

Dynamics of Fluorescent Probes in Biological Systems

Mallela Manikya Gopala Krishna

Department of Chemical Sciences

Tata Institute of Fundamental Research

Mumbai 400 005

INDIA

*A thesis submitted to the University of Mumbai
for the Ph. D. degree in Physical Chemistry*

March 1999

To the memory of my father

Acknowledgements

I would like to express my sincere gratitude to Prof. N. Periasamy for his excellent guidance and for his constant support throughout the course of this work. I would also like to thank him for introducing me to the fascinating field of fluorescence spectroscopy and for many helpful discussions that improved my understanding of the subject. I am indebted to him for his moral support and encouragement in my difficult times.

I would like to thank Prof. G. Krishnamoorthy for his keen interest in my work and for his help whenever I needed it. I would like to thank Prof. K. V. R. Chary for his help and for the collaborative projects on NMR experiments and on HSPI protein. I thank Dr. Ranjan Das for all his help. My sincere thanks to Prof. S. R. Kasturi, Prof. V. R. Marathe, Prof. S. Doraiswamy, Dr. Sanjay Wategaonkar, Dr. Sudipta Maiti, Prof. S. Mitra and Prof. G. Govil for their kind help. I also thank Prof. R. V. Hosur for guiding me in one of the research projects.

I thank Prof. Rajaram Nityananda of Raman Research Institute, Bangalore, and Dr. S. N. Mazumdar and Prof. Deepak Dhar of Theoretical Physics Group, TIFR for the discussions regarding the analytical solution for the surface diffusion problem. I would like to acknowledge Prof. Y. K. Levine of University of Utrecht, Netherlands for the discussions on the orientation of molecules in bilayer membranes. I thank Mr. Amaresh Mishra and Prof. G. B. Behera of Sambalpur University for the collaborative projects on the aminostyrylpyridinium dyes. I would like to thank Prof. Jayant Udgaonkar of NCBS, Bangalore for providing the Barstar single tryptophan mutant.

I thank Nakul Maiti for many helpful discussions and his help in many ways. I would like to thank my labmates Arvind, Vetri, Swami, Naresh, Lakshmikanth, Ira, Koti, Meenakshi, Parijat, Neel and Balaji for their help. I would also like to acknowledge Vinit for his help regarding the work on HSPI protein. With great pleasure, I thank my VIBGYOR friends Anant, Apurba, Britto, Gunjan, Prasanta and Sarata with whom I shared many of my dreams and for many memorable and cheerful moments during our stay at TIFR. I would like to thank my friends at other Institutes Anthony, Hotha, Sarma, Lakshminarayana, Rajesh, Hema, Gayathri, Ramalakshmi and others for their help and for providing the journal references.

I gratefully thank all the faculty members of the Department of Chemical Sciences for their kind help in different ways during the course of this work. I thank my M. Sc. teachers at University of Hyderabad for their constant encouragement. I thank my friends H. P. Maity, Mita, Bhaumik, Ravikanth, Kishore, Shilpi, Madhu, Sanjay, Krishnananda, Sridevi and others for their help. I would like to thank Ajit, Bhagat, Kamat, Madhuri, Geetanjali, Biswajit, Limaye, Bankar, Sachin and Tambi for their help. My thanks for the help taken from computer, library, drawing, photography and xerox sections of the Institute.

I take this opportunity to thank Prof. A. S. Verkman of University of California at San Francisco for offering me a fellowship to visit his lab and for introducing me to the molecular biology techniques such as gene cloning, protein expression and site directed mutagenesis. I would also like to thank him for the collaborative projects on AQP1 and CFTR proteins. I thank my labmates at UCSF Tongui, Yuxin, Neel, Bauxue, TK, Fuminori, Joechim, Javier, Mark, Sujatha and Cathy for their kind help. I also thank Swami, Kishore and Shilpi for their help during my stay at San Francisco. I gratefully acknowledge the organizers of MAFS5 conference and SMD workshop at Berlin for providing me the financial assistance to attend the same.

I would like to thank my cousins at Mumbai for all their help and also for those nice weekends I spent at their home. I am short of words in expressing my gratitude to my family members for bearing the difficulties they had to undergo during the course of this work. Without their constant support and encouragement, this thesis would not have taken shape.

Statutory Declarations

Name of the Candidate:	Mallela Manikya Gopala Krishna
Name of the Supervisor:	Professor N. Periasamy
Degree:	Ph. D.
Subject:	Physical Chemistry
Title of thesis:	Dynamics of Fluorescent Probes in Biological Systems
Registration Number:	TIFR-83 (15 th June 1995)
Place of Research:	Tata Institute of Fundamental Research, Homi Bhabha Road, Mumbai 400005

Statements required under the ordinances 0.770 and 0.771

The work presented in this thesis has not been submitted to this or any other University for Ph. D. or any other degree.

All the work presented in this thesis has been carried out by me under the supervision of Prof. N. Periasamy. Preparation of samples, data collection and analysis of the experimental results were performed by me. The results were discussed and interpreted by me with the help of Prof. N. Periasamy.

Statements regarding the new facts:

The following new facts have emerged during the studies conducted as part of this thesis.

(1) A new method of spectrally constrained global analysis of multiple fluorescence decays in a multi-component aqueous system was developed for the accurate estimate of fluorescence lifetimes and spectra of fluorescent dye molecules in lipid bilayer membranes.

(2) It was identified that the fluorescence decay of Nile red in lipid vesicles, surfactant micelles and viscous organic solvents is biexponential with a negative fraction for the short lifetime indicating subnanosecond excited state kinetics.

(3) The sites of solubilization of fifteen organic dyes in a bilayer membrane (Egg PC) were identified to be surface, interface or core region based on the combined effects of viscosity and refractive index on the fluorescence lifetimes. Dicarboyanines were identified to be oriented in the core of the bilayer membrane based on the decrease of fluorescence lifetime with refractive index.

(4) The second rank order parameters determined from fluorescence lifetime and anisotropy differed significantly in the case of DODCI in bilayer membranes. This discrepancy was explained by a bimodal orientational distribution with one population centered about the membrane normal and the other parallel to the membrane surface. A unimodal distribution was not adequate.

(5) The fluorescence anisotropy due to translational diffusion of oriented dipoles on the surface of a sphere is found to be double exponential with the correlation times $R^2/6D_{tr}$ and $R^2/2D_{tr}$ where R is the radius of the sphere and D_{tr} is the translational diffusion coefficient. The amplitudes of the two correlation times depend on the angle made by the dipoles with the surface normal. From the translational dynamics of Nile red in SDS micelles, it was calculated that the molecular dipole makes an angle of $25 \pm 7^\circ$ with the surface of the micelle.

(6) The fluorescence anisotropy due to the rotational diffusion of surface dipoles on the surface of a sphere decays exponentially to a residual anisotropy which is one fourth of the initial value.

Signature of the candidate

I agree with the above statements

Signature of the supervisor

SYNOPSIS

I. Introduction

Biological systems are natural complex systems. Fluorescence Spectroscopy is one of the widely used tools for the study of dynamics in biological systems. Biological Fluorescence techniques make use of the fluorescence emitted by the chromophores which is sensitive to their local environment. Biologically useful chromophores can be intrinsic like the aromatic amino acids in proteins or extrinsic like fluorescent dye molecules. The three useful properties of fluorescence are fluorescence spectrum, intensity and polarization. These fluorescence properties tell us about the nature of the environment of the fluorescent probe. The time dependence of the above properties tells us about the dynamics of the chromophore and its immediate neighbourhood.

Bilayer membranes and proteins form two important classes of biological systems. Micelles form a model system for membranes. The bilayer membranes are made up of lipid molecules. A lipid molecule has a hydrophilic head group (e.g., Phosphatidyl Choline) and two hydrophobic tails (saturated or partially unsaturated hydrocarbon chains). In water, they form closed spherical bilayer structures called lipid vesicles or liposomes. Hydrocarbon chains form the interior of the bilayer with the head groups exposed to the water. The structure and dynamics of these bilayer membranes and the way the lipid molecules control the dynamics of small molecules inside a bilayer membrane has been the subject of numerous studies. Micelles are formed by the aggregation of amphiphilic surfactant molecules in water. Surfactant molecules are similar to the lipid molecules except that they contain only one hydrophobic chain. Micelles contain a hydrophobic core with the hydrophilic head groups exposed to water and hence these form model systems for lipid bilayer membranes. Proteins are macromolecules which are uniquely folded polypeptides. The function of a protein depends upon its structure and dynamics. Tryptophan, one of the three fluorescent aromatic amino acids, is the commonly used intrinsic fluorophore in protein fluorescence studies. Fluorescent organic dye molecules are commonly used as extrinsic fluorophores in the study of bilayer lipid membranes and surfactant micelles.

Steady state and time resolved fluorescence techniques provide valuable information about the biological system under study. The Stokes' shift, fluorescence spectra and quantum yield give information about the interaction of the chromophore with the surrounding medium. Fluorescence decay characterizes the excited state kinetics. The method of decay associated spectra allows us to obtain the spectra of individual components in a multi-component system. The quenching of fluorescence of fluorophores by quenchers tells us about the accessibility of fluorophore to the quenchers. One can measure the distances in a biological system using fluorescence resonance energy transfer between a donor and an acceptor. The fluorescence anisotropy describes the rotational and orientational freedom of the fluorophore. The information gained about a biological system (e.g., conformational changes, biomolecular complexation) by using fluorescence spectroscopy increases with the combined analysis of many of the above mentioned fluorescence parameters.

In spite of the multi-faceted research on the dynamics of probes in biological systems using fluorescence and other techniques, there still remain unanswered questions concerning the location, orientation and dynamics of small molecules (e.g., drug molecules) at extremely low concentrations in lipid bilayers and micelles. The fluorescence dynamics of a few fluorescent probes in bilayer membranes, micelles and proteins using conventional and new methods were investigated. The results and conclusions are described below.

II. Fluorescence Characteristics of membrane-bound probes

The determination of location, orientation and dynamics of fluorophores in membranes requires measurement of fluorescence properties of the membrane-bound probes. It was found necessary to examine carefully the assumptions and methods used for obtaining the fluorescence properties of membrane-bound fluorophores.

(a) Spectrally Constrained Global Analysis of Fluorescence Decays

Most biological systems are multi-component consisting of an aqueous phase and one or more nonaqueous phases. Although fluorescent dye probes are often targeted to a specific phase, it is not uncommon that the fluorophore finds its way to the aqueous compartment. Time

resolved and steady state fluorescence measurements of the whole system are a sum of the spectral and dynamic properties of the targeted component and the aqueous component. Separation of the fluorescent characteristics of the fluorophore in the targeted component is essential for the interpretation of the results. A popular method of fluorescence analysis is to combine the time resolved fluorescence data with the steady state spectrum and obtain the decay associated spectra for the multicomponent system [1]. This method of global analysis of multiple fluorescence decays collected at different emission wavelengths fails in resolving the spectra when the lifetimes of the dye in the aqueous phase and nonaqueous phase are close to each other.

A new method of global analysis was developed which takes advantage of the known spectrum and lifetime of the fluorescent probe in the aqueous phase. The intensity ratios at different wavelengths for the aqueous component were calculated using the known steady state spectrum of the fluorophore in water. These were used in calculating the partial derivatives of the fluorescence response with respect to the free parameters which are needed for the nonlinear least squares analysis using Levenberg - Marquardt algorithm. This procedure reduces the number of free parameters in the global analysis.

Spectrally constrained global analysis of multiple fluorescence decays was applied to the case of a fluorescent probe DODCI (3,3'-diethyloxadicarbocyanine iodide) in Egg PC (Egg Phosphatidyl Choline) membrane. DODCI in water exhibits a single fluorescence lifetime. DODCI in Egg PC showed a double exponential fluorescence decay with the lifetimes and amplitudes varying as a function of the emission wavelength. This indicates that two-species-two-lifetime model is not correct. A three exponential global analysis with a fixed lifetime for the aqueous component resulted in unsatisfactory oscillations in the amplitudes (spectra) for the aqueous and non-aqueous components. The spectrally constrained global analysis produced smoothly varying amplitudes (spectra) for the non-aqueous components. The method allows accurate estimate of the lifetimes of membrane-bound fluorophores.

(b) Excited State Kinetics of Nile Red in Membranes and Micelles

Nile red (Nile Blue A Oxazone) is a commonly used hydrophobic dye for probing the

structure, environment and dynamics in biological systems. The fluorescence of this dye is strongly dependent on polarity and Nile red has been used as a micropolarity probe in biological systems. A single emissive state was generally assumed to explain the fluorescence decay kinetics of Nile red in organic solvents as well as in micelles and vesicles.

Our experiments showed that the fluorescence intensity decay is different at different emission wavelengths in the case of Nile red in Egg PC membrane. The global analysis of multiple fluorescence decays collected over the emission spectrum of Nile red gave two exponentials with lifetimes 1.26ns and 3.88ns and the amplitudes varying with the emission wavelength. Nile red in SDS (Sodium Dodecyl Sulfate) micelles also showed a double exponential fluorescence decay with the lifetimes 0.68ns and 2.53ns and the amplitudes varying with the emission wavelength. The fluorescence decays collected as a function of emission wavelength in the case of Nile red in methanol fit to a single exponential (2.88ns) at all wavelengths.

In both the cases of Nile red in Egg PC vesicles and SDS micelles as well as in 1-octanol and glycerol, the amplitudes of short lifetime component become negative at longer emission wavelengths. This indicates an excited state reaction of Nile red in these systems. Analytical equations for irreversible and reversible two state excited state reaction were consistent with the experimental results. It is concluded that the short lifetime observed in the case of Nile red in Egg PC and SDS corresponds to the initially excited state and the long lifetime is due to the newly formed species in the excited state.

Negative amplitudes were not observed for several other dyes in bilayer membranes indicating the absence of excited state kinetics.

III. Effect of Viscosity and Refractive Index on the Fluorescence Lifetimes in Biological Systems

The fluorescence lifetimes of fluorophores in biological systems are affected by the viscosity and refractive index of the aqueous and non-aqueous components. The mechanism by which the viscosity modifies the fluorescence lifetime is different from that of refractive index. Fluorescence lifetime is the inverse of the sum of radiative and nonradiative rates. Viscosity

affects the nonradiative rate whereas the refractive index affects the radiative rate. The effect of viscosity on the lifetime is based on the collision mechanism between the solvent molecules and the excited state of the dye. Hence, the effect of viscosity on fluorescence lifetime depends upon the extent of exposure of the fluorophore to the solvent. The effect of refractive index is optical and depends upon isotropic/anisotropic electric field experienced in the vicinity of the probe. In the case of a fluorophore in a 'spherical' cavity such as tryptophan in a protein, the refractive index effect on the radiative rate will be proportional to the fifth power of the refractive index of the aqueous medium. In the case of a fluorophore in a thin layer such as a bilayer lipid membrane, the effect of refractive index depends on the probe orientation with respect to the membrane normal. In the extreme cases of probe orientation parallel and perpendicular to the membrane normal, the radiative rate varies as the fifth and first powers of the refractive index of the aqueous medium respectively [2]. An increase of refractive index decreases the fluorescence lifetime whereas the increase of viscosity increases the fluorescence lifetime. The effect of refractive index on the fluorescence lifetimes of fluorophores in biological systems has generally been ignored in the literature. This effect is more pronounced in the case of fluorophores with high quantum yield. The combined effects of viscosity and refractive index on the fluorescence lifetime depend on the relative values of the nonradiative and radiative rates.

(a) Protein Fluorescence in Aqueous Glycerol Solutions

The fluorescence lifetime of a tryptophan in a protein is expected to be strongly viscosity dependent if it is solvent exposed. If the tryptophan is not solvent exposed, then the viscosity will not affect the fluorescence lifetime but refractive index will affect the fluorescence lifetime. Experiments were carried out on two structurally compact proteins Human Seminal Plasma Prostatic Inhibin (HSPI) and Barstar W38,44F mutant. HSPI is a two-tryptophan protein which exhibits a two exponential fluorescence decay. The two lifetimes (5.86ns and 2.44ns) were assigned to the two sterically constrained, solvent exposed tryptophans (W32 and W92) existing as single rotamer populations based on the combined analysis of Fluorescence and NMR (Nuclear Magnetic Resonance) results [3]. Barstar W38,44F mutant contains a single tryptophan that is inaccessible to solvent and exhibits a single exponential fluorescence decay

(4.85ns) [4]. In these two proteins, the tryptophans have no independent rotational motion other than the rotation of the entire protein. In aqueous glycerol solutions, the proteins retained the structural integrity as indicated by the fluorescence anisotropy and increase of the rotational correlation time of the protein. Increase of glycerol concentration from 0% to 55.75% w/w increases the relative viscosity from 1 to 8.21 whereas the refractive index increases from 1.334 to 1.407. In the control experiments, the fluorescence lifetime of NATA (N-Acetyl Tryptophanamide) increases steadily with glycerol, which is the viscosity effect. The fluorescence lifetime of W38,44F Barstar shows no variation with the increase of glycerol. The fluorescence lifetimes of HSPI at first show no variation and then steadily increase with the glycerol concentration. These trends are consistent with the combined effect of viscosity and refractive index on a low quantum yield probe such as tryptophan.

(b) Fluorescence of Organic Dyes in Bilayer Membranes: Site of Solubilization

The determination of site of solubilization of a small molecule (e.g., drug molecule, fluorophore etc.) at low concentrations in a bilayer membrane is a non-trivial problem. Fluorescence measurements can be judiciously used for the determination of the probe location. The sites of solubilization of fifteen organic dye molecules in a lipid bilayer membrane were identified from the combined effects of viscosity and refractive index on the fluorescence lifetime.

Sucrose was used to vary the viscosity and refractive index of the aqueous medium in which the lipid vesicles were prepared by sonication. Variation of sucrose from 0% to 44.4% w/w increases the relative viscosity from 1 to 10.74 whereas the refractive index increases from 1.334 to 1.413. Fluorescence decay measurements were carried out on fifteen organic dye molecules incorporated in Egg PC vesicles. The strategy of global analysis of multiple files was adopted to reduce the errors associated with the fluorescence lifetimes. The fluorescence lifetime distributions obtained by Maximum Entropy Method (MEM) show one or more well resolved peaks, which match well with the results of discrete exponential analysis. The fluorescence decay of the membrane-bound dye was associated with at least two spectroscopically distinct species, with only one being prominent in most cases.

There are three regions in the membrane phase in which an organic dye molecule is expected to have different degrees of hydrophobicity and exposure to the solvent. These are the surface region, in which the dye is exposed to the solvent; the interface region, in which the exposure to the solvent is limited; and the hydrocarbon core region where the dye is not exposed to solvent. The viscosity effect dominates if the dye is located near the surface and the refractive index dominates when the dye is solubilized in the core. In the case of the dye DiA (4-(4-dihexadecylamino)styryl)-N-methylpyridinium iodide), the fluorescence decay becomes slower whereas the decay is faster for DODCI with the increase of sucrose concentration. Hence, the viscosity effect is dominant in the case of DiA whereas the refractive index effect is dominant in the case of DODCI. Therefore, the sites of solubilization of the two dyes DiA and DODCI are attributed to the surface and core regions of the bilayer, respectively. Similar strategy was followed in determining the sites of solubilization for the other dyes in the bilayer membrane.

The dependence of the radiative rate of a membrane-bound fluorescent probe on the refractive index of the aqueous medium depends upon its orientation with respect to the membrane normal [2]. Such an effect can be observed only for the dyes that have a linear structure such as DODCI and located in the core of the bilayer. Three dicarbocyanines and DPH (1,6-diphenyl-1,3,5-hexatriene), which show the refractive index effect are identified to be solubilized in the core of the bilayer.

IV. Orientational Distribution of Linear Dye Molecules in Bilayer Membranes

The anisotropic nature of the bilayer restricts the orientational freedom of the fluorescent dye molecules in a bilayer membrane. The question of the orientational distribution of probe molecules in a bilayer has been the focus of numerous studies using fluorescence anisotropy as the measured parameter. In this thesis, the effect of the refractive index on the fluorescence lifetime has been used as an additional constraint to determine the orientational distribution of linear dye molecules in a lipid bilayer. In addition to DPH, dicarbocyanines are

the only molecules which show the refractive index effect. Among dicarbocyanines, DODCI was found to show the maximum effect. The orientational and dynamical freedom of a dye molecule in a biological system is characterized by the order parameters. The second rank order parameter, $\langle P_2(\cos\theta) \rangle$ was calculated from the initial and limiting anisotropy values in the fluorescence anisotropy decay. The second rank order parameter was also calculated from the dependence of the fluorescence lifetime on the refractive index. These two order parameters determined from the lifetime and anisotropy measurements do not match with one another.

Different models of orientational distributions were considered to explain the discrepancy between the two order parameters. A unimodal orientational distribution with a single population cannot explain this discrepancy. A bimodal orientational distribution function where one population is centered about the membrane normal and the other parallel to the membrane surface was found to be adequate. Two models (Gaussian model and Maier-Saupe model [5]) were considered for the distributions in the bimodal orientational distribution. Both the models explain the discrepancy between the two order parameters of DODCI and it was not possible to discriminate between the two models.

The lifetime and anisotropy experiments were carried out on DODCI in seven synthetic lipids with different chain lengths (C12, C14 and C16) and varying unsaturation. The ratios of the amplitudes of the long (dye population in the core region) and short (dye in the surface region) lifetimes of the membrane-bound DODCI decrease with the increase of the hydrocarbon chain length and decrease of unsaturation. The refractive index effect of the long fluorescence lifetime is different for different lipids. The two order parameters determined from lifetime and anisotropy measurements were used to determine the bimodal orientational distributions. The fractional amplitudes of the two populations depend on unsaturation and alkyl chain length of the lipid. The ratio of the populations oriented parallel and perpendicular to the membrane normal increase with the increase of the alkyl chain length or with the decrease of unsaturation.

V. Translational and Rotational Diffusion of Surface Probes: Monte Carlo Simulations and Fluorescence Anisotropy Experiments

The time resolved fluorescence anisotropy decay measurements provide direct information about the rotational dynamics of fluorescent probes. The fluorescence anisotropy decay is not affected by the translational diffusion dynamics of the fluorophore in liquids. On the other hand, if the fluorophore is bound to the surface of a nanometer-size particle (vesicles, micelles and proteins), the fluorescence depolarization dynamics is determined by both translational and rotational dynamics of the dye on the surface. In addition, the fluorescence anisotropy decay depends upon the orientation of the transition dipole and the shape of the particle. In spite of numerous studies of fluorescence dynamics of fluorophores bound to micelles, membranes and proteins, analytical equations are not available for the anisotropy due to translational diffusion of surface bound fluorophores.

Monte Carlo simulations of the surface diffusion of molecular dipoles on a spherical surface were performed. A computer program was developed for this purpose in C language with graphics. The simulation for the translational diffusion consists of three steps: (i) selection of the initial distribution of the dipoles in the excited state with $\cos^2\theta$ dependence where θ is the angle made by the dipole with the polarization axis (z-axis) of the exciting laser beam, (ii) diffusion of the dipoles on the spherical surface in random directions through small steps using three dimensional rotational matrix, and (iii) calculation of the anisotropy function from the intensities along x, y and z-axes after each step. Test of the simulations was performed for the case where the dipoles are oriented perpendicular to the spherical surface for which the decay is single exponential.

The anisotropy decay due to the translational diffusion of oriented molecular dipoles on a spherical surface was found to be two exponential with the correlation times $R^2/6D_{tr}$ and $R^2/2D_{tr}$ where R is the radius of the sphere and D_{tr} is the translational diffusion coefficient. The amplitudes of the two exponentials depend upon the angle θ between the dipoles and the normal to the spherical surface. When the dipoles are perpendicular to the spherical surface ($\theta=0$), the anisotropy decay is single exponential with the correlation time $R^2/6D_{tr}$. The second exponential appears when $\theta \neq 0$. In the case where the dipoles are oriented perpendicular to the normal to the spherical surface ($\theta=\pi/2$), the amplitude ratio of the two exponentials with correlation times $R^2/6D_{tr}$ and $R^2/2D_{tr}$ is 1:3. These equations were used in the analysis of anisotropy decay of Nile

red in SDS micelles. The anisotropy decay for the dye in the micelle is caused by three depolarizing motions: wobbling dynamics of the dye in the micelle, the translational motion of the dye on the spherical surface of the micelle and the rotational diffusion of the micelle. Using the appropriate equations for these three processes, it was calculated that Nile red wobbles in a cone of semiangle of 54° with the order parameter 0.47. From translational dynamics, it was calculated that the molecular dipole makes an angle of $25 \pm 7^\circ$ with the surface of the micelle.

Monte Carlo simulations were also carried out for the rotational diffusion of the dipoles on planar and spherical surfaces. The procedure is similar to the one described for simulating the translational diffusion. The decay is simulated for two cases: (i) where the dipoles are distributed over the entire spherical surface and the simulated anisotropy decay is the average of all the dipoles (e.g., sonicated vesicles) and (ii) where the dipoles are distributed on a planar membrane. The anisotropy decay is found to be $r(t) = r(0)\exp(-4D_{\text{rot}}t)$ in the case of diffusion in a plane and $r(t) = r(0)[0.25 + 0.75\exp(-4D_{\text{rot}}t)]$ in the case of rotational diffusion of dipoles on a spherical surface. These equations were applied to the case of DiIC₁₈(5) (1,1'-dioctadecyl-3,3,3',3'-tetramethylindocarbocyanine perchlorate) in sonicated and giant Egg PC vesicles. The fluorescence anisotropy decay of DiIC₁₈(5) on a single giant liposome was fitted to a single exponential function whereas in the case of DiIC₁₈(5) in sonicated vesicles, a short correlation time was found in addition to the one predicted for the rotational diffusion of dipoles which was attributed to the wobbling-in-cylinder dynamics of the dye about the surface of the membrane.

VI. Summary

The location and orientation of small molecules in a lipid bilayer membrane has been addressed in this thesis with the help of the effects of viscosity and refractive index of the aqueous medium on the fluorescence lifetimes. This thesis makes use of the refractive index effect on the fluorescence lifetimes of fluorophores, which has been ignored in the past. The sites of solubilization of fifteen organic dye molecules in a bilayer membrane were identified as either in the core, interface or surface regions of the bilayer. The orientational distribution of the oriented dye molecule DODCI in the core of the bilayer is bimodal with the two populations oriented parallel and perpendicular to the membrane normal. The surface to core populations

and the fractions of the two populations in the bimodal orientational distribution in the core depend on the nature of the alkyl chain of the lipid.

In the course of the above work, a new method of spectrally constrained global analysis was developed to separate the fluorescence lifetimes of the membrane-bound dye. A slow excited state kinetics leading to negative amplitudes was observed in the case of Nile red in membranes, micelles and viscous organic solvents.

The fluorescence anisotropy decay due to translational diffusion of dipoles on a spherical surface was found to be two exponential with the amplitudes varying with the angle made by the dipoles with the normal to the spherical surface. The rotational diffusion of surface probes results in a single exponential fluorescence anisotropy decay. The residual anisotropy is zero and one-fourth of the initial anisotropy in the case of diffusion on a plane and on a spherical surface respectively. These equations were applied in interpreting the fluorescence anisotropy decays of fluorescent probes in lipid vesicles and micelles.

Ref:

- [1] J. R. Lakowicz, Principles of Fluorescence Spectroscopy, Plenum Press, New York, 1983.
- [2] D. Tóptygin and L. Brand, Biophys. Chem., **48**, 1993, 205.
- [3] M. M. G. Krishna, V. K. Rastogi, N. Periasamy and K. V. R. Chary, J. Phys. Chem. B, **102**, 1998, 5520.
- [4] R. Swaminathan, U. Nath, J. B. Udgaonkar, N. Periasamy and G. Krishnamoorthy, Biochemistry, **35**, 1996, 9150.
- [5] C. Zannoni, A. Arcioni and P. Cavarota, Chem. Phys. Lipids, **32**, 1983, 179.

Contents

1	Introduction	1
1.1	Dynamics in Biological systems	1
1.1.1	Lipid bilayer membranes	2
1.1.2	Micelles	9
1.1.3	Proteins	11
1.1.4	Small molecules in biology	12
1.2	Fluorescence Spectroscopy	16
1.2.1	Fluorescence Spectra	19
1.2.2	Fluorescence Intensity and Quantum yield	20
1.2.3	Fluorescence Intensity Decay and Lifetime	21
1.2.4	Fluorescence Anisotropy	22
1.2.5	Time Resolved Emission Spectra and Decay Associated Spectra . .	25
1.2.6	Fluorescence Quenching	28
1.2.7	Fluorescence Resonance Energy Transfer	29
1.3	Scope of the thesis	31
2	Experimental: Materials and Methods	34
2.1	Materials	34
2.2	Preparation of samples	36
2.2.1	Preparation of lipid vesicles	36
2.2.2	Preparation of surfactant micelles	37

2.3	Experimental Methods	38
2.3.1	Absorption measurements	38
2.3.2	Steady State Fluorescence Measurements	38
2.3.3	Quantum yield and Radiative rate	39
2.3.4	Time Resolved Fluorescence Measurements	40
2.3.5	Fluorescence Microscopy Experiments	45
2.3.6	NMR Measurements	46
2.4	Fluorescence Decay Data Analysis	46
2.4.1	Nonlinear Least squares Levenberg-Marquardt Algorithm	47
2.4.2	Discrete Exponential analysis of fluorescence intensity decays	49
2.4.3	Global Analysis of multiple fluorescence intensity decays	53
2.4.4	Maximum Entropy Method	54
2.4.5	Analysis of time resolved fluorescence anisotropy	57
3	Fluorescence Characteristics of Membrane Bound Probes	62
3.1	Spectrally Constrained Global Analysis (SCGA) of Fluorescence Decays	63
3.1.1	Method:	64
3.1.2	Application: DODCI in Egg PC membrane	68
3.2	Excited State Kinetics of Nile red in Membranes and Micelles	78
3.2.1	Nile red in Egg PC vesicles and SDS micelles	79
3.2.2	Fluorescence decay kinetics and Species Associated Spectra	81
3.2.3	Nile red in viscous solvents	88
3.3	General Characteristics of membrane-bound fluorescent probes	93
4	Effects of Viscosity and Refractive Index on the Fluorescence Lifetimes in Biological Systems	94
4.1	Effect of Viscosity	95
4.2	Effect of Refractive Index	95
4.3	Protein Fluorescence in Aqueous Glycerol Solutions	98
4.3.1	Barstar W38,44F: Solvent inaccessible single tryptophan	99

4.3.2	HSPI: Solvent accessible tryptophans	99
4.3.3	Effects of viscosity and refractive index	108
4.4	Fluorescence of Organic Dyes in Bilayer Membranes	113
4.4.1	Fluorescence Lifetimes in Ethanol and Water	115
4.4.2	Fluorescence Lifetimes in Membrane	118
4.4.3	Effects of viscosity and refractive index on the fluorescence lifetimes: Determination of the Site of Solubilization	122
4.4.4	Location of DODCI and DiIC ₁₈ (5) in Egg PC: NMR experiments .	133
4.4.5	Oriented dye molecules in the core of the bilayer membrane	137
5	Orientational Distribution of Linear Dye Molecules in Bilayer Mem-	
	branes	140
5.1	Order parameters	141
5.1.1	Theory	141
5.1.2	Measurement	143
5.2	Refractive index of the membrane	145
5.3	Orientation of the linear dye molecules: Dicarbocyanines and DPH	147
5.4	Location and Orientation of a linear dye molecule DODCI in lipid bilayer membranes: Effects of chain length, unsaturation and temperature	159
5.4.1	Location of DODCI	162
5.4.2	Orientation of DODCI	169
6	Translational and Rotational Diffusion of Surface Probes: Monte Carlo	
	Simulations and Fluorescence Anisotropy Experiments	180
6.1	Models for the rotational dynamics of fluorophores in biological systems . .	182
6.2	Fluorescence anisotropy decay of Fluorescent Probes in bilayer membranes	183
6.3	Dynamics of surface probes: Diffusion on the surface of a macroparticle . .	188
6.4	Monte Carlo Simulations	189
6.4.1	Translational diffusion	189
6.4.2	Rotational diffusion	196

6.5	Translational Diffusion: Simulations and Experiment	197
6.5.1	Results of the Monte Carlo Simulations	197
6.5.2	Theoretical justification of the simulation results	205
6.5.3	Experiment: Nile red in SDS micelles	211
6.6	Rotational Diffusion: Simulations and Experiment	217
6.6.1	Results of the Monte Carlo Simulations	217
6.6.2	Theoretical justification of the simulation results	219
6.6.3	Rotational Dynamics of DiIC ₁₈ (5) in Egg PC	220
7	Summary	227
7.1	Summary	227
7.2	Future Directions	230
A	C program developed for Monte Carlo simulations of the translational diffusion of surface probes on the surface of a sphere	233

Chapter 1

Introduction

1.1 Dynamics in Biological systems

Biological systems are natural complex systems. The diverse but coordinated functions carried out by these systems are responsible for the functioning of complex living organisms. Studying the structure and dynamics of these systems is essential to understand the physicochemical processes associated with them.

Examples of these simple biological systems include membranes, proteins and nucleic acids. These biological systems are organized molecular assemblies constituted by small individual molecular units which are covalently linked (in the case of proteins and nucleic acids) or non-covalently self-assembled (membranes). The diversity of the functions carried out by a biological system depend on the collective behaviour and cooperativity of these individual units and on the nature of hydrophobic and hydrophilic interactions between these subunits and with water. Biological membranes are formed because of the noncovalent hydrophobic interaction between the amphiphilic molecules known as lipids that contain one hydrophilic head group attached to two long hydrophobic alkyl chains. The nature of the lipid regulates the processes that are associated with the membranes. Natural membranes also contain proteins and the organization i.e., the structure and function of these membrane proteins, in most cases, is controlled by their nature of

the interaction with the surrounding sea of lipids. Proteins are formed by the covalent peptide bonds between amino acids. The nature of the amino acid side chains (polarity, hydrophobicity and charge) controls the structure and function of the proteins. The interactions between the side chains of amino acids among themselves and with water decide the complete three dimensional structure of the protein and its function. Nucleotides are the individual subunits in the nucleic acids such as DNA and RNA. Each nucleotide contains a purine/pyrimidine base linked to a sugar. Covalent phosphate bonds between the individual nucleotides make the nucleic acids. The sequence and the stacking interactions between these individual nucleotides carry the genetic information and the three dimensional structures of the nucleic acids that are necessary for their function.

This thesis deals with the dynamics of fluorescent probes in biological systems: mainly, in lipid bilayer membranes and to some extent, in proteins and in micelles. These three systems are described in detail as follows.

1.1.1 Lipid bilayer membranes

All living cells and many organelles inside the cell are enclosed by membranes. These membranes separate the components of vital metabolic processes inside the cell from external environment, and inside the cell, they separate the cellular constituents such as nucleus, mitochondria, golgi apparatus, lysosomes, endoplasmic reticulum etc. from the surrounding cytosol. These membranes modulate different processes ranging from permeability and transport of small molecules, cell-cell communication and as a support for membrane proteins. Figure 1.1 shows the various processes modulated by the membranes [1].

Nagelli, in the year 1855, first suggested the presence of an impermeable membrane based on the observation that the surface of the cells are impermeable to certain pigments present inside or outside the cell [2]. The rates of permeation of various compounds into this membrane are similar to the partition of these compounds between oil and water which suggested the fatty (hydrophobic) nature of the membrane (Overton, 1896).

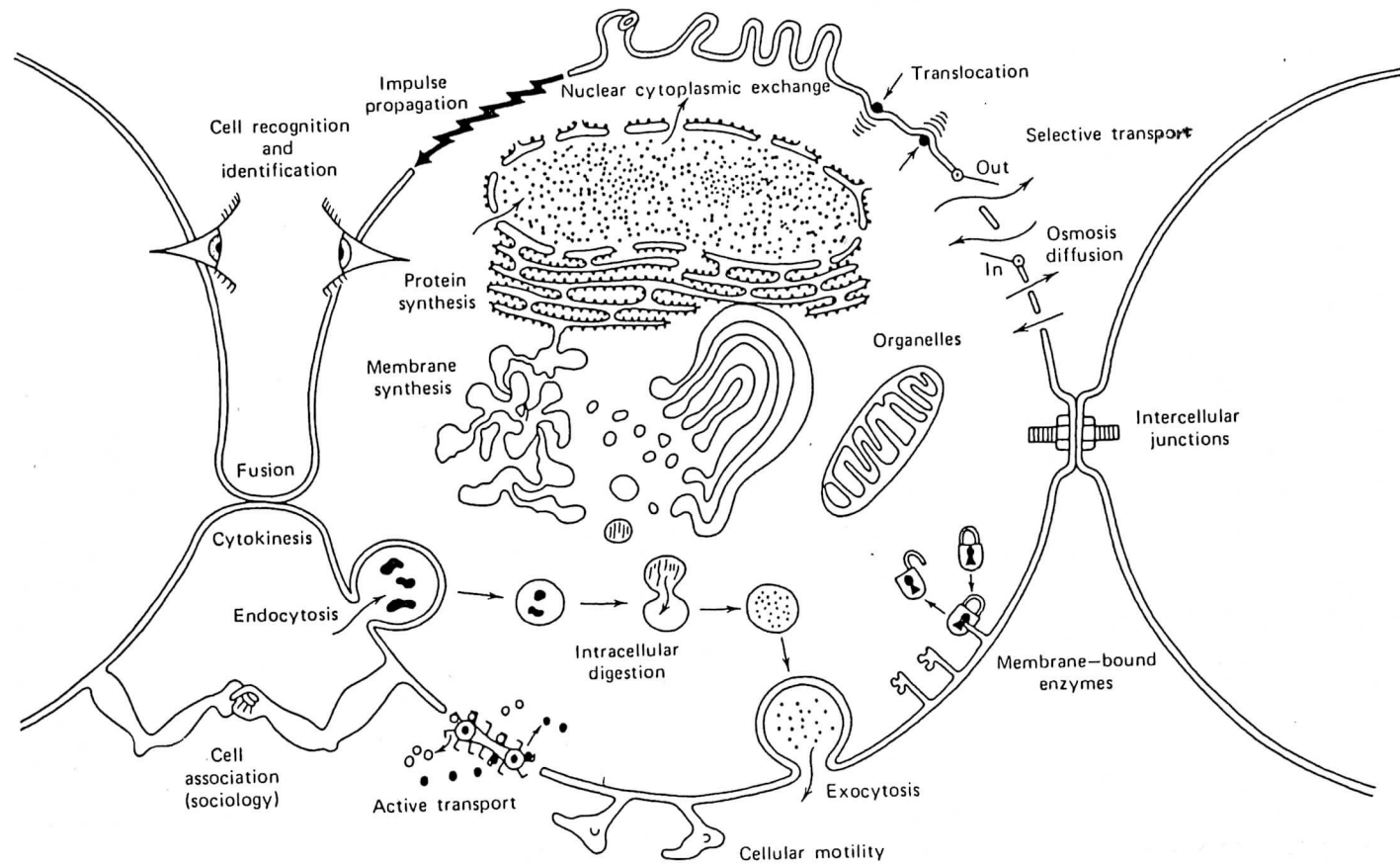


Figure 1.1: Cartoon of a typical cell. This figure shows the various processes modulated by the cell membrane [1].

The membranes are identified to be formed by the small molecules that are called lipids which are amphiphilic. Most of the lipids have a hydrophilic head group and two long hydrophobic alkyl chains. Langmuir (1917) has shown that fats and fatty acids with long alkyl chains, when dissolved in water, stack in parallel because of the van der Waals forces between the hydrocarbon chains and by repulsion between the water and the hydrophobic hydrocarbon chains. Lipids extracted from biological membranes formed monolayers on the surface of water whose surface area is found to be twice that of the natural membranes which led to the conclusion that the membranes are of two molecules thick and the lipid molecules are arranged in the form of a bilayer with the hydrophilic head groups pointed towards water and the hydrocarbon tails stacked with one another in two layers excluding water (Gorter, 1925; Danielli, 1935). Later experimental studies on the solubility and permeability of small molecules have proven the bimolecular nature of the lipid bilayer [2]. Based on several experimental studies, classical fluid mosaic model was proposed for the biological membranes which states that membranes are two-dimensional fluids of oriented lipids, and membrane proteins are like boats in the sea of lipids [3]. A general picture of this model that is accepted for the structure of biological membranes is shown in the figure 1.2.

Lipid molecules are the main constituents of biological membranes [4, 5, 6]. These molecules are amphiphilic in nature containing a hydrophilic head and two long hydrophobic alkyl chains. A typical structure of a lipid molecule which is a phospholipid is shown in the figure 1.3. The basic structure of a lipid contains a glycerol moiety (in the case of phospholipids) or a sphingosine (in the case of sphingolipids) with different substitutions. The long hydrophobic chains can be either saturated or partially unsaturated. In most cases, the hydrophilic head group is a phosphate group attached with one of the polar moieties such as choline. There are other lipids present in the biological membranes known as glycolipids where the headgroup is a sugar. The phospholipid shown in the figure 1.3 is the naturally occurring lipid, sn-1-Palmitoyl, sn-2-Oleoyl, sn-3-Phosphatidyl Choline (POPC) which is the major constituent of the lipid extracted from fresh egg yolk (Egg PC) [7]. Here the numbering sn-1, sn-2 and sn-3 represent the substitution on the

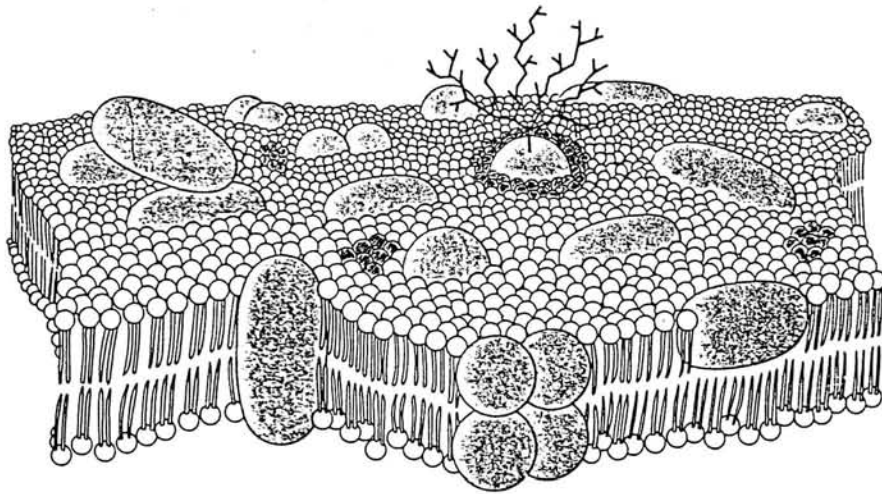
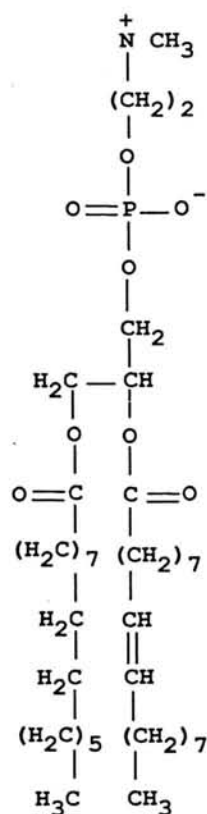


Figure 1.2: A general model for the structure of biological membranes based on the classic fluid mosaic model. The membrane proteins can be seen in the picture as boats floating in the sea of lipids.

glycerol moiety. This lipid contains two alkyl chains attached at sn-1 and sn-2 positions, one is of 16 carbon atoms length with no double bonds (Palmitoyl) and the other is of 18 carbon atoms length with one cis- double bond (Oleoyl) and a phosphatidyl choline attached at the sn-3 position of the glycerol. Phosphatidyl Choline does not have any net charge because of the positive charge on the choline and negative charge on the phosphate groups. Some of the lipids such as Phosphatidyl inositol, Phosphatidyl serine have a net negative charge.

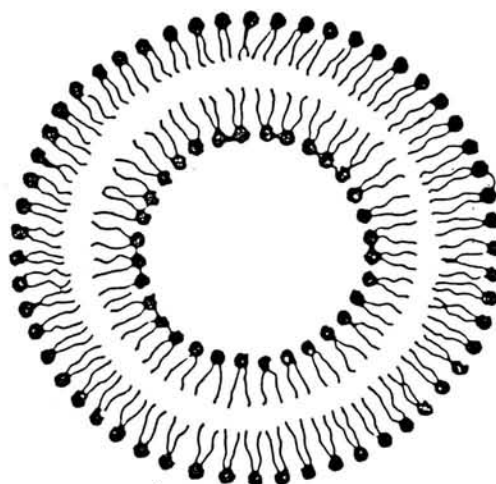
When the lipid is dissolved in water, the lipid molecules organize to form closed spherical structures known as lipid vesicles or liposomes. The interior and exterior of these spherical structures is water and the boundary which separates the two aqueous phases is the lipid bilayer. The typical structure of a lipid vesicle is shown in the figure 1.3. One can control the size of the lipid vesicles in a controlled manner using different methods of preparation [8, 9, 10].

The following basic facts have emerged as a result of several biophysical, biochemical and spectroscopic studies on the structure and dynamics of lipid bilayer membranes [1, 2, 11]. Phosphatidyl Cholines are the major lipids found in animal membranes. Most naturally occurring lipids are with even numbered acyl chains. Lipids with odd numbered acyl chains hardly ever exceeds 2%. The unsaturation in the acyl chain is of cis-type. The introduction of a cis-double bond in an all-trans chain yields a bent configuration [4] and reduces the interaction between the neighbouring linear chains. Approximately eleven water molecules bind tightly to a phospholipid molecule in a bilayer at the water/lipid interface. Water molecules penetrate into the bilayer to atleast the second carbon atom of the acyl chain. Based on the experiments on unmediated exchange of phospholipids between liposomes, it was observed that the residence time of a phospholipid in the lipid bilayer is more than three hours. The thickness of the bilayer measured by X-Ray diffraction is smaller than that calculated on the basis of fully extended alkyl chain and the polar group conformation, indicating the folding of the lipid chains in the core of the bilayer. Thickness of the bilayer increases with increasing chain length of the phospholipid. The thickness of the hydrocarbon region in the bilayer has been found

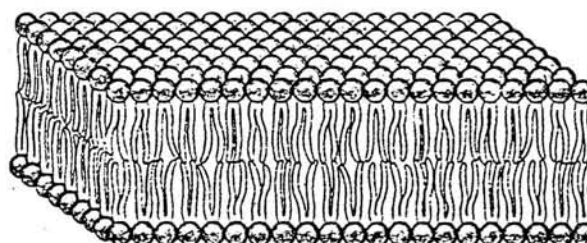


POPC

A



B



C

Figure 1.3: (A) Structure of a typical phospholipid molecule. The structure shown is that of 1-Palmitoyl, 2-Oleoyl Phosphatidyl Choline (POPC). (B) Lipid vesicle (or liposome) and (C) bilayer membrane formed by the aggregation of lipid molecules when dissolved in water. The hydrophilic headgroups of the lipids point towards water whereas the hydrophobic lipid chains form the interior of the bilayer excluding water.

to be 25, 33 and 38 Å for the bilayers made up of lipid chains (with one double bond) of alkyl chain length of 18, 22 and 24 carbon atoms, respectively [12]. Microviscosity of bilayer membranes measured from the tumbling rates of the fluorophores, decreases with increasing unsaturation, temperature and the presence of lipid soluble agents such as organic solvents, detergents and anesthetics. The dielectric constants of aqueous and lipid phases are 80 and 2, respectively. Many studies suggest that there is a gradient of fluidity that increases toward the centre of the bilayer and a gradient of polarity that decreases from about the second methylene residue toward the centre of the bilayer [13, 14]. Free volumes in the lipid bilayer are created by gauche-trans-gauche (also known as 2gl-type) kinks in the lipid chain. Small molecules enter these free volumes created by such kinks [15]. In natural membranes which is a mixture of several lipids, domains of different lipids were observed [16, 17].

The lipid bilayers undergo a phase transition with the increase of temperature. The temperature at which the bilayer undergoes a phase transition is known as the phase transition temperature and it is characteristic of the lipid. The bilayer phase below the transition temperature is called the gel phase whereas the one above the phase transition is termed as the liquid crystalline phase [1]. These temperature dependent phase transitions are particularly sharp in the case of bilayers prepared from pure (single molecular species) phospholipids. In biological membranes which is a mixture of several lipids, the gel and liquid crystalline phases exist over a broad temperature range. In Dimyristoyl PC (of 14 carbon atoms length), the peak width is $\approx 0.2^\circ\text{C}$ for 10% to 90% conversion. For most lipids, the width of the transition is 0.8 to 1.5°C . The transition temperature increases with the increase of chain length and decreases with the increase of unsaturation and also depends upon the nature of the polar head group. For example, the phase transition temperatures of the PC lipids with the alkyl chain length as 12, 14 and 16 carbon atoms falls at -2°C , 24°C and 41°C , respectively [18, 1, 19]. The phase transition temperatures of the same lipids with unsaturation in the lipid chain are below 0°C . With the phase transition, the thickness of the bilayer decreases and the area per lipid molecule increases. The lateral diffusion of lipid probes in the gel phase of the bilayer are of 100-fold lower than

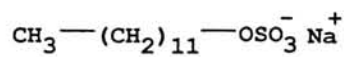
those in the case of liquid crystalline phases. Above the phase transition temperature, the number of 2gl kinks in the bilayer increases. At the phase transition temperature, the lipid bilayer is very fragile and the transport of small molecules and ions through the bilayer is maximum at the midpoint of the phase transition.

1.1.2 Micelles

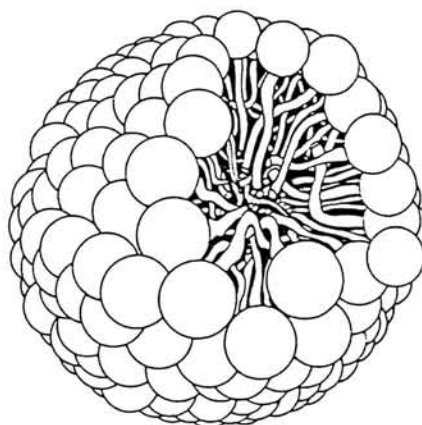
Micelles are the model systems for lipid bilayer membranes. Micelles made up of bile salts are found to be involved in the digestion systems [20, 21, 22, 23]. Micelles are formed by the aggregation of surfactant molecules. Like lipid molecules, surfactant molecules are also amphiphilic. These contain a hydrophilic head group and one long hydrophobic tail of long alkyl chain. When these molecules are dissolved in water, these form small spherical particles with the hydrocarbon tails constituting the core that is completely hydrophobic and the polar head groups pointing towards water. Figure 1.4 shows a typical surfactant Sodium dodecyl sulfate (SDS) and the structure of the micelle formed by the aggregation of these surfactant molecules. SDS is an anionic micelle and there are other surfactants that are cationic (e.g., Cetyl Trimethyl ammonium bromide (CTAB)) and neutral (e.g., Triton X-100). The micelles are of smaller in size than that of lipid vesicles and typical radii are in the range of 15-30Å.

Lipid molecules form spherical vesicles with the interior and exterior of the vesicle as the water separated by the bilayer whereas the surfactants form a closed spherical particles with the hydrocarbon interior. The reason for this being that lipid molecules contain two hydrophobic tails whereas the surfactants contain only one hydrophobic chain. So the basic shape of a lipid molecules is like a cylinder whereas the shape of a surfactant is like a cone. Cylinders cannot be packed into a closed spherical structures whereas cones can be packed into spherical structures. Hence, surfactants form spherical micelles and the lipids form closed bilayers [24].

Micelles form model systems for bilayer membranes because of their structural similarity with the bilayers having hydrophobic interior and polar head groups pointing towards

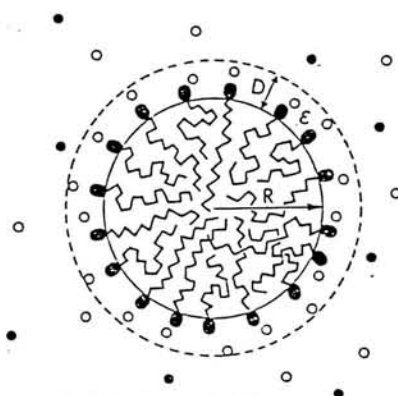


SDS



A

B



C

Figure 1.4: (A) Structure of Sodium Dodecyl Sulfate (SDS), (B) the structure of the micelle formed by the aggregation of surfactant molecules, and (C) a two dimensional crosssection of the micelle indicating the chain folding at the core of the micelle.

the aqueous phase. The shape and size of micelles depend on the nature and length of the hydrocarbon chain, the head group, surfactant concentration, solvent medium, additives and many other factors [25, 11, 26, 27]. Surfactants form micelles with fixed aggregation number only after the concentration of surfactant exceeds a particular concentration known as Critical Micelle Concentration (CMC). The concentration of monomer at and above CMC remains constant, that is less than the CMC value. CMC and the aggregation number are characteristics of a particular surfactant. For the case of SDS, CMC is about 8mM at room temperature [25] and the aggregation number is 60 ± 6 , i.e., approximately 60 surfactant molecules aggregate to form a single micelle [28, 29, 25]. Micellar core is fluid-like, but less fluid than a comparable hydrocarbon solvent of the same chain length [30, 31]. There are 10-12 water molecules bound per one surfactant molecule. Water molecules penetrate the micellar surface upto a distance of approximately six carbon atoms [30]. Addition of electrolytes to ionic micelles results in an increased micellar size and in some cases, worm-like micelles are formed with significant increase in the aggregation number [32, 33]. Worm-like micelles are known to form also at high surfactant concentrations or at reduced levels of aqueous phase [25, 28]. Organic molecules are easily solubilized in the micelles.

1.1.3 Proteins

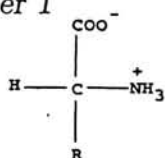
Proteins play major roles in biology in several ways such as enzyme catalysts in the biochemical reactions, aiding in the transport of molecules, in the generation and transmission of signals and in controlling the growth and differentiation [6, 5, 34, 35]. Proteins are polypeptides which are the covalent polymers formed by the peptide bonds between amino acids. Figure 1.5 shows the typical structure of an amino acid, the structure of two fluorescent amino acids: tryptophan and tyrosine, and the three dimensional structure of a protein Barstar that contains 89 amino acids [36]. Most of the amino acids are chiral in nature(L-type, except glycine). These are zwitter ionic having both acid and base properties. These amino acids may be charged or uncharged; polar or nonpolar; or,

hydrophilic or hydrophobic. Due to the interaction between the individual amino acid side chains and with water, the polypeptide chain assumes a unique structure that is responsible for the stability and function of that protein. Different types of structures that a folded polypeptide chain can assume include structures like α -helix, β -sheet etc. These secondary structures are folded into an array of tertiary structures that constitute the final three dimensional structure of the protein. Some of the proteins contain disulfide bridges that stabilize the compact structure of the protein. In addition to the amino acids, some proteins contain metal centers such as metallo porphyrins and iron sulphur clusters. The proteins containing metallo centers such as cytochrome and hemoglobin are particularly involved in the processes of electron transfer, energy conversion and as oxygen carriers.

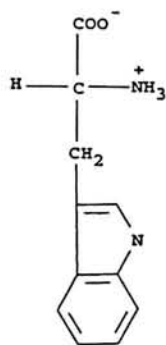
Most proteins are either of fibrous or globular type. Fibrous proteins usually serve structural roles whereas globular proteins function as enzymes and in many other capacities. Water soluble proteins fold into compact structures with the nonpolar amino acids at the core and the polar residues exposed to the water. In the case of proteins that exist in natural membranes, the location of the amino acids on the polypeptide chain depends on the location of this protein in the membrane. There are examples where a protein takes different structural forms when present in the aqueous phase and when it is inserted into membranes [37, 38, 39]. The difference comes because the structure assumed by a protein depends on its interaction with the surrounding medium. Proteins recognize and bind to small molecules and they are highly proficient at forming complementary surfaces and clefts necessary for the binding. The catalytic power of proteins comes from their capacity to bind substrate molecules in precise orientations and to stabilize the transition states in the making and breaking of chemical bonds.

1.1.4 Small molecules in biology

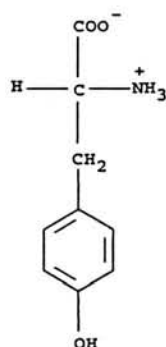
Small molecules play different roles in the biological world. Among all the molecules in a living cell, half of them are small molecules. Ion transporters across the membrane, receptors and other signal transmitting molecules, drug molecules, hormones, antibodies



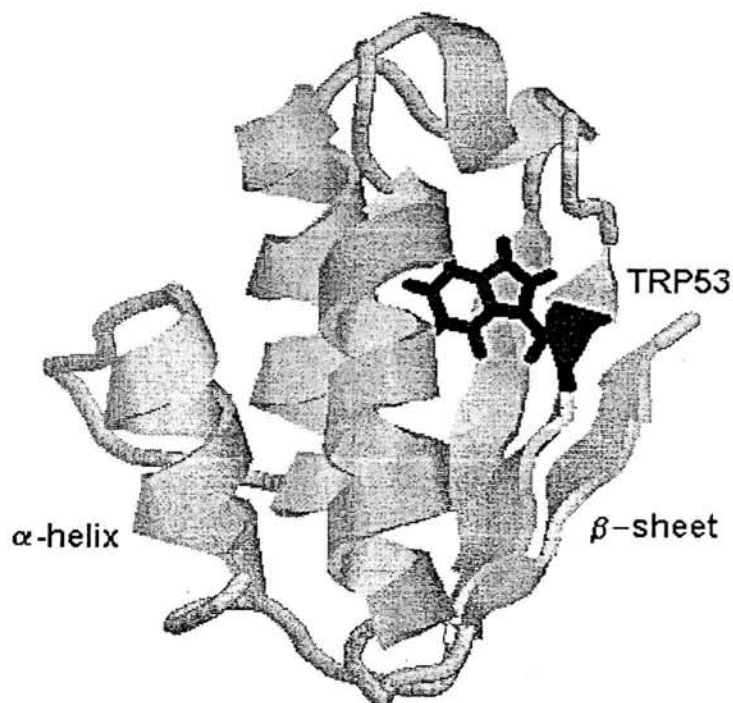
Amino acid



Tryptophan



Tyrosine



A

B

Figure 1.5: (A) Structure of an amino acid. R denotes the side chain which varies with the amino acid. This structure is true in the case of nineteen essential amino acids except proline which contains a cyclised side chain attached to the α carbon atom. The figure also shows the two amino acids, tryptophan and tyrosine whose fluorescence is commonly explored in literature in probing the protein structure and function. (B) Structure of a protein, Barstar, that is made up of peptide bonds between 89 amino acids [36]. The different structural elements formed such as α -helix and β -sheet because of the hydrophobic interactions can be seen in the structure. The figure also shows the tryptophan at 53rd position (W53) along the amino acid sequence, that is buried in the protein matrix whose fluorescence is used for the studies carried out in Chapter 4.

and vitamins are some of the examples of the roles played by the small molecules. The use of spin labels [40, 41], voltage sensitive dyes [42, 43, 44, 45] and fluorescent probes [46, 47, 48] are some of the well known examples of the use of small molecules in the study of biological systems.

To understand the mechanisms involved in the different processes carried out by the small molecules, one needs to know the location, orientation and dynamics of these small molecules in biological systems. This thesis deals with such aspects mainly in the case of one biological system, i.e., bilayer membranes.

Among the many spectroscopic techniques available for the study of structural dynamics of biological systems, X-Ray, Nuclear Magnetic Resonance (NMR), Electron Spin (or paramagnetic) Resonance (ESR or EPR) and fluorescence techniques are of wide use. Electron microscopy, Atomic Force Microscopy (AFM), Differential Scanning Calorimetry (DSC) are also some of the widely used techniques. X-Ray and NMR techniques are mainly used for the elucidation of the structure of the biological systems. Dynamics of biological systems is studied mainly by the NMR, ESR and fluorescence techniques. X-Ray uses the diffraction patterns from the samples to obtain the structural information about the system under study. NMR uses the chemical shifts of the paramagnetic nuclei and the relaxation measurements (spin-spin and spin-lattice) for the study of biological systems. ESR techniques require a free radical to detect the electron paramagnetic signal and hence these techniques use spin labels, mainly nitroxide spin labels such as TEMPO (2,2,6,6-Tetramethylpiperidine-N-oxyl), DOXYL (4,4-Dimethyloxazolidine-N-oxyl), for this purpose. Fluorescence techniques make use of the fluorescent probes in the study of biological systems.

Two aspects have to be noted in all these techniques: concentration limits and time scales. NMR requires millimolar concentrations. In the study of interaction of small molecules with bilayer membranes, one needs to maintain a high probe to lipid ratio (minimum of 1:25) in order to observe the probe signals, such a high ratio may disturb the bilayer structure to a large extent. In some cases, spectra of the probe and lipid may overlap significantly making the assignment of the probe resonances difficult. To

avoid these two problems, the use of deuterated lipids was suggested which is a costly affair. The timescales of the dynamic processes that can be studied by NMR is down to milliseconds. In ESR, one uses the spin labels to study the structure and dynamics of biological systems. This requires concentrations of few hundred micromoles per liter and can probe the dynamics down to the time scales of microseconds. In fluorescence spectroscopy, the concentration of the fluorescent probes used for the study of biological systems is extremely low. The time scale can be as low as femtoseconds.

Most of the elementary chemical and biological processes such as molecular collisions, molecular motions, solvent relaxation, rotational and translational diffusion, proton and electron transfer reactions, energy transfer, photosynthesis, photochemical isomerization, cage recombination, internal motions within a complex biological system, host-guest dynamics, dynamics of small molecules in biological systems occur in the time scales of femtoseconds to microseconds. Hence, fluorescence spectroscopy is the best technique available to probe these different processes. It is the most widely used technique in the study of dynamics of biological systems.

The structure and dynamics of the biological membranes (lipid bilayer membranes) and the way the lipid molecules control the dynamics of small molecules inside a bilayer membranes has been the subject of many studies. These studies have used several spectroscopic techniques [49] such as Fluorescence spectroscopy [50, 51, 52, 53, 54, 46], NMR spectroscopy [55, 56, 57, 58, 59, 60], X-Ray techniques [61, 62, 63], ESR spectroscopy using spin labels [40, 41, 64], calorimetric studies [65], electron microscopy [1, 62], Neutron Scattering [66], Infrared Spectroscopy [67], Raman spectroscopy [68], Atomic Force Microscopy (AFM) [69, 70], and the recent Single Particle Tracking (SPT) techniques [71].

In spite of this multi-faceted research on the dynamics of biological membranes, there still remain unanswered questions concerning the location, orientation and dynamics of small molecules in these lipid bilayer membranes. Some of these questions are: Where are these small molecules located in the membrane? Are there any specific sites in the membrane or is it a continuous distribution of sites? How are these molecules oriented in

the membrane? How do the lipid chains affect the site of solubilization and orientation of small molecules? What are the effects of aqueous phase properties such as viscosity and refractive index on the properties of molecules bound to the membranes? How is the dynamics of small molecules in biological systems different from those in homogeneous solutions? This thesis addresses these questions in the context of biological membranes using the methodologies of fluorescence spectroscopy.

1.2 Fluorescence Spectroscopy

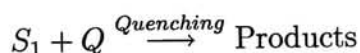
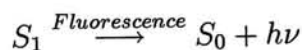
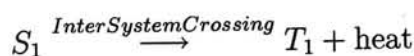
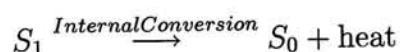
Fluorescence spectroscopy is the most widely used technique for the study of dynamics of biological systems. Fluorescence spectroscopists have studied the biological fluorescence down to the time scales of femtoseconds [72, 73, 74] and down to the concentration and space limits of single molecules [75, 76, 77, 78]. In fluorescence techniques, the photon emitted by the fluorescent probes is like a torch shining light on the biological environment. The fluorescence emitted by a chromophore is very sensitive to the physical properties of its environment. The biological fluorescent probes are of two types: intrinsic and extrinsic. Aromatic amino acids such as tryptophan and tyrosine are examples of intrinsic fluorescent probes (structures shown in the figure 1.5) in proteins whereas organic fluorescent dyes are the commonly used extrinsic probes in the study of biological systems (some of the extrinsic probes are shown in the figure 4.6). In the case of proteins, extrinsic fluorescent probes such as iodoacetamide probes (e.g., IAEDANS (5-(2-((iodoacetyl)amino)ethyl)amino-naphthlene-1-sulfonic acid), IAF (5-iodoacetamidofluorescein)) [79, 80, 81], are linked covalently to one of the side chains of the amino acids to probe the structural dynamics of the protein or its environment [82, 83, 48]. The main assumption made in the use of extrinsic probes is that the properties of the system under study are not perturbed with the incorporation of the extraneous dye which is valid in most cases. In some cases, when the small molecule of interest is not fluorescent, the appropriate fluorescent analogs were used to take advantage of the sensitivity of fluorescence techniques. For example, the ATP fluorescent analog TNP-ATP

(2'-(or-3')-O-(trinitrophenyl)-adenosine-5'-triphosphate) is generally used to monitor the structural dynamics of ATP binding proteins [81, 84, 85].

Dynamics of fluorescent probes in biological systems differ considerably from that in a homogeneous solvent. In a homogeneous liquid, dynamics of the fluorescent probe is not hindered, i.e., the probe can rotate in all directions. In the case of a biological system which is microheterogeneous, the probe finds itself in a pocket of restricted environment resulting in the hindered dynamics that does not allow the fluorescent probe to rotate/orient in all random directions.

The three useful properties of fluorescence are fluorescence spectrum, intensity and polarization. These fluorescence properties tell us about the nature of the probe environment and changes in it that provides information regarding the system. The time dependence of the above properties adds a new dimension to the fluorescence spectroscopy and tells us about the dynamics of the fluorescent probe and its environment. The information that can be extracted from different steady state and time resolved fluorescence experiments can be described as follows [46, 47].

The general processes of light absorption and emission and other excited state processes in the case of a chromophore are represented in a Jablonski diagram of molecular energy levels as shown in the figure 1.6 [86, 87]. The deactivation of an excited fluorophore can happen in multiple ways such as



In the above equations, the last one represents the quenching reaction of the excited fluorophore by a quencher Q. k_{IC} , k_{ISC} , k_r and k_q represent the rate constants for internal conversion, intersystem crossing, fluorescence and quenching, respectively.

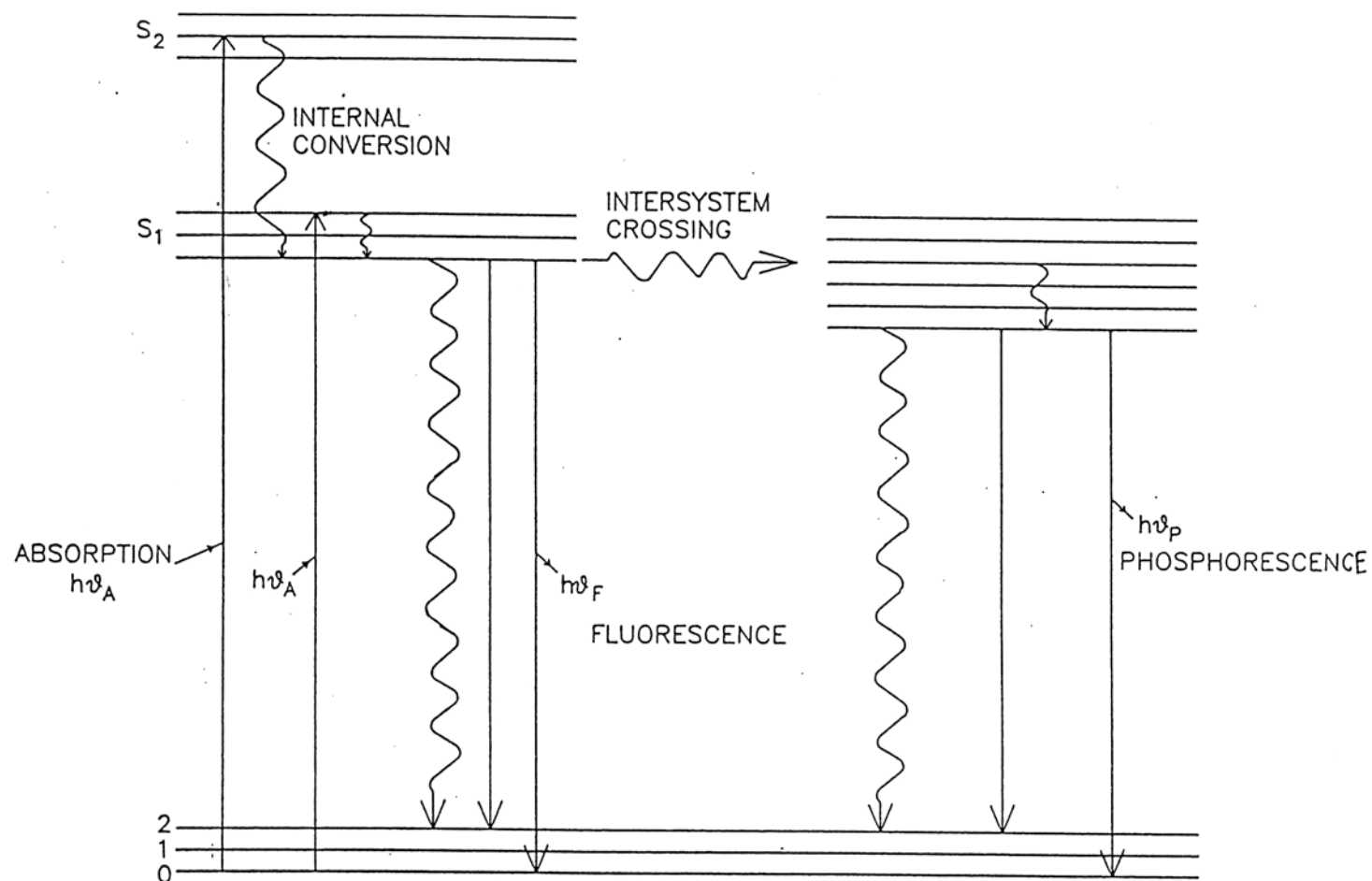


Figure 1.6: Jablonski diagram showing the excitation of the ground state fluorophore and different deactivation processes of the excited fluorophore

Some of the important parameters that can be obtained from the fluorescence spectroscopic studies which are useful for understanding the dynamics of biological systems are described as follows.

1.2.1 Fluorescence Spectra

Fluorescence spectra and changes in it give information about the interaction of the chromophore with the surrounding medium. Fluorescence spectra are characteristic of the energy levels involved in the transitions and the excited state relaxation of the fluorescent probe. A large spectral width compared to absorption spectral width generally implies multiple species in the excited state. Fluorescence spectra can be recorded as emission and excitation spectra. Emission spectrum is recorded by exciting the sample at a fixed wavelength and scanning the fluorescence over a range of emission wavelengths. Excitation spectrum is recorded by observing the fluorescence at a fixed emission wavelength and scanning the excitation wavelengths. The emission spectra reflect characteristics of the excited state whereas the excitation spectra represent those of the ground state. Multiple peaks appearing in the fluorescence emission spectrum can be from different vibrational levels or they can be from multiple species. If the origin of multiple peaks is due to the presence of multiple species, then the excitation spectra corresponding to each emission maximum should be different. The fluorophore heterogeneity in a given system can be determined by recording emission and excitation spectra at different wavelengths. The fluorescence emission spectra recorded at different excitation wavelengths should be identical if the system contains a single fluorophore in a single environment. The same is true with the excitation spectra recorded at different emission wavelengths. Non-overlap of the spectra recorded at different wavelengths indicates multiple fluorescent species in the system.

The emission maximum does not occur at the same wavelength as that of absorption maximum and occurs at a red shifted wavelength. The difference between the absorption and emission maxima is known as Stokes' shift. The origin for a non-zero Stokes' shift can

be the difference in the excited state and ground state geometries, or solvent relaxation or some chemical mechanisms. The fluorophore is initially excited to one of the highest vibrational levels of S_1 state that has the maximum Franck-Condon factor or, in other words, whose geometry is very close to that of the ground state. It relaxes to the lowest vibrational state of S_1 and the fluorescence is observed from this state. Solvent plays a major role in altering the energy levels involved in these transitions. Solvent dependent Stokes' shift is interpreted using Lippert-Mataga equation which relates it to the change in the dipole moment and the solvent properties, refractive index and dielectric constant of the solvent [87, 46]. Very large Stokes' shift may indicate a chemical mechanism resulting in the formation of a new fluorescent molecule and the emission is observed from this new product.

The shift in the fluorescence spectral maximum of a fluorophore with solvent is useful to characterize its environment in complex systems. For example, in the case of tryptophan in proteins, the emission maximum varies from 320nm to 360nm depending on the hydrophobicity of the environment of tryptophan. For the buried tryptophans, the maximum occurs at around 320nm whereas it shifts to 360nm in the case of exposed tryptophans [46]. Similarly, the emission maxima of extrinsic fluorescent probes such as Nile red and PRODAN (6-propionyl-2-(dimethylamino)-naphthalene) are used to estimate the polarity of the environment [46, 88, 89, 90, 91].

1.2.2 Fluorescence Intensity and Quantum yield

Fluorescence intensity measures the flux of photons or number of photons emitted by the excited fluorophore. Fluorescence quantum yield, ϕ , is a measure of the probability that an excited fluorophore decays radiatively by the emission of a photon. If I_a and I_f represent the absorbed and fluorescence intensities in absolute units (photons/sec) of the sample, then

$$\phi = \frac{I_f}{I_a} \quad (1.1)$$

Fluorescence quantum yield is related to the radiative and nonradiative rates of the

fluorophore by the equation

$$\begin{aligned}\phi &= \frac{k_r}{k_r + k_{nr}} \\ &= \frac{k_r}{k_r + k_{IC} + k_{ISC} + k_q[Q]}\end{aligned}\quad (1.2)$$

where k_r and k_{nr} represent the radiative and nonradiative rates of the fluorophore.

The two processes that determine the fluorescence intensity and quantum yield are themselves sensitive to the probe environment. Optical properties of the probe environment affects the radiative property. Refractive index of the environment and the relative geometry are the important parameters. Nonradiative processes are mainly controlled by the viscosity of the medium if the main origin of these deactivation processes is through the collisional mechanism. In addition to these changes in the parameters, the intensity will also be affected by the variation in the location of the fluorophore due to change in structural organization/conformation in the biological system. Sometimes, the fluorescence of the fluorophore may get quenched because of these structural changes.

1.2.3 Fluorescence Intensity Decay and Lifetime

Fluorescence decay measures the excited state kinetics of the fluorophore. Here the sample is excited with a pulse of light and the fluorescence intensity is recorded as a function of time. The fluorescence lifetime represents the average time for which the fluorophore spends in the excited state and is given by the equation

$$\begin{aligned}\tau &= \frac{1}{k_r + k_{nr}} \\ &= \frac{1}{k_r + k_{IC} + k_{ISC} + k_q[Q]}\end{aligned}\quad (1.3)$$

As discussed before, the radiative rate k_r depends upon the optical environment of the probe. In homogeneous solvents, it is proportional to the square of the refractive index and in biological systems, the exact functional form depends upon the anisotropy of the probe environment. This is more elaborated in Chapter 4. The nonradiative rate depends upon the viscosity of the probe environment and decreases with the increase of viscosity thus increasing the lifetime.

If the sample contains only one fluorophore, then the fluorescence decay is ideally a single exponential as

$$I(t) = I_0 \exp(-t/\tau) \quad (1.4)$$

When the system under study contains multiple fluorescent species, then the intensity decay becomes multiexponential with the number of exponentials equal to the number of species present in the system. In this case, the intensity decay equation becomes

$$I(t) = \sum_i \alpha_i \exp(-t/\tau_i) \quad (1.5)$$

where τ_i and α_i represent the i th lifetime and the corresponding preexponential factor in the multiexponential intensity decay. Here the average lifetime is defined as the area under the fluorescent intensity decay curve that is proportional to the quantum yield as

$$\tau_{ave} = \frac{\sum_i \alpha_i \tau_i}{\sum_i \alpha_i} \quad (1.6)$$

The changes in the fluorescence lifetimes and preexponential factors with the changes in the physical parameters of the system can be used to gain information about the dynamics of the system under study. These changes can be explained by the changes in the probe environment such as viscosity, polarity, quenchers near the fluorophore, conformational changes in the biological system affecting the local environment etc. These changes can be used to decipher the quenching mechanisms in complex biological systems or can be used to measure distances in a biological system as will be described in the subsequent sections.

1.2.4 Fluorescence Anisotropy

The excitation probability of a fluorescent probe when shined with light depends on the square of the cosine of the angle made by the molecular dipole with the polarization axis of the excitation light. Hence, the initially created probe population in the excited state is orientationally anisotropic when the sample is excited with a polarized light. Fluorescence anisotropy measures the relaxation of this anisotropic probe population to the equilib-

rium population. Hence, the anisotropy decay characterizes the different mechanisms contributing to this depolarization process.

Experimentally, the fluorescence anisotropy is measured by measuring the intensities along the parallel and perpendicular orientations of the emission polarizer in the right angle geometry with the excitation polarizer oriented in the vertical direction. If I_{\parallel} and I_{\perp} represent these two intensities, then fluorescence anisotropy is calculated using the equation

$$r = \frac{I_{\parallel} - I_{\perp}}{I_{\parallel} + 2I_{\perp}} \quad (1.7)$$

The steady state anisotropy measures the average depolarization during the lifetime of the excited fluorophore whereas the time resolved anisotropy measures the time course of this depolarization.

In the case of time resolved measurements, when the sample is excited with a pulsed light, the two polarized decays $I_{\parallel}(t)$ and $I_{\perp}(t)$ are related to the total intensity decay $I(t)$ and the fluorescence anisotropy decay $r(t)$ according to the equations

$$\begin{aligned} I_{\parallel}(t) &= \frac{1}{3}I(t)[1 + 2r(t)] \\ I_{\perp}(t) &= \frac{1}{3}I(t)[1 - r(t)] \end{aligned} \quad (1.8)$$

Hence these two polarized decays can be used to compute $r(t)$ according to the equation 1.7 and $I(t)$ as

$$I(t) = I_{\parallel}(t) + 2I_{\perp}(t) \quad (1.9)$$

Note that the final expression for $r(t)$ does not contain the total intensity decay term $I(t)$. Hence fluorescence anisotropy decay and total intensity decay are two independent measurements that can be used to obtain the information about the system.

The initially created anisotropy at zero time $r(0)$ or r_0 depends upon the excitation and emission wavelengths. The corresponding relation is given by

$$r(0) = \frac{2}{5} \frac{(3\cos^2\delta - 1)}{2} \quad (1.10)$$

where δ is the angle between the excitation and emission dipoles. Hence the value of $r(0)$ can vary between 0.4 to -0.2 depending on the excitation and emission wavelengths.

The anisotropy decay parameters depend on the size and shape of the fluorophore and the environment of the fluorophore in the system [92]. In homogeneous solvents, as the rotational motion of the solute is unhindered, the fluorescence anisotropy decays to zero. In the case of spherical solutes, this decay is single exponential

$$r(t) = r(0)\exp(-t/\phi) \quad (1.11)$$

where ϕ is the rotational correlation time. This rotational correlation time is related to the molecular volume V and the viscosity of the liquid η by the Stokes-Einstein relation

$$\phi = \frac{\eta V}{kT} \quad (1.12)$$

where k is the Boltzmann constant and T is the temperature of the sample. This relation (sometimes using $V' = fV$ where f is a correction factor for nonspherical solutes) has been explored in literature to determine the microviscosities of the probe environment in biological systems by measuring the rotational correlation times. When the fluorophore is an ellipsoidal (prolate or oblate) solute, the fluorescence decay becomes double exponential. In theory, the fluorescence anisotropy of any fluorophore of any shape can never exceed five exponentials [93, 94, 92].

When the fluorophore is in a biological system such as a lipid membrane or a protein, the fluorophore is in a restricted environment that does not allow the probe to rotate/orient in all random directions. Therefore the fluorescence anisotropy does not decay to zero with time resulting in a finite residual anisotropy (or non-zero anisotropy at infinite time, r_∞). In general, the fluorescence anisotropy decay of a fluorophore can be fitted to a multiexponential function with the residual anisotropy part as

$$r(t) = (r_0 - r_\infty)\sum_i \beta_i \exp(-t/\phi_i) + r_\infty \quad (1.13)$$

where ϕ_i and β_i represent the correlation times and the respective amplitudes. Many models such as wobbling-in-a-cone model, asymmetric rotation, chromophores rotating between many barriers were proposed in literature to account for this complex anisotropy decay in microheterogeneous systems [95, 96, 50, 97, 98, 99, 100, 53, 101].

The two limiting values of the fluorescence anisotropy, r_0 and r_∞ can be used to calculate the model-independent order parameter S that describes the order of the probe environment and is given by [102, 103]

$$S = \sqrt{\frac{r_\infty}{r_0}} \quad (1.14)$$

When the probe rotates freely, then the order parameter becomes zero. In the other case, when the probe molecule is fixed, i.e., without any rotational freedom, the order parameter is one. For biological systems, the order parameter varies between these two extremes, indicating the order of the probe environment.

When a probe molecule is attached to a macroparticle, the dynamics of the macroparticle also gets reflected in the anisotropy decay of the probe. If the size of the macroparticle is small in size, then the rotational diffusion of the macroparticle also contributes to the depolarization of the anisotropy. This is particularly true in the case of micelles and proteins of small size whose rotational correlation time falls in the range of the excited state lifetimes of fluorescent probes. In the case of lipid vesicles, the rotational diffusion is of the order of microseconds and hence it does not contribute to the anisotropy decay. In addition to this parameter, the surface diffusion of the fluorescent probes on the surface of the macroparticle also contributes to the fluorescence decay [104, 105].

1.2.5 Time Resolved Emission Spectra and Decay Associated Spectra

Time Resolved Emission Spectra (TRES) and Decay Associated Spectra (DAS) are two important methods to characterize the excited state dynamics. These two use the multiple fluorescence decays collected at varying emission wavelengths.

TRES measures the variation of the fluorescence spectrum with time. These spectra were constructed using the multiple fluorescence decays collected at different emission wavelengths [106, 107]. Each fluorescence decay was fitted to a sum of exponentials to deconvolute the instrument response from the experimentally measured decay data.

Generally, three exponentials are enough to fit the experimental data. The purpose of these fits is simply to represent the decay curves and no physical meaning is attributed to the obtained lifetimes and amplitudes. TRES is constructed using the results of these fits and the steady state emission spectrum using the following equation. The emission intensity at the wavelength λ at time $t = t'$ is

$$I_{\lambda}(t') = \frac{I_{SS,\lambda}}{\tau_{ave,\lambda}} \sum_{i=1}^N \alpha_{i,\lambda} \exp(-t'/\tau_{i,\lambda}) \quad (1.15)$$

where $\alpha_{i,\lambda}$ and $\tau_{i,\lambda}$ are the amplitudes and lifetimes in the Nth exponential fluorescence decay at λ such that $\sum \alpha_{i,\lambda} = 1$. $\tau_{ave,\lambda}$ is the average lifetime and $I_{SS,\lambda}$ is the steady state fluorescence intensity at the emission wavelength λ . These spectra, constructed at different times after the sample is excited, represent the variation of the fluorescence emission spectrum with time.

These TRES are generally fitted to a log-normal line shape function [108] to obtain a smooth spectrum according to the equation 1.16

$$g(\nu) = \begin{cases} g_0 \exp \left[-\ln(2) \left(\frac{\ln[1+\alpha]^2}{b} \right) \right] & \text{for } \alpha > 1 \\ 0 & \text{for } \alpha \leq 1 \end{cases} \quad (1.16)$$

where

$$\alpha = \frac{2b(\nu - \nu_p)}{\Delta} \quad (1.17)$$

Here g_0 , ν_p and b represent the peak height, peak frequency and asymmetry factor, respectively. The full width at half maximum (FWHM), Γ is calculated using the value of the optimized parameters Δ and b with the relation

$$\Gamma = \Delta \left(\frac{\sinh(b)}{b} \right) \quad (1.18)$$

Time Resolved Emission Spectra provide information regarding the dynamic processes in the excited state occurring on the same time scale as that of the lifetime of the fluorophore. TRES has been used in resolving the excited state kinetics such as dynamic solvent relaxation or a slow interconversion between multiple species where the spectrum of the sample continuously changes with time in the excited state [46, 109, 110, 111, 112].

When the sample exhibiting TRES shows two or three lifetimes that are constant over the emission range, then the method of DAS can be used to resolve the spectra of these components using appropriate model.

Decay Associated Spectra (DAS) is a commonly used technique to resolve the multiple fluorescent components in a complex multicomponent system [113, 46]. These multiple components can be either from multiple fluorophores or the same fluorophore in different environments. This method takes advantage of the difference between the fluorescence properties of different fluorescent components. This method resolves the spectra of the different species using the fluorescence decays collected at varying values of some parameters.

The method of DAS is described as follows. Let the system contain N fluorescence components, each with a characteristic fluorescence lifetime τ_i . The spectra of each species can be obtained by resolving the steady state spectrum into the spectra of the individual components using the amplitudes of the lifetimes obtained at multiple emission wavelengths as

$$I_{\lambda,i} = I_{\lambda} \frac{\alpha_{\lambda,i} \tau_i}{\sum_j \alpha_{\lambda,j} \tau_j} \quad (1.19)$$

Here $\alpha_{\lambda,i}$ represent the emission wavelength dependent amplitudes for the lifetime τ_i . I_{λ} and $I_{\lambda,i}$ represent the steady state intensity and intensity corresponding to the i th component at the wavelength λ . The amplitudes of the N lifetimes can be obtained from the global analysis of the fluorescence decays of the system collected at multiple emission wavelengths.

The above case illustrates the method of DAS resolved by taking advantage of the difference in the lifetimes for multiple species. There are examples in literature where DAS was used to resolve the spectra of the species based on the differences in the rates of fluorescence quenching (QDAS, [114, 115]) and differences in the anisotropy of the fluorophores (ADAS, [116, 117]). In this thesis, a new method of DAS was developed that takes advantage of the known spectrum of one of the component in resolving the spectra of the other components in a multicomponent system (Chapter 3).

1.2.6 Fluorescence Quenching

The quenching of the probe fluorescence by the quenchers can be used to obtain information about the biological system under study [118, 46]. The fluorescence quenching is of two types: dynamic and static. Dynamic quenching occurs through the collisions between the excited fluorophore and the quencher during the lifetime of the fluorophore. Static quenching occurs through the formation of a ground state complex between the fluorophore and the quencher. The changes in the steady state intensity with the addition of the quencher can be used to obtain the quenching constant using the Stern-Volmer equation

$$\frac{I_0}{I} = 1 + K_{SV}[Q] \quad (1.20)$$

where I_0 and I are the steady state intensities in the absence of the quencher and at the quencher concentration $[Q]$ and K_{SV} is the Stern-Volmer constant. The above equation is linear for purely dynamic or purely static quenching mechanisms. In the case of the pure dynamic quenching mechanism, the Stern-Volmer constant is equal to $k_q\tau_0$, where k_q is the dynamic quenching rate constant and τ_0 is the fluorescence lifetime in the absence of the quencher. In the case of static quenching mechanism, K_{SV} becomes K_s , the association constant for the quencher with the fluorophore. The above equation can be used to calculate the quenching rate constant k_q or the association constant K_s depending on the quenching mechanism. The clear distinction between these two mechanisms can be made from time resolved measurements. The dynamic quenching mechanism is reflected in the changes in the lifetimes, whereas the static quenching mechanism does not change the lifetimes. In the case of dynamic quenching mechanism, the lifetimes follow the above equation with K_{SV} replaced by $k_q\tau_0$, that is

$$\frac{\tau_0}{\tau} = 1 + k_q\tau_0[Q] \quad (1.21)$$

where τ is the fluorescence lifetime at the quencher concentration $[Q]$. When the collision dependent quenching mechanism approaches the diffusion controlled reaction (k_q close to the diffusion limited rate), then the fluorescence intensity decay will deviate from the exponential behaviour and in this case, the fluorescence decay contains $\exp(-t^{\frac{1}{2}})$ term

in addition to $\exp(-t)$ term [119, 120, 121, 122, 123]. The use of quenchers with varying properties can give information about the probe environment, for example, ionic quenchers tells about the charge effects near the fluorophore in a biological system. When the system contains multiple fluorophores such as multiple tryptophans in a protein, then the Stern-Volmer equation for the change of steady state fluorescence intensity with the addition of quencher is the product of the Stern-Volmer equations for individual fluorophores.

Fluorescence quenching methods have been used to obtain information about the accessibility of fluorophores to quenchers, to study the ligand binding reactions and conformational changes, protein folding mechanisms, to model the diffusion processes on the surface of membranes, in determining the location of fluorophores in the membrane with quenchers attached to the lipid chains at different positions and to study the membrane transport. [118, 124, 125, 126, 127, 128, 129, 130, 131].

1.2.7 Fluorescence Resonance Energy Transfer

The technique of Fluorescence Resonance Energy Transfer (FRET) is considered as a biological ruler to measure distances between a pair of fluorophores in a complex biological system and hence to obtain structural and dynamical information about the system [132, 133, 134, 46, 135]. The fluorescence energy transfer occurs between a donor and an acceptor because of the long range dipole-dipole interactions. The rate of energy transfer depends upon the extent of overlap of the emission spectrum of donor with the absorption spectrum of the acceptor, the relative orientation of the donor and acceptor transition dipoles, and the distance between these molecules.

The rate of energy transfer between a donor and an acceptor is given by

$$k_T = \frac{1}{\tau_d} \left(\frac{R_0}{R} \right)^6 \quad (1.22)$$

where τ_d is the lifetime of the donor in the absence of acceptor, R_0 is the Forster distance at which 50% of the excitation energy is transferred to the acceptor and R is the distance between the donor and the acceptor. The Forster critical distance R_0 is related to the

molecular parameters by the relation

$$R_0 = 9.78 \times 10^3 (\kappa^2 n^{-4} \phi_d J)^{\frac{1}{6}} \text{ (in } \text{\AA}) \quad (1.23)$$

where κ^2 is the factor describing the relative orientation of the transition dipoles of the donor and the acceptor, n is the refractive index of the medium, ϕ_d is the quantum yield of the donor in the absence of the acceptor and J is the normalized overlap integral that expresses the overlap between the donor emission and the acceptor absorption. The overlap integral is calculated using the relation

$$J = \frac{\int F_d(\lambda) \epsilon_a(\lambda) \lambda^4 d\lambda}{\int F_d(\lambda) d\lambda} \quad (1.24)$$

where $F_d(\lambda)$ is the fluorescence intensity of the donor in the absence of the acceptor at the wavelength λ and $\epsilon_a(\lambda)$ is the molar absorption coefficient of the acceptor at λ . $\kappa^2=2/3$ for randomly oriented donor acceptor pairs. The Forster distance R_0 is characteristic of a particular donor-acceptor pair in a specific medium (of refractive index n) for a particular orientation factor (κ^2). The experimentally measured quantity is the efficiency of the energy transfer, E , which is the ratio of photons transferred to the acceptor to that absorbed by the donor. This quantity is given by

$$E = \frac{k_T}{\tau_d^{-1} + k_T} = 1 - \frac{\tau_{da}}{\tau_d} = \frac{R_0^6}{R_0^6 + R^6} \quad (1.25)$$

where τ_{da} is the lifetime of the donor in the presence of the acceptor. Hence by knowing the value of the Forster distance R_0 , one can calculate R , the distance between a donor and an acceptor in unknown systems by measuring the energy transfer efficiency E . The lifetime ratio τ_{da}/τ_d in the above equation can be replaced by the steady state fluorescence intensity ratio F_{da}/F_d (or a quantum yield ratio) where F_{da} and F_d represent the fluorescence intensities of the donor in the presence and absence of the acceptor.

The accuracy of the distances determined by FRET depends on the accuracy of the calculation of R_0 that involves the measurement of κ , n , ϕ_d and the overlap integral J (equation 1.23). In the event of no information regarding the orientation of donor and acceptor dipoles, the orientation factor κ^2 is generally assumed to be $2/3$, which is the

value when the donor and acceptor are in random directions. This approach may not be correct in the case of biological systems where the donor and acceptor can not occupy all random orientations because of their restricted environments. To take care of this uncertainty factor, methods were proposed in literature that allow the determination of the values for κ^2 in a given biological system from the fluorescence anisotropy measurements that measures the rotational freedom of the donor and acceptor molecules [134, 136].

FRET has been successfully used in measuring distances in complex biological systems. When there are no intrinsic fluorescent probes in the system which is the case in most of the systems, a pair of donor and acceptor are attached covalently at the desired positions for this purpose. When the distance between the donor and acceptor is dynamic, that is, the distance varies during the lifetime of the donor, the observed fluorescence intensity decays with multiple lifetimes corresponding to the multiple distances between the donor and acceptor. The time resolved data was used to determine the distance distributions and these were used in deducing the dynamical information about the system under study [137, 134, 135]. FRET has been used in measuring the distances in biological systems such as proteins and membranes, and thus providing structural models for the biomolecules, in monitoring the self-association of proteins in membranes, in locating the functional sites in membrane proteins, in studying the interaction between different subunits in a multiunit system, in measuring enzyme kinetics, in monitoring the protein folding reactions and in studying the protein-nucleotide interactions [134, 135, 138, 139, 133, 81, 140].

The information gained about a biological system by using fluorescence spectroscopy with the help of intrinsic or extrinsic fluorescent probes increases tremendously with the combined analysis of many of the above mentioned fluorescence methods.

1.3 Scope of the thesis

This thesis deals with the study of dynamics of the fluorescent probes in biological systems, mainly in the case of lipid bilayer membranes, and to some extent in micelles and proteins from the viewpoint of a physical chemist. One of the main aims is to determine the

location, orientation and dynamics of fluorescent probes in lipid bilayer membranes. The assumptions and methods used for obtaining the fluorescence properties of membrane-bound fluorophores were also examined. New methods were developed during the course of this thesis. The next six chapters give the details of the work carried out in this thesis according to the outline as follows.

Chapter 2: Experimental: Materials and Methods

This chapter gives the details about the different fluorescent probes, lipids, surfactants and proteins used in this thesis. The methods of preparation of vesicles and micelles, and different techniques used in the study of these systems, mainly steady state and time resolved fluorescence measurements, are described. The fluorescence decay data analysis is also discussed in this chapter.

Chapter 3: Fluorescence characteristics of membrane-bound probes

Here the methods and assumptions used in determining the properties of membrane-bound fluorescent probes are discussed. The first section in this chapter describes a new method of global analysis procedure that was used to estimate the lifetimes and spectra of the membrane-bound dye. The second section deals with the case of excited state kinetics in the case of Nile red which gives rise to multiple lifetimes for the membrane-bound dye.

Chapter 4: Effect of viscosity and refractive index on the fluorescence lifetimes in biological systems

In this chapter, the effects of viscosity and refractive index of the aqueous medium on the fluorescence lifetimes of probes in bilayer membranes and proteins were examined. These effects were made use of in determining the site of solubilization (location) of fluorescent probes in the bilayer membrane. The main aim of these studies was also to identify the oriented fluorescent probes that show the refractive index effect.

Chapter 5: Orientational distribution of linear dye molecules in bilayer membranes

Here the orientation of linear dye molecules in the bilayer membrane has been addressed through the measurement of order parameters from anisotropy and lifetime measurements. The effect of the nature of the lipid chain on the location and orientation of fluorescent

probes in bilayer membranes was examined.

Chapter 6: Translational and rotational diffusion of surface probes: Monte Carlo simulations and fluorescence anisotropy experiments

The dynamics of the fluorescent probes in bilayer membranes is addressed in this chapter. Surface diffusion of fluorescent probes were modeled with the help of Monte Carlo simulations and the appropriate equations were applied in explaining the dynamics in the case of micelles and in small and giant vesicles.

Chapter 7: Summary

This chapter gives a summary of the research work described in this thesis. Future directions in the field of dynamics of fluorescent probes in biological systems are also discussed.

Chapter 2

Experimental: Materials and Methods

2.1 Materials

The lipids used in this thesis were the lipids containing L- α -Phosphatidyl Choline (PC) as the head group with varying hydrophobic chains. These include natural lipids such as egg PC (from fresh egg yolk, Sigma Chemicals, USA) which is a mixture of several lipids, and synthetic lipids such as C12:0 (DLPC, Dilauroyl PC), C14:0 (DMPC, Dimyristoyl PC), C16:0 (DPPC, Dipalmitoyl PC), C18:0 (DSPC, Distearoyl PC), C20:0 (DAPC, Diarachidoyl PC), C14:1 (Dimyristoleoyl PC) and C16:1 (Dipalmitoleoyl PC). The synthetic lipids are obtained from Avanti Polar Lipids, USA. The nomenclature used in representing a synthetic PC lipid is as follows. The lipid is represented as Cx:y where x represents the length of the alkyl chain and y represent the number of double bonds in the alkyl chain. The single double bond in the alkyl chain of the lipids, C14:1 and C16:1, is at the 9th position in the alkyl chain and is of cis type. The structure of a typical PC lipid, POPC (Palmitoyl (16:0), oleoyl (18:1) PC), which is the major component of egg PC is shown in the figure 4.13. The surfactant SDS (Sodium Dodecyl Sulfate) was obtained from Sigma Chemicals, USA.

Fluorescence measurements were carried out on fluorescent probes incorporated in lipid vesicles or surfactant micelles. The fluorescent probes used in this thesis were Nile red (Nile Blue A Oxazone; Exciton Inc., USA), R6G (Rhodamine 6G, Exciton Inc., USA), BODIPY 611/627 (3,5-bis-(2-thienyl-4,4-difluoro-4-bora-3a,4a-diaza-s-indacene; Molecular Probes Inc., USA), MC540 (Merocyanine 540, Sigma Chemicals, USA), RH421 (N-(4-sulfobutyl)-4-(4-(4-dipentylamino)-phenyl)-butadienyl)-pyridinium, inner salt; Molecular Probes Inc., USA), FM4-64 (N-(3-triethylammoniumpropyl)-4-(6-(4-(diethylamino)phenyl)-hexatrienyl)-pyridinium dibromide; Molecular Probes Inc., USA), DiA (4-Di-16-ASP, (4-(4-dihexadecylamino)-styryl)-N-methyl-pyridinium iodide; Molecular Probes Inc., USA), DPH (1,6-diphenyl-1,3,5-hexatriene; Molecular Probes Inc., USA), TMA-DPH (1-(4-trimethylammonium-phenyl)-6-phenyl-1,3,5-hexatriene p-toluenesulfonate; Molecular Probes Inc., USA), DiOC₂(5) (DODCI, 3,3'-diethyloxadecarbocyanine iodide; Exciton Inc., USA), DiSC₂(3) (3,3'-diethylthiacarbocyanine iodide; Molecular Probes Inc., USA), DiSC₂(5) (3,3'-diethylthiadecarbocyanine iodide; Molecular Probes Inc., USA), DiSC₃(5) (3,3'-dipropylthiadecarbocyanine iodide; Molecular Probes Inc., USA), DiIC₁₈(3) (DiI, 1,1'-dioctadecyl-3,3,3',3'-tetramethyl-indo-carbocyanine perchlorate; Molecular Probes Inc., USA), DiIC₁₈(5) (DiD, 1,1'-dioctadecyl-3,3,3',3'-tetramethyl-indo-dicarbocyanine perchlorate; Molecular Probes Inc., USA). The structures of these dyes are shown in figure 4.6.

Barstar W38,44F single tryptophan mutant was obtained from Prof. Jayant Udgaonkar's lab at National Centre for Biological Sciences, TIFR centre, Bangalore and Human Seminal Plasma Prostatic Inhibin was obtained from Prof. K. V. R. Chary's lab at TIFR. NATA (N-acetyl L-Tryptophanamide) was obtained from Sigma Chemicals, USA.

All the solvents used were of spectroscopic or HPLC grade and tested to be free of fluorescence. The lipid vesicles and surfactant micelles were also tested to be free of fluorescence before the addition of the fluorescent dyes. Deionized water was used in the sample preparation of all aqueous samples.

2.2 Preparation of samples

2.2.1 Preparation of lipid vesicles

Lipid vesicles can be prepared from the lipids by different methods [141, 8, 9, 10]. In this thesis, lipid vesicles were prepared mainly using the sonication procedure, and in some cases, using ether evaporation method. In the sonication procedure, the required amount of the lipid was initially dissolved in chloroform. This solution was dried to form a thin film at the bottom of a long glass tube (1cm diameter, 20cm length). The lipid film was hydrated with 1.5ml of the appropriate buffer and vortexed to form a highly turbid solution consisting of Multilamellar vesicles (MLVs). These were sonicated under nitrogen atmosphere in a bath type sonicator (Imeco Ultrasonics, Bombay) to obtain Unilamellar vesicles (ULVs) [142]. The extent of sonication was controlled by monitoring the turbidity of the solution. Two main factors affect the sonication procedure: (i) water level in the bath sonicator and (ii) position of the glass tube in the sonicator. At first, water level in the sonicator was adjusted such that good standing waves are formed in the bath. Next, the height of the glass tube in the bath sonicator was adjusted such that the water level in the sonicator and in the glass tube are at the same level. This ensures the formation of good standing waves that results in efficient sonication. In general, it was enough to sonicate for a time period of 20 min and the turbid solution becomes clear after sonication indicating the formation of ULVs. Nitrogen atmosphere was maintained during the sonication procedure to avoid the lipid peroxidation [143]. The sonicated vesicles are of a single bilayer with diameters in the range of 200-400Å, with nearly 70% of the vesicles having diameters $\approx 300\text{\AA}$ [142].

Some of the initial experiments carried out in the course of this thesis were done on the vesicles prepared by ether evaporation procedure [141]. In this method, a lipid solution prepared in ether is injected into the aqueous phase kept at 55-65°C. As the ether solution comes in contact with the aqueous phase, ether gets evaporated resulting in the formation of lipid vesicles. Several parameters such as the lipid concentration in ether, rate of injection and the temperature of the water bath has to be optimized to ensure

the formation of unilamellar vesicles with uniform size distribution. The typical size of the vesicles prepared by the ether evaporation method varies from 0.1 to 1.0 μm . The vesicles prepared by the ether evaporation procedure were of larger size compared to the those prepared by sonication. This procedure is mainly used in literature for trapping the molecules inside the lipid vesicles [141]. In our hands, with the vesicles prepared by the ether evaporation procedure, the reproducibility of the experimental results was not as good as that for sonicated vesicles and hence in most cases, sonicated vesicles were used for the experiments, unless otherwise mentioned.

For the preparation of giant vesicles with the fluorescent dye incorporated inside, the lipid and the dye mixture in the required concentration ratio was first dissolved in chloroform and it was dried on a glass plate to form a lipid-dye film. This film was then hydrated with the appropriate buffer for about two to three hours to obtain the giant liposomes with the fluorescent dye incorporated [144]. The typical diameter of these giant liposomes were in the range of 5-20 μm .

2.2.2 Preparation of surfactant micelles

SDS micellar solutions were prepared by stirring the surfactant in warm (about 35°C) deionized water for about an hour. The concentration of the surfactant (69mM) used was above its CMC. Critical Micelle Concentration (CMC) is the concentration of the surfactant above which micelles are formed with fixed aggregation number. For SDS, CMC is 8mM [25]. The concentration of the micelle $[M]$ was calculated using the equation

$$[M] = \frac{[S] - \text{CMC}}{N_{\text{agg}}} \quad (2.1)$$

where $[S]$ is the surfactant concentration and N_{agg} is the aggregation number of the micelles. In the case of SDS, $N_{\text{agg}}=60\pm6$ [28, 25]. Hence the concentration of the SDS micelles used in our experiments was 1.02mM.

The stock solutions of the dyes were prepared in absolute ethanol and stored at -20°C. The concentrations were calculated using the absorption measurements and the literature values of the molar extinction coefficients. In general, the dye to lipid ratio or the dye to

micelle ratio was kept above 1:500. The dyes were added to the lipid vesicles or surfactant micelles and kept overnight before doing the fluorescence measurements.

2.3 Experimental Methods

2.3.1 Absorption measurements

Absorption measurements were carried out on a double beam Shimadzu-2100 spectrophotometer. Absorption spectra give information about the ground state of the absorbing molecules. The absorbance A is related to the concentration of the sample C as

$$A = \log \left(\frac{I_0}{I} \right) = \epsilon Cl \quad (2.2)$$

where I_0 and I are the intensities of the incident and transmitted light, ϵ is the molar extinction coefficient and l is the path length of the light beam through the sample which is 1 cm in our case. This equation can be used to calculate the concentration of the sample of unknown concentration by knowing the value of the molar extinction coefficient or vice versa.

2.3.2 Steady State Fluorescence Measurements

Steady state fluorescence experiments were done on a SPEX Fluorolog 1681 T format or a Shimadzu RF 540 spectrofluorometer. Fluorescence measurements were carried out in the right angle geometry. The excitation light was an unpolarized light from a Xe-lamp. Appropriate filters were used at the emission side to avoid the excitation light when necessary. Emission spectrum was recorded by keeping the excitation wavelength fixed and varying the emission wavelength. Excitation spectrum was recorded by keeping the emission wavelength fixed and scanning the excitation wavelength. The emission spectra recorded at different excitation wavelengths and the excitation spectra recorded at different emission wavelengths can be used to deduce information about the fluorophore heterogeneity of the sample.

For measuring fluorescence anisotropy, a polarizer was attached before the exciting beam which results in the vertical polarization of the exciting beam and the emission intensities were measured in the directions parallel ($I_{\parallel} = I_{VV}$) and perpendicular ($I_{\perp} = I_{VH}$) to the polarization of the exciting light beam. Because of the difference in the monochromator response to different polarizations of the light, these intensities have to be corrected by a factor known as G-factor (Geometry factor) [46]. When the polarization of the exciting beam is horizontal, the sample fluorescence intensities along the vertical and horizontal directions at the right angle geometry to the exciting light should be the same if the response of the emission monochromator and detector to the horizontally and vertically polarized fluorescence light is the same. Hence G factor is taken as the ratio of these two intensities ($G = I_{HV}/I_{HH}$) and the anisotropy is calculated using the equation

$$r_{ss} = \frac{I_{\parallel} - GI_{\perp}}{I_{\parallel} + 2GI_{\perp}} = \frac{I_{VV} - \frac{I_{HV}}{I_{HH}} I_{VH}}{I_{VV} + 2\frac{I_{HV}}{I_{HH}} I_{VH}} \quad (2.3)$$

Most of the steady state anisotropy experiments were carried out on the T-format spectrofluorometer which uses two detection channels on the emission side at the right angle geometry with respect to the excitation light. One channel is kept at the vertical polarization and the other is kept at the horizontal polarization which allows the measurement of two polarized fluorescence intensities at the same time. This procedure eliminates the effect of any sample instability problems on the fluorescence anisotropy measurements.

2.3.3 Quantum yield and Radiative rate

Radiative rate of a fluorophore k_r was estimated using the Strickler-Berg equation [145]:

$$k_r = 2.88 \times 10^{-9} n^2 \langle \nu_f^{-3} \rangle_{av}^{-1} \int \frac{\epsilon_{\nu} d\nu}{\nu} \quad (2.4)$$

where

$$\langle \nu_f^{-3} \rangle_{av}^{-1} = \frac{\int I(\nu) d\nu}{\int \nu^{-3} I(\nu) d\nu}$$

If the absorption and emission spectra follow the mirror symmetry relationship, then the equation 2.4 turns out to be

$$k_r = 2.88 \times 10^{-9} n^2 \int \frac{(2\nu_0 - \nu)^2}{\nu} \epsilon_{\nu} d\nu \quad (2.5)$$

where n is the refractive index of the medium, ϵ_ν and $I(\nu)$ are the molar extinction coefficient and fluorescence intensity at the frequency ν (in cm^{-1}), and ν_0 is the frequency of 0-0 transition of $S_0 - S_1$.

Quantum yield (ϕ_f) which is the ratio of the fluorescence photons to the ratio of the photons absorbed by the sample was measured from the values of the radiative rate (k_r) and the fluorescence lifetime (τ) as

$$\phi_f = \frac{k_r}{k_r + k_{nr}} = k_r \tau \quad (2.6)$$

where k_{nr} represents the nonradiative rate. Quantum yield of the sample was measured in some cases using a reference of known quantum yield by using the equation

$$\phi_s = \frac{F_s}{F_r} \times \frac{A_r}{A_s} \times \phi_r \quad (2.7)$$

where F_s , F_r , A_s , A_r , ϕ_s and ϕ_r represent the total fluorescence (area under the fluorescence spectrum), absorbances and quantum yields of the sample and reference, respectively.

2.3.4 Time Resolved Fluorescence Measurements

Time resolved fluorescence decay measurements were carried out on a Time Correlated Single Photon Counting (TCSPC) setup coupled with a picosecond laser [119, 146, 147]. Schematic diagram of the TCSPC setup is shown in figure 2.1. The exciting laser source was a cavity dumped, mode-locked, picosecond Rhodamine 6G dye laser (570-630 nm) (Spectra Physics Inc., USA) synchronously pumped by the frequency doubled (532 nm) output of CW, mode locked Nd-YAG laser (Spectra Physics Series 3000). In some experiments, frequency doubled output of a mode-locked picosecond Spectra Physics Ti-Sapphire Tsunami laser (720-900 nm) pumped by a diode pumped CW Spectra Physics Millennia X Nd-Vanadate laser (532 nm) was used. The pulse width of the exciting laser pulses were typically of the order of 1-4 ps and were cavity dumped from 82 MHz to a repetition rate of 800 KHz using a cavity dumper. The average power was typically between

10-50 mW. Most of the fluorescent probes studied here were excited using the fundamental wavelengths (570-630 nm) of the Rhodamine 6G dye laser. Some of the fluorescent probes were excited with the frequency doubled output (290-310 nm) of the fundamental of Rhodamine 6G dye laser using a KDP crystal. For the excitation of tryptophan in proteins and its derivatives such as NATA, the wavelength of 295 nm was used which can be either the frequency doubled output of the fundamental (590 nm) of the dye laser or the frequency tripled output of the fundamental (888 nm) of the Ti-Sapphire laser.

The Time Correlated Single Photon Counting (TCSPC) setup used for measuring the fluorescence decays from the excited fluorescent probe molecules can be described as follows [148, 46, 149]. Here, the time interval between the exciting photon (laser pulse) and a single fluorescence photon from the fluorescent sample excited by the same laser pulse is measured in repeated cycles and the data was used to construct the fluorescence decay of the sample. For this purpose, a Time to Amplitude converter (TAC) coupled with a multi channel pulse height analyzer (MCPHA) was used. A small part of the exciting laser beam is taken and fed to a Photomultiplier tube to start the reference signal which is called the START signal. This signal starts TAC, which generates a constant voltage ramp that increases linearly with time. When the fluorescent photon arrives at the detection end which is the microchannel plate photomultiplier (MCP-PMT, Hamamatsu 2809), a STOP signal is generated which stops the increasing voltage ramp generated by the TAC. The device now contains a voltage whose height is proportional to the time difference between the START and STOP signals. If no STOP pulse is detected, the voltage is reset to zero. The height of the pulse which is proportional to the time difference between these two signals, i.e., START and STOP signals is recorded in a digital manner into the MCPHA. A Constant Fraction Discriminator (CFD) was used for the precise timing of the detection of START and STOP signals. Parameters such as threshold of detection and the zero cross jitter of the CFD have to be optimized for this purpose. The procedure of detection of single fluorescent photons for each exciting laser pulse was repeated until a large number of photons is collected and the number of times each voltage was generated by the TAC in repeated cycles of the exciting pulses is recorded in the form of a histogram by the

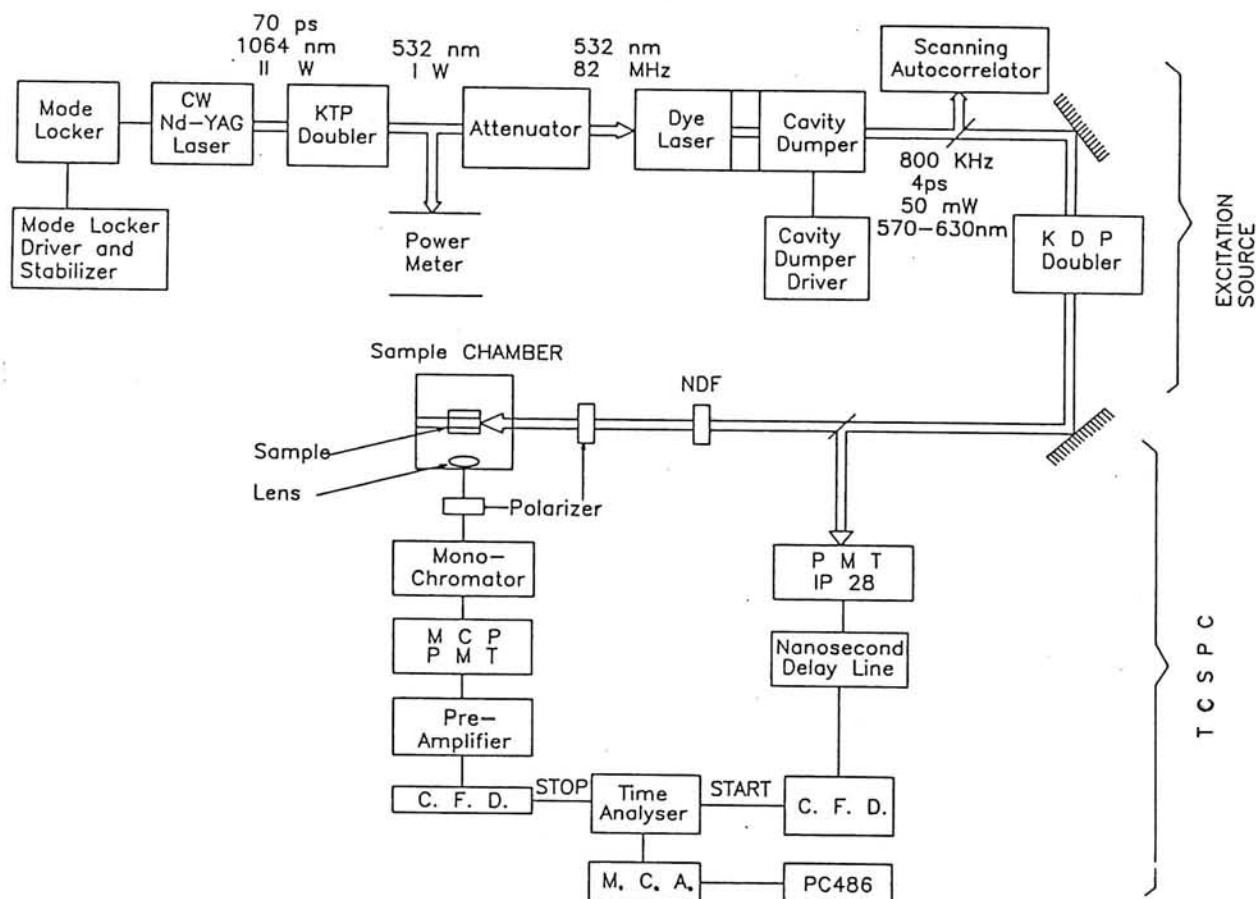


Figure 2.1: Time Correlated Single Photon Counting (TCSPC) setup used to measure the time resolved fluorescence decays of the excited fluorescent probes. The figure shows the picosecond Rhodamine 6G dye laser as the excitation source. The other excitation source which is the Tsunami laser is shown in the next figure.

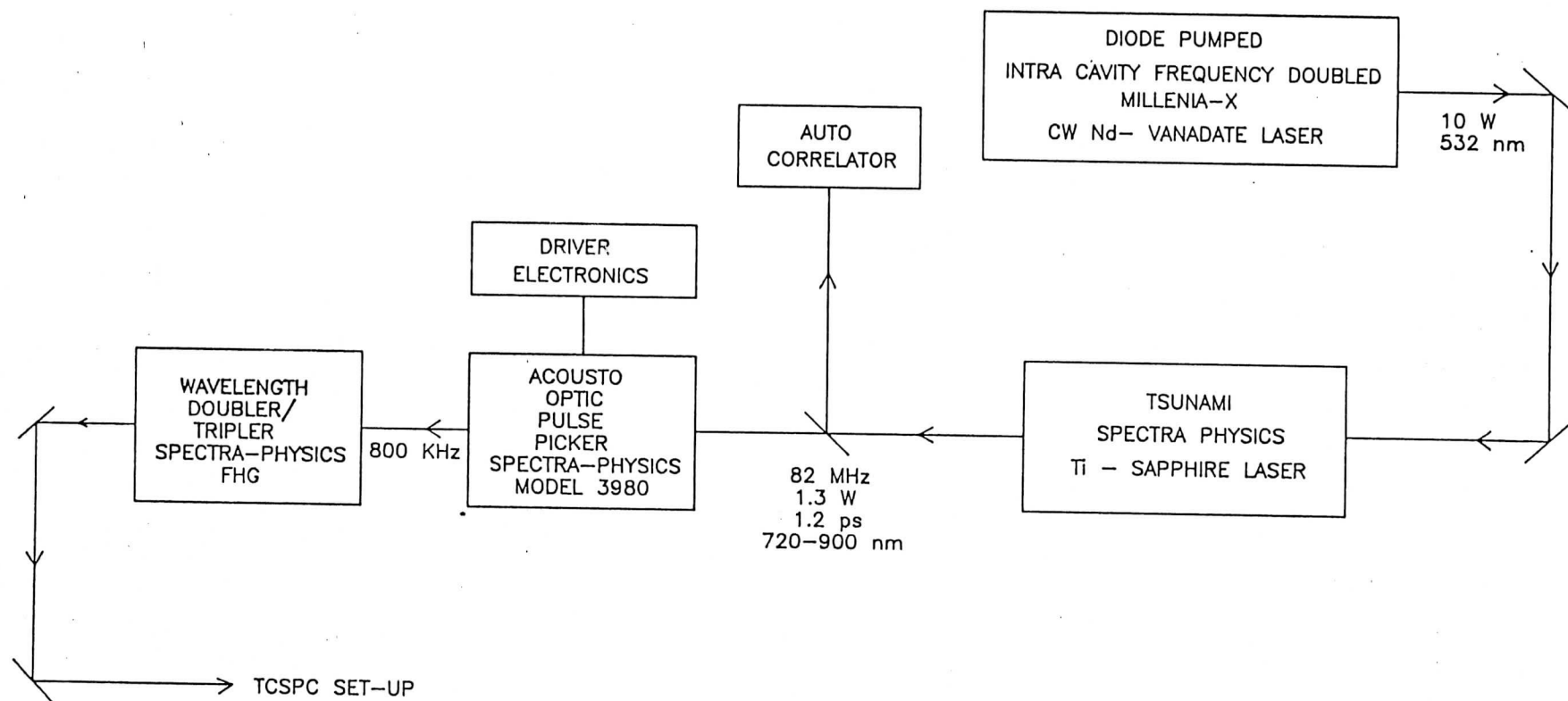


Figure 2.2: Block diagram of the Tsunami laser used as the excitation source in some of the TCSPC experiments.

MCPHA. At low count rates, the time difference between the START and STOP photons follows the fluorescence statistics and hence the histogram generated by the MCPHA represents the fluorescence decay of the sample [148]. For this purpose, the count rate of the fluorescent photons were kept below 1% of the repetition rate of the exciting laser pulses. In our case, the pulse repetition rate of the laser pulses was 800 KHz and hence the fluorescence photons were collected at the count rate of < 6000 counts/sec. The time per channel of the MCPHA was determined using laser pulses with a fixed separation time of 12.195 ns ($=1/82\text{MHz}$). The Instrument Response Function (IRF) was measured using a scattering solution made using a dilute solution of non-dairy creamer or MgO in water. The Full Width at Half Maximum (FWHM) of the IRF is typically about 100 ps.

For the measurement of fluorescence lifetimes, fluorescence decay was collected from the sample after excitation with the emission polarizer oriented at the magic angle (54.7°) with respect to the excitation polarizer. The fluorescence decay collected at the magic angle represents that of the total fluorescence intensity decay because of the absence of any anisotropy components in the fluorescence decay at this particular angle.

For the measurement of time resolved fluorescence anisotropy, the fluorescence decays were collected with the emission polarizer kept at parallel (I_{\parallel}) and perpendicular (I_{\perp}) orientations with respect to the excitation polarizer. These polarized components were corrected for the G factor. G factor of the TCSPC setup was measured by two methods: tail-matching [148] and area matching method, using a fluorophore in a homogeneous solvent of low viscosity such as ethanol where the rotational correlation time is much shorter than its fluorescence lifetime ($\phi \ll \tau$). If the emission monochromator response is the same for both the polarizations, then the time taken to match the tails of the two polarized fluorescence decays (I_{\parallel} and I_{\perp}) at long times after excitation for this case should be the same. Hence G-factor is equal to the ratio of the times taken to match the tails of I_{\perp} and I_{\parallel} ($G = t_{\perp}/t_{\parallel}$). In the second method of area matching, the two polarized fluorescence decays I_{\parallel} and I_{\perp} were collected for a fixed time. A region is selected in the tail region of the polarized fluorescence decays at long times ($t > 10\phi$) after excitation where the initially created anisotropic population decays to a random isotropic population because of the

short rotational correlation time of the fluorophore compared to its fluorescence lifetime ($\phi \ll \tau$). Similar to the arguments in the tail-matching method, the areas of the selected region for the two polarized fluorescence decays should be the same if the monochromator and detector respond equally to both the polarizations. Hence the ratios of the areas gives the G-factor (A_{\parallel}/A_{\perp}) in this method. The average of several measurements was taken for the accurate estimate of the G-factor. Using the thus obtained G-factor, for the sample whose anisotropy decay has to be experimentally measured, I_{\perp} was collected for the time $t_{\parallel} \times G$ where t_{\parallel} is the time for which I_{\parallel} was collected. These two polarized intensity decays were used to compute the fluorescence anisotropy decay according to the following equation

$$r(t) = \frac{I_{\parallel} - I_{\perp}}{I_{\parallel} + 2I_{\perp}} \quad (2.8)$$

The observed fluorescence responses are the convolution of the IRF with the intensity decay function of the sample. Hence to analyze the observed fluorescence responses, one needs to employ specific data analysis methods to obtain lifetime and anisotropy parameters about the system under study. These are discussed briefly in the next section (section 2.4).

2.3.5 Fluorescence Microscopy Experiments

Time resolved fluorescence microscopy is a powerful technique for studying the various localized aspects of structure, dynamics and function of cells and membranes [150, 151, 152]. In this thesis, this technique was used to obtain the fluorescence decays of the probe DiIC₁₈(5) from a localized portion of a giant liposome (refer figure 6.4A). An inverted epifluorescence microscope (Nikon, Diaphot 300) coupled with the above mentioned Rhodamine 6G picosecond dye laser was used for this purpose. The laser beam (600nm), after passing through a dichroic mirror (XF44 of Omega Optical Co., USA) was focussed on to a single giant liposome with the help of an objective lens (40X, NA 0.55, Nikon). The diameter of the focussed laser beam was typically about 1.0 μm . The fluorescence was collected by the same objective lens, passed through a 645 nm cut-off filter, a Glan-Thomson

polarizer and detected by a photon counting photomultiplier (XP2020Q). The G factor was determined by using the Kiton red (Sulforhodamine B, Exciton Inc., USA) solution in water whose rotational correlation time (0.20 ns) is faster than its lifetime (1.55 ns). The instrument response function (IRF) was measured by monitoring the fluorescence of Oxonol VI (Propyl Oxonol) in Ethanol whose fluorescence lifetime is less than 30 ps. Since Oxonol VI shows fluorescence in the wavelength region of DiIC₁₈(5) and Kiton red, the same optical elements were used in collecting both the IRF and the emission profiles. The FWHM of the IRF was about 280 ps. Typical peak count in the emission decay for fluorescence intensity and anisotropy measurements was about 10,000 and the time per channel was 43.22 ps. The fluorescence intensity and polarized fluorescence decays were analyzed with the appropriate data analysis methods described in section 2.4 to obtain the fluorescence lifetimes and the rotational correlation times.

2.3.6 NMR Measurements

The proton NMR experiments were carried out on a Varian Unity Plus spectrometer with a ¹H frequency of 600MHz. The experiments included one dimensional (1D) ¹H spectra and two dimensional (2D) Nuclear Overhauser Effect Spectroscopy (NOESY) [153] with a mixing time of 500ms. All the NMR experiments were carried out at 25°C.

2.4 Fluorescence Decay Data Analysis

The fluorescence decay data obtained from time resolved fluorescence measurements by using either TCSPC setup or a fluorescence microscope has to be fitted to the appropriate nonlinear functions (in most cases, exponential functions). The parameters to be optimized are fluorescence lifetimes, rotational correlation times, preexponential factors etc. The commonly used method is the nonlinear analysis by the Levenberg-Marquardt algorithm which is described in the next section.

2.4.1 Nonlinear Least squares Levenberg-Marquardt Algorithm

Levenberg-Marquardt algorithm is the most widely accepted method for the non-linear analysis of the experimental data in physical sciences. The method is described as follows [154, 155, 156].

Let (x_i, y_i) be the experimental data points that have to be fitted to a nonlinear function

$$y(x) = f(a_1, a_2, \dots, a_j, \dots, a_m, x) \quad (2.9)$$

where f is a nonlinear function of x and all a_j . For a good fit of the experimental data, the quantity which measures the sum of the squares of the deviations between the experimental and fitted data, known as χ^2 has to be minimized.

$$\chi^2 = \sum \left(\frac{(y_i - y(x_i))^2}{\sigma_i^2} \right) \quad (2.10)$$

Here σ_i represents the standard deviation associated with the experimental value y_i .

In the method of non-linear least squares, one starts at an initial set of guess values a'_j for the parameters to be optimized and arrives at the optimized values a_j through small increments δa_j in successive iterations. The fitting function $y(x)$ can be expanded in a Taylor series to first order in the parameter increments as

$$y(x) \simeq y'(x) + \sum_{j=1}^m \left[\frac{\partial y'(x)}{\partial a_j} \delta a_j \right] \quad (2.11)$$

where $y'(x)$ is the value of the fitting function calculated with the starting values a'_j and the derivatives are calculated at the starting values. Hence χ^2 becomes

$$\chi^2 = \sum \left[\frac{1}{\sigma_i^2} \left(y_i - y'(x_i) - \sum_{j=1}^m \left(\frac{\partial y'(x)}{\partial a_j} \delta a_j \right) \right)^2 \right] \quad (2.12)$$

In each successive iteration, the parameter increments δa_j are determined such that χ^2 gets minimized. The next iteration starts with the new values $a'_j + \delta a_j$. To minimize χ^2 with respect to the parameter increments δa_j , the partial derivatives of χ^2 with respect to each δa_k should be equal to zero.

$$\frac{\partial \chi^2}{\partial \delta a_k} = 0 \quad (2.13)$$

The above equation results in m simultaneous equations which can be expressed as the matrix equation

$$\beta = \delta a \alpha \quad (2.14)$$

where

$$\beta_k = -\frac{1}{2} \frac{\partial \chi'^2}{\partial a_k} \quad (2.15)$$

and

$$\alpha_{jk} = \Sigma \left[\frac{1}{\sigma_i^2} \frac{\partial y'(x_i)}{\partial a_j} \frac{\partial y'(x_i)}{\partial a_k} \right] \quad (2.16)$$

where χ'^2 is the χ^2 determined at the parameter values a'_j . The matrix α is known as the curvature matrix.

The Levenberg-Marquardt algorithm uses the above first order expansion of the fitting function and an adjustable parameter λ to arrive at the best parameters which fits the experimental data. The matrix equation to be solved for the parameter increments in this method is

$$\beta = \delta a \alpha' \quad (2.17)$$

with

$$\alpha'_{jk} = \begin{cases} \alpha_{jk}(1 + \lambda) & \text{for } j = k \\ \alpha_{jk} & \text{for } j \neq k \end{cases} \quad (2.18)$$

The recipe in this algorithm for fast and efficient convergence of the parameters to be optimized for the best fit of the experimental data with a global minimum for χ^2 is as follows:

1. Compute $\chi^2(a)$.
2. Start initially with $\lambda = 0.001$.
3. Compute δa and $\chi^2(a + \delta a)$ with this choice of λ .
4. If $\chi^2(a + \delta a) > \chi^2(a)$, increase λ by a factor of 10 and repeat step 3.
5. If $\chi^2(a + \delta a) < \chi^2(a)$, decrease λ by a factor of 10, consider $a' = a + \delta a$ to be the new starting point, and return to step 3, substituting a' to a .

The value of λ in the successive cycles decides the rate of convergence of χ^2 to its global minimum. As the solution reaches minimum, the value of λ will decrease.

Levenberg-Marquardt algorithm which is also known as the gradient-expansion algorithm is the most simple and most direct and efficient method available for the nonlinear least squares fitting of any kind of experimental data. The values of the optimized parameters by this method are independent of the starting values when the global minimum of χ^2 is reached [155].

2.4.2 Discrete Exponential analysis of fluorescence intensity decays

The analysis of the experimentally measured fluorescence intensity decay to a sum of discrete exponentials is described as follows [157, 158, 159]. The observed fluorescence response $F(t)$ is the convolution of the instrument response function $R(t)$ and the fluorescence intensity decay function $I(t)$ as

$$F(t) = \int_0^t R(s + \delta) I(t - s) ds \quad (2.19)$$

where δ is the shift parameter that has to be optimized in the analysis. This parameter takes care of the slight time shift (an instrumental artifact) between the measured IRF and the fluorescence response. The slight mismatch arising between these two due to the measurement of IRF and the fluorescence response at two different wavelengths, will be taken care in the data analysis by the shift parameter. When the intensity decay function $I(t)$ is the sum of exponentials such as

$$I(t) = \sum_{k=1}^p a_k \exp(-t/\tau_k) \quad (2.20)$$

where τ_k and a_k are the k th lifetime and the corresponding amplitude, equation 2.19 becomes

$$F(t) = \int_0^t R(s + \delta) \left[\sum_{k=1}^p a_k \exp(-(t - s)/\tau_k) \right] ds \quad (2.21)$$

The above convolution integral can be written as

$$F_m = \epsilon \sum_{j=1}^m R_j \sum_{k=1}^p a_k \exp[-(m - j)\epsilon/\tau_k] \quad (2.22)$$

or

$$F_m = \sum_{k=1}^p F_m^k \quad (2.23)$$

where F_m^k is the calculated fluorescence response in the m th channel due to the k th exponential component. Here ϵ represents the time duration of one channel.

For trapezoid integration, the following recursion relation can be used to calculate the F_m^k .

$$F_m^k = (F_{m-1}^k + 0.5\epsilon a_k R_{m-1}) \cdot \exp(-\epsilon/\tau_k) + 0.5\epsilon a_k R_m \quad (2.24)$$

This equation results in the recursion relations between the partial derivatives of F_m^k with respect to the parameters to be optimized as given below.

$$\frac{\partial F_m^k}{\partial \tau_k} = \left[\frac{\partial F_{m-1}^k}{\partial \tau_k} + \frac{\epsilon}{\tau_k^2} [F_{m-1}^k + 0.5\epsilon a_k R_{m-1}] \right] \exp(-\epsilon/\tau_k) \quad (2.25)$$

and

$$\frac{\partial F_m^k}{\partial a_k} = \frac{F_m^k}{a_k} \quad (2.26)$$

These recursion relations (equations 2.25 and 2.26) can be used to calculate the matrix elements of the two matrices β and α' in the equation 2.17 using the relations 2.15 and 2.16. Using these two matrices, the best fit values of the parameters were optimized using the Levenberg-Marquardt algorithm described in the previous section.

In TCSPC experiments, the statistics of photon counting follows Poisson distribution [148] and hence the standard deviation in the number of counts in the i th channel, σ_i , will be

$$\sigma_i = \sqrt{F_i} \quad (2.27)$$

where F_i is the number of photon counts in the i th channel. Hence, the expression for reduced χ^2 becomes

$$\chi^2 = \frac{1}{N} \sum_{i=1}^n \frac{(F_i - F(t_i))^2}{F_i} \quad (2.28)$$

where N is the number of degrees of freedom which is equal to $n - l$ where n is the number of data points fitted and l is the number of free parameters in the analysis. $F(t_i)$ is the calculated fluorescence response in the i th channel during the fitting procedure. When

$n \gg l$, then $N \simeq n$. The best fit of the experimental data is judged by the value of χ^2 that should be around 1.0 ± 0.2 .

For a good fit, the weighted residuals $r(t_i)$ for all the data points should also be randomly distributed about the zero value. The weighted residual $r(t_i)$ for the i th channel is defined as

$$r(t_i) = \frac{F_i - F(t_i)}{\sqrt{F_i}} \quad (2.29)$$

The randomness of the weighted residuals can be checked by making use of the autocorrelation function defined as

$$C(t_j) = \frac{\frac{1}{m} \sum_{i=1}^m r(t_i) r(t_{i+j})}{\frac{1}{n} \sum_{i=1}^n [r(t_i)]^2} \quad (2.30)$$

where $m = n - j$ with j set to an upper limit of $n/2$. Here $C(t_j)$ represents the correlation between the weighted residuals in the i th and $(i+j)$ th channels, summed over a selected i channels.

Figure 2.3 shows the experimentally measured time resolved fluorescence response and the calculated fluorescence response for the best fit in the case of Merocyanine 540 in Egg PC, using the methods described in the above two sections. The fluorescence decay data was fitted to a double exponential function. The χ^2 value (1.10) and the randomness of the residuals as shown in the bottom panel indicates the goodness of the fitting of the experimental data to the two exponential intensity decay function.

Several improvements were proposed in the above discussed analysis of the experimental data for the generation of accurate parameters such as using Simpson's rule or law of the mean instead of the trapezoidal approximation for the numerical integration as done in the equation 2.24. These methods are found to be equally good to the above method that uses the Trapezoidal approximation [148]. When one of the lifetimes in a multiexponential decay function is very short or very close to that of the IRF, an improvement in the above described method of data analysis was suggested in literature to extract these short lifetimes [159, 160].

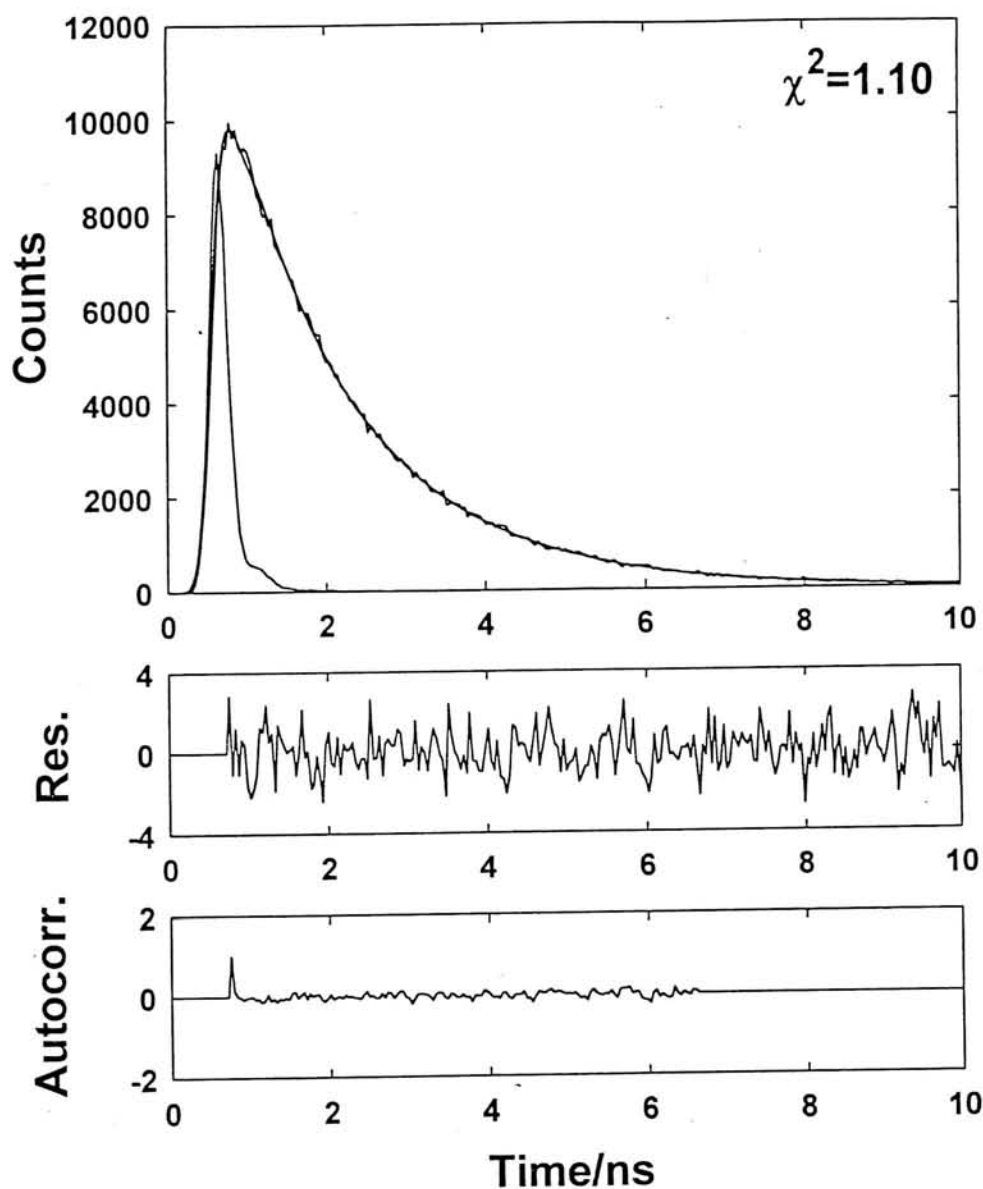


Figure 2.3: Fluorescence decay of Merocyanine 540 in Egg PC (pH 7.4, 25°C) measured at magic angle using a TCSPC setup. The sample was excited at 570nm and the emission was collected at 680nm. The figure also shows the instrument response function and the calculated fluorescence decay for the best fit of the experimental data. The fluorescence decay was fitted to a double exponential function and χ^2 value for the best fit was about 1.10. The obtained lifetimes are 1.68ns and 0.64ns with the respective amplitudes 0.81 and 0.19. The bottom panels show the random weighted residuals and the autocorrelation function of the weighted residuals.

2.4.3 Global Analysis of multiple fluorescence intensity decays

Global analysis of multiple fluorescence decays collected at different experimental conditions such as at multiple emission or excitation wavelengths, varying concentrations or solvent composition has been well established in the literature of fluorescence spectroscopy as a convenient tool for the extraction of physically meaningful parameters with increased confidence limits and to test different models that account for the observed structural dynamics of the fluorescent probes in the systems under study [161, 162, 163, 164, 165, 166, 116, 117, 167]. The global analysis procedure is particularly useful in the method of constructing Decay Associated Spectra (DAS). In the global analysis procedure, multiple fluorescence decays are analyzed combinely keeping some of the parameters common to all the decays and other parameters that are particular to each data set. This can be illustrated with the following example [161].

Consider the system of a mixture of two fluorophores which exhibit single exponential fluorescence decays with differing emission spectra. For this system, the fluorescence decays collected at multiple emission wavelengths should be analyzed to a double exponential intensity decay function with the two lifetimes τ_1 and τ_2 common to all the decay data sets whereas the amplitudes a_{1i} and a_{2i} varying with the decay data set of index i . If these n fluorescence decays are analyzed individually, the total number of parameters to be optimized becomes $4n$. But when the linkage between these different data sets were made through the two common lifetimes, the total number of parameters to be optimized decreases from $4n$ to $2n+2$. The reduction in the total number of parameters to be optimized increases the confidence limits on the thus obtained values. Global analysis procedure optimizes these $2n+2$ parameters by the nonlinear least squares Levenberg-Marquardt algorithm described in the previous sections using the equations 2.17, 2.18, 2.15 and 2.16.

Calculation of the matrix elements of β and α (equations 2.15 and 2.16) involves the calculation of the partial derivatives of fluorescence decays with respect to the parameters to be optimized. The partial derivatives of the n fluorescence decays with the global

parameters τ_1 and τ_2 are non-zero. If there is no amplitude relationship between the individual decay sets, the partial derivatives of the i th fluorescence decay with respect to the local parameters a_{1i} and a_{2i} are non-zero whereas the partial derivatives becomes zero with respect to the local parameters a_{1j} and a_{2j} corresponding to the other, say, j th ($j \neq i$) decay data set. Hence most of the off-diagonal elements of the curvature matrix α are zero which makes the procedure of solving the matrix equation 2.17 for determining parameter increments in successive cycles, quite easier and faster. If there is any amplitude relationship known between different decay data sets, that will further reduce the number of free parameters to be optimized in the global analysis procedure and this relationship has to be taken into account while calculating the elements of the curvature matrix. One such case known as the Spectrally Constrained Global Analysis (SCGA) is described in the next chapter (section 3.1).

Global analysis of multiple fluorescence decays is a very useful technique and has been used in calculating the DAS, QDAS (Quenching DAS) and ADAS (Anisotropy DAS) [168, 114, 169, 116, 117], (e.g., figure 4.3 shows the DAS of the two fluorescence lifetimes arising from two tryptophans of the HSPI protein), in the analysis of excited state kinetics [169, 164] (section 3.2 illustrates one such case of excited state kinetics for the fluorescent dye Nile red), in the combined analysis of polarized fluorescence decays to obtain information about the fluorescence anisotropy parameters (section 2.4.5) (e.g., figure 2.5), in the study of protein folding dynamics [170, 171], in the analysis of distribution of distances through fluorescence resonance energy transfer measurements [172, 167], in the analysis of multiexcitation anisotropy experiments [173, 165] etc.

2.4.4 Maximum Entropy Method

The fluorescence decay data analysis by the Maximum Entropy Method (MEM) [174, 175, 176, 177, 178] is an unbiased way of data analysis. In MEM, the fluorescence intensity decay was analyzed to the model of continuous distribution of lifetimes

$$I(t) = \int_0^{\infty} \alpha(\tau) \exp(-t/\tau) d\tau \quad (2.31)$$

where $\alpha(\tau)$ corresponds to the amplitude of the lifetime τ in the intensity decay. In practice, the limits on the above integration is set based on the information regarding the system under study and the detection limit of the instrument. In our case, the lower and upper limits of the integration was set as 10 ps and 20 ns respectively. For the practical purpose, the above equation can be written in terms of a discrete sum of exponentials as

$$I(t) = \sum_{i=1}^N \alpha_i \exp(-t/\tau_i) \quad (2.32)$$

where N represents the total number of exponentials. In our data analysis, N is taken as 150 exponentials equally spaced in the $\log(\tau)$ space between the lower and upper limits. MEM initially starts with a flat distribution of amplitudes $\alpha(\tau)$, that is, each lifetime has equal weightage in the beginning and arrives at the amplitude distribution which best describes the observed experimental fluorescence intensity decay. The optimization of the amplitude distribution $\alpha(\tau)$ is carried out in successive cycles by minimizing the χ^2 (equation 2.28) and maximizing the entropy S . The expression used for S is the Shannon-Jaynes entropy function [179] which is

$$S = -\sum p_i \log p_i \quad (2.33)$$

where $p_i = \alpha_i / \sum \alpha_i$.

The optimization procedure is done as follows [176, 178]. The initial flat distribution is improved in successive iterations as

$$\alpha_i(\text{new}) = \alpha_i(\text{old}) + x \delta \alpha_i \quad (2.34)$$

where $\delta \alpha_i$ are the amplitude increments. These are determined using three search directions constructed using $\nabla \chi^2$, ∇S and $\nabla \nabla \chi^2$. The multiplication factor x which minimizes χ^2 and maximizes S was determined by the α -chop and p -chop techniques. When negative amplitudes are not possible for the system under study (not true for some systems, e.g., those undergoing excited state kinetics show negative amplitudes, example in section 3.2), care is taken to avoid the negative values by using only a fraction of x or equating the negative values to zero (which increases χ^2 slightly in that iteration). Successive iterations

give distributions that minimize χ^2 and maximize S . If the χ^2 criterion is satisfied by many distributions in a particular iteration, then the distribution with maximum entropy is selected among these distributions. The analysis is terminated when χ^2 reached the specified lower limit or when χ^2 and $\alpha(\tau)$ show no change in successive iterations.

MEM analysis gives a lifetime distribution that is model independent. If the system under study truly represents a multiexponential system, then MEM will give rise to a multimodal gaussian distribution with the number of peaks equal to the number of lifetimes. The average lifetimes obtained for each peak in the MEM distribution shows one-to-one correspondence with the lifetimes obtained in the discrete exponential analysis. The resolvability and widths of the lifetime peaks in a MEM distribution depend on several factors such as the signal to noise ratio (counting statistics), position of the first channel (shift parameter), discretization in τ space (equation 2.32), and the completeness of the experimentally measured fluorescence decay [174, 178]. The width of the lifetime peaks in the MEM distribution becomes narrower with the increase of the signal-to-noise ratio, i.e., with the increase of peak counts and reaches a plateau value at higher peak counts [178, 174]. Hence for the MEM analysis carried out in this thesis, the fluorescence decays were collected upto the peak count of 10000 counts. The resolvability of the lifetime peaks depends on the discretization of the integral 2.31 into the numerical summation 2.32. The resolvability increases with the increase of the number of exponentials used in the discretization procedure. If there is a slight shift between the IRF and the measured fluorescence decay, it will result in an artifact in the MEM distribution where the width of the shortest lifetimes close to the IRF becomes higher than what they should be [174]. The resolvability and widths of the peaks in MEM distribution also depend upon the completeness of the experimental data. It was shown that the decay which was complete by more than 99.5% resulted in a well resolved lifetime distribution [178]. Hence in the case of our experiments, the fluorescence decays were collected which were complete by 99.9% of the peak counts, i.e., upto 10 counts in the tail region with the peak counts at 10000.

Figure 2.4 shows a typical MEM distribution obtained for the case of Merocyanine 540

in Egg PC whose fluorescence decay and the results of the discrete exponential analysis are shown in the figure 2.3. Note that the two well resolved peaks in the MEM distribution show one-to-one correspondence with the two lifetimes obtained in the discrete exponential analysis.

2.4.5 Analysis of time resolved fluorescence anisotropy

The analysis of time resolved fluorescence anisotropy decay $r(t)$ was carried out through the global analysis of the two polarized decays I_{\parallel} and I_{\perp} collected with the emission polarizer oriented parallel and perpendicular to the excitation polarizer [92]. These two polarized decays are related to the total intensity decay $I(t)$ and the anisotropy decay $r(t)$ according to the following equations:

$$\begin{aligned} I_{\parallel}(t) &= \frac{1}{3}I(t)[1 + 2r(t)] \\ I_{\perp}(t) &= \frac{1}{3}I(t)[1 - r(t)] \end{aligned} \quad (2.35)$$

Here the intensity decay $I(t)$ is a multiexponential function

$$I(t) = \sum_{i=1}^N \alpha_i \exp(-t/\tau_i) \quad (2.36)$$

with $\sum_i \alpha_i = 1$. Here τ_i and α_i corresponds to the i th lifetime and the corresponding amplitude in the N exponential intensity decay.

The equation for time resolved fluorescence anisotropy for any system can be expressed as

$$r(t) = (r_0 - r_{\infty}) \sum_{j=1}^M \beta_j \exp(-t/\phi_j) + r_{\infty} \quad (2.37)$$

where ϕ_j and β_j represent the j th rotational correlation time and the corresponding pre-exponential factor in the M exponential anisotropy decay with $\sum_j \beta_j = 1$. r_0 and r_{∞} represent the anisotropies at zero time (initial anisotropy) and at infinite time (residual anisotropy).

The initial anisotropy r_0 can vary between 0.4 and -0.2 depending upon the excitation and emission wavelengths. The residual anisotropy r_{∞} in the anisotropy equation 2.37

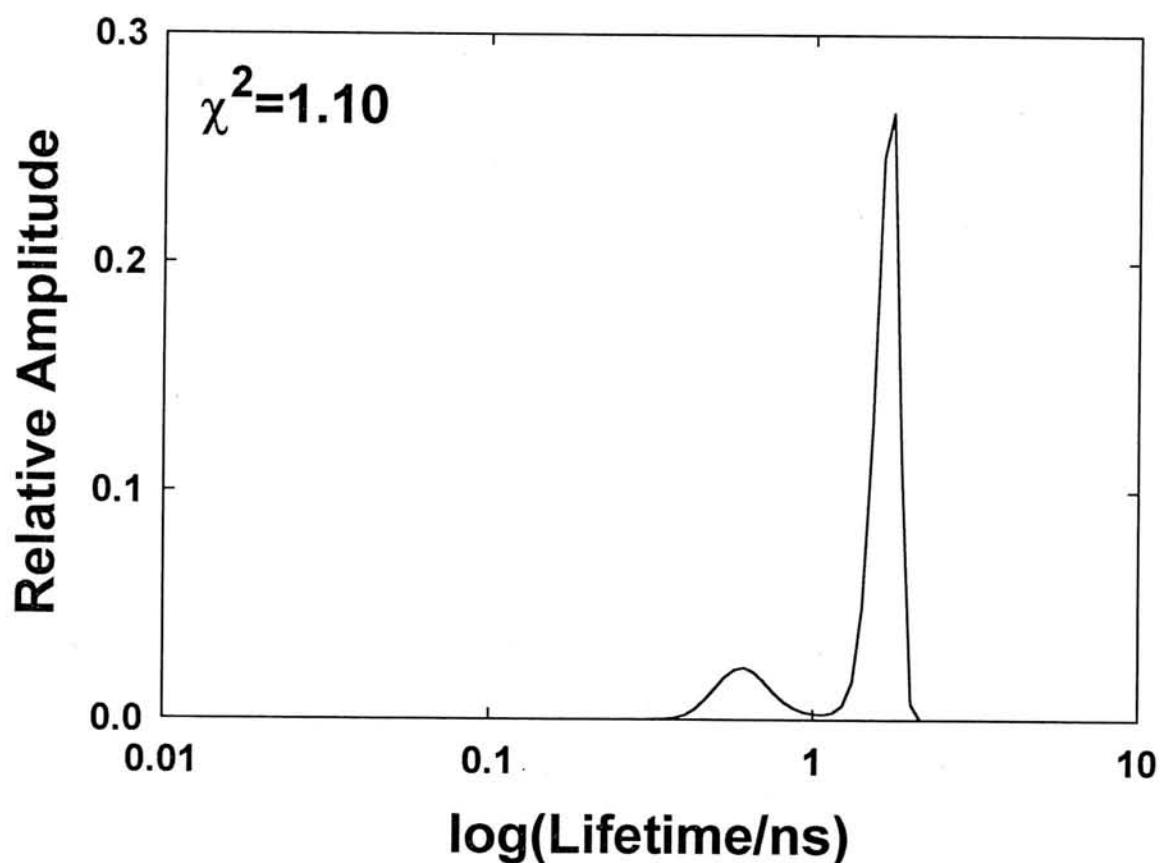


Figure 2.4: Fluorescence lifetime distribution obtained by the MEM analysis of the fluorescence decay of Merocyanine 540 in Egg PC (pH 7.4, 25°C). The experimental fluorescence decay along with the IRF is shown in the figure 2.3. The χ^2 was about 1.10 for the MEM analysis. The two lifetime peaks are in one-to-one correspondence with the two lifetimes obtained by the discrete exponential analysis (figure 2.3)

represents the rotational freedom of the molecule. When the probe molecule is in a homogeneous medium where it can rotate freely in all directions, then r_∞ becomes zero. When the probe molecule is in restricted environments such as membranes, micelles or proteins, the probe molecule can not rotate freely in all random directions and hence r_∞ becomes finite. The ratio of the residual and initial anisotropy values can be used to calculate the order of the probe environment which will be more elaborated in Chapter 5.

In the case of micelles and proteins, because of their small size, the rotation of the micelle or protein will also result in the fluorescence depolarization. In this case, the equation for fluorescence anisotropy decay becomes

$$r(t) = r_p(t) \times r_m(t) \quad (2.38)$$

where $r_p(t)$ and $r_m(t)$ represent the contribution to the fluorescence depolarization from the rotational motions of the probe and the macroparticle (micelle or protein) to which the probe is attached. $r_p(t)$ will have a form similar to the equation 2.37 whereas $r_m(t)$ becomes single exponential in the case of a spherical macroparticle. In the above equation, the fluorescence depolarization due to the surface diffusion of fluorescent probes on the surface of the macroparticle is not considered. This part is more elaborated in Chapter 6.

In the above global analysis procedure of polarized fluorescence anisotropy decays, additional constraint was used such that the calculated steady state anisotropy from the fitted data should match with that of the experimentally measured value, r_{ss} . The r_{ss} can be calculated from the time resolved data using the equation

$$r_{ss} = \frac{\int_0^\infty I(t)r(t)dt}{\int_0^\infty I(t)dt} \quad (2.39)$$

Substituting the expressions for $I(t)$ and $r(t)$ (equations 2.36 and 2.37), the above equation becomes

$$r_{ss} = \frac{(r_0 - r_\infty) \sum_i \sum_j \alpha_i \beta_j \left(\frac{1}{\tau_i} + \frac{1}{\phi_j} \right)^{-1}}{\sum_i \alpha_i \tau_i} + r_\infty \quad (2.40)$$

In the case of a fluorescent probe with a single fluorescent lifetime τ and a single rotational correlation time ϕ with no residual anisotropy ($r_\infty=0$), the equation for the steady state

anisotropy becomes

$$r_{ss} = \frac{r_0\phi}{\tau + \phi} \quad (2.41)$$

In some cases, the total intensity decay was calculated from the two polarized decays as $I(t) = I_{\parallel} + 2I_{\perp}$ and was analyzed for the fluorescence lifetimes and the corresponding amplitudes in the intensity decay. These were incorporated as fixed parameters in the anisotropy decay analysis to reduce the number of free parameters to be optimized. In some cases, the value of r_0 was determined from an independent anisotropy experiment on the probe solution in highly viscous solvent such as glycerol at the same excitation and emission wavelengths and the thus obtained value of r_0 is used in the anisotropy decay analysis procedure.

Figure 2.5 shows the experimentally measured polarized fluorescence decays and the corresponding anisotropy function for the case of Merocyanine 540 in Egg PC. The figure also shows the random residuals obtained after the global analysis procedure.

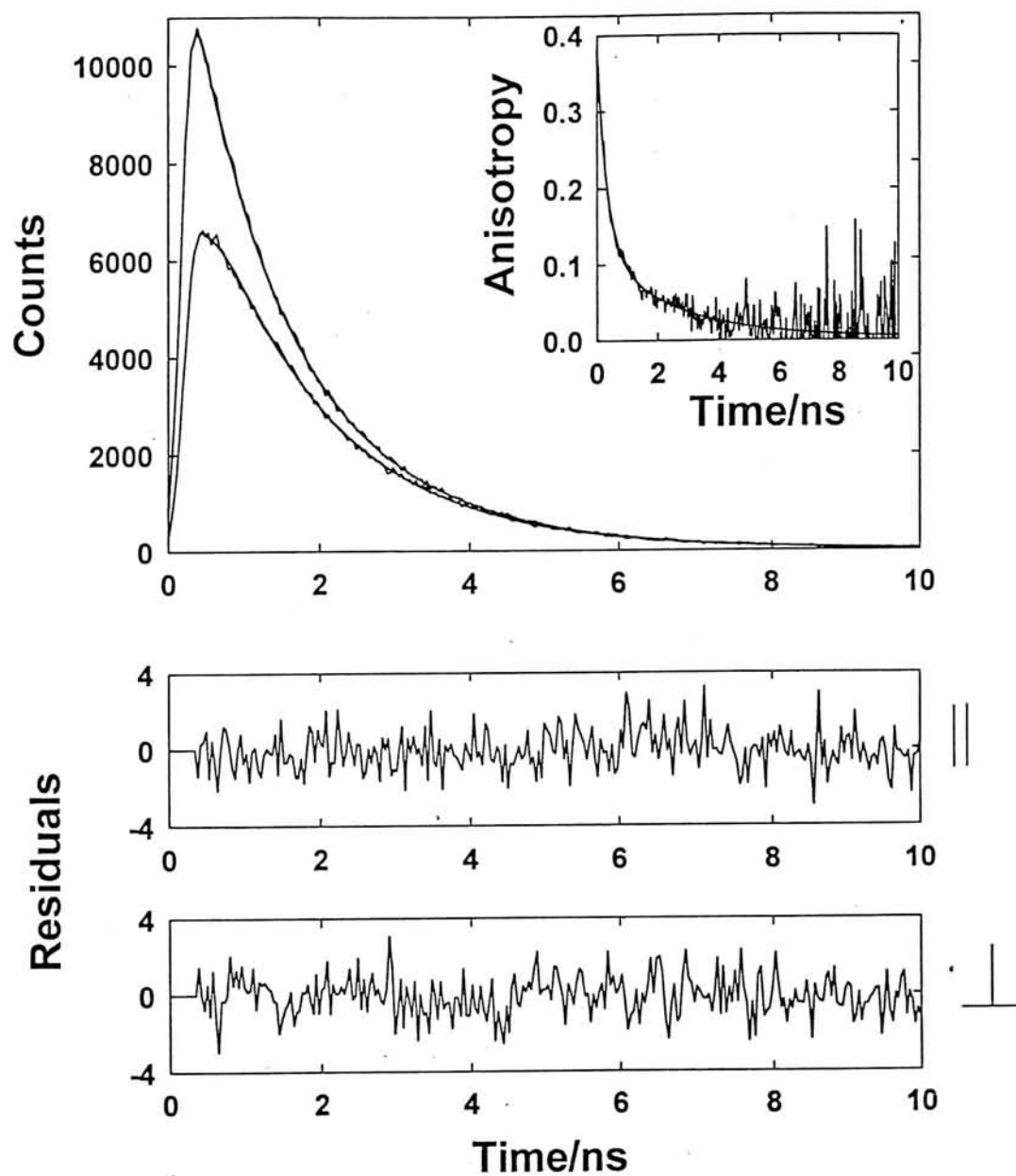


Figure 2.5: Polarized fluorescence decays of Merocyanine 540 in Egg PC. The excitation and emission wavelengths are 570nm and 680nm respectively. The anisotropy decay calculated from the two polarized decays is shown in the inset of the figure. The solid lines show the best fit of the experimental data. The bottom panels show the residuals for the two polarized decays. The results of the anisotropy decay analysis are given in Table 6.1

Chapter 3

Fluorescence Characteristics of Membrane Bound Probes

Most of the biological systems are multi-component and in most cases, the fluorophore exists in two or more distinct environments. The determination of the location, orientation and dynamics of fluorescent probes in membranes requires accurate estimation of fluorescence properties of the membrane-bound probes. Therefore, one needs to employ a method which can give accurately the fluorescence properties related to a particular phase in which we are interested. The first part in this Chapter (section 3.1) describes one such method named as Spectrally Constrained Global Analysis (SCGA) developed for this purpose.

Multiple lifetimes for a fluorophore in a biological system, does not always mean multiple sites of solubilization or locations. Multiple lifetimes for a fluorophore can also arise for the dye located at a single site and undergoing excited state kinetics. The characteristic features of excited state kinetics were examined in the case of a fluorescent probe Nile red in membranes, micelles and viscous solvents and this is described in this chapter (section 3.2)

3.1 Spectrally Constrained Global Analysis (SCGA) of Fluorescence Decays

Most of the biological systems are complex multicomponent systems consisting of aqueous and one or more nonaqueous phases. Though fluorescent probes are often targeted to a specific phase, organelle or compartment it is not uncommon that the fluorophore (especially, the polar or charged dyes) finds its way to the aqueous compartment which is the major compartment in all biological systems. Dynamic and steady state fluorescence measurements of the whole system is a simple or convoluted sum of the spectral and dynamic properties of the targeted component and the aqueous component. Separation of the fluorescence characteristics of the fluorophore in the targeted component is essential for the interpretation of the results.

A popular method of fluorescence analysis is to combine the dynamic time resolved fluorescence data with steady state emission spectrum and obtain Decay Associated Spectra (DAS) for the multicomponent system [113, 46] as described in Chapter 2. Suppose that the fluorescence from a sample originates from n species of structurally distinct fluorophores in an m -component system and the spectra of the n species overlap. The fluorescence emission decays obtained at all emission wavelengths can be used to construct the spectrum of each species if the lifetimes of each species are sufficiently distinct from each other. The fluorescence decays are globally or individually fitted to the n -exponential function and the decay associated spectra are constructed using equation 3.1,

$$I_{\lambda,i} = I_{\lambda} \frac{\alpha_{\lambda,i} \tau_i}{\sum \alpha_{\lambda,j} \tau_j} = I_{\lambda} \frac{\alpha_{\lambda,i} \tau_i}{\tau_{av,\lambda}} \quad (3.1)$$

where $I_{\lambda,i}$ is the intensity of the i th species with a lifetime τ_i , $\alpha_{\lambda,i}$ is the preexponent associated with the lifetime τ_i for the fluorescence decay collected at λ , I_{λ} is the steady state intensity of the sample at λ , and $\tau_{av,\lambda}$ is the amplitude-weighted average lifetime. In practice, the decay associated spectra can be constructed for a maximum of 3-4 species because of the limitations of fitting decay equations containing more than four exponentials.

The conventional method of decay associated spectra fails even for $n=3$ if the lifetimes of the dye in the aqueous phase and nonaqueous phase are close to each other such that they are not resolvable. A method which takes advantage of the differences in the anisotropy decay of the fluorophore in a multicomponent system has been described [116, 117] to obtain anisotropy decay associated spectra (ADAS). A new method was developed which was named as Spectrally Constrained Global Analysis (SCGA) which takes advantage of the fact that the spectrum and lifetime of the dye in the aqueous phase is known.

The method of SCGA has been applied in the case of DODCI in EggPC membrane to obtain the spectra and lifetimes of the fluorescent probe associated with the membrane.

3.1.1 Method:

The experimentally measured fluorescence decay data is a convolution of the instrument response function (IRF) and the intensity decay function (single or multiexponential). The popular method of deconvolution of individual fluorescence decay data is by the method of iterative reconvolution using the IRF and an assumed decay function whose parameters are improved in successive iterations. The iterative procedure for the optimization of the parameters (lifetimes, amplitudes and shift) by the Levenberg-Marquardt algorithm has been described in Chapter 2. Global analysis for the simultaneous fitting of multiple fluorescence decays is a very useful technique for the accurate estimate of the parameters which are common to all the decay data sets [161]. The main advantage of this method is the reduction in the number of free parameters to be optimized. Suppose there are n fluorescence decay data sets available for a sample (such as for example, decays obtained at different emission wavelengths) for which the excited state decay is described by a three exponential decay function, global analysis would treat the three lifetimes as common parameters for all the decay curves. The number of optimized parameters becomes $(4n+3)$ ($3n$ amplitudes, n shift parameters and 3 lifetimes) instead of $7n$ in the case of individual analysis of the n decays. Further reduction in the parameters is possible if amplitude

relationship (that is the spectrum for one component), if known, is incorporated. The method of spectrally constrained global analysis (described below) requires only $(3n+4)$ free parameters to be optimized; that is, a further reduction of $(n-1)$ parameters, and thus increases the confidence limits on the optimized parameters.

Let λ_p be either the peak wavelength or any other wavelength where the emission intensity is not equal to zero. Let $I_p(t)$ be the three exponential decay equation for the emission at λ_p :

$$I_p(t) = \alpha_p e^{-t/\tau_1} + \beta_p e^{-t/\tau_2} + \gamma_p e^{-t/\tau_3} \quad (3.2)$$

where α_p , β_p and γ_p are the amplitudes for the three lifetimes, τ_1 , τ_2 and τ_3 , respectively. Let $I_{s,p}$ be the steady state spectral intensity of the sample at λ_p . The steady state intensity $I_{s,p}$ is a sum of the intensities contributed by the three lifetime components. The intensity associated with τ_1 is given by

$$I_{s,p,\tau_1} = I_{s,p} \frac{\alpha_p \tau_1}{\alpha_p \tau_1 + \beta_p \tau_2 + \gamma_p \tau_3} \quad (3.3)$$

Similarly, the intensity decay equation of the sample at any other wavelength λ_i is given as,

$$I_i(t) = \alpha_i e^{-t/\tau_1} + \beta_i e^{-t/\tau_2} + \gamma_i e^{-t/\tau_3} \quad (3.4)$$

and the steady state intensity associated with τ_1 at λ_i is given by

$$I_{s,i,\tau_1} = I_{s,i} \frac{\alpha_i \tau_1}{\alpha_i \tau_1 + \beta_i \tau_2 + \gamma_i \tau_3} \quad (3.5)$$

Let us assume that the steady state spectrum associated with τ_1 is known (in our case, the fluorophore in water) and the intensities at λ_p and λ_i are $I_{w,p}$ and $I_{w,i}$, respectively. Since the species (and spectrum) associated with τ_1 in membrane system and the dye in water are identical, the following equality holds.

$$\frac{I_{w,i}}{I_{w,p}} = \frac{I_{s,i,\tau_1}}{I_{s,p,\tau_1}} \quad (3.6)$$

Using equations 3.3, 3.5 and 3.6 one gets,

$$\frac{\alpha_i \tau_1}{\alpha_i \tau_1 + \beta_i \tau_2 + \gamma_i \tau_3} = \frac{\alpha_p \tau_1}{\alpha_p \tau_1 + \beta_p \tau_2 + \gamma_p \tau_3} x_i \quad (3.7)$$

where

$$x_i = \frac{I_{w,i}I_{s,p}}{I_{w,p}I_{s,i}} \quad (3.8)$$

The values of x_i can be independently determined from the spectra of the fluorophore in water and in the membrane system. Equation 3.7 can be resolved with respect to α_i :

$$\alpha_i = \frac{\alpha_p x_i}{(1 - x_i)\alpha_p \tau_1 + \beta_p \tau_2 + \gamma_p \tau_3} (\beta_i \tau_2 + \gamma_i \tau_3) \quad (3.9)$$

Thus, the parameter α_i in equation 3.4 is not an independent parameter. α_p is the only amplitude parameter that has to be determined for τ_1 in the global analysis procedure for multiple decays collected at various emission wavelengths.

The fluorescence response $F(t)$ at a given wavelength is a convolution of the instrument response function $R(t)$ and the intensity decay function $I(t)$. Levenberg-Marquardt algorithm for the optimization of the values of free parameters requires the calculation of the convolution of integral $F(t)$ and partial derivatives of $F(t)$ with respect to the free parameters [157].

$$F_i(t) = \int_0^t R(s + \delta) I_i(t - s) ds \quad (3.10)$$

where δ is the shift parameter. The intensity decay function $I_i(t)$ at λ_i is given by equations 3.4 and 3.9. Numerical calculation of $F_i(t)$ and its partial derivatives are performed using recursion relations similar to the ones described by Grinvald and Steinberg [157]. Here the amplitude parameter α_i is a function of all other parameters ($\alpha_p, \beta_p, \gamma_p, \beta_i, \gamma_i, \tau_1, \tau_2$ and τ_3) and hence the recursion relations for the partial derivatives are different from those given by Grinvald and Steinberg [157].

In our case, the intensity decay function $I(t)$ is a three exponential function and hence the convolution integral can be written as [157],

$$F_m = \epsilon \sum_{j=1}^m R_j \sum_{k=1}^3 a_k \exp[-(m - j)\epsilon/\tau_k] \quad (3.11)$$

or

$$F_m = \sum_{k=1}^3 F_m^k \quad (3.12)$$

where F_m^k is the calculated fluorescence response in the m th channel due to the k th exponential component. a_k is the pre-exponential factor in the k th exponential. ϵ is the time duration of one channel.

For trapezoid integration, the following recursion relation can be used to calculate the F_m^k [157].

$$F_m^k = (F_{m-1}^k + 0.5\epsilon a_k R_{m-1}) \cdot \exp(-\epsilon/\tau_k) + 0.5\epsilon a_k R_m \quad (3.13)$$

This equation results in the recursion relations between the partial derivatives of F_m^k with respect to the lifetimes

$$\begin{aligned} \frac{\partial F_m^1}{\partial \tau_1} &= \left[\frac{\partial F_{m-1}^1}{\partial \tau_1} + 0.5\epsilon R_{m-1} \frac{\partial a_1}{\partial \tau_1} + \frac{\epsilon}{\tau_1^2} [F_{m-1}^1 + 0.5\epsilon a_1 R_{m-1}] \right] \exp(-\epsilon/\tau_1) + 0.5\epsilon \frac{\partial a_1}{\partial \tau_1} R_m \\ \frac{\partial F_m^1}{\partial \tau_l} &= \left[\frac{\partial F_{m-1}^1}{\partial \tau_l} + 0.5\epsilon R_{m-1} \frac{\partial a_1}{\partial \tau_l} \right] \exp(-\epsilon/\tau_1) + 0.5\epsilon \frac{\partial a_1}{\partial \tau_l} R_m; \text{ for } l = 2, 3 \\ \frac{\partial F_m^k}{\partial \tau_k} &= \left[\frac{\partial F_{m-1}^k}{\partial \tau_k} + \frac{\epsilon}{\tau_k^2} [F_{m-1}^k + 0.5\epsilon a_k R_{m-1}] \right] \exp(-\epsilon/\tau_k); \text{ for } k = 2, 3 \\ \frac{\partial F_m^k}{\partial \tau_l} &= 0; \text{ for } l \neq k \neq 1 \end{aligned} \quad (3.14)$$

The partial derivatives of a_k with respect to the τ_1 , τ_2 and τ_3 are nonzero only in the case of a_1 which are given below.

$$\begin{aligned} \frac{\partial a_1}{\partial \tau_1} &= -\frac{a_1(1-x_i)\alpha_p}{(1-x_i)\alpha_p\tau_1 + \beta_p\tau_2 + \gamma_p\tau_3} \\ \frac{\partial a_1}{\partial \tau_2} &= a_1 \left[\frac{\beta_i}{\beta_i\tau_2 + \gamma_i\tau_3} - \frac{\beta_p}{(1-x_i)\alpha_p\tau_1 + \beta_p\tau_2 + \gamma_p\tau_3} \right] \\ \frac{\partial a_1}{\partial \tau_3} &= a_1 \left[\frac{\gamma_i}{\beta_i\tau_2 + \gamma_i\tau_3} - \frac{\gamma_p}{(1-x_i)\alpha_p\tau_1 + \beta_p\tau_2 + \gamma_p\tau_3} \right] \end{aligned} \quad (3.15)$$

In the case of λ_p , the partial derivatives of F_m with the amplitudes α_p , β_p and γ_p are

$$\begin{aligned} \frac{\partial F_m}{\partial \alpha_p} &= \frac{F_m^1}{\alpha_p} \\ \frac{\partial F_m}{\partial \beta_p} &= \frac{F_m^2}{\beta_p} \\ \frac{\partial F_m}{\partial \gamma_p} &= \frac{F_m^3}{\gamma_p} \end{aligned} \quad (3.16)$$

and at other wavelengths λ_i , the partial derivatives become

$$\begin{aligned}
 \frac{\partial F_m}{\partial \alpha_p} &= \frac{F_m^1(\beta_p \tau_2 + \gamma_p \tau_3)}{\alpha_p[(1 - x_i)\alpha_p \tau_1 + \beta_p \tau_2 + \gamma_p \tau_3]} \\
 \frac{\partial F_m}{\partial \beta_p} &= -\frac{F_m^1 \tau_2}{[(1 - x_i)\alpha_p \tau_1 + \beta_p \tau_2 + \gamma_p \tau_3]} \\
 \frac{\partial F_m}{\partial \gamma_p} &= -\frac{F_m^1 \tau_3}{[(1 - x_i)\alpha_p \tau_1 + \beta_p \tau_2 + \gamma_p \tau_3]} \\
 \frac{\partial F_m}{\partial \beta_i} &= \frac{F_m^1 \tau_2}{\beta_i \tau_2 + \gamma_i \tau_3} + \frac{F_m^2}{\beta_p} \\
 \frac{\partial F_m}{\partial \gamma_i} &= \frac{F_m^1 \tau_3}{\beta_i \tau_2 + \gamma_i \tau_3} + \frac{F_m^3}{\gamma_p}
 \end{aligned} \tag{3.17}$$

These recursion relations in calculating the partial derivatives of $F(t)$ with the parameters to be optimized were incorporated into the non-linear least squares Levenberg-Marquardt algorithm.

This method is applied in the case of DODCI in Egg PC membrane to separate the fluorescence properties of the dye associated with the aqueous and membrane phases.

3.1.2 Application: DODCI in Egg PC membrane

The fluorescence decay of DODCI is single exponential in water ($\tau = 0.68\text{ns}$ in buffer) and in ethanol ($\tau = 1.07\text{ns}$). A single exponential decay is a clear evidence that only one species is present in these samples. The fluorescence experiments were carried out on DODCI incorporated in Egg PC membranes prepared by sonication in pH 4.3 buffer. When the dye is bound to lipid vesicle membranes the fluorescence decay is not single exponential. The number of distinct fluorescent species cannot be assumed even in this two component system. An elegant method of analysis which does not assume the number of distinct species is the maximum entropy method (MEM) [174]. This method gives distributions of lifetimes and the peaks of distributions are generally consistent with the discrete lifetimes obtained by a discrete exponential analysis. MEM is useful to limit the discrete exponential fit to the number of distribution (gaussian) peaks.

Figure 3.1A and 3.1B show the instrument response functions and the fluorescence decays of DODCI in vesicle membranes at two wavelengths (590 and 690 nm) and the results of analysis by MEM and discrete exponential analysis. The distribution of lifetimes is bimodal with peak positions at 0.66ns and 1.78ns for the fluorescence decay at 590 nm, and 0.90ns and 2.00ns for the decay at 690 nm. The bimodal gaussian-like distribution of lifetimes suggests that a two exponential function would be adequate to fit the data. More positively, there is no evidence for the existence of a third lifetime component. The two lifetimes obtained in the two exponential fits of the decays at 590 nm are 0.65ns and 1.75ns, and at 690 nm are 0.90ns and 2.02ns. In this case the two lifetimes are wavelength dependent. Figure 3.1C shows the distribution of weighted residuals for the two decays which indicate the absence of any fast decay components. Figure 3.2 shows the variation of the two lifetimes with emission wavelength.

Variation of fluorescence lifetime(s) with emission wavelength is a strong evidence that the two-species-two-lifetime model is not correct. It is therefore necessary to consider a three exponential model. Since the fluorescence could be individually fitted adequately to two exponential function, a three exponential fit of individual decays is superfluous. However, a global analysis of multiple fluorescence decays collected at all the emission wavelengths for three lifetimes which are common for all decays is still meaningful. The result of the global analysis gave the three lifetimes as 0.68ns (fixed to that of the aqueous component), 0.74ns and 1.90ns for a $\chi^2_{global}=1.09$. The variation in the amplitudes of the two short lifetime components with the emission wavelength is shown in figure 3.3A and the decay associated spectra for these components are shown in figure 3.3B. The amplitudes for the lifetime components 0.68ns and 0.74ns showed wild oscillations which are unphysical. The reason for the oscillations is presumably due to the closeness of the two lifetimes and as a result the values of the amplitudes for these two lifetimes become highly correlated. That is, a lower value of amplitude 1 is compensated by a higher value of amplitude 2. A straight forward global analysis is therefore not useful when two lifetimes are close to each other.

The solution to this problem lies in finding additional constraints in the global fitting

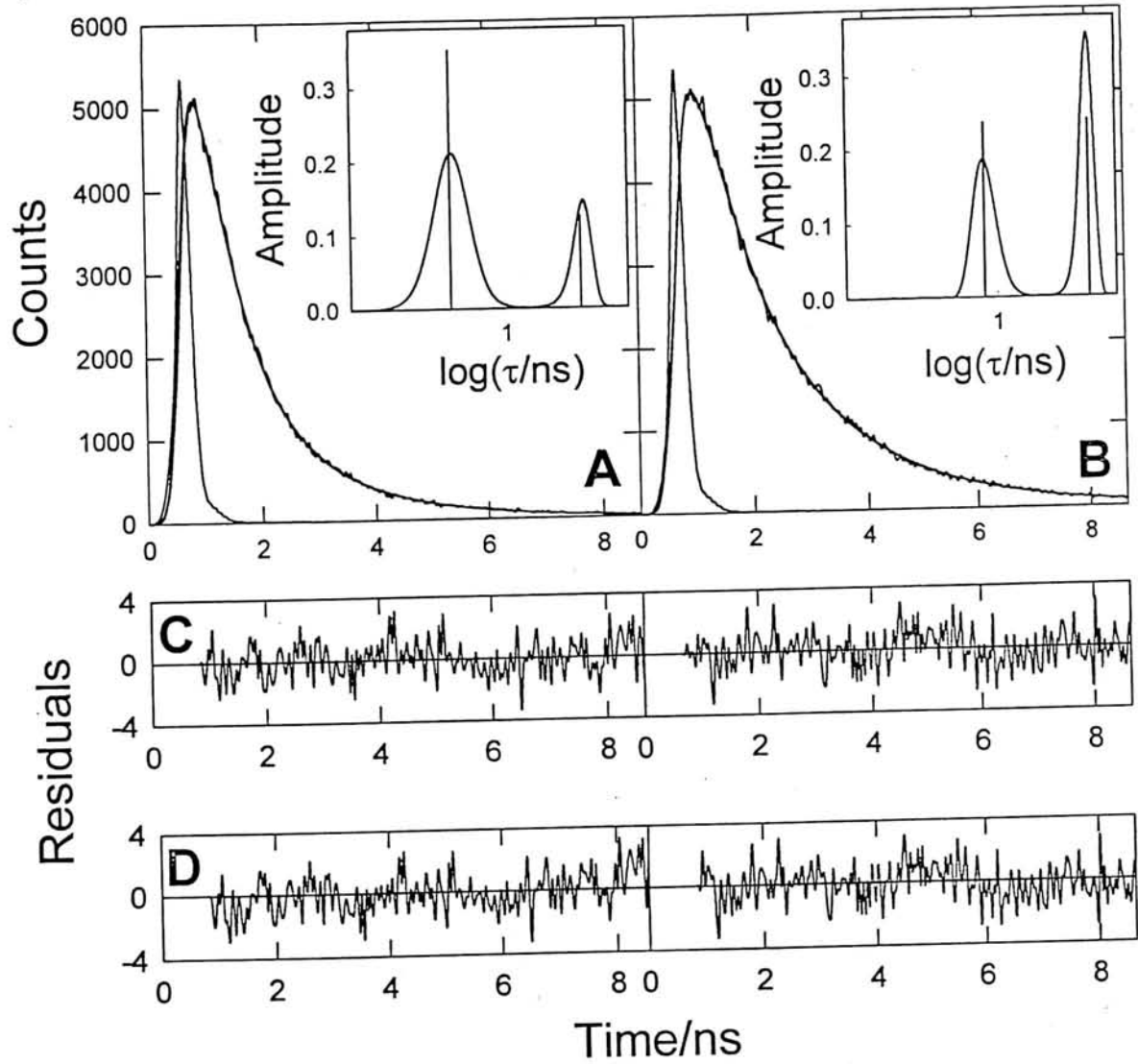


Figure 3.1: Fluorescence decays of DODCI in EggPC vesicles for emission wavelengths at (A) 590 nm and (B) 690 nm. The instrument response functions at the excitation wavelength of 570 nm are also shown. The time per channel was 37.84 ps. The distribution of lifetimes obtained by MEM analysis ($\chi^2 = 1.02$ for 590 nm and $\chi^2 = 1.20$ for 690 nm) and discrete two exponential fit ($\chi^2 = 1.04$ for 590 nm and $\chi^2 = 1.17$ for 690 nm) are shown in the insets. C and D show the distribution of weighted residuals obtained in the case of two exponential fit where all the parameters are kept free and in the case of spectrally constrained global analysis respectively. The obtained mean lifetime values are (C) 590 nm: $\tau_{av} = 0.94\text{ns}$, $\chi^2 = 1.04$; 690 nm: $\tau_{av} = 1.42\text{ns}$, $\chi^2 = 1.17$; (D) 590 nm: $\tau_{av} = 0.96\text{ns}$, $\chi^2 = 0.97$; 690 nm: $\tau_{av} = 1.42\text{ns}$, $\chi^2 = 1.08$.

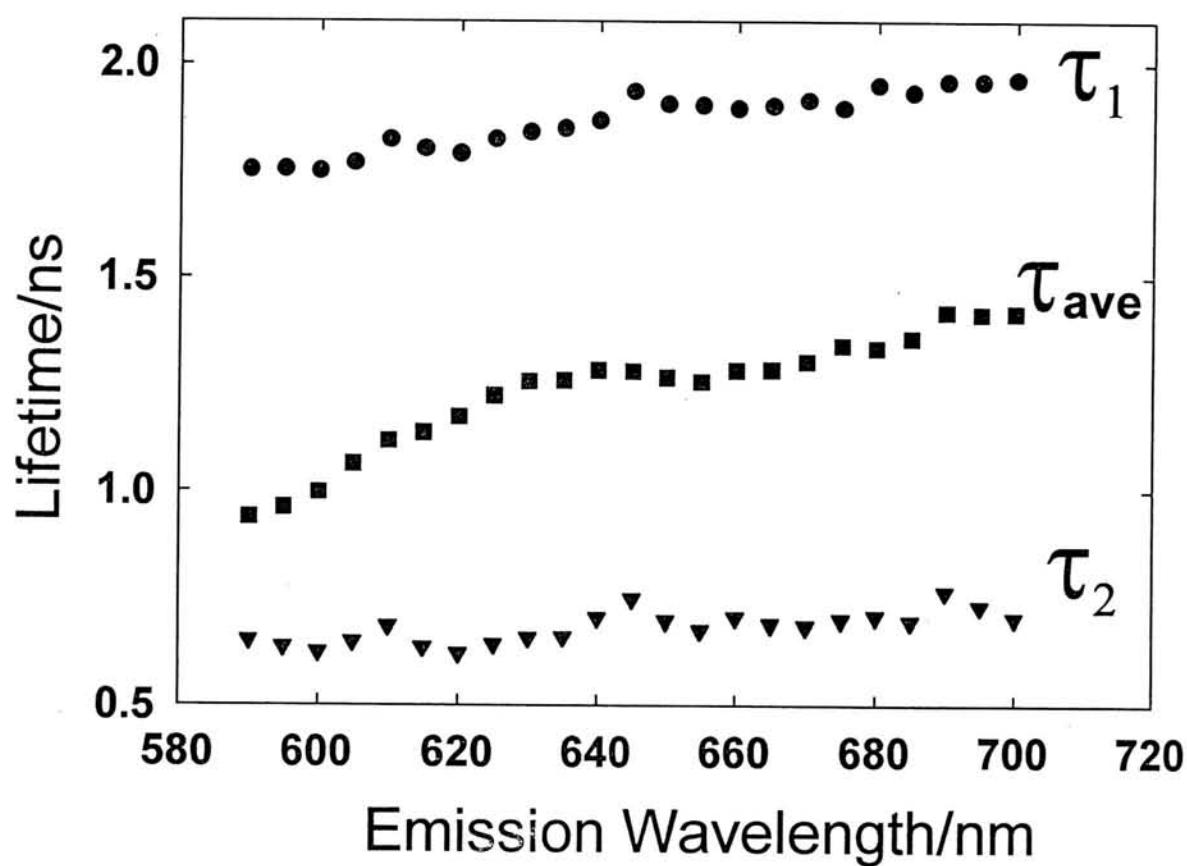


Figure 3.2: Variation of the two lifetimes and the average lifetime obtained in the discrete two exponential fit of the fluorescence decays of DODCI in EggPC vesicles with emission wavelength.

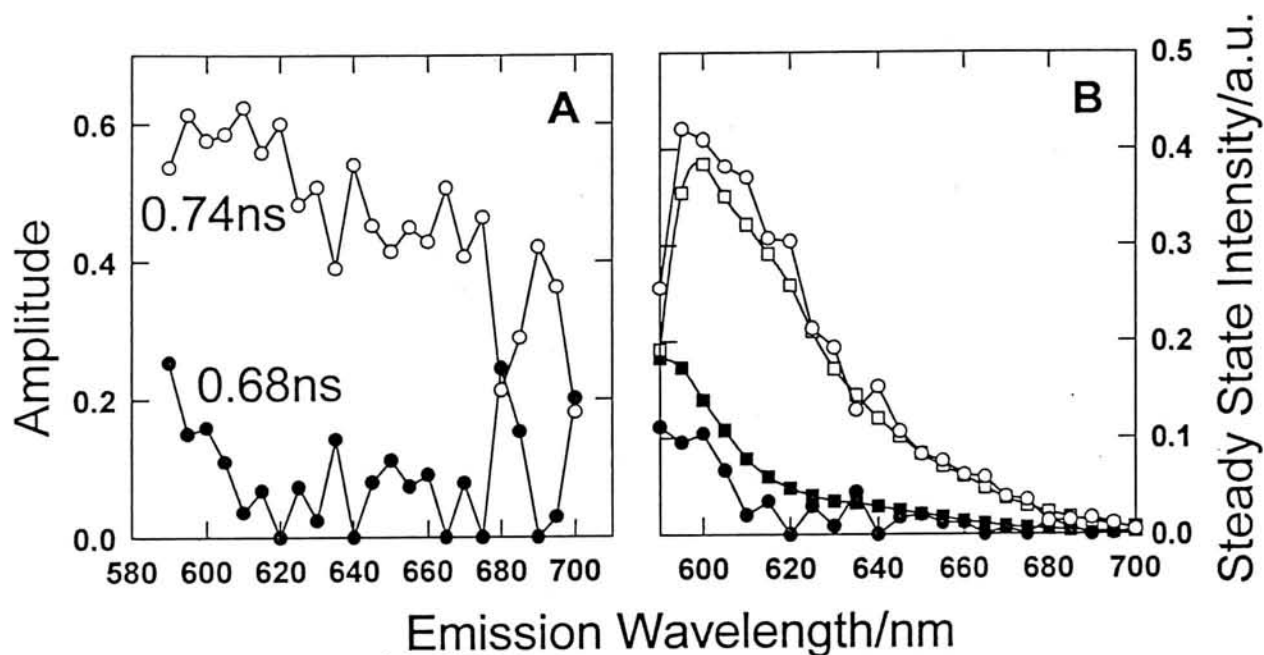


Figure 3.3: (A) The amplitudes of the two short lifetime components obtained in a global analysis of 23 fluorescence decays collected at different emission wavelengths. The unphysical oscillations in the amplitudes for lifetimes 0.68ns and 0.74ns are due to correlation effects due to the proximity of the lifetimes. (B) Decay Associated Spectra for $\tau_1 = 0.68\text{ns}$ (aqueous component, solid symbols) and τ_2 (membrane-bound component, hollow symbols). The circles indicate the spectra obtained using the global analysis where the lifetime of DODCI in water is fixed. The squares indicate the spectra obtained with the spectrally constrained global analysis.

strategy. In the case of polar fluorescent probes such as DODCI (and similar potential sensing membrane cationic probes [48]) in membrane systems one of the lifetime components may be expected to be from the dye in the aqueous phase. The presence of a significant fraction of the dye in the aqueous phase could be confirmed by plotting the steady state fluorescence anisotropy versus lipid concentration, as shown in figure 3.4, for DODCI and nilered. In this experiment, the dye concentration was kept constant and the steady state anisotropy values were measured as a function of the lipid concentration. If the dye exists completely in the aqueous phase, the steady state anisotropy will be less because the rotation of the dye is very fast in low viscous solvents such as water and leads to a fast depolarization. On the other hand, if the dye exists completely in the membrane phase, the steady state anisotropy will be high because of the hindered rotation of the dye and of high viscosity of the surrounding medium. The partitioning of the dye into the aqueous and membrane phases depends on the partition coefficient and the relative amounts of the two phases in the system. As we increase the lipid concentration, more and more dye gets partitioned into the membrane phase and hence the steady state anisotropy steadily increases and reaches a constant value. In the case of nilered, the dye is completely solubilized in the membrane even at lipid concentration of 0.01 mg/ml and the steady state anisotropy attains a constant value above this concentration. On the other hand, the binding of DODCI to the membrane is much less and therefore the steady state anisotropy does not saturate below 0.05 mg/ml. For the experiments described here, the lipid concentration used was 0.1 mg/ml and the steady state anisotropy plot shows that the contribution of the dye present in the aqueous phase to the total fluorescence anisotropy is small but significant. Time resolved fluorescence anisotropy measurements also give evidence for the presence of DODCI in the aqueous phase. Figure 3.5 shows the time resolved fluorescence anisotropy decays collected as a function of the emission wavelength. A sharp anisotropy component can be clearly seen in the anisotropy decay collected at lower emission wavelengths and it slowly disappears with the increase of the emission wavelength. This indicates that a significant fraction of DODCI is present in the aqueous phase whose contribution to the total fluorescence properties of the system

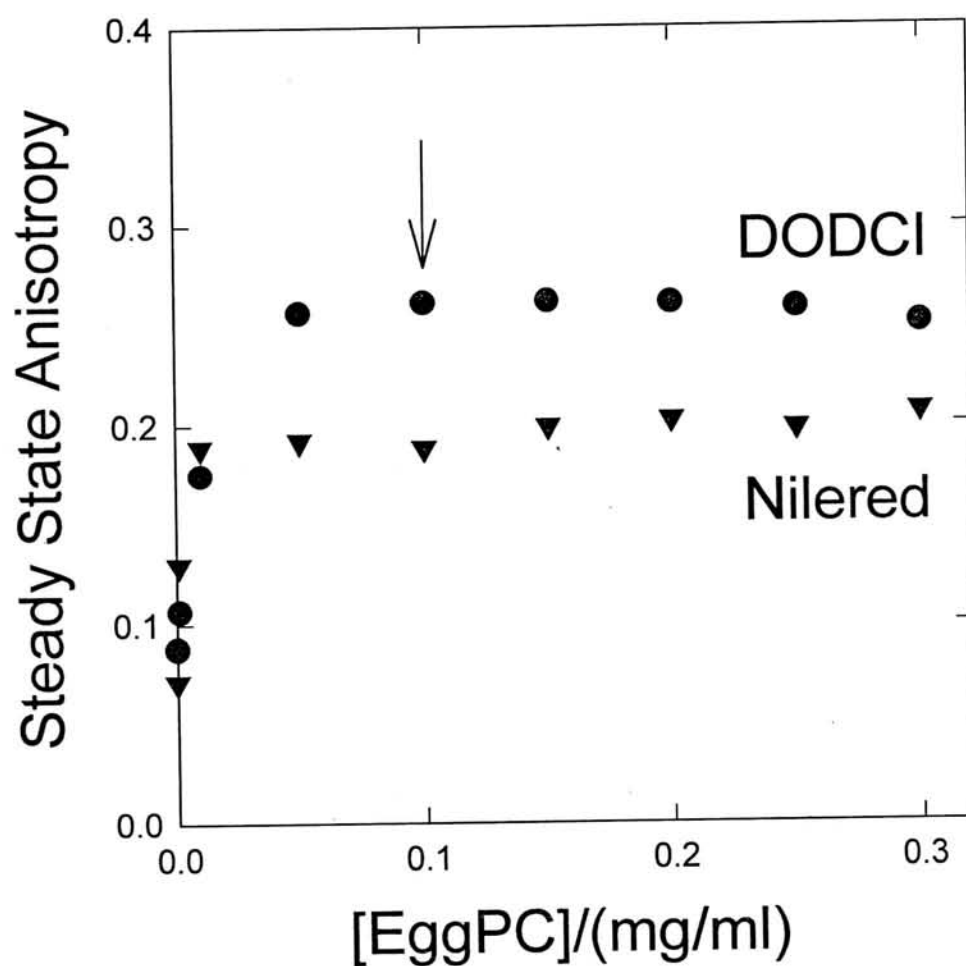


Figure 3.4: Variation of steady state anisotropy of DODCI and Nilered as a function of lipid concentration. The concentration of lipid used in the experiments where the spectra and lifetimes of the membrane bound dye were determined using the method of SCGA is indicated by an arrow.

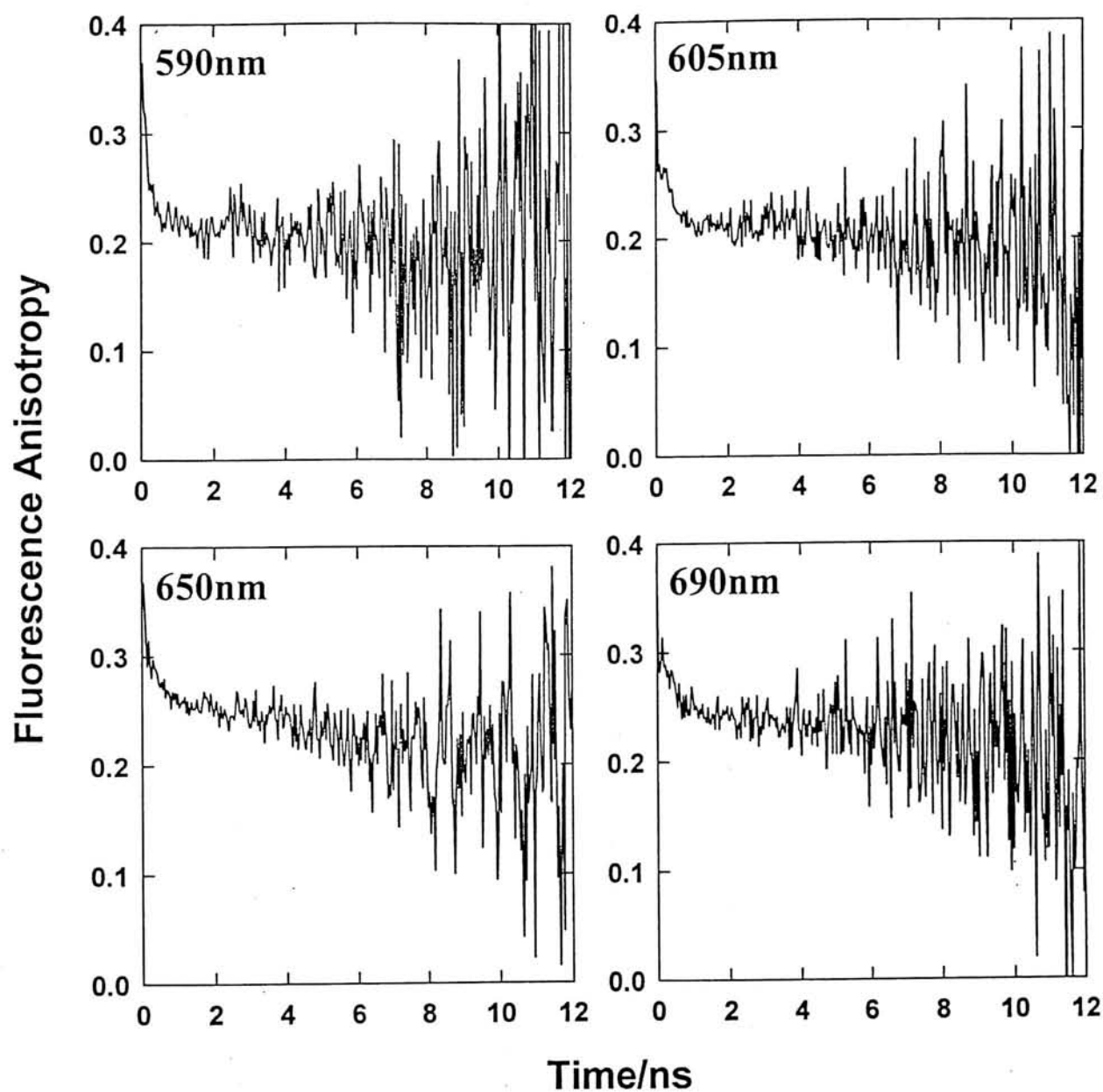


Figure 3.5: Time resolved fluorescence anisotropy decays for DODCI in Egg PC collected as a function of the emission wavelength. The sample was excited at 570nm and the respective emission wavelengths are indicated on the plots

is significant at lower emission wavelengths. The discrete exponential analysis clearly shows that the short lifetime obtained at lower emission wavelengths matches with that of the dye in water. The emission spectrum of DODCI in buffer shows that the emission maximum is at 590 nm and there is negligible fluorescence at 690 nm. The fluorescence parameters (lifetime and spectrum) for the dye in the aqueous phase is known and these can be included in the spectrally constrained global analysis as described in the previous section (section 3.1.1).

The analysis of the fluorescence decays by the method of SCGA described here in which the spectrum and lifetime (0.68ns) of DODCI in the aqueous phase were fixed gave the remaining two lifetimes as 0.84ns and 1.97ns. Figure 3.1D shows the distribution of weighted residuals for the two decays (Figure 3.1A and 3.1B) obtained in the spectrally constrained global analysis. It may be noted that the decay associated spectrum for the membrane-bound component (0.84ns) is smooth in contrast to the spectrum associated with 0.74ns component obtained in global analysis in which only the lifetime of the aqueous component (0.68ns) was fixed (Figure 3.3B). Figure 3.6 shows the decay associated spectra for the three lifetimes. The species with lifetimes of 0.84 and 1.97ns are attributed to two structural variations of the dye in the membrane based on the effects of the external viscosity and refractive index on the fluorescence lifetimes and this will be described more in detail in Chapter 4.

The above experimental example illustrates the usefulness of SCGA in identifying the decay-associated-spectra of the membrane-bound dye. The method of Spectrally Constrained Global Analysis (SCGA) described here can be used in any multicomponent system to obtain the fluorescence properties of the fluorophore in a particular component if the fluorescence properties of the other components are known. This method will be useful in most biological fluorescence studies if the fluorescent probe (especially the water soluble one) is present or suspected to be present in the aqueous fraction.

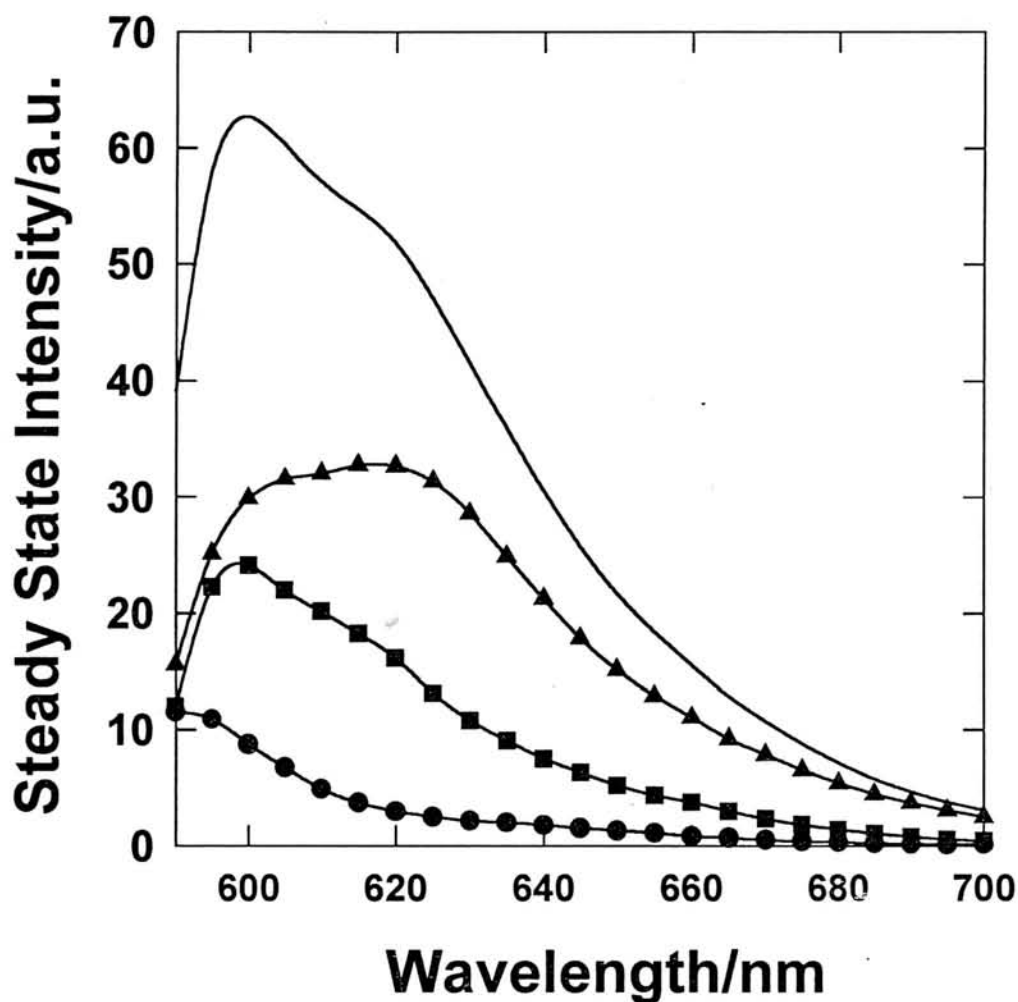


Figure 3.6: The decay associated spectra for the three lifetime components (\circ , $\tau_w = 0.68\text{ns}$; \square , $\tau_{short} = 0.84\text{ns}$ and \triangle , $\tau_{long} = 1.97\text{ns}$, $\chi^2_{global}=1.03$) obtained by the spectrally constrained global analysis method described in this paper. The solid line is the steady state spectrum of DODCI in Egg PC vesicles prepared in pH 4.3 buffer.

3.2 Excited State Kinetics of Nile red in Membranes and Micelles

Observation of multiple lifetimes in a biological system may not be always from the dye located in multiple sites. A dye located at a single site can also give rise to multiple lifetimes if the dye undergoes excited state kinetics. Hence before assigning the multiple lifetimes to multiple sites, one should make sure the absence of excited state kinetics as a cause of multiple lifetimes. Excited state kinetics was observed in the case of Nile red which exhibits dual lifetimes, arising from the initially excited species and a product of the excited state kinetics.

Nile red is a commonly employed hydrophobic dye in the study of biological systems such as membranes [180, 181], micelles [105, 182], reverse micelles [91], proteins [183, 184] and for staining biological tissues [185]. This dye has also been widely used in the studies of various organized assemblies such as zeolites [186], liquid crystals [187], LB films [188] and planar supported membranes [189]. The fluorescence properties of Nile red highly depend upon the polarity of the probe environment [88, 89]. A Twisted Intramolecular Charge Transfer (TICT) state has been proposed to account for the polarity sensitive fluorescence of Nile red [186, 190]. However, unlike most other TICT molecules, dual fluorescence spectra was not observed and hence the TICT of Nile red was proposed to be nonemissive [186]. In all the above reports, a single emissive state was assumed to explain the fluorescence properties of Nile red. Interestingly, excited state kinetics of Nile red has not been discussed in any of the above studies. Our experiments show that Nile red in vesicles, micelles and viscous solvents show wavelength dependent fluorescence intensity decay because of the excited state kinetics.

Fluorescence measurements were carried out on Nile red incorporated in Egg PC vesicles and SDS micelles in 10mM NaH_2PO_4 pH 7.4 Buffer. The Egg PC liposomes were prepared by sonication. The lipid concentration used in these experiments was 0.3 mg/ml (0.42 mM). SDS micelles were prepared by stirring the surfactant in warm deionized water for 1 hr. The dye ($0.77\mu\text{M}$) was added from the stock solution made in ethanol to

the samples and kept overnight. The final sample contains less than 1% v/v ethanol. The dye to lipid ratio was kept at 1:543 and the dye to micelle ratio was kept at 1:1272. All measurements were carried out in air-saturated solutions at room temperature ($25 \pm 1^\circ\text{C}$). All solvents used in the fluorescence studies were of spectroscopic grade and tested to be free of any fluorescence impurities. Fluorescence experiments were carried out at the excitation wavelength of 570nm.

3.2.1 Nile red in Egg PC vesicles and SDS micelles

The fluorescence decay of Nile red in Egg PC vesicles is strongly emission wavelength dependent. The fluorescence emission maximum is at 630nm. Figure 3.7 shows the fluorescence decays obtained at three emission wavelengths 580nm, 630nm and 750nm. The fluorescence decay collected at the blue end of the emission spectrum (580nm) shows a short lifetime component in addition to the long lifetime component whereas the fluorescence decay collected at the red end of the emission spectrum (750nm) shows a rising component. Hence a single fluorescence lifetime cannot explain the fluorescence decay kinetics of Nile red in Egg PC vesicles at all emission wavelengths. A two exponential global analysis of multiple fluorescence decays collected as a function of emission wavelength from 580nm to 750nm gave two lifetimes 1.26ns and 3.88ns with the amplitudes varying with the emission wavelength.

The fluorescence of Nile red in SDS micelles is also emission wavelength dependent as in the case of Nile red in Egg PC vesicles. The emission maximum occurs at 640nm for Nile red in SDS. The global analysis of multiple fluorescence decays collected at wavelengths ranging from 585nm to 750nm fit to a two-exponential function with the lifetimes 0.68ns and 2.53ns with the amplitudes varying with the emission wavelength.

Are the observed two lifetimes in the case of Nile red in Egg PC vesicles and SDS micelles from the dye present at two different sites? Before searching for the origin of two lifetimes, the role of any fluorescence impurity giving rise to the second lifetime was ruled out. The purity of Nile red was checked using thin-layer chromatography on silica plates

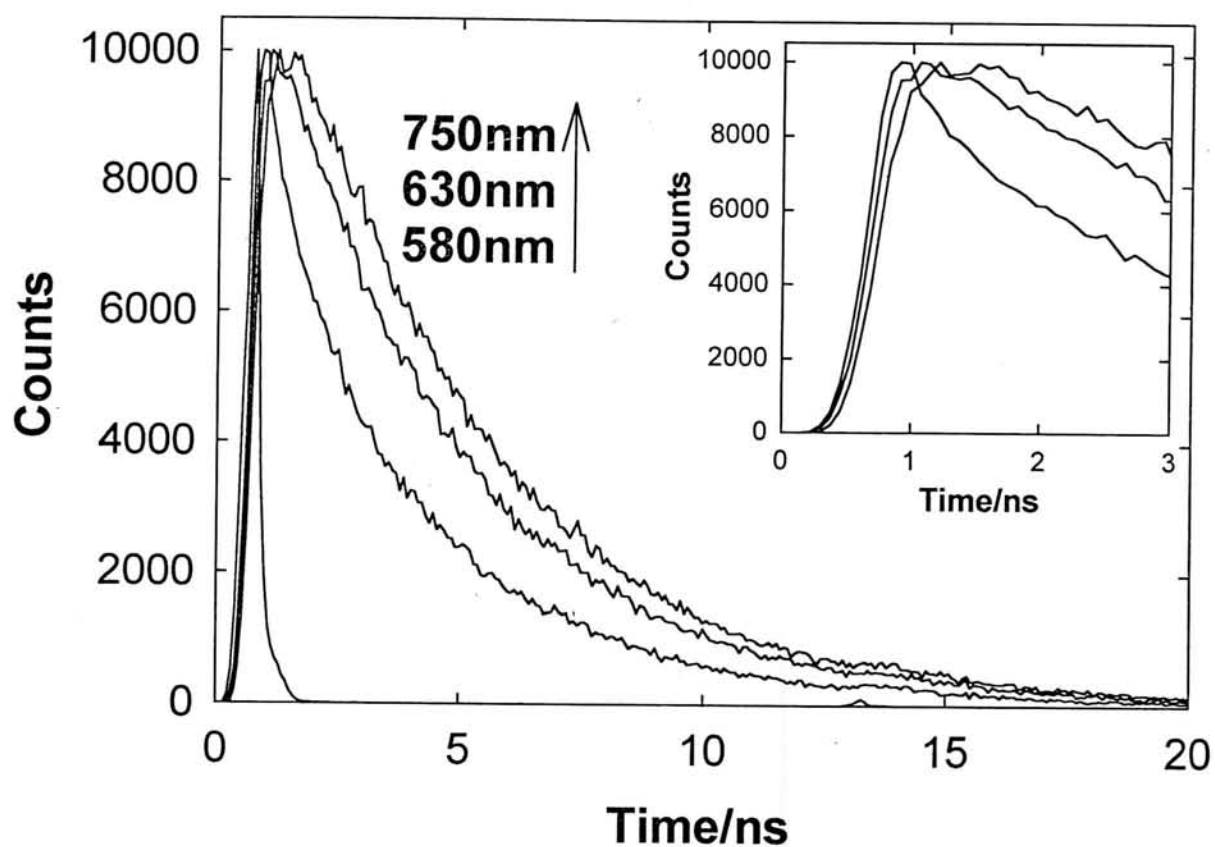


Figure 3.7: Fluorescence intensity decays of Nile red (0.77 μ M) in Egg PC (0.42 mM) at the emission wavelengths 580 nm, 630 nm and 750 nm with the excitation wavelength 570 nm. The Instrument Response Function (IRF) is also shown in the figure. The inset shows the three fluorescence decays plotted over a more expanded time scale to indicate the differences in the rising edges.

in different solvent mixtures (chloroform, acetonitrile-water, acetonitrile-tetrahydrofuran (THF), chloroform-methanol mixtures) as described in [90]. Single spots were observed on silica plates indicating that Nile red is pure. Nile red in Methanol exhibits single exponential fluorescence decay at all emission wavelengths ranging from 580nm to 750nm with a lifetime of 2.88ns. The single exponential decay confirms the purity of the sample and the presence of a single emitting species in the excited state.

Figure 3.8 shows the variation of the amplitudes of the short and long lifetimes observed in the case of Nile red in Egg PC vesicles and SDS micelles. The amplitudes of the short lifetime become negative for the emission wavelengths $> 630\text{nm}$ and 640nm in the case of Nile red in Egg PC vesicles and SDS micelles respectively. The negative amplitudes for one of the two lifetimes rules out the possibility that these two lifetimes are from two different sites of the dye. This can only be explained if the fluorophore undergoes excited state kinetics during the lifetime of the initially excited state leading to a new emitting state. Analytical equations were derived for the fluorescence intensity decays and species associated spectra (SAS) in the case of a two state kinetics in the excited state.

3.2.2 Fluorescence decay kinetics and Species Associated Spectra

Figure 3.9 shows the model for the excited state kinetics. Let A^* be the initially excited species and B^* be the newly formed species. In the case of irreversible reaction of A^* (Fig. 3.9A), let k_A and k_B represent the rate constants (radiative and nonradiative processes) at which the species A^* and B^* emit and k_{AB} be the rate of formation of B^* from A^* . In this case, the rate of change of the concentrations of A^* and B^* becomes

$$\begin{aligned}\frac{d[A^*]}{dt} &= -(k_A + k_{AB})[A^*] \\ \frac{d[B^*]}{dt} &= k_{AB}[A^*] - k_B[B^*]\end{aligned}\tag{3.18}$$

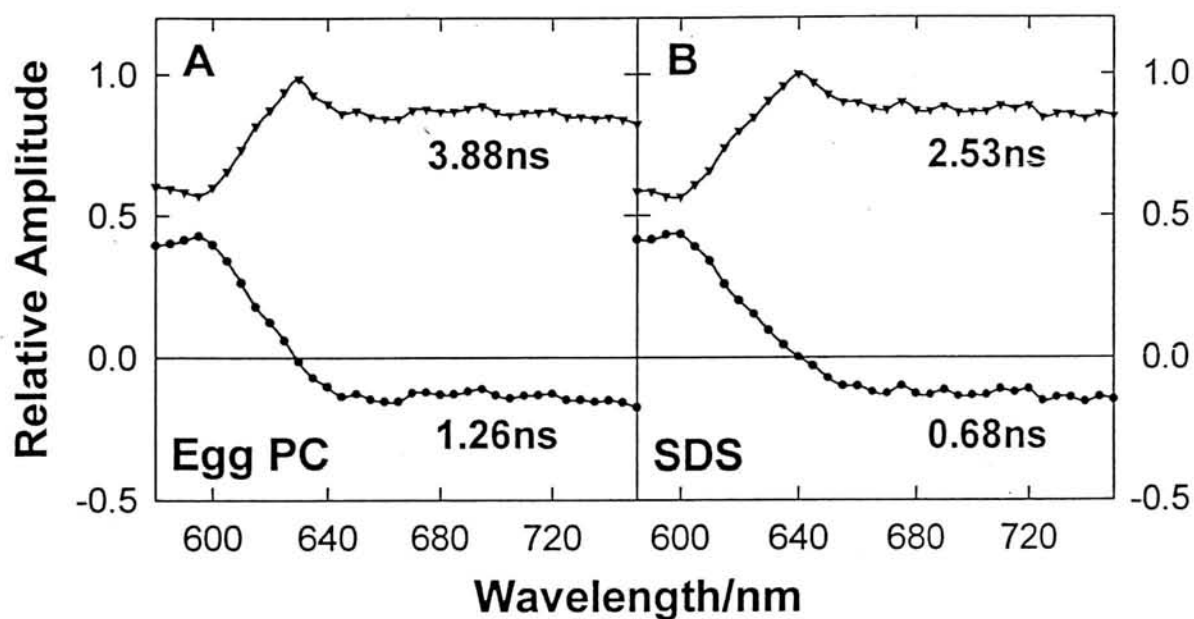
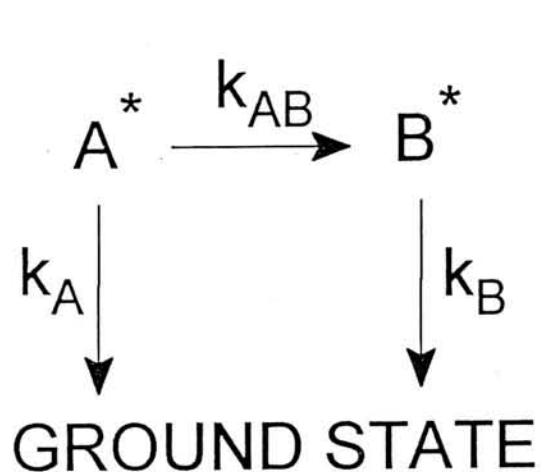
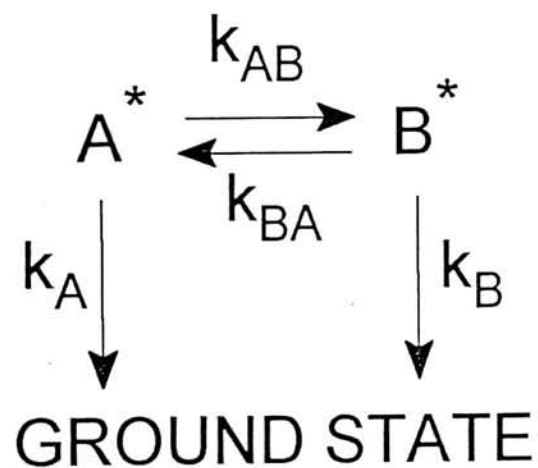


Figure 3.8: Relative amplitudes of the two lifetimes obtained by the global analysis of multiple fluorescence intensity decays collected at different emission wavelengths with the excitation wavelength 570nm in the case of Nile red ($0.77\mu\text{M}$) in (A) Egg PC (0.42mM) vesicles and (B) SDS (69mM) micelles. The amplitudes were normalized such that the sum of the absolute values becomes one.



Scheme A



Scheme B

Figure 3.9: Model for the excited state kinetics of Nile red: (A) Irreversible reaction in the excited state and (B) Reversible reaction in the excited state. A^* and B^* represent the initially excited and newly formed species in the excited state.

These equations were solved using the standard Laplace Transform method [191]. With the condition that the initial concentration of B^* is zero, the solutions become

$$\begin{aligned} [A^*]_t &= [A^*]_0 \exp[-(k_A + k_{AB})t] \\ [B^*]_t &= \frac{k_{AB}[A^*]_0}{k_B - (k_A + k_{AB})} [\exp[-(k_A + k_{AB})t] - \exp[-k_B t]] \end{aligned} \quad (3.19)$$

The intensity at a particular wavelength λ becomes

$$I_\lambda(t) = a_\lambda[A^*]_t + b_\lambda[B^*]_t \quad (3.20)$$

where a_λ and b_λ are the wavelength dependent spectral contours of A^* and B^* . Integration of these over the entire emission spectrum give the fluorescence rate constants of A^* and B^* . From the two equations 3.19 and 3.20 and with $\tau_A = (k_A + k_{AB})^{-1}$ and $\tau_B = k_B^{-1}$, the equation for wavelength dependent fluorescence intensity decay becomes

$$I_\lambda(t) = [A^*]_0 \left[\left(a_\lambda + \frac{b_\lambda k_{AB} \tau_A \tau_B}{\tau_A - \tau_B} \right) \exp\left(-\frac{t}{\tau_A}\right) - \frac{b_\lambda k_{AB} \tau_A \tau_B}{\tau_A - \tau_B} \exp\left(-\frac{t}{\tau_B}\right) \right] \quad (3.21)$$

When the lifetime of the initially excited species τ_A is longer than that of the newly formed species τ_B , equation 3.21 predicts negative amplitudes for the short lifetime component τ_B at all emission wavelengths. In the other case where $\tau_B > \tau_A$, the negative amplitudes for the short lifetime component τ_A occur at longer emission wavelengths where $a_\lambda < b_\lambda k_{AB} \tau_A \tau_B / (\tau_B - \tau_A)$, i.e., at the wavelengths where the emission from the newly formed species dominates over the emission from the initially excited species.

In the case of Nile red in Egg PC vesicles and SDS micelles, negative amplitudes for the short lifetime component occurs only at the long emission wavelengths. Hence, in both these cases, the short lifetime can be associated with that of the initially excited species and the long lifetime with that of the newly formed species.

The spectra associated with the two species A^* and B^* can be obtained as

$$\begin{aligned} SAS_A(\lambda) &= \frac{I_{SS}(\lambda)}{\tau_{ave}(\lambda)} \int_0^\infty a_\lambda[A^*]_t dt \\ SAS_B(\lambda) &= \frac{I_{SS}(\lambda)}{\tau_{ave}(\lambda)} \int_0^\infty b_\lambda[B^*]_t dt \end{aligned} \quad (3.22)$$

where $\tau_{ave}(\lambda) = \int_0^\infty I_\lambda(t)dt$. If α_A and α_B represent the amplitudes of the two exponentials in the intensity decay equation 3.21 with the time constants τ_A and τ_B , the equations for SAS (Species Associated Spectra) of A and B becomes

$$\begin{aligned} SAS_A(\lambda) &= \frac{(\alpha_A(\lambda) + \alpha_B(\lambda))\tau_A I_{ss}(\lambda)}{\tau_{ave}(\lambda)} \\ SAS_B(\lambda) &= \frac{\alpha_B(\tau_B - \tau_A)I_{ss}(\lambda)}{\tau_{ave}(\lambda)} \end{aligned} \quad (3.23)$$

These equations show that for determining species associated spectra of A^* and B^* , there is no need to know the values of the individual rate constants k_A , k_B and k_{AB} or the values of a_λ and b_λ .

The species associated spectra of the two species were resolved from the steady state spectra and the wavelength-dependent amplitudes of the two lifetimes using equation 3.23 in the case of Nile red in Egg PC vesicles and SDS micelles. These are as shown in figure 3.10. The species associated spectra of A^* and B^* differ by about 5 to 10nm in their emission maxima.

The analytical equations for the fluorescence intensity decay and the SAS were solved when there is a reversible reaction between A^* and B^* . The kinetic scheme for this is shown in figure 3.9B. Let k_A and k_B represent the rate at which the two species A^* and B^* emit and k_{AB} and k_{BA} represent the forward and backward rates in the reaction equilibrium between A^* and B^* . In this case, the rates of change of $[A^*]$ and $[B^*]$ can be written as

$$\begin{aligned} \frac{d[A^*]}{dt} &= -(k_A + k_{AB})[A^*] + k_{BA}[B^*] \\ \frac{d[B^*]}{dt} &= k_{AB}[A^*] - (k_B + k_{BA})[B^*] \end{aligned} \quad (3.24)$$

The solutions of the above coupled differential equations, as solved by the laplace transform method, with the initial condition $[B^*]_0=0$ are

$$\begin{aligned} [A^*]_t &= \frac{[A^*]_0}{2c} \left[(c + dk) \exp \left[-\frac{(sk + c)t}{2} \right] + (c - dk) \exp \left[-\frac{(sk - c)t}{2} \right] \right] \\ [B^*]_t &= \frac{[A^*]_0 k_{AB}}{c} \left[-\exp \left[-\frac{(sk + c)t}{2} \right] + \exp \left[-\frac{(sk - c)t}{2} \right] \right] \end{aligned} \quad (3.25)$$

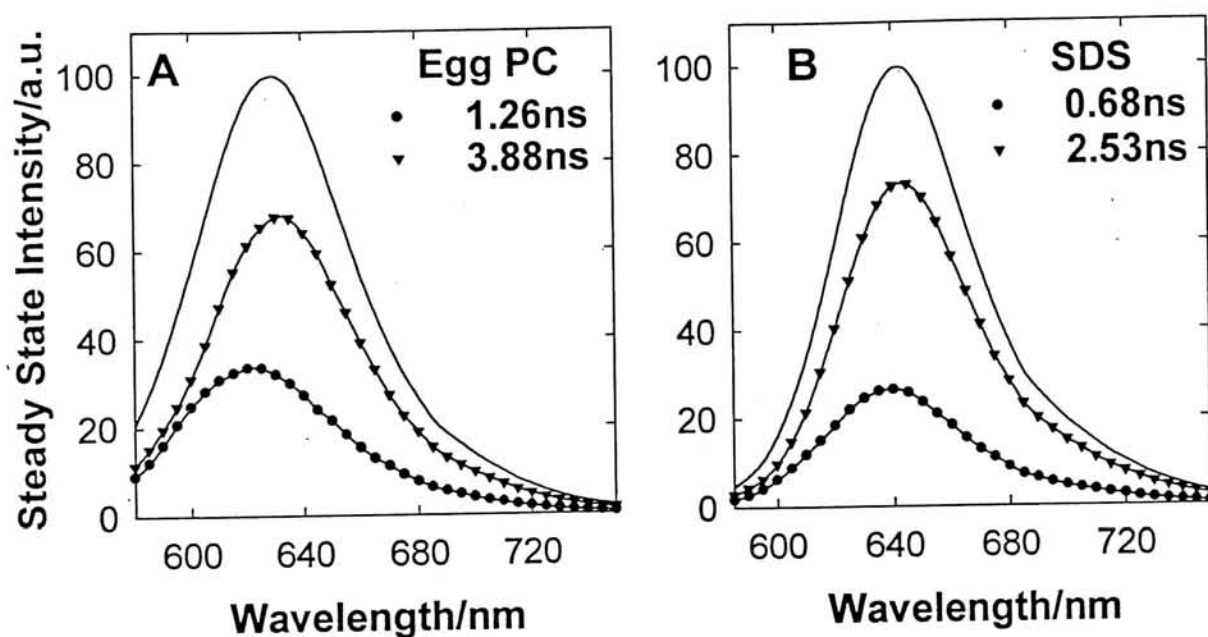


Figure 3.10: Species associated spectra of Nile red in (A) Egg PC vesicles and (B) SDS micelles in the case of irreversible reaction in the excited state (Figure 3.9A). Here 1.26ns and 3.88ns represent the lifetimes of the initially excited species and the newly formed species in the case of Nile red in Egg PC vesicles whereas in the case of Nile red in SDS micelles, 0.68ns and 2.53ns corresponds to the lifetimes of the initially excited and newly formed species respectively.

with

$$sk = k_A + k_{AB} + k_B + k_{BA}$$

$$dk = (k_A + k_{AB}) - (k_B + k_{BA})$$

and

$$c = (k_A^2 + k_{AB}^2 + k_B^2 + k_{BA}^2 + 2k_A k_{AB} - 2k_A k_B - 2k_A k_{BA} - 2k_{AB} k_B + 2k_{AB} k_{BA} + 2k_B k_{BA})^{\frac{1}{2}}$$

Here, the decay of the two species A* and B* is double exponential at all emission wavelengths. With these solutions, the intensity decay equation is

$$I_\lambda(t) = [A^*]_0 \left[\left(\frac{a_\lambda(c + dk)}{2c} - \frac{b_\lambda k_{AB}}{c} \right) \exp\left(-\frac{(sk + c)t}{2}\right) + \left(\frac{a_\lambda(c - dk)}{2c} + \frac{b_\lambda k_{AB}}{c} \right) \exp\left(-\frac{(sk - c)t}{2}\right) \right] \quad (3.26)$$

The two decay constants in the intensity decay equation can not be associated with any individual species and all the four rate constants affect the decay constants. If α_1 and α_2 represent the amplitudes and τ_1 and τ_2 represent the decay constants in the intensity decay equation 3.26, the species associated spectra of the two species A* and B* become

$$SAS_A(\lambda) = \frac{(\alpha_1(\lambda) + \alpha_2(\lambda))(k_B + k_{BA})\tau_1\tau_2 I_{ss}(\lambda)}{\tau_{ave}(\lambda)}$$

$$SAS_B(\lambda) = I_{ss}(\lambda) - SAS_A(\lambda) \quad (3.27)$$

For resolving the species associated spectra of the initially excited and newly formed species, one needs to know the value of $(k_B + k_{BA})$.

Lofroth [169] suggested a method to determine the value of $(k_B + k_{BA})$. From equation 3.27, one can write

$$(k_B + k_{BA}) = \frac{SAS_A(\lambda)\tau_{ave}(\lambda)}{(\alpha_1(\lambda) + \alpha_2(\lambda))\tau_1\tau_2 I_{ss}(\lambda)} \quad (3.28)$$

and at the wavelengths where B* emission is negligible, $SAS_A(\lambda) \approx I_{ss}(\lambda)$ and hence

$$(k_B + k_{BA}) \approx \frac{\tau_{ave}(\lambda)}{(\alpha_1(\lambda) + \alpha_2(\lambda))\tau_1\tau_2} \quad (3.29)$$

Hence a quantity $(k_B + k_{BA})^{app}$ is defined with the above definition (equation 3.29) and from the plot of $(k_B + k_{BA})^{app}$ with the emission wavelength λ , the value of $(k_B + k_{BA})$ is

obtained as the limiting value at the short end of the emission spectrum. A constant value for $(k_B + k_{BA})^{app}$ in the blue end of the spectrum confirms the assumption that the emission from B^* is negligible compared to that of A^* in this region. $(k_B + k_{BA})$ can not be determined in the cases where the spectra of A^* and B^* overlap at all emission wavelengths.

Figure 3.11 shows the plots of $(k_B + k_{BA})^{app}$ as a function of the emission wavelength in the case of Nile red in Egg PC vesicles and SDS micelles. The value of $(k_B + k_{BA})^{app}$ approaches a constant value as we go towards lower emission wavelengths and this value is taken as $(k_B + k_{BA})$ for determining SAS. The species associated spectra for Nile red in Egg PC vesicles and SDS micelles are as shown in figure 3.11. The SAS of the two species differs by about 5 to 10nm in their emission maxima as in the case of irreversible reaction in the excited state (Figure 3.10).

Although the emission maxima of the two species A^* and B^* are almost same whether the excited state kinetics is reversible or irreversible, the relative spectral intensities of the two species get interchanged based on the kinetics assumed (Figures 3.10 and 3.11). That means, in the case of an irreversible reaction between A^* and B^* , the spectral intensity of B^* is higher than that of A^* . In the other case, i.e., in the case of a reversible reaction between A^* and B^* , the spectral intensity of A^* is higher than that of B^* . The possible explanation for this inversion is that in the case of reversible reaction, B^* repopulates A^* through a back reaction.

It is not possible to identify whether the observed excited state kinetics in the case of Nile red is irreversible or reversible, solely based on the fluorescence results.

3.2.3 Nile red in viscous solvents

Are the observed excited state kinetics characteristic of lipid or surfactant media or characteristic of viscous media? Fluorescence measurements were carried out on Nile red in two viscous solvents 1-Octanol and Glycerol to verify this.

The fluorescence intensity decay of Nile red in 1-octanol (emission maximum at 622nm)

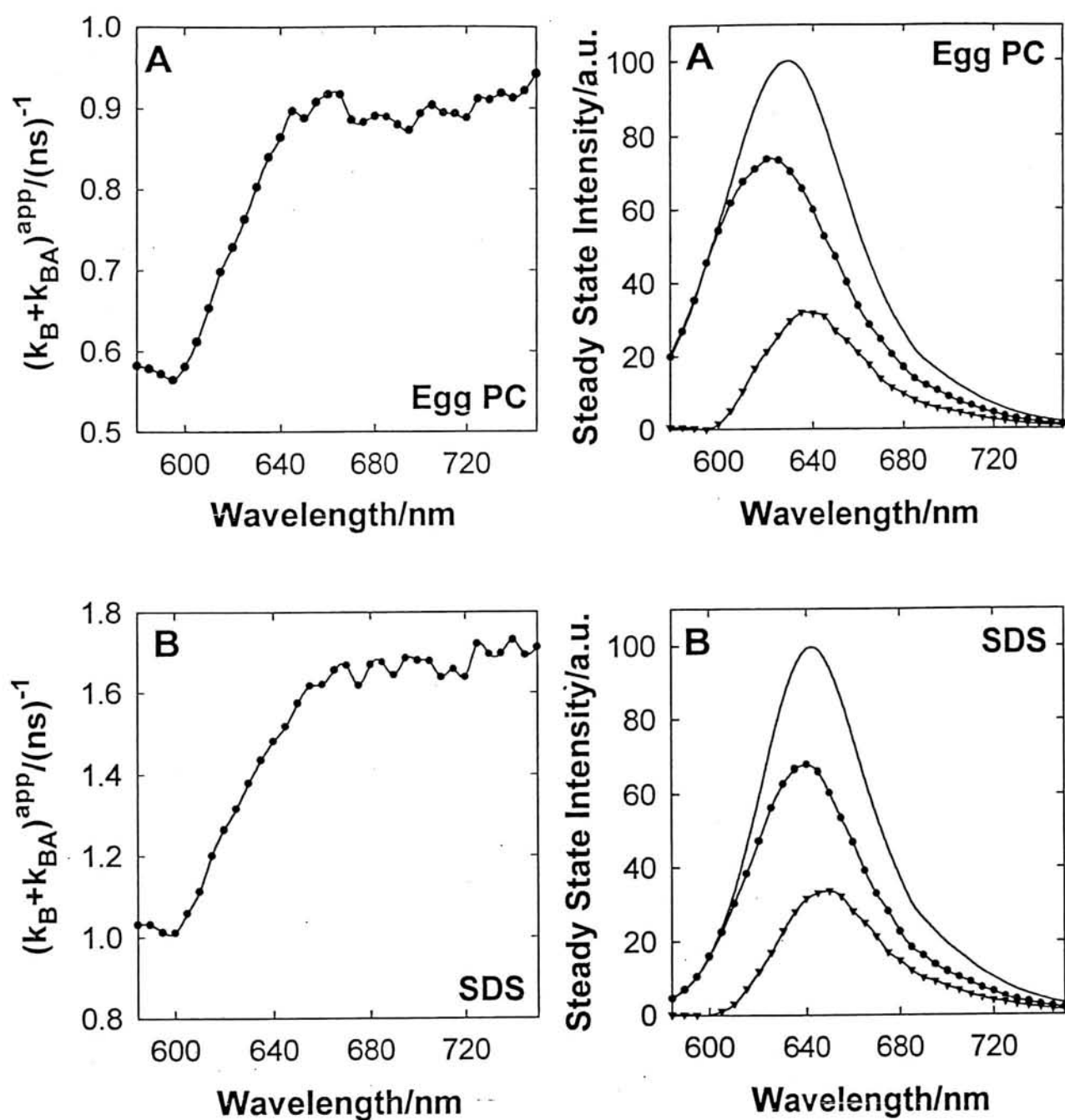


Figure 3.11: Plot of $(k_B + k_{BA})^{app}$ with the emission wavelength and Species Associated Spectra (SAS) of the two species in the case of reversible reaction in the excited state of Nile red in (A) Egg PC vesicles and (B) SDS micelles. The circles and triangles represent the SAS of the initially excited and newly formed species respectively.

is also emission wavelength dependent, similar to the case of Nile red in membranes and micelles. The multiple fluorescence intensity decays collected at various emission wavelengths ranging from 580nm to 750nm for the excitation wavelength of 570nm can be globally fitted to a double exponential function with the two lifetimes 0.42ns and 4.12ns and the amplitudes of the two lifetimes are wavelength dependent. The amplitudes of the short lifetime (0.42ns) become negative at emission wavelengths $\lambda_{em} \geq 625\text{nm}$. The species associated spectra for the two lifetimes in both cases of irreversible and reversible reaction in the excited state are as shown in figure 3.12.

The excited state kinetics was also observed in the case of Nile red in glycerol (emission maximum at 647nm). The global analysis of multiple fluorescence decays collected at varying emission wavelengths ranging from 590nm to 750nm at the excitation wavelength of 570nm gave two lifetimes 0.56ns and 2.63ns with the amplitudes varying with the emission wavelength. Negative amplitudes were observed for the short lifetime component (0.56ns) at the emission wavelengths $\lambda_{em} \geq 650\text{nm}$. The species associated spectra for Nile red in glycerol are as shown in figure 3.13.

The observation of two lifetimes with negative amplitudes for the short lifetime component in the case of Nile red in viscous solvents 1-octanol and glycerol leads to the conclusion that the excited state kinetics of Nile red is characteristic of viscous media. Hence, before interpreting the multiple lifetimes for a fluorescent probe in a biological system in terms of the multiple sites or some other phenomenon related to the biological system under study, one should make sure that the origin of these multiple lifetimes are not the excited state kinetics of the fluorophore such as that observed in the case of Nile red.

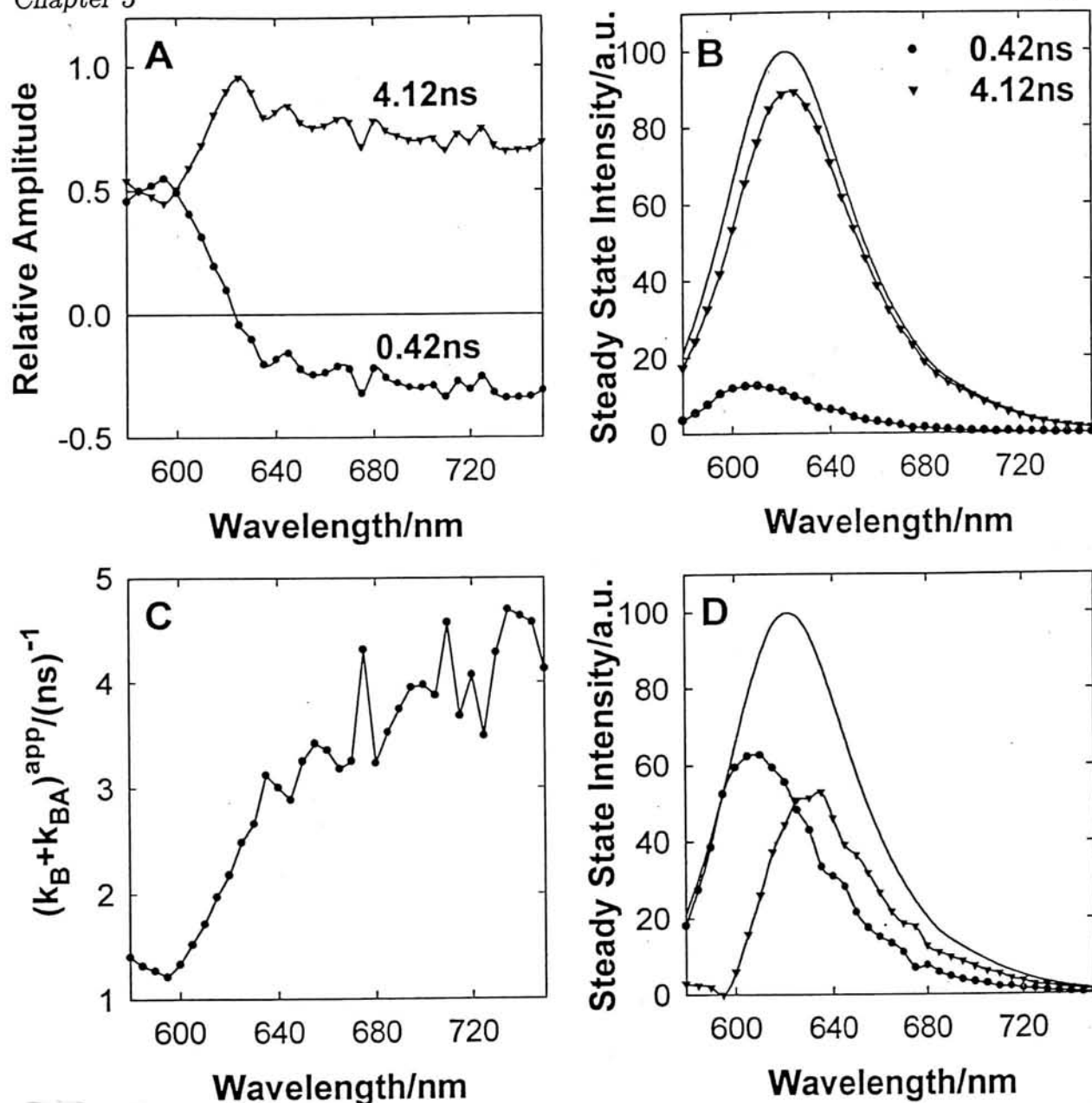


Figure 3.12: Nile red ($0.77\mu\text{M}$) in 1-octanol: (A) Relative amplitudes of the two lifetimes obtained by the global analysis of multiple fluorescence decays collected as a function of the emission wavelength at the excitation wavelength 570nm, (B) SAS in the case of irreversible reaction in the excited state. Here 0.42ns and 4.12ns correspond to the lifetimes of the initially excited and newly formed species. (C) Plot of $(k_B + k_{BA})^{app}$ with the emission wavelength, (D) SAS in the case of reversible reaction in the excited state. The circles and triangles represent the SAS of the initially excited and newly formed species respectively.

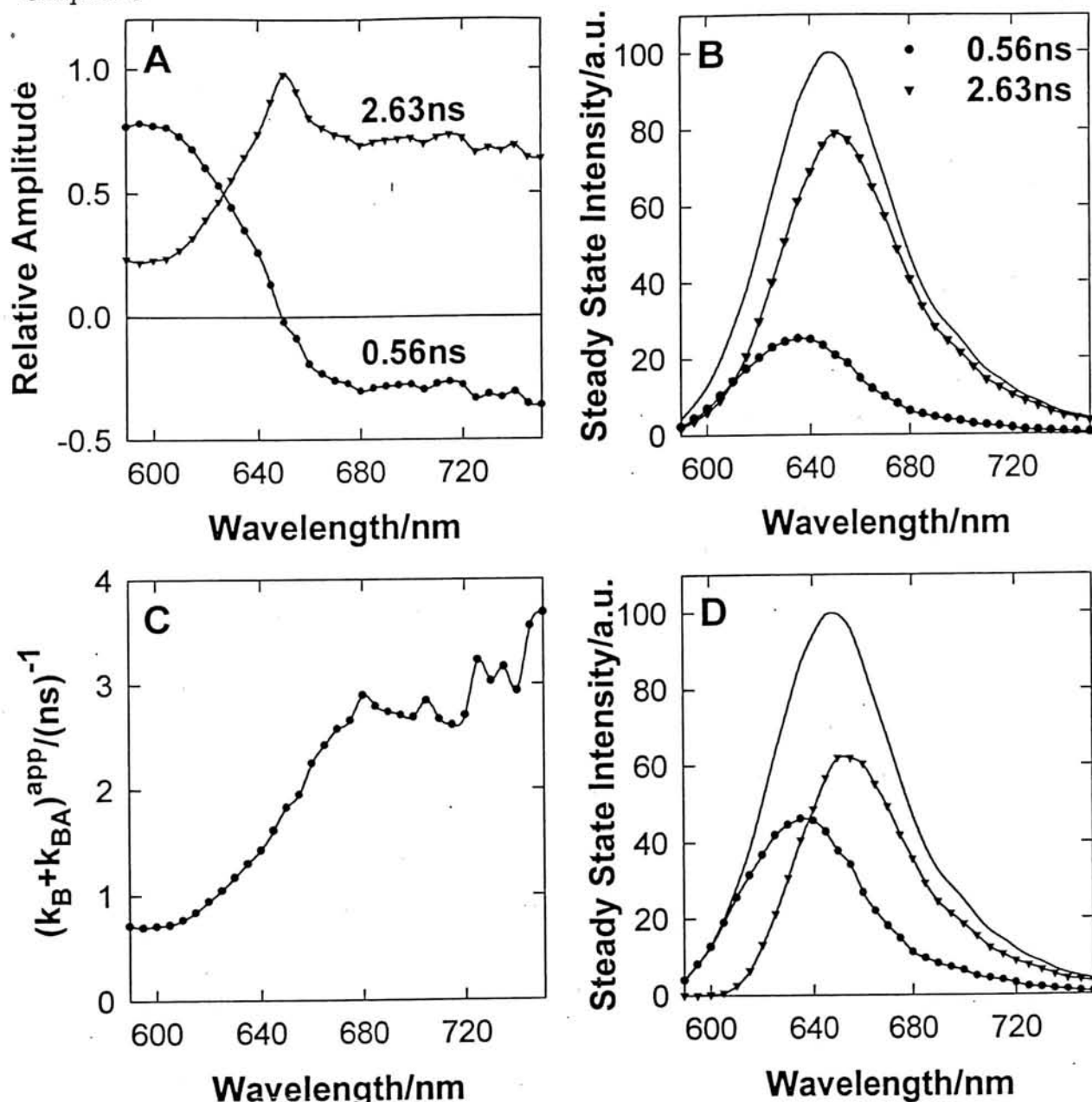


Figure 3.13: Nile red ($0.77\mu\text{M}$) in glycerol: (A) Relative amplitudes of the two lifetimes obtained by the global analysis of multiple fluorescence decays collected as a function of the emission wavelength at the excitation wavelength 570nm, (B) SAS in the case of irreversible reaction in the excited state. Here 0.56ns and 2.63ns correspond to the lifetimes of the initially excited and newly formed species. (C) Plot of $(k_B + k_{BA})^{app}$ with the emission wavelength, (D) SAS in the case of reversible reaction in the excited state. The circles and triangles represent the SAS of the initially excited and newly formed species respectively.

3.3 General Characteristics of membrane-bound fluorescent probes

The fluorescence properties of a membrane-bound fluorophore are considerably different from those of the fluorophore present in the aqueous phase. As can be seen from figure 3.6, the emission spectrum of the membrane-bound dye is red shifted compared to that of the dye present in the aqueous phase. The fluorescence lifetimes are also different for the membrane bound dye and the dye present in the aqueous phase. The membrane-bound dye exhibits a longer fluorescence lifetime compared to that present in the aqueous phase. This is because of the reduced collision dependent nonradiative processes in the membrane phase. When the dye is present in the aqueous phase, the fluorescence anisotropy decays to zero with a faster correlation time. For a membrane-bound dye, the fluorescence anisotropy decays with a slower correlation time related to the microviscosity of the fluorophore environment that is higher compared to the viscosity of the aqueous phase. The anisotropy of the membrane-bound dye may not decay to zero as the fluorophore can not get randomly oriented in the membrane phase because of the anisotropic nature of the orientation of the lipid chains with the membrane surface.

One of the aims of this thesis is to determine the location, orientation and dynamics of fluorescent probes in bilayer membranes. The method of Spectrally Constrained Global Analysis (SCGA) was applied to determine the fluorescence properties of membrane-bound probes, particularly in those cases where the spectra of the membrane-bound fluorophore overlaps considerably with that present in the aqueous phase. It was made sure that the multiple lifetimes observed for a membrane-bound fluorescent dye are not arising due to the excited state kinetics of the dye. Using the thus obtained fluorescence properties, the question of the location, orientation and dynamics of fluorescent probes in bilayer membranes has been addressed in the next three chapters.

Chapter 4

Effects of Viscosity and Refractive Index on the Fluorescence Lifetimes in Biological Systems

Fluorescence lifetimes of the fluorescent probes in biological systems are affected by the viscosity and refractive index of the aqueous and the non-aqueous phases. Two types of processes are responsible for the deexcitation of the excited fluorophore: radiative and nonradiative processes. Fluorescence lifetime is the inverse of the sum of these two rates (non-radiative and radiative).

$$\tau = \frac{1}{k_r + k_{nr}} \quad (4.1)$$

where τ is the fluorescence lifetime, and k_r and k_{nr} are the radiative and non-radiative rates, respectively. Non-radiative processes constitute of Internal Conversion, Intersystem Crossing, Fluorescence quenching, Energy Transfer etc. These processes occur without the emission of radiation. The radiative rate is defined by the spontaneous emission. The effects of viscosity and refractive index on the fluorescence lifetime is through two different mechanisms: viscosity affects the non-radiative rate whereas the refractive index affects the radiative rate.

4.1 Effect of Viscosity

Viscosity affects the non-radiative rate through a collisional mechanism between the excited fluorophore and the surrounding solvent molecules. As we increase the solvent viscosity, the collisions between the excited chromophore and the solvent molecules decrease as the diffusion of the two for a collision is slowed down and hence deactivation by a collisional mechanism (nonradiative rate) decreases. Hence, the lifetime of the fluorophore tends to increase with the increase of the solvent viscosity. In a biological system such as membrane or protein, the effect of viscosity of the aqueous medium on the fluorescence lifetime of the dye strongly depends on how much the fluorophore is exposed to the solvent. If the fluorophore is completely exposed to the solvent, then the viscosity effect will be prominent compared to the fluorophores which are inaccessible to the solvent. Hence the viscosity effect is location dependent for the fluorophore in a biological system.

4.2 Effect of Refractive Index

Spontaneous emission from an excited fluorophore depends upon its optical environment. Electromagnetic field is characterized by various modes of radiation. The excited dipole resonantly couples to a mode and transfers energy that satisfies the fundamental laws of conservation of energy and momentum. In an optically isotropic environment, there exists a continuum of field modes that can be coupled to a dipole and the radiative rate is independent of the location and orientation of the dipole in the medium.

The situation is completely different in the case of optically anisotropic environments where the radiative rate becomes location and orientation dependent. This was illustrated with the experiments carried out on fluorescent dye molecules in front of mirrors and in cavities. When a Europium dibenzoylmethane complex was doped into Langmuir-Blodgett films of cadmium arachidate on a gold mirror with varying distance between the dye molecule and the gold mirror [192], it was found that the lifetime of the dye depends on the location of the dye molecule, i.e., the distance between the dye molecule and the

gold mirror. Similar is the case with the dye molecule between two mirrors [192]. When an excited dipole is placed in a cavity of two mirrors with the cavity size comparable to that of the light wavelength [193], no spontaneous emission was observed for the dipole oscillating parallel to the mirrors (σ or s -polarization) when the distance between the two mirrors was less than half of the wavelength. For the case where the polarization is perpendicular to the mirrors (π or p -polarization), excited state decays rapidly. That means, the excited state lifetime of the dipole strongly depends on its orientation. There were many examples in the literature of Quantum Electrodynamics [193, 194, 195, 196] which show that the spontaneous emission rate of an excited dipole differs considerably in optically anisotropic environments compared to that in optically isotropic environment. Lifetimes of the excited cesium atoms increased several fold when placed between two mirrors [197, 198]. In the case of a dipole placed in a spherical resonant cavity, it was observed that spontaneous emission rate increases by about five hundred times [199].

The parameter which characterizes the optical environment is the refractive index of the medium. Increase of refractive index increases the electromagnetic field density i.e., the number of modes that can be resonantly coupled with the excited dipole. Hence the radiative rate increases and the lifetime decreases with the increase of the refractive index. The dependence of the rate of spontaneous emission i.e., the radiative rate on the refractive index depends upon the anisotropy of the optical environment around the excited dipole. In general, the radiative rate is proportional to the electromagnetic field density and to the square of the local electric field experienced by the probe. In the case of optically isotropic environments, the radiative rate is proportional to the square of the refractive index. In the case of optically anisotropic environments, the exact functional form for the dependence of radiative rate on the refractive index depends on the geometry of anisotropic environment.

Biological systems are optically anisotropic. Radiative rates of the fluorophores in these systems such as lipid bilayer membranes and proteins depend upon the refractive indices of the biological medium (lipid matrix in the case of bilayer membranes and peptide matrix in the case of proteins) and the surrounding aqueous medium. The exact

functional form depends upon the anisotropy of the optical medium. In general, with the increase of the refractive index, the radiative rate increases and hence the lifetime decreases.

Refractive index effect on the fluorescence lifetime is purely optical and hence does not depend upon the extent of solvent exposure of the fluorophore like the case of the effect of viscosity. Increase of refractive index decreases the fluorescence lifetime through the increase of radiative rate and the increase of viscosity increases the fluorescence lifetime through the decrease of the nonradiative rate. Hence the combined effects of viscosity and refractive index depend upon the relative magnitudes of the radiative and nonradiative rates contributing to the fluorescence lifetime. Refractive index effect on the fluorescence lifetime has been ignored in the literature and this can be severe in the case of high quantum yield dyes where the radiative rate is much higher than the nonradiative rate.

The effect of viscosity and refractive index on the fluorescence lifetimes of the fluorophores in two important biological systems: proteins and lipid bilayer membranes has been examined in the next two sections. In the case of lipid bilayer membranes (section 4.4), these effects were used in assigning the site of solubilization (or location) of fluorescent probes.

4.3 Protein Fluorescence in Aqueous Glycerol Solutions

Tryptophan is the intrinsic fluorescent probe in proteins which is generally used in the study of structure and dynamics of proteins. If the tryptophan in a protein is solvent exposed, then the fluorescence is sensitive to the properties of the aqueous medium. In the case of tryptophans which are buried inside the protein matrix and inaccessible to solvent, the fluorescence lifetime is not affected by the aqueous phase properties such as quenchers. Similarly viscosity of the aqueous medium is not expected to affect the fluorescence of buried tryptophans.

Refractive index affects the fluorescence lifetime of the tryptophan irrespective of whether it is solvent exposed or not. If n_0 and n_1 are the refractive indices of the aqueous and protein media, the electric field changes by n_0^2/n_1^2 because of the refraction at the interface between the water and the protein phases. Hence the radiative rate which is proportional to the square of the electric field experienced by the probe and the density of the electromagnetic states which is proportional to the macroscopic refractive index n_0 when the medium with the refractive index n_1 (protein medium) is very small compared to the medium with the refractive index n_0 (aqueous medium) [200], becomes

$$k_r \propto n_0 \left(\frac{n_0^2}{n_1^2} \right)^2 = \left(\frac{n_0^5}{n_1^4} \right) \quad (4.2)$$

Hence the radiative rate increases as the fifth power of the external refractive index in the case of proteins. This is based on the assumption that the dipole is embedded in a sphere of protein matrix.

The combined effects of viscosity and refractive index on the fluorescence lifetime of tryptophan in proteins depends on the relative magnitudes of the nonradiative and radiative rates. Fluorescence experiments were carried out on two proteins, Barstar W38,44F mutant [201] and Human Seminal Plasma Prostatic Inhibin (HSPI) [202, 131] in aqueous glycerol solutions. Here glycerol was used to vary the external viscosity and refractive index of the aqueous solution in which the proteins were dissolved.

4.3.1 Barstar W38,44F: Solvent inaccessible single tryptophan

Barstar W38,44F mutant where the two tryptophans W38 and W44 are mutated to phenylalanines, contains a single tryptophan (W53) which is located in the core of the protein [201]. This protein shows an emission maximum at 321nm which shows that the tryptophan is solvent inaccessible. The emission maximum for tryptophans in proteins vary from 310nm to 360nm depending on whether the tryptophan is accessible to the solvent or not and the emission maximum for a protein can be used qualitatively to identify the solvent accessibility of a tryptophan [46]. The solvent inaccessibility of the single tryptophan in Barstar W38,44F was also confirmed by the observation that the quenchers KI and acrylamide are unable to quench the tryptophan fluorescence in Barstar W38,44F mutant. This single tryptophan protein exhibits a single exponential fluorescence decay with a lifetime of 4.84ns. A single fluorescence lifetime indicates that the conversion between the three rotamers that are responsible for the multiexponential decay of tryptophans in proteins is absent and the tryptophan exists as a single rotamer. This will be more elaborated in the next section where it was found that the two tryptophans in HSPI are also in sterically rigid environments. The rigidity of the environment of W53 in the Barstar mutant was also confirmed by the observation that the protein shows a single rotational correlation time of 4.59ns which corresponds to the rotation of the entire protein and shows that the tryptophan does not have any independent motion.

4.3.2 HSPI: Solvent accessible tryptophans

Human Seminal Plasma Prostatic Inhibin contains two tryptophans at positions W32 and W92 [202]. This protein shows a double exponential fluorescence decay with the lifetimes 5.86ns and 2.44ns and the respective amplitudes 0.64 and 0.36 [131]. The three quenchers Potassium Iodide (anionic), acrylamide (neutral) and Cesium Chloride (cationic) quenches the fluorescence by a dynamic quenching mechanism. The Stern-Volmer quenching curves in the case of steady state fluorescence intensity and average fluorescence lifetime are identical. Linear Stern-Volmer curves were observed for the two lifetimes which is in favour of

associating the two lifetimes to separate tryptophans. The fluorescence anisotropy decay is single exponential with a correlation time of 9.2ns, which is due to the rotation of the entire protein and indicating no independent rotational motions for the two tryptophans in HSPI like the case of W38,44F Barstar.

The two lifetimes in HSPI are from the two different tryptophans: NMR evidence

As described above, the two fluorescence lifetimes of HSPI are in favour of associating with two separate tryptophans. There are only a few examples of multi-trp proteins for which it was possible to identify the lifetimes with individual tryptophans [203, 204]. Multi exponential fluorescence decay is commonly observed in several proteins [164], including many proteins containing only one tryptophan [164, 205, 118, 206, 207, 208]. There are very few single trp proteins which show a single exponential fluorescence decay [209, 210, 211, 201]. It is usually difficult to associate fluorescence lifetimes with individual tryptophans in a multi-trp protein without modifying the protein to a simple single trp protein. Fluorescence anisotropy of HSPI has also revealed the compact structure of the protein devoid of segmental or local dynamics in the region of the tryptophan. This gives rise to the possibility that indole moieties of the two tryptophans are held rigidly in one of three rotamer structures (see below) which can be unambiguously confirmed from NMR studies.

Tryptophan in water at pH 7 shows a biexponential fluorescence decay and the lifetimes are assigned to rotamer structures [164]. Multiexponential decay of tryptophan fluorescence in proteins has been generally attributed to multiple conformations (χ^1 rotamers) around the C^α - C^β bond of the tryptophan side chain [212, 213], multiple microstates of the protein [214], or multiple structures of the protein [215, 207]. The recent work [208] on the lifetime distributions of single tryptophan proteins has strongly suggested that multiexponential decay of the tryptophan arises due to the presence of various rotamers, the tryptophan side chain can adopt. The two fluorescence lifetimes for the free tryptophan in water has been assigned to these rotamer structures about the C^α - C^β bond, which makes

the indole group proximal to the carboxyl group in two of the three structures [216]. The three rotamer structures (χ^1 conformations whose structures are shown in figure 4.1) are found to be long lived on millisecond timescale using NMR experiments [217]. Hence the three tryptophan rotamers would show up as distinctly different species in the nanosecond/picosecond time scale fluorescence lifetime experiments. The fluorescence decay of a tryptophan analog that has restricted rotation about the $C^\alpha-C^\beta$ bond is found to be biexponential, which is correlated with the two conformational populations calculated from 1H NMR coupling constants [218, 219]. The combined study of fluorescence decay and NMR of tryptophan containing polypeptide has shown that the population of the three rotamers derived from NMR experiments were in excellent agreement with the amplitudes of the three fluorescence decay components [217]. All these strongly suggest that the fluorescence decay of a tryptophan in a protein depends on its relative populations of the three rotamers.

In the light of the above discussion, the assignment of the two lifetimes to two individual tryptophans in HSPI implies that the two tryptophans are in sterically constrained environments and the tryptophan side chain is in a single conformation. The absence of any fast decays in the fluorescence anisotropy is also in support of the argument that the tryptophans in HSPI are in rigid environments.

The 1H NMR can be used to calculate the relative populations of the three rotamers (shown in figure 4.1) from the experimental values of the coupling constants (J s) between H^α and $H^{\beta R}(H^{\beta S})$ using the equations [217]

$$\begin{aligned}
 p_I &= [^3J(H^\alpha - H^{\beta R}) - ^3J_g] / \Delta^3J \\
 p_{II} &= [^3J(H^\alpha - H^{\beta S}) - ^3J_g] / \Delta^3J \\
 p_{III} &= 1 - p_I - p_{II} = (^3J_t + ^3J_g - [^3J(H^\alpha - H^{\beta R}) + ^3J(H^\alpha - H^{\beta S})]) / \Delta^3J \quad (4.3)
 \end{aligned}$$

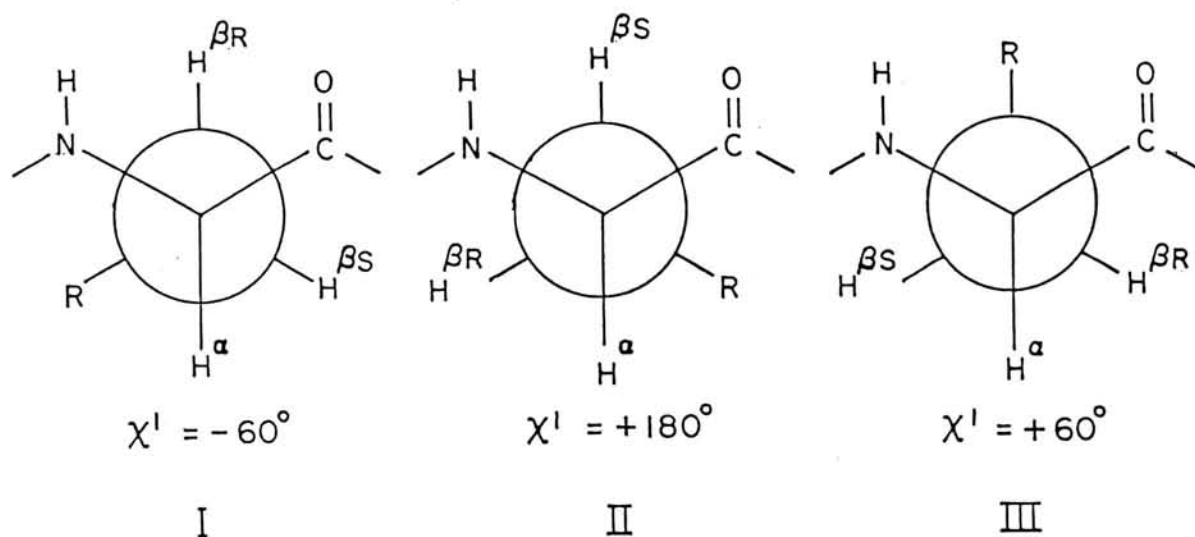
where $\Delta^3J = ^3J_t - ^3J_g$, and 3J_t and 3J_g are the nominal values of the coupling constants for vicinal protons in trans and gauche conformations respectively.

The information about J helps in fixing the three rotamer populations which in turn can be used to explain the fluorescence decay kinetics [217]. The estimation of these cou-

pling constants is not straight forward except in the case of small peptides and proteins (containing less than fifty amino acids). For larger proteins, the 2D NMR spectral resolution suffers from extensive spectral overlaps, large resonance linewidths, antiphase active coupling constants and inphase passive coupling constants. For HSPI with 94 amino acids, the conformational dependent characteristic multiplet structures of the individual COSY crosspeaks were not resolved and hence could not aid in the estimation of the J couplings. In situations where the J-couplings were less than the individual resonance linewidths, corresponding COSY crosspeaks are either weak or absent. In view of this, we have made an attempt to qualitatively fix the χ^1 rotamer populations from the crosspeak patterns observed in the 2D NMR spectra of HSPI and compare them with the independent parameters obtained from the fluorescence experiments.

For a tryptophan side chain, the three most probable staggered rotamer conformations are with $\chi^1 = -60^\circ$, $+180^\circ$ and $+60^\circ$ (figure 4.1) and for all these rotamers, the $J(H^\alpha-H^{\beta R}, H^{\beta S})$ values are χ^1 dependent. They can be calculated for various values of χ^1 by using appropriate Karplus-type relations (equations 4.3) and these 'J' values decide the COSY crosspeak intensities. Likewise, the nOe intensities between H^α and $H^{\beta R} / \beta S$ are also χ^1 dependent. Hence, the COSY and NOESY crosspeak intensities between H^α and $H^{\beta R} / H^{\beta S}$ protons can together be used to qualitatively fix the χ^1 populations and to know whether the tryptophan is in a single staggered rotamer conformation or not.

For a staggered rotamer conformation with $\chi^1 = -60^\circ$ and $\chi^1 = +180^\circ$, the COSY crosspeak between H^α and one of the H^β protons is very intense, while the crosspeak with the other β proton is at the same time below the lowest contour level because of the coupling constants involved (trans protons show a large coupling constant compared to the gauche protons) (see figure 4.1). On the other hand, the COSY crosspeaks between the H^α and $H^{\beta R} / H^{\beta S}$ for the rotamer population with $\chi^1 = +60^\circ$ will be of the same intensity. Similarly the NOESY crosspeak intensities between H^α and $H^{\beta R} / H^{\beta S}$ protons is also χ^1 dependent. For $\chi^1 = -60^\circ$ and $+180^\circ$, the H^β proton which is in trans orientation with respect to the H^α proton expectedly shows weaker nOe compared to the other H^β proton which is in the gauche (g^\pm) conformation with respect to the H^α proton. For the



	$\chi^1 = -60^\circ$	$\chi^1 = +180^\circ$	$\chi^1 = +60^\circ$
$J(H^\alpha - H^{\beta R})$	Large (~13.56 Hz)	Small (~2.6 Hz)	Small (~2.6 Hz)
$J(H^\alpha - H^{\beta S})$	Small (~2.6 Hz)	Large (~13.56 Hz)	Small (~2.6 Hz)
$\text{COSY}(H^\alpha - H^{\beta R})$	Strong	Weak	Weak
$\text{COSY}(H^\alpha - H^{\beta S})$	Weak	Strong	Weak
$\text{nOe}(H^\alpha - H^{\beta R})$	Weak	Strong	Strong
$\text{nOe}(H^\alpha - H^{\beta S})$	Strong	Weak	Strong

Figure 4.1: The three rotamer structures seen along $C_\alpha - C_\beta$ bond of tryptophan. The table indicates the expected $J(H^\alpha - H^{\beta R}/H^{\beta S})$ values and COSY and NOESY crosspeak intensities between the H^α and $H^{\beta R}/H^{\beta S}$ protons that one would observe for the above three rotamer structures.

other conformation ($\chi^1 = +60^\circ$), both the NOESY crosspeaks between the H^α and H^β protons are equal and strong in intensity. In the event of rotational averaging between the three rotamer conformations about the C^α - C^β bond, the $J(H^\alpha, H^{\beta R})$ and $J(H^\alpha, H^{\beta S})$ values average out and result in equal crosspeak intensities between H^α and $H^{\beta R}/H^{\beta S}$. Similarly, interproton distances between H^α and $H^{\beta R}/H^{\beta S}$ also average out and result in equal nOe crosspeak intensities between H^α and $H^{\beta R}/H^{\beta S}$ in the NOESY spectrum. It is very difficult to differentiate this rotational averaging with the case where the single rotamer with $\chi^1 = +60^\circ$ is populated because in both the cases, the COSY and NOESY crosspeak intensities between H^α and $H^{\beta R}/H^{\beta S}$ protons are similar.

Figure 4.2 shows the crosspeak patterns observed in the 2QF COSY (A) and NOESY (B) spectra of HSPI between the H^α and H^β protons of the two tryptophans (the data taken from [220]). For both W32 and W92, the 2QF COSY spectrum (figure 4.2A) shows only one crosspeak between one of the $C_\beta H$ protons and $C_\alpha H$ proton. The upfield shifted $C_\beta H$ protons show up strong J correlation to $C_\alpha H$ proton while the downfield shifted ones do not. Such an observation directly indicates that the side chains of these residues are locked in a single staggered rotamer conformation, which is either with $\chi^1 = -60^\circ$ or $+180^\circ$. The NOESY spectrum of HSPI (figure 4.2B) also shows up different nOe intensities between the H^α and H^β protons for the two tryptophans. The downfield shifted $C_\beta H$ protons show a strong nOe with the C_α protons compared to the upfield shifted $C_\beta H$ protons. The trend in the intensities of the COSY and NOESY crosspeaks for the two tryptophans is as explained in the previous paragraphs. That is, the β proton which shows a strong COSY crosspeak (which is in trans conformation) with the α proton shows a weak NOESY crosspeak and vice versa. This substantiates our earlier conclusion that the tryptophan sidechains are locked in a single staggered rotamer conformations. In order to further differentiate between the two possible rotamer conformations with $\chi^1 = -60^\circ$ and $+180^\circ$, one would require stereospecific resonance assignments of all the $C_\beta H$ protons of both the tryptophans.

2D NMR experiments clearly proves that the two tryptophans exist in sterically rigid, single rotamer populations and hence each tryptophan shows a single fluorescence lifetime.

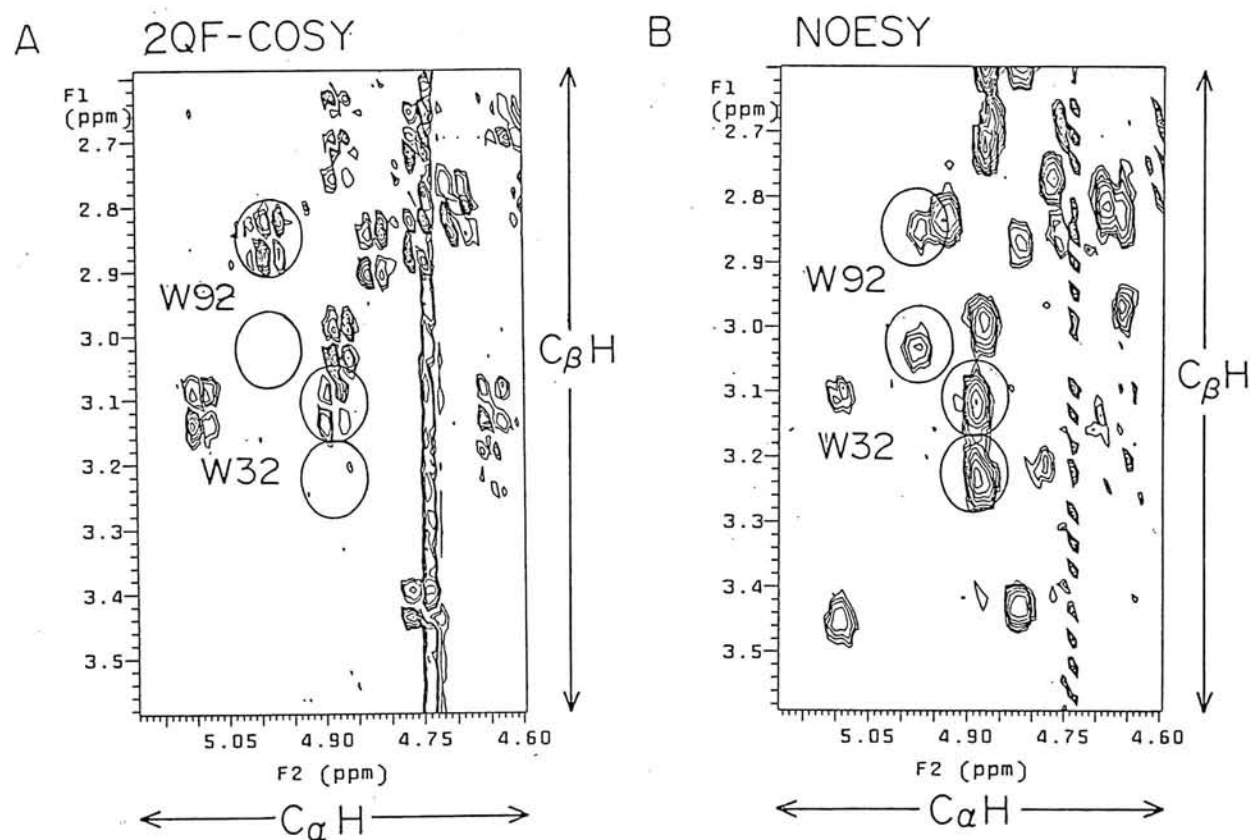


Figure 4.2: Selected spectral regions ($\omega_1 = 2.6 - 3.6$ ppm; and $\omega_2 = 4.6 - 5.15$ ppm) of 600 MHz phase sensitive 2QF COSY (A) and NOESY (B) spectra of HSPI (protein concentration 2.5 mM; pH 3.0; temperature 20°C) showing through-bond (J) and through-space (nOe) connectivities, respectively, from $C_\beta H$ protons to $C_\alpha H$ protons. The J and nOe correlations arising from the $C_\alpha H$ and $C_\beta H$ protons of W32 and W92 are highlighted with circles around them. The J and nOe correlations arising from the $C_\alpha H$ and $C_\beta H$ protons of W32 and W92 are highlighted with circles around them. The absence of the J correlations in the COSY spectrum, between the down-field shifted $C_\beta H$ protons and the $C_\alpha H$ protons of both the tryptophans is clearly evident. Though one of the nOe crosspeak for W32 partially suffers from spectral overlaps, the nOe correlation from the down-field shifted $C_\beta H$ protons to $C_\alpha H$ protons are significantly stronger than the correlation from the upfield shifted $C_\beta H$ protons for both the tryptophans.

However, the specific assignment of the two lifetimes to the two tryptophans is possible only after mutating the protein to a single tryptophan protein like in the case of Barstar.

Decay associated spectra of tryptophans:

The fluorescence emission maximum of tryptophan depends on the local environment in the protein i.e., on the neighbouring amino acid groups surrounding the tryptophan. The Trp emission maximum in water (completely exposed to solvent) occurs at 360 nm. If the Trp is in the hydrophobic region of the protein, the emission maximum gets blue shifted to 310 nm [46]. The fluorescence emission maximum of HSPI occurs at 346 nm indicating that the Trp residues are significantly exposed to the solvent. As described earlier, the fluorescence of HSPI is due to two lifetimes which can be associated with different tryptophans. The steady state fluorescence spectrum of HSPI was resolved into the spectra associated with the two lifetimes (DAS) as described in Chapter 2. The fluorescence decays collected at emission wavelengths varying from 320 nm to 430 nm at an interval of 5 nm with the excitation wavelength at 295 nm were analyzed globally to obtain the two lifetimes which are common to all the emission wavelengths, and amplitudes varying as a function of the emission wavelength. The decay associated spectra are shown in figure 4.3. As seen in figure 4.3, the emission maxima (345 nm) and the spectral shapes of both the lifetimes are identical. As described earlier [131], the quenching rate constants of the two lifetimes by the three quenchers acrylamide, potassium iodide and cesium chloride fall in the range expected for the solvent-exposed tryptophans. These results confirm that the two tryptophans in HSPI are solvent-exposed.

In summary, we have two proteins: Barstar W38,44F mutant where the single tryptophan is inaccessible to the solvent and HSPI where the two tryptophans are solvent exposed. In both cases, each tryptophan exhibits a single fluorescence lifetime indicating that the tryptophans are locked in one of the three rotamer (figure 4.1) populations. Time resolved anisotropy studies on these two proteins indicate that there are no independent motions for the tryptophans other than the rotation of the entire protein.

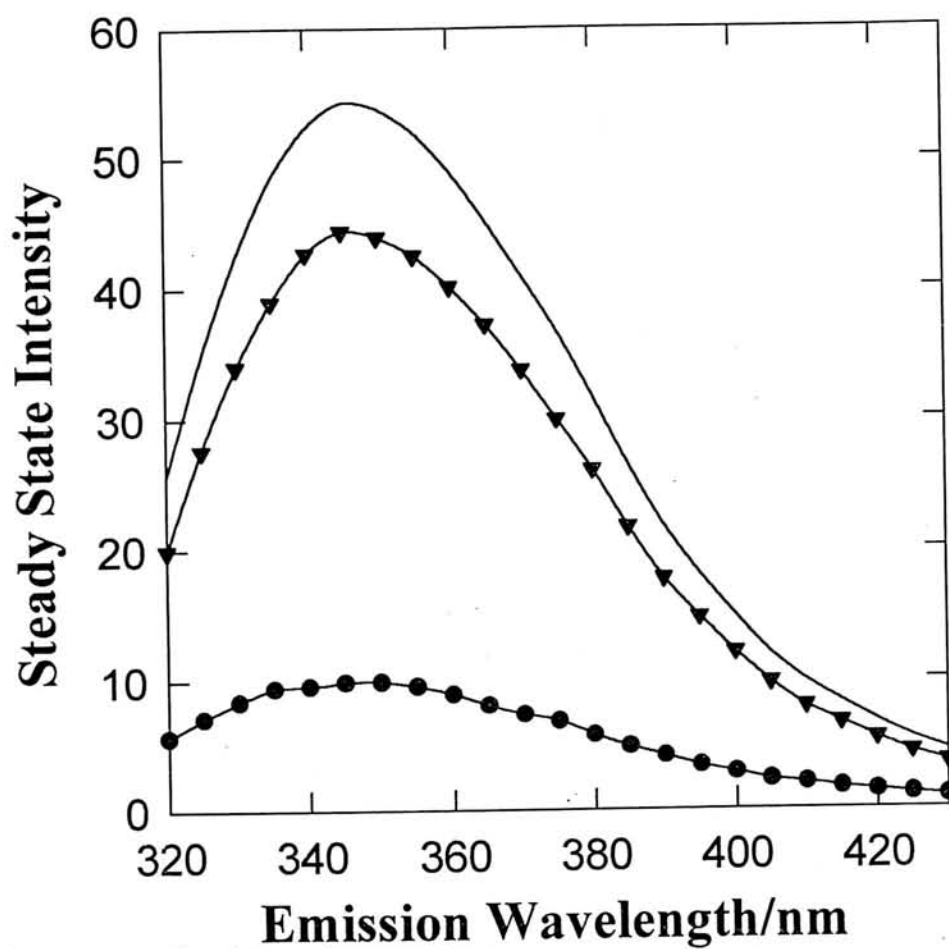


Figure 4.3: DAS of the two lifetimes of HSPI. The solid curve represents the steady state intensity. The solid triangles and circles represent the spectra of the long (5.86ns) and short lifetime (2.44ns) respectively.

4.3.3 Effects of viscosity and refractive index

Protein solutions were prepared in aqueous glycerol solutions where glycerol is used to vary the viscosity and refractive index of the aqueous medium. One needs to confirm that the addition of glycerol does not perturb the structural integrity of these proteins. If the trp environment loses its structural rigidity, then the tryptophan may exist in the other rotamers which gives rise to multiple lifetimes for a single tryptophan and hence the observed trends in the fluorescence lifetimes with glycerol may not truly represent the effects of viscosity and refractive index. Time resolved fluorescence anisotropy experiments were carried out on these two proteins in aqueous glycerol solutions for this purpose. Since in these two proteins, the tryptophans do not have any independent motion and the fluorescence depolarization is caused only by the rotation of the entire protein, the two proteins should give a single rotational correlation time in all glycerol solutions that corresponds to the rotation of the entire protein. Figure 4.4 shows the rotational correlation times of these two proteins in glycerol solutions. The variation in the case of NATA where the fluorophore is exposed to the solvent is also shown in the figure 4.4. The two proteins, Barstar W38,44F and HSPI exhibit a single rotational correlation time in all glycerol solutions which is because of the rotation of the entire protein and this correlation time increases with the increase of glycerol. More importantly, no fast depolarization was detected in the glycerol solutions which indicate that the structural integrity of the tryptophan environment is retained.

Figure 4.5 shows the variation of fluorescence lifetimes for the two proteins Barstar W38,44F and HSPI and for NATA in aqueous glycerol solutions. Increase of glycerol concentration from 0% to 55.75% w/w increases the relative viscosity from 1 to 8.21 whereas the refractive index increases from 1.334 to 1.407.

The fluorescence lifetime of NATA where the fluorophore is completely exposed to the solvent increases from 2.82ns to 3.64ns (i.e., by 29%) with the increase of glycerol from 0% to 55.75% w/w. This is the viscosity effect on the fluorescence lifetime and shows that the nonradiative processes dominate over the radiative process in the case of NATA.

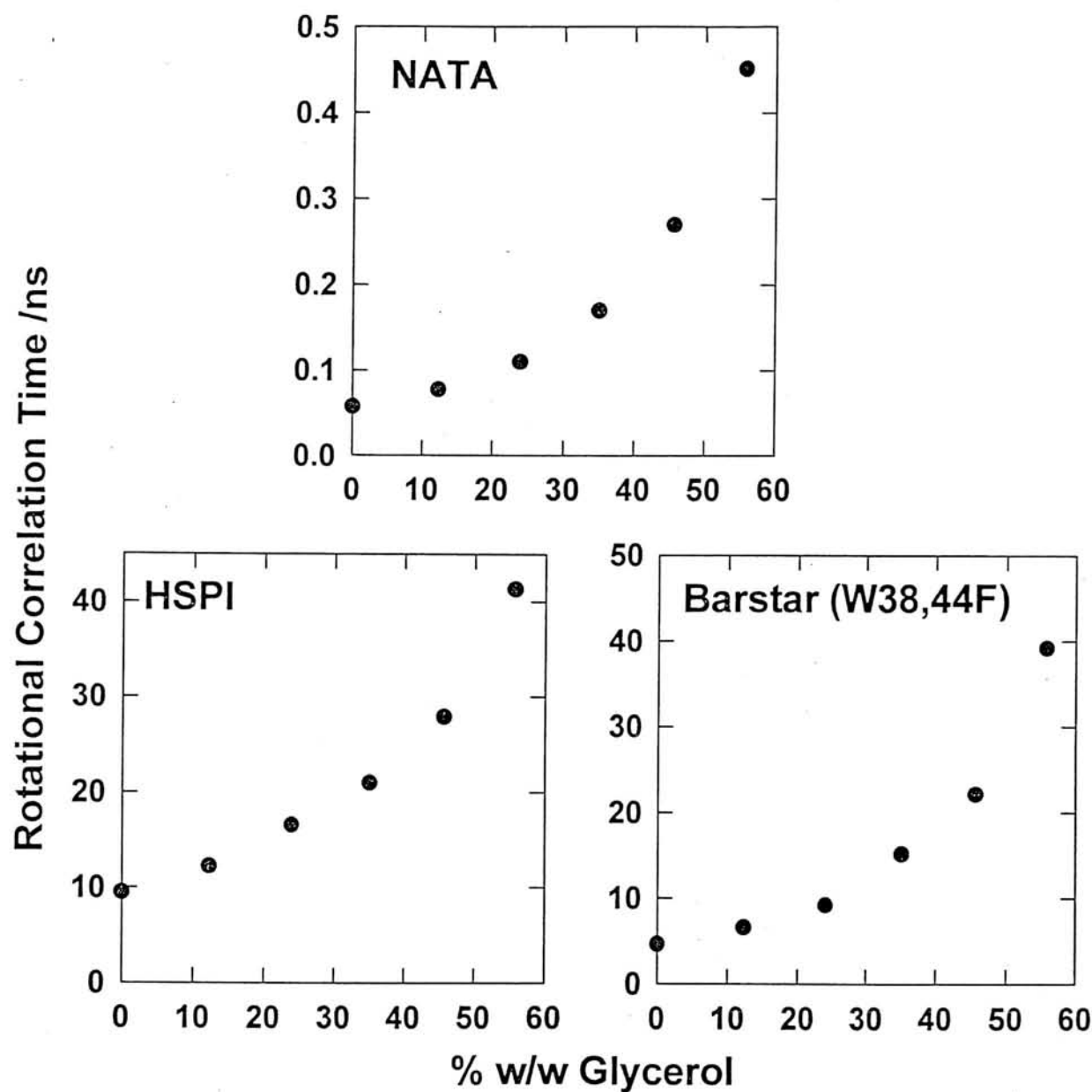


Figure 4.4: Rotational correlation times of NATA, HSPI and Barstar W38,44F in aqueous glycerol solutions. The samples were excited at 295nm and the emission was at 360nm for NATA (10 μ M), 350nm for HSPI (10 μ M) and 330nm for Barstar W38,44F (10 μ M). The experiments were done in pH 7.4 10mM NaH₂PO₄ buffer for NATA and Barstar W38,44F, and in pH 3.0 100mM sodium acetate buffer for HSPI.

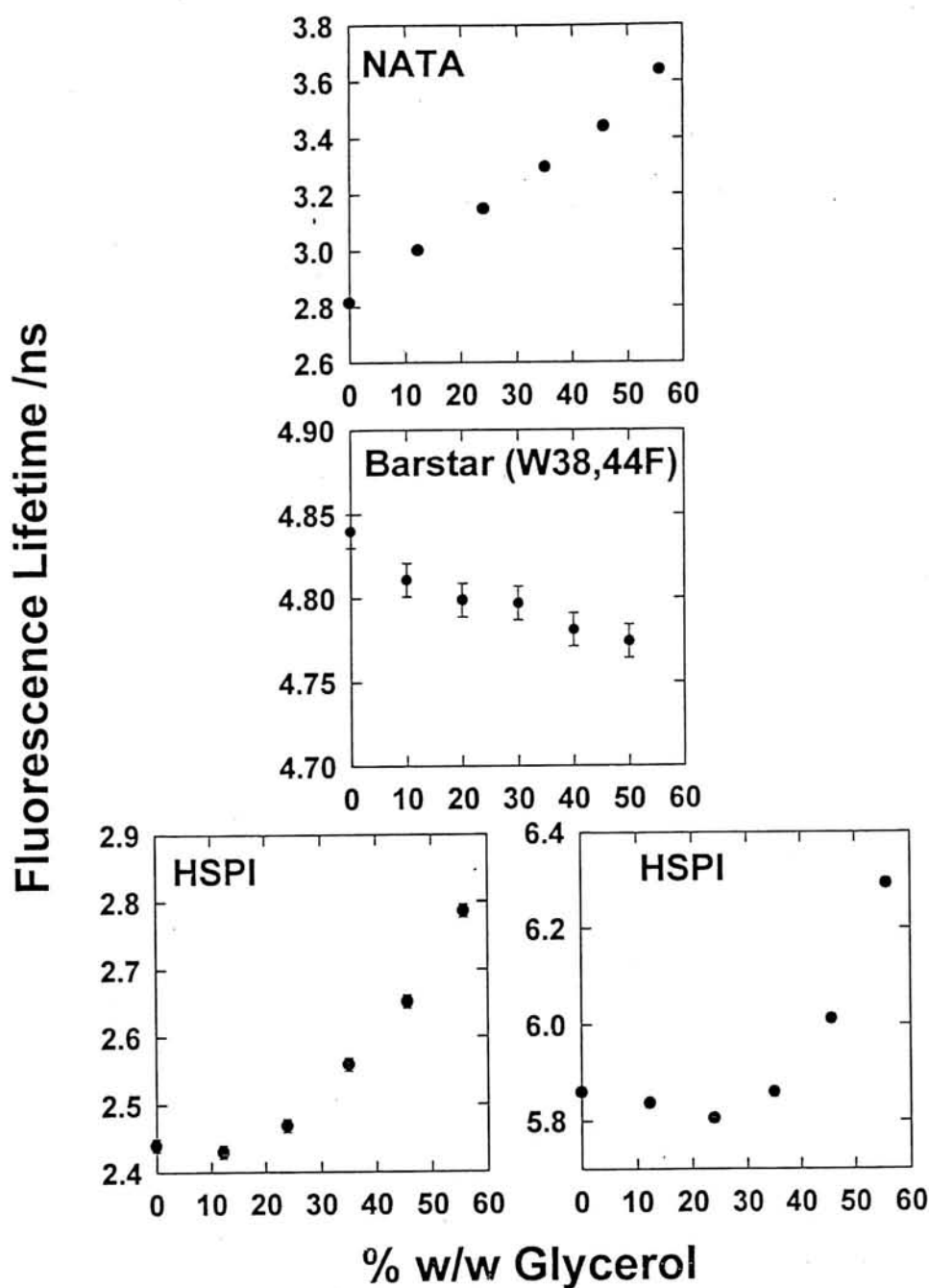


Figure 4.5: Variation of the fluorescence lifetimes of NATA, Barstar W38,44F and HSPI in aqueous glycerol solutions. The samples were excited at 295nm and the emission was at 360nm for NATA (10 μ M), 350nm for HSPI (10 μ M) and 330nm for Barstar W38,44F (10 μ M). The experiments were done in pH 7.4 10mM NaH₂PO₄ buffer for NATA and Barstar W38,44F, and in pH 3.0 100mM sodium acetate buffer for HSPI.

In the case of Barstar W38,44F, a single fluorescence lifetime was observed in glycerol solutions which shows a slight decrease (from 4.84ns to 4.77ns, i.e., by 2%) with the increase of glycerol concentration. The observation of single fluorescence lifetime for Barstar W38,44F in glycerol solutions is in agreement with the time resolved anisotropy studies which shows that the structural rigidity of the tryptophan environment is maintained and the tryptophan exists in a single rotamer population. As mentioned before, increase of viscosity increases the fluorescence lifetime whereas the increase of refractive index decreases the fluorescence lifetime. The decrease of the fluorescence lifetime with the increase of glycerol concentration observed in the case of Barstar W38,44F clearly shows that the refractive index effect is dominant over the viscosity effect as expected for the solvent inaccessible tryptophans. The decrease in the fluorescence lifetime is not inversely proportional to the fifth power of the refractive index of the aqueous medium as expected from the dependence of the radiative lifetime which is the inverse of the radiative rate on the refractive index (equation 4.2). For tryptophan, the radiative lifetime is known to be around 20-25ns [221, 222]. Hence the nonradiative processes dominate over the radiative process in the case of Barstar W38,44F (fluorescence lifetime of 4.84ns), but since the tryptophan is solvent inaccessible, the refractive index effect dominates over the viscosity effect as the viscosity effect is through a collisional mechanism between the excited tryptophan and the solvent molecules.

In the case of HSPI, the two lifetimes 5.86ns and 2.44ns at first shows a slight decrease or no variation which is followed by an increase with the increase of glycerol concentration. This is the result of combined effects of viscosity and refractive index effects on the fluorescence lifetimes. Increase of viscosity and refractive index does not follow the same trend with the increase of the glycerol concentration. Refractive index increase is almost linear whereas the increase of viscosity is linear at lower glycerol concentrations and the viscosity increases exponentially at higher glycerol concentrations. Hence in the case of solvent exposed fluorophores where both the nonradiative and radiative processes are responsible for the deexcitation of the fluorophore, the refractive index effect will be dominant at lower glycerol concentrations whereas the viscosity effect will be dominant

at higher glycerol concentrations. This is what has been observed in the case of the two lifetimes of HSPI.

The trends in the variation of the fluorescence lifetimes with the increase of glycerol concentration observed in the case of the two proteins Barstar W38,44F and HSPI are consistent with the combined effects of viscosity and refractive index on a low quantum yield probe such as tryptophan and the solvent accessibility of the tryptophan. The effects of viscosity and refractive index on the fluorescence lifetimes offers another method of determining whether a tryptophan in a protein is exposed to solvent or not.

4.4 Fluorescence of Organic Dyes in Bilayer Membranes

Fluorescence of organic dye molecular probes is widely used in the investigation of the physical properties of lipid membranes in model and biological systems [52, 223, 53]. The structure and dynamics of the dye molecule bound to the membrane is of great interest because of the usefulness of the fluorescence property in a wide variety of biological applications [224, 48]. One or more fluorescence properties (spectra, quantum yield, lifetime and anisotropy) of the molecule are sensitive to variations in the structure and/or dynamics of the membrane and hence their usefulness in the investigation of the biomembranes. A large number of applications are based on the increase in the fluorescence quantum yield of the membrane-bound dye. The exact molecular mechanism for the change in fluorescence property in some applications (for example, the action of dyes that are sensitive to the membrane potential [45, 225, 226]) is not clearly understood. Identification of the solubilization sites for the dye in the membrane and its local structure (site of solubilization, surface vs. core and orientation with respect to the interface) is a prerequisite for an understanding of the molecular mechanism for the change in the fluorescence parameters. Location of small molecules inside a bilayer membrane at extremely low concentrations (micromolar) can not be easily determined. Here the combined effects of viscosity and refractive index were used to determine the site of solubilization (location) of fluorescent probes in bilayer membranes.

Fluorescence properties of dye molecules incorporated in membranes are perturbed by the physical properties of the external aqueous medium such as viscosity and refractive index. Viscosity of the aqueous medium affects the lifetime through a collisional mechanism and hence depends on where the dye is solubilized in the membrane. Refractive index effect on the fluorescence lifetime is purely optical and can be expected for the dye molecules located inside the core of the bilayer. The combined effects of viscosity and refractive index on the fluorescence lifetime of a dye molecule incorporated inside a bilayer membrane is determined by the relative magnitudes of the radiative and nonradiative

rates of the excited state. Viscosity affects the nonradiative rate whereas the refractive index affects the radiative rate. The effect of refractive index on the radiative property of a fluorophore in a biological system has been ignored in the past.

Lukosz [227] obtained the analytical expression for the spontaneous emission rate for a emission dipole embedded in an extremely thin planar dielectric layer of refractive index and optical thickness less than $\lambda/8$ (λ being the wavelength of light) sandwiched between media of different refractive indices. The theory is based on the fact that the local electric field experienced by the probe differs from the macroscopic electric field depending on its location in the layer and/or orientation with respect to the thin layer. This theory has been applied by Toptygin et al [228, 229, 200] for the case of lipid bilayer membranes. According to the theory, the radiative decay rate, k_r of a fluorescent probe in the membrane of refractive index n_1 is given as

$$k_r = \frac{4\omega^3}{3\hbar c^3} f^2 |\mu|^2 n_0 (\sin^2 \theta + \frac{n_0^4}{n_1^4} \cos^2 \theta) \quad (4.4)$$

where ω is the circular frequency of fluorescence light, \hbar is Planck's constant, c is the speed of light, f is the factor which accounts for the difference between the local electric field experienced by the probe inside the layer and the macroscopic field, μ is the matrix element of the emission electric dipole operator, n_0 is the refractive index of the aqueous medium present on either side of the membrane bilayer and θ is the angle between the molecular emission dipole and the normal to the surface of the layer. According to the above equation, the radiative rate varies as the fifth power or the first power of the refractive index n_0 of the aqueous medium for the emission dipoles which are oriented perpendicular ($\theta = 0^\circ$) or parallel ($\theta = 90^\circ$) to the membrane surface, respectively. Thus for the dye molecules of high quantum yield, the refractive index effect on the fluorescence lifetime can be severe and can not be ignored in interpreting the fluorescence results.

Lukosz's theory of the dependence of the spontaneous emission rate on the refractive index and the orientation of the dye molecule has been experimentally observed in the case of single molecule fluorescence studies on a fluorescent dye molecule DiIC₁₈(3) incorporated in a PMMA (Poly methyl methacrylate) film using time resolved fluorescence

microscopy [230]. In the case of bilayer membranes, the refractive index effect has been observed in the case of the commonly used fluorescent dye molecule DPH in DPPC membranes [200]. DPH is the only fluorophore which is reported in literature to exhibit the refractive index effect.

Time resolved fluorescence experiments were carried out on fifteen organic dye molecules incorporated inside Egg PC membrane. The lipid vesicles were prepared by sonication as described in Chapter 2 in pH 7.4 buffer (10mM sodium acetate, 10mM NaH_2PO_4 , 10mM MES and 150mM NaCl). There are mainly two aims for this study: (i) to identify the site of solubilization (or location) of these organic molecules in the bilayer membranes using the combined effects of viscosity and refractive index on the fluorescence lifetime and (ii) to identify the dye molecules which are oriented in the bilayer membrane, i.e., whose fluorescence lifetime decreases with the increase of the external refractive index (equation 4.4).

4.4.1 Fluorescence Lifetimes in Ethanol and Water

The molecular structures of the fifteen organic dye molecules used in this study are shown in figure 4.6. The fluorescence decay of all the dye molecules, except FM464, investigated in this study is single exponential (or nearly so) in dilute solutions ($<10 \mu\text{M}$) in ethanol (table 4.1). Observation of single exponential decay for the dye in ethanol confirms that the dye is pure and that the photophysics of fluorescence is due to a single structurally distinct species.

The fluorescence decay of the dyes in water (containing ethanol 2% v/v) is predominantly single exponential for water-soluble charged dyes (Rhodamine 6G, RH421, FM464, DODCI, DiSC_m(n)) and multiexponential for other neutral dyes (Table 4.1). The fluorescence emission and excitation spectra are consistent with the presence of a single monomer species for those dyes for which the fluorescence decay is single exponential. The dyes which exhibited multiexponential decay in the aqueous solutions are presumed to have multiple species including aggregates.

(1) $m=1$ DiIC ₁₈ (3) (2) $m=2$ DiIC ₁₈ (5)	
(3) Nile red	
(4) Rhodamine 6G	
(5) Merocyanine 540	
(6) RH421	
(7) FM4-64	
(8) DiA	
(9) DPH	
(10) TMA-DPH	
(11) A=O $m=2$ $n=1$ DiOC ₂ (5) (12) A=S $m=1$ $n=1$ DiSC ₂ (3) (13) A=S $m=2$ $n=1$ DiSC ₂ (5) (14) A=S $m=2$ $n=2$ DiSC ₃ (5)	
(15) BODIPY 611/627	

Figure 4.6: Structures of different dyes with the abbreviated names used in the text

Table 4.1: Fluorescence lifetimes and amplitudes of organic dyes in ethanol and water

Dye	Ethanol		Water						
	τ	χ^2	τ_1	τ_2	τ_3	α_1	α_2	α_3	χ^2
DiIC18(3)	0.31	1.15	0.1	0.66	1.84	0.76	0.19	0.05	0.98
DiIC18(5)	1.26	1.02	0.1	0.51	3.6	0.77	0.19	0.04	1.2
Nilered	3.58	1.09	0.59	3.18	-	0.9	0.1	-	1
Rhodamine 6G	3.83	1	3.98	-	-	1	-	-	1.18
Merocyanine 540	0.49	0.96	0.14	1.41	-	0.88	0.12	-	1.18
RH421	1.11	1.01	0.14	1.12	-	0.96	0.04	-	0.8
FM4-64	0.36(0.85), 0.82(0.15)	0.76	0.08	0.8	-	0.98	0.02	-	0.84
DiA	0.12	0.95	0.17	0.75	2.34	0.78	0.17	0.05	0.9
DPH	4.82	0.85	0.17	2.25	10	0.53	0.42	0.05	1.21
TMA DPH	0.09(0.99), 1.85(0.01)	0.89	0.05	0.74	3.3	0.96	0.03	0.01	1.08
DiOC2(5) (DODCI)	1.07	0.82	0.65	-	-	1	-	-	0.98
DiSC2(3)	0.19	0.7	0.13	1.1	-	0.97	0.03	-	1.14
DiSC2(5)	1.38	1.07	0.77	2.25	-	0.95	0.05	-	0.96
DiSC3(5)	1.44	0.95	0.9	-	-	1	-	-	0.95
BODIPY 611/627	5.56	1.08	1.69	4.45	-	0.7	0.3	-	1.19

4.4.2 Fluorescence Lifetimes in Membrane

All the dyes (charged and neutral dyes) listed in Table 4.1 (structures shown in figure 4.6) are readily solubilized in membrane. There is no evidence for the formation of aggregates in membranes for $[\text{dye}] < 10\mu\text{M}$. The readiness of solubilization is indicated by the increase in the quantitative parameters such as fluorescence anisotropy for the dye molecule when it is incorporated in the membrane.

Figure 4.7 shows the typical variation of steady state fluorescence anisotropy (r_{ss}) for two dyes (Nile red and DODCI) as a function of lipid concentration at a fixed dye concentration. In both the cases, the fluorescence anisotropy increases with the concentration of lipid but the rate of increase is different. For DODCI, the anisotropy variation depends upon the excitation and emission wavelengths as well. The difference in the trends for the two dyes can be understood from the fact that Nile red is not soluble in water whereas DODCI is water soluble. Even at a low concentration of the lipid, the dye Nile red is solubilized only in the lipid phase and the anisotropy attains the limiting maximum value. In the case of water soluble dyes such as DODCI, the variation of fluorescence anisotropy with the concentration of lipid, and the wavelength dependence are solely attributable to the partitioning of the dye between the aqueous and lipid phase. At short excitation and emission wavelengths (570 and 590nm) the fluorescence of the dye in water is selectively excited and detected. But at long wavelengths of excitation and emission (580 and 690nm) the fluorescence is predominantly due to the membrane-bound dye and the plot of r_{ss} vs lipid concentration resembles that of Nile red. The fluorescence lifetimes of the membrane-bound dye population obtained by the method of Spectrally Constrained Global Analysis (SCGA) of fluorescence decays (section 3.1) closely match with those obtained at long wavelengths of excitation and emission. Hence for obtaining the lifetimes of the membrane bound dye, the fluorescence experiments were carried out at long wavelengths of excitation and emission.

The fluorescence decay of all the dyes bound to the membrane is either two or three exponentials (except R6G which is single exponential). The values of lifetimes and am-

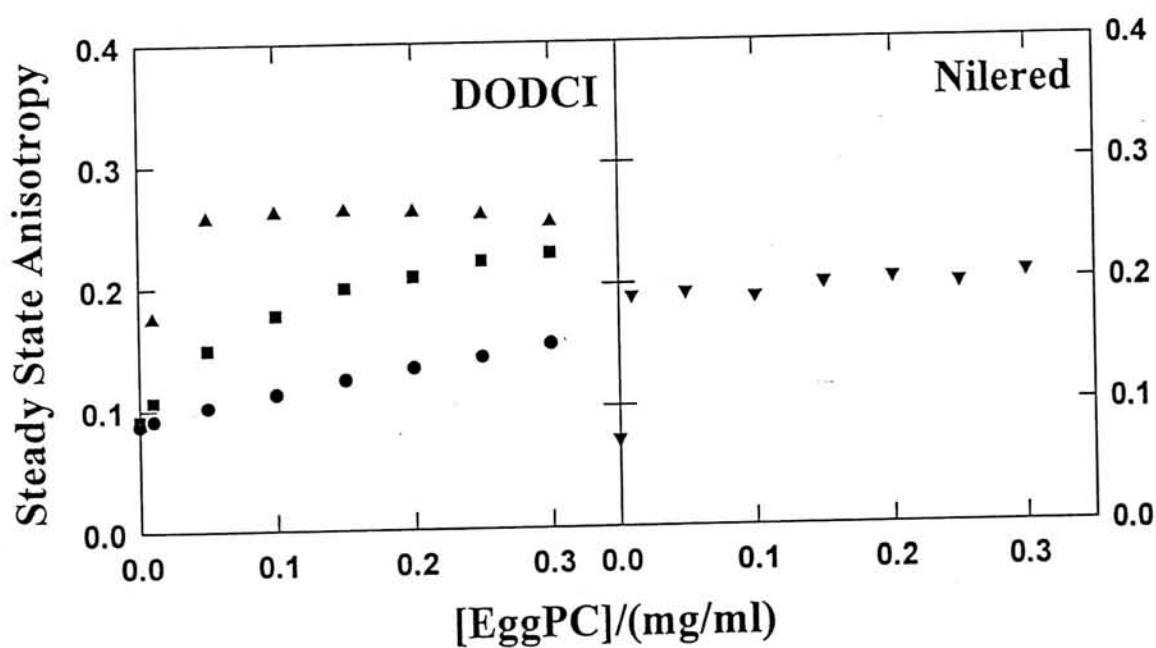


Figure 4.7: Variation of steady-state anisotropy of Nile red ($\lambda_{ex}=570\text{nm}$, $\lambda_{em}=615\text{nm}$ and DODCI [(●) $\lambda_{ex}=570\text{nm}$, $\lambda_{em}=590\text{nm}$, (■) $\lambda_{ex}=570\text{nm}$, $\lambda_{em}=690\text{nm}$, (▲) $\lambda_{ex}=580\text{nm}$, $\lambda_{em}=690\text{nm}$] in aqueous solution as a function of lipid concentration.

plitudes for the dyes and the wavelengths of excitation and emission are given in Table 4.2. The fluorescence of each dye (except R6G) consists of a long lifetime component and a short lifetime component. In a few cases there was a middle lifetime component as well. The long lifetime in membrane is comparable to or longer than the lifetime in ethanol. In several cases the fraction of the long lifetime component was the major one or a significant fraction. Existence of multiple lifetimes was also confirmed by analysis of the fluorescence decay data by maximum entropy method (MEM).

The fluorescence decays of the membrane-bound dye were subjected to the analysis by MEM to obtain the distribution of lifetimes. MEM is an unbiased method which does not assume any a priori model for the excited state kinetics or lifetimes. It assumes that the lifetimes are distributed with equal probability (amplitude) in a range (typically, 10ps to 20ns in our case) and the shape of the distribution (amplitude vs. lifetime) is obtained as the final outcome of analysis [174]. Figure 4.8 shows the results of MEM analysis of fluorescence decays for all the dyes bound to the membrane. The fluorescence of the dyes in membrane is not due to a single continuous distribution of lifetimes. The distribution shows one or more well resolved peaks for all the dyes and for most dyes the width of the prominent peak is relatively sharp. A comparison of the average lifetime for each prominent peak in the multi-peaked distribution of lifetimes with the lifetimes (Table 4.2) obtained by discrete exponential analysis shows a one-to-one correspondence. It is clear from the above results and discussion that the fluorescence decay of the membrane-bound dye can be associated with at least two spectroscopically distinct species, only one is however prominent in several cases. These two species could be the same dye incorporated in two different sites in the membrane or from the excited state kinetics of the dye located at a single site as observed for the case of Nile red (section 3.2). Excited state kinetics of the dye molecule leading to a new fluorescent state would be indicated by negative amplitudes for the short lifetime component like the case of Nile red in membranes and micelles (section 3.2). This has not been observed in most of the dyes studied. Hence, the two lifetimes are associated with two species which ought to be the dye molecule incorporated at two different sites in the membrane. In the case of some

Table 4.2: Fluorescence lifetimes and amplitudes of organic dyes in Egg PC vesicles. The table also shows the excitation and emission wavelengths at which the fluorescence decays were collected.

Dye	λ_{ex}	λ_{em}	τ_1	τ_2	τ_3	α_1	α_2	α_3	χ^2
DiIC18(3)	570	650	0.13	0.48	1.51	0.63	0.31	0.06	1.04
DiIC18(5)	600	750	0.34	1.29	-	0.63	0.37	-	1.02
Nilered	570	615	0.72	3.71	-	0.19	0.81	-	1.11
Rhodamine 6G	300	630	4.11	-	-	1	-	-	1.07
Merocyanine 540	570	680	0.62	1.69	-	0.21	0.79	-	1.08
RH421	570	700	0.55	1.72	-	0.14	0.86	-	0.99
FM4-64	570	690	0.1	0.57	1.13	0.69	0.21	0.1	0.93
DiA	570	630	0.19	0.59	1.74	0.71	0.26	0.03	0.98
DPH	300	500	1.79	5.92	9.61	0.14	0.62	0.24	0.98
TMA DPH	300	470	0.91	3.67	6.11	0.35	0.51	0.14	1.05
DiOC2(5) (DODCI)	580	690	0.66	1.74	-	0.43	0.57	-	0.96
DiSC2(3)	570	690	0.3	1.04	-	0.37	0.63	-	0.94
DiSC2(5)	630	760	0.98	2.03	-	0.29	0.71	-	0.9
DiSC3(5)	630	760	1.09	2	-	0.16	0.84	-	1.02
BODIPY 611/627	610	730	2.75	5.35	-	0.18	0.82	-	1.18

voltage sensitive dyes such as FM464, RH421, DiA, negative amplitudes were observed for short lifetimes at longer emission wavelengths as reported previously in the literature [226]. This led us to conclude that the short lifetimes correspond to that of the initially excited species in these cases. The lifetime of the initially excited species depends on the interconversion rate between the initially excited species and the newly formed species (section 3.2), in addition to the effects of viscosity and refractive index. Therefore, one cannot assign the location of the dye molecules giving rise to the short lifetime from the variation of the fluorescence lifetime with the aqueous phase parameters such as viscosity and refractive index. Hence in these cases, the location of the dye molecules giving rise to the long lifetime component was determined whose variation of lifetime truly represents the combined effect of viscosity and refractive index on the fluorescence lifetime.

4.4.3 Effects of viscosity and refractive index on the fluorescence lifetimes: Determination of the Site of Solubilization

The viscosity and refractive index of the aqueous medium in which the vesicles were prepared can be increased by the addition of an organic solute. Sucrose was chosen in our study as the solute because the membrane vesicles were stable. Figure 4.9 shows the change in the fluorescence intensity decay for the two representative dyes DiA and DODCI with the presence of sucrose (44.4% w/w) in the aqueous phase. In the case of DiA, the fluorescence decay becomes slower whereas in the case of DODCI, the decay becomes faster with the addition of sucrose. This shows that the mechanism which is operating in these two cases is different. The change of sucrose concentration from 0% to 44.4% w/w increases the relative viscosity from 1 to 10.74 and refractive index increases from 1.334 to 1.413. Immediate conclusion which can be drawn is that the viscosity effect is dominant for DiA, whereas the refractive index effect is dominant for DODCI. The next question that arises is where are these molecules located in the bilayer. Can we identify the sites of solubilization of these dye molecules from the combined effects of viscosity and refractive index on the fluorescence lifetime of the membrane-bound dye?

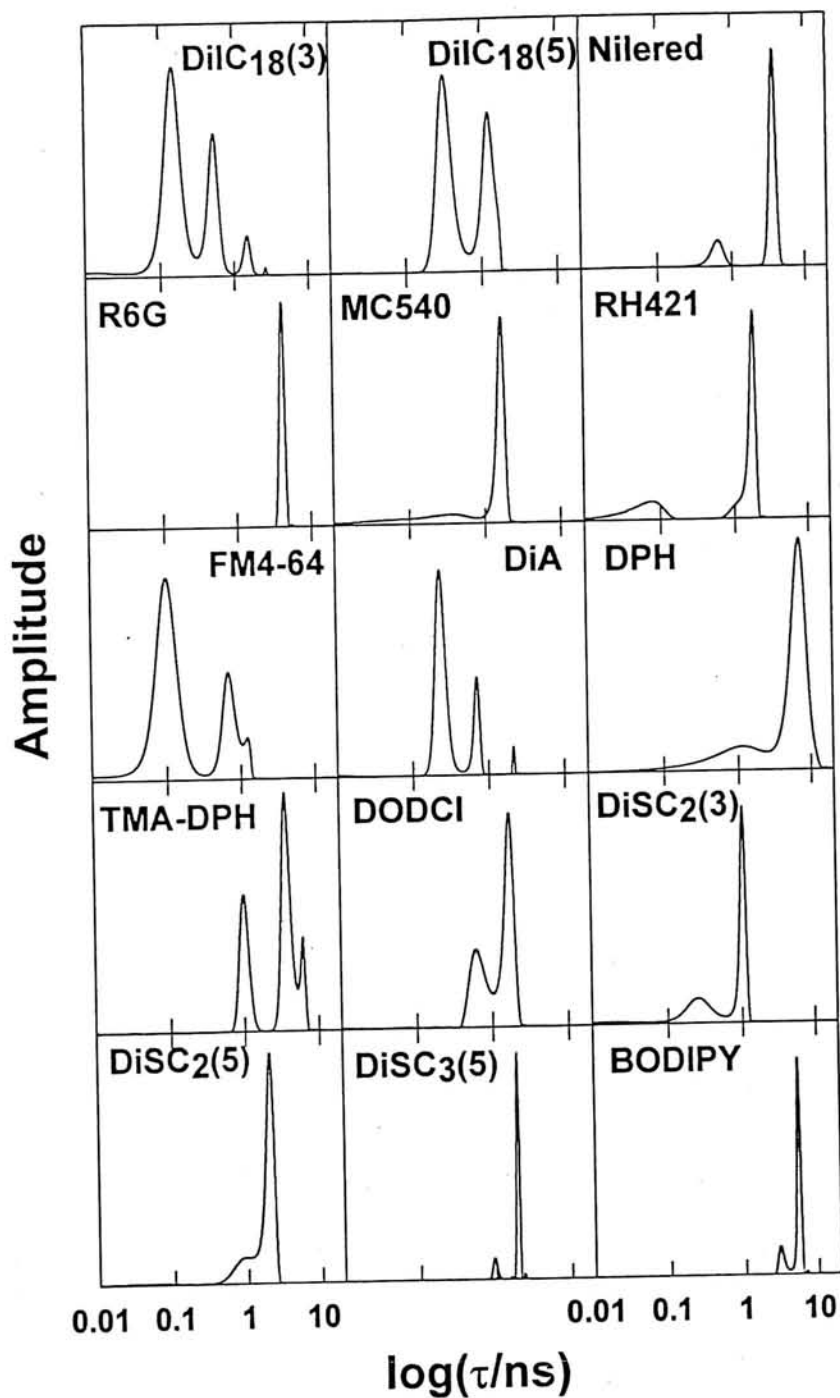


Figure 4.8: Distribution of fluorescence lifetimes obtained by the analysis of Maximum Entropy Method for the fluorescence decay of fifteen dyes in Egg PC membrane. The excitation and emission wavelengths are given in Table 4.2.

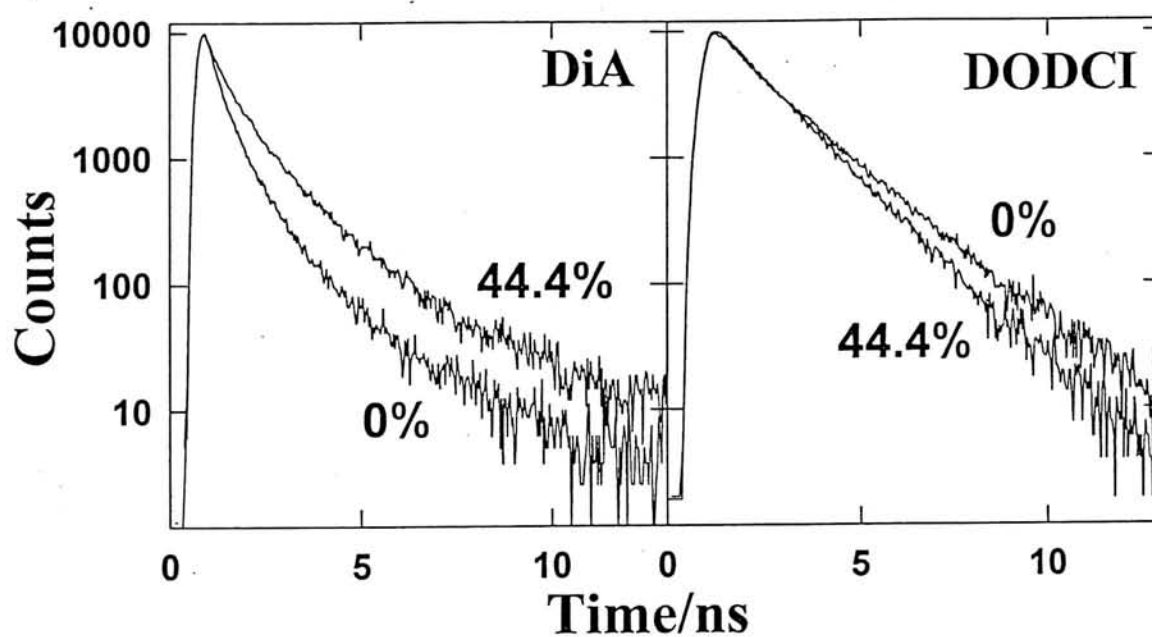


Figure 4.9: Fluorescence decay of DiA ($\lambda_{ex}=570\text{nm}$, $\lambda_{em}=630\text{nm}$) and DODCI ($\lambda_{ex}=580\text{nm}$, $\lambda_{em}=690\text{nm}$) in membrane with and without sucrose in the aqueous solution.

There are three different regions in the membrane phase in which an organic dye molecule is expected to have different degrees of solvent exposure. These are the surface region in which the dye is exposed to the solvent, the interface region in which the exposure to the solvent is limited, and the core region. The core region could be anywhere from the centre of the bilayer to the interface. Figure 4.10 shows a cartoon of the membrane structure and three sites of solubilization marked s (surface), i (interface) and c (core). The combined effects of viscosity and refractive index can be used to identify the site of solubilization of the fluorescent probes. Figure 4.10 also shows the expected trends in the fluorescence lifetimes for the dyes solubilized in the three regions of the bilayer with the increase of the sucrose concentration in the aqueous medium. If the dye is solubilized in the interior region, then it is expected to be insulated from the variation in some of the physical properties of the aqueous medium. The effect of viscosity on the lifetime is based on collisional mechanism between the solvent molecules and the excited state of the dye. Therefore, viscosity of aqueous medium should have no effect on the lifetime of the dye molecule bound in the interior region of the membrane. However, the dye molecule bound in the surface region of the membrane which is exposed to the aqueous phase is still subjected to the collisions of solvent molecules and hence a viscosity effect is observable. On the other hand, the effect of refractive index on the radiative rate is an optical phenomenon and this effect would be observable even for the molecule bound in the interior region of the membrane. Thus, identification of the site of solubilization (surface vs. interior region) of the membrane-bound dye molecule is possible from the variation of the lifetime of the membrane-bound dye in sucrose solutions. The prerequisite for a dye whose location in the bilayer membrane has to be determined is that the fluorescence lifetime of the dye should be highly viscosity sensitive.

Assuming that the dye is highly viscosity sensitive, the fluorescence lifetime of the dye located in one of the three regions of the membrane varies with the increase of the sucrose concentration as follows. If the dye is located on the surface of the membrane (region s in figure 4.10), the viscosity effect dominates over the refractive index effect as the molecule is completely exposed to the solvent and the variation of the fluorescence

Variation of τ with [sucrose] in a bilayer membrane :

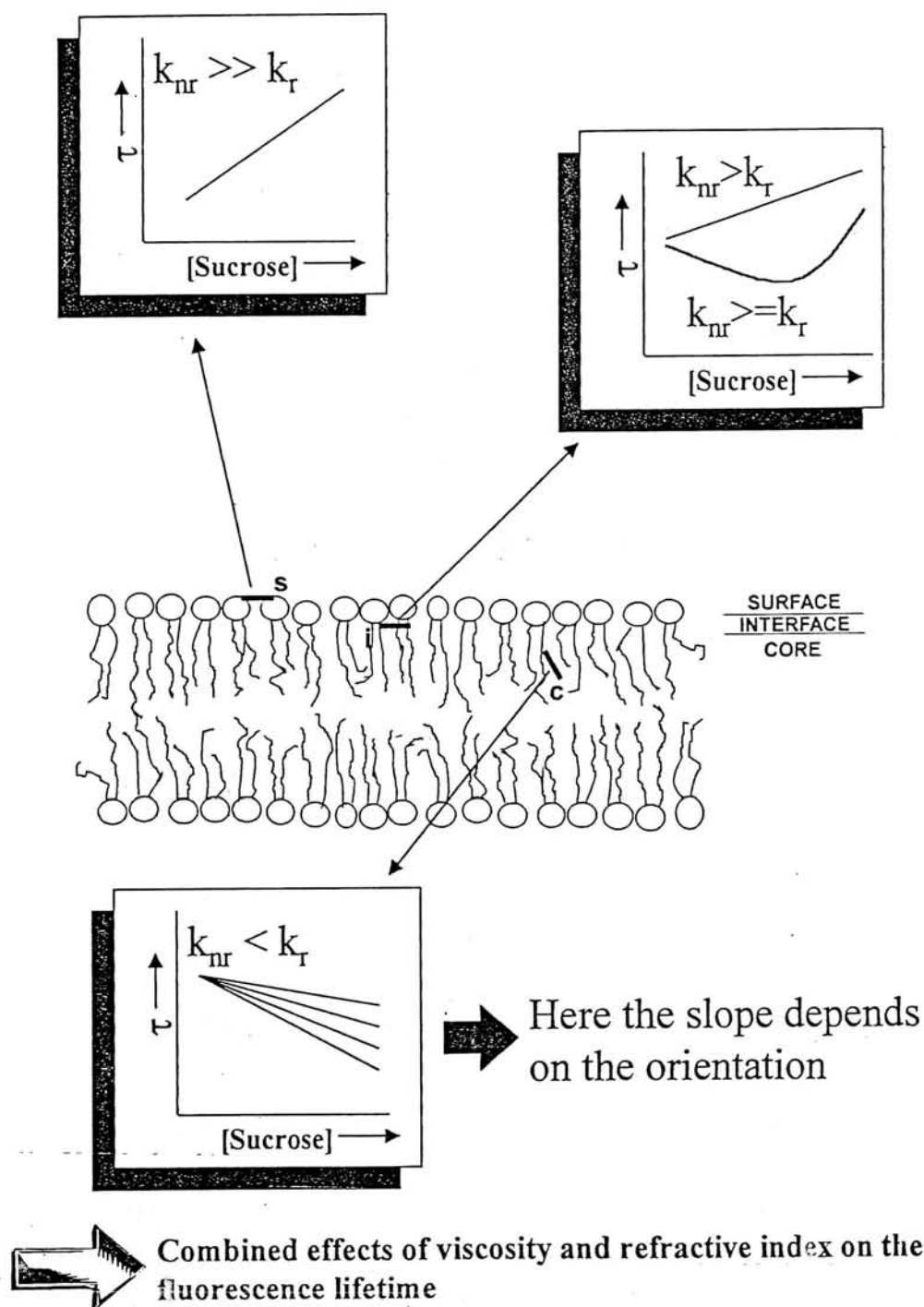


Figure 4.10: Cartoon of the structure of the bilayer membrane. The site of solubilization for a fluorescent probe can be in one of the three regions: Surface (s), Interface (i), Core (c) regions. The figure also shows the expected trends in the fluorescence lifetimes for the dyes located in these three regions with the increase of sucrose concentration in the aqueous medium. These trends are because of the combined effects of external viscosity and refractive index on the fluorescence lifetime of the membrane-bound dye.

lifetime almost follows that of the dye present in the aqueous medium. If the dye is located in the interface region (region i in figure 4.10), the fluorescence lifetime of the dye can show two trends depending on the relative magnitudes of the nonradiative and radiative rates. The fluorescence lifetime can increase with the increase of the sucrose concentration if the collision dependent nonradiative rates dominates over radiative rates but the extent of increase will be less pronounced compared to that of the dye present in the aqueous medium. If the nonradiative and radiative rates are almost same, then the lifetime at first decreases or shows no variation and then increases with the increase of the sucrose concentration. That means, the refractive index dominates at low sucrose concentrations whereas the viscosity effect dominates at high sucrose concentrations. If the dye is located in the core of the bilayer where the dye is inaccessible to solvent, viscosity effect will be absent. If the nonradiative rates are low compared to radiative rate, the fluorescence lifetime decreases with the sucrose concentration which is the refractive index effect.

Global analysis of multiple fluorescence decays (minimum of six decays) [161] collected at fixed excitation and emission wavelengths was carried out to obtain the fluorescence lifetimes with increased confidence limits. Figures 4.11 and 4.12 show the variation of the fluorescence lifetimes of the dyes in the aqueous phase and the membrane phase with the sucrose concentration. Three distinct cases were observed for the variation of the fluorescence lifetimes of the dyes present in the aqueous phase. The fluorescence lifetimes of all the dyes except Rhodamine 6G and BODIPY increases with the increase of the sucrose concentration which is the viscosity effect on lifetime (i.e., $k_{nr} \gg k_r$). In the case of Rhodamine 6G, lifetime decreases which is the refractive index effect indicating that this dye is of high quantum yield (i.e., $k_{nr} \ll k_r$). In the case of BODIPY, lifetime remains unchanged with the increase of the sucrose concentration which is because of the combined effects of viscosity and refractive index on the fluorescence lifetime (i.e., here $k_{nr} \leq k_r$). Table 4.3 shows the percentage changes in the fluorescence lifetimes of the dyes present in the aqueous phase and the membrane phase with the increase of the sucrose concentration. In the case of membrane-bound probes where excited state kinetics was observed, the percentage changes were indicated only for the long lifetime components.

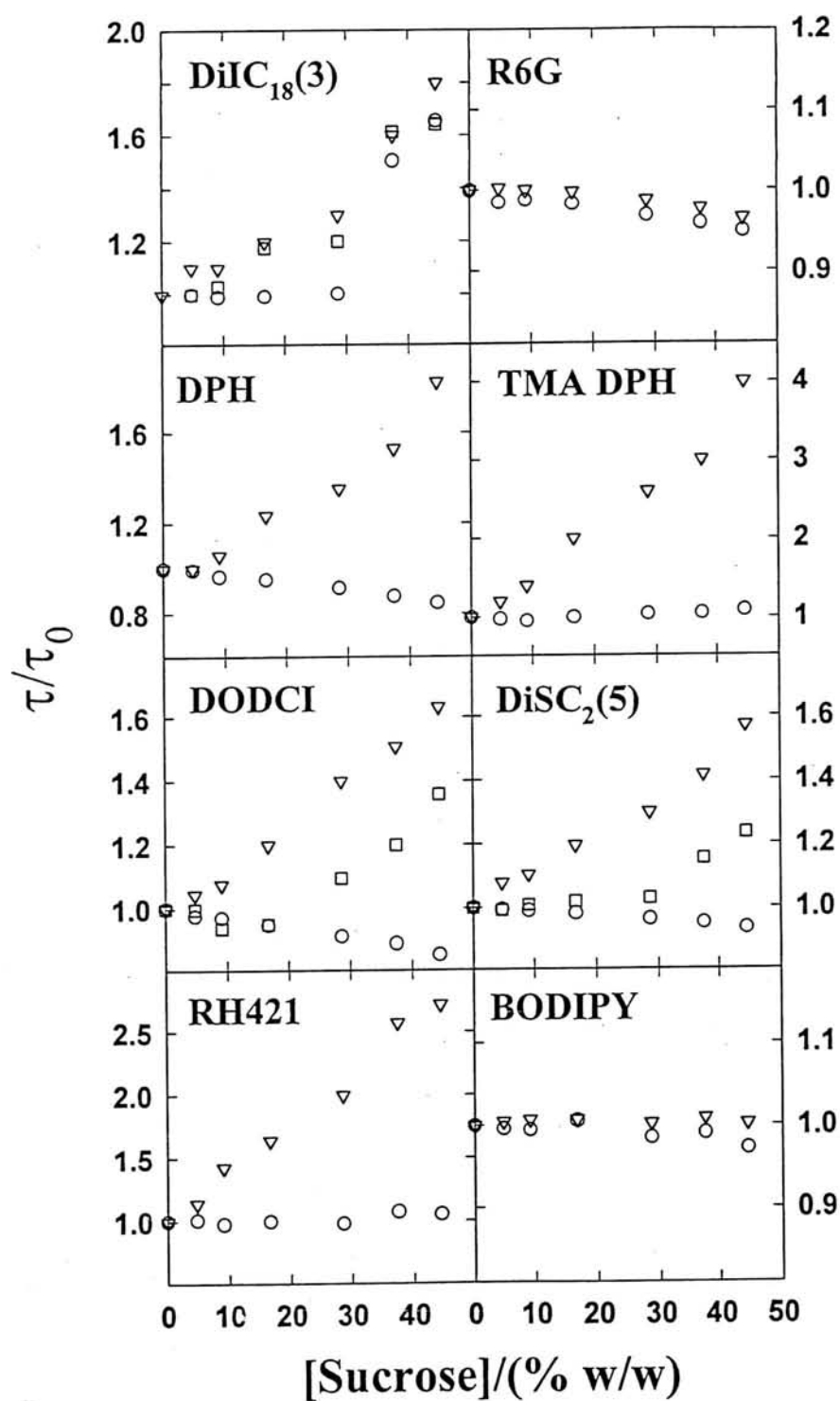


Figure 4.11: Variation of the fluorescence lifetime ratio (τ/τ_0) for the dye with the concentration of sucrose. (∇) Dye in aqueous solution. (○) Dye bound to the membrane (long lifetime or major component). (□) Dye bound to the membrane (short lifetime component).

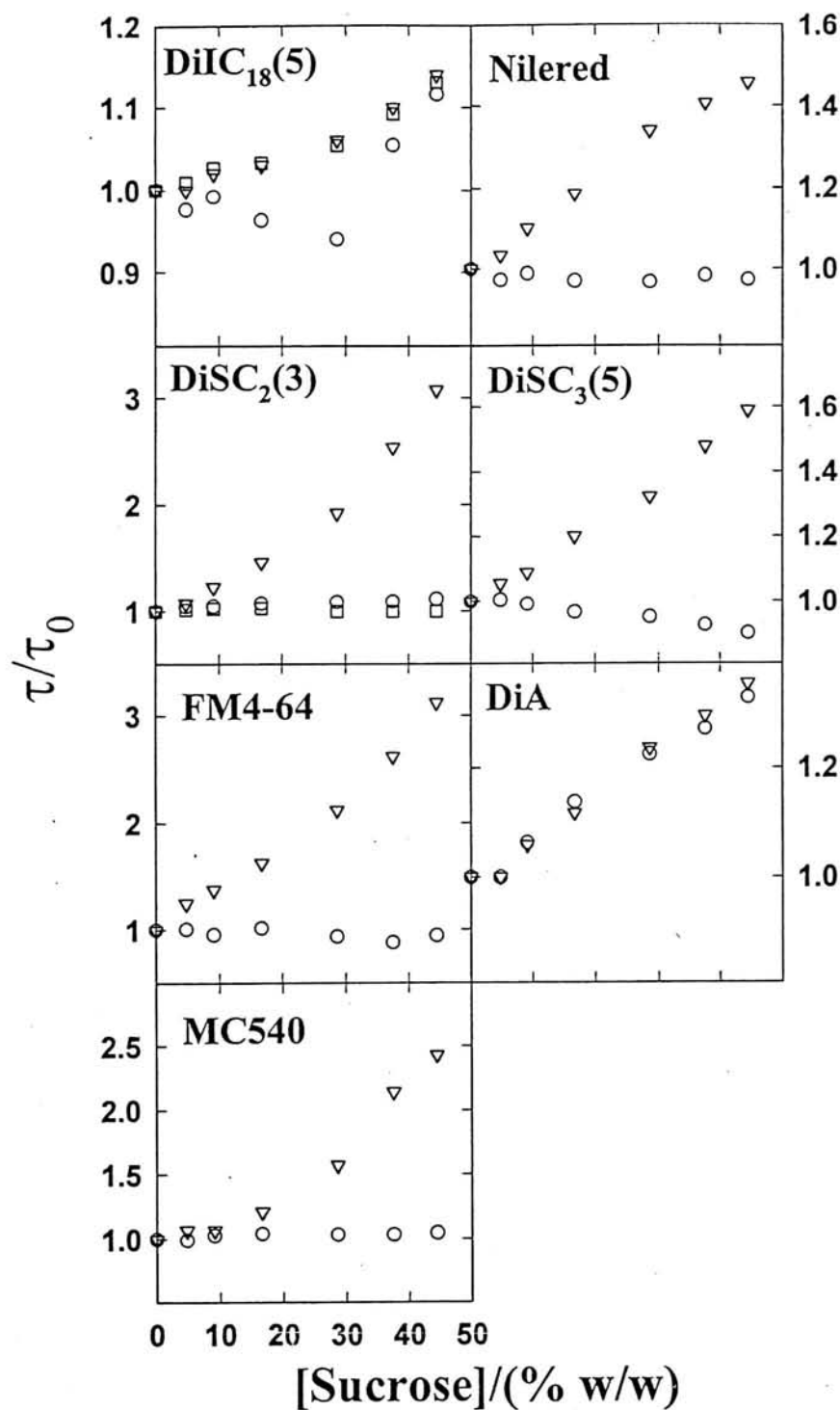


Figure 4.12: Variation of the fluorescence lifetime ratio (τ/τ_0) for the dye v with the concentration of sucrose. (▽) Dye in aqueous solution. (○) Dye bound to the membrane (long lifetime or major component). (◻) Dye bound to the membrane (short lifetime component).

Table 4.3: Site of solubilization of major lifetime components of organic dyes in Egg PC membrane

Dye Number	Dye	τ_w	% Change	τ_1	% Change	Site	τ_2	% change	Site
1	DiIC18(3)	0.10	+80	1.51	x	Interface	0.13	+64	Surface
2	DiIC18(5)	0.10	+14	1.29	x	Interface	0.34	+13	Surface
3	Nilered	0.59	+46	3.71	0	Core			
4	Rhodamine 6G	3.98	-4	4.11	-5				
5	Merocyanine 540	0.14	+143	1.69	+5	Interface			
6	RH421	0.14	+171	1.72	0	Interface			
7	FM4-64	0.08	+213	1.13	-5	Interface			
3	DiA	0.17	+36	0.59	+33	Surface			
9	DPH	0.17	+82	9.61	-15	Core			
10	TMA DPH	0.05	+300	6.11	x	Interface			
11	DiOC2(5) (DODCI)	0.65	+63	1.74	-14	Core	0.66	x	Interface
12	DiSC2(3)	0.13	+208	1.04	+12	Core	0.30	0	Interface
13	DiSC2(5)	0.77	+57	2.03	-7	Core	0.98	x	Interface
14	DiSC3(5)	0.90	+59	2.00	-10	Core			
15	BODIPY 611/627	4.60	0	5.35	-3				

The fluorescence decay of DiA in Egg PC membrane indicates three lifetime components: 0.19ns, 0.59ns and 1.74ns with the respective amplitudes 0.71, 0.26 and 0.03. Negative amplitudes were observed for short lifetime component (0.19ns) at longer emission wavelengths indicating excited state kinetics. The value of the long lifetime (0.59ns) have increased by 33% in the presence of sucrose (44.4% w/w) (figure 4.12 and Table 4.3). The variation of the lifetime with sucrose is shown in figure 4.12. DiA in water also shows three lifetimes (Table 4.1) and the major lifetime (0.17ns) increases with the increase of sucrose which is the viscosity effect (triangles in figure 4.12 and Table 4.3). A comparison of this variation with that of the major component (0.59ns) in membrane suggests that the dye in the membrane is exposed to the aqueous solution and the increase in the lifetime of the membrane-bound dye with sucrose is a viscosity effect. Therefore, we conclude that the site of solubilization of DiA in membrane is on the surface exposed to water. This conclusion is consistent with the structure of the dye where the chromophore is attached to a long alkyl chain.

The fluorescence decay of DODCI in membrane consists of two major components: 0.66ns and 1.74ns with the respective amplitudes 0.43 and 0.57. The lifetime of the short component (0.66ns) shows a decrease followed by a marginal increase and the lifetime of the long component (1.74ns) decreases by 14% with the addition of sucrose (44.4% w/w). The opposite trends of variation of these two components indicate that the site of solubilization for these two species are different. The short component shows the refractive index effect followed by viscosity effect at high sucrose concentrations and hence its site is inferred to be the interfacial region where the exposure to water is partial. On the other hand, the long component shows refractive index effect and hence its site is inferred to be the core region of the membrane.

The change of lifetime of the major components of other membrane-bound dyes in sucrose (44.4%) are given in Table 4.3. The variations are also shown in figures 4.11 and 4.12. Three distinct cases were observed which can be associated with the three different sites of solubilization (figure 4.10) in the bilayer membrane.

(i) The lifetime increases with sucrose and the increase is similar to the case in the aqueous

solution for several dyes: DiIC₁₈(3) (0.13ns), DiIC₁₈(5) (0.34ns), and FM464 (0.1ns). This is the viscosity effect. That means the chromophore is exposed to the solvent in these cases and the site of solubilization for these species (lifetime components) is inferred to be the surface region (indicated s in figure 4.10).

(ii) For a few cases the fluorescence lifetime decreases with sucrose (figures 4.11 and 4.12, and Table 4.3) which is clearly the refractive index effect. These are, DPH (9.61ns), DiISC₂(5) (2.03ns) and DiSC3(5) (2.0ns). For these cases, the fluorescence lifetime is highly viscosity sensitive in aqueous solutions. The species associated with these lifetime components are therefore inferred to be in the core region (indicated c in figure 4.10). All the molecules which show refractive index effect are linear dye molecules and these cases are further discussed in the next section.

(iii) The fluorescence lifetime of some components of the above dyes and several other membrane-bound dyes do not fall in the above two categories. For example, the 0.66ns lifetime component of DODCI in membrane shows a decrease followed by a marginal increase with sucrose compared to that of DODCI in water (figure 4.11). The dye molecule which is placed in the interfacial region of the membrane (indicated i in figure 4.10) is expected to exhibit relatively less viscosity effect than its counterpart which is exposed to water. The lifetime components which show such trends are marked X in Table 4.3. For some other dyes such as RH421, the membrane-bound lifetime (1.72ns) shows no variation whereas the fluorescence lifetime of the dye present in the aqueous phase is highly viscosity sensitive (figure 4.11 and Table 4.3). The sites of solubilization for these dyes were assigned as the interfacial region of the membrane (indicated i in figure 4.10).

Finally, the fluorescence lifetimes of BODIPY and Rhodamine 6G are not sensitive to viscosity like all the other dyes (figure 4.11). Even if these dye molecules are present on the surface it is not possible to observe the viscosity effect. The site of solubilization cannot be assigned for these dyes. The lifetimes of these dyes bound to the membrane show marginal decrease which is consistent with the refractive index effect. Table 4.3 summarizes the sites of solubilization determined for the fluorescent probes in Egg PC membrane based on the combined effects of viscosity and refractive index on the fluorescence lifetime(s) of

the membrane-bound dye.

4.4.4 Location of DODCI and DiIC₁₈(5) in Egg PC: NMR experiments

Nuclear Magnetic Resonance (NMR) experiments were carried out on DODCI and DiIC₁₈(5) in Egg PC vesicles to obtain independent information about the location of these dyes in the membrane phase. The strategy was to monitor the changes in the chemical shifts of the proton resonances of the lipid by the addition of the dye. In addition, it was also intended to characterize the lipid-dye interactions in the 2D NOESY spectra of the respective complexes.

The proton NMR experiments were carried out on a Varian Unity Plus spectrometer with a ¹H frequency of 600MHz. The experiments included one dimensional (1D) ¹H spectra and two dimensional (2D) Nuclear Overhauser Effect spectroscopy (NOESY) [153] with a mixing time of 500ms. All the experiments were carried out at pH 4.3 (deuterated acetate buffer, 100mM) and temperature 25°C. For the NMR experiments concentrations of the lipid and the dye used were 25 and 5 mM respectively, that is in the dye to lipid ratio of 1:5. NMR spectra recorded at the dye to lipid ratios 1:10 and 1:25 showed very weak or no signals for the dye protons compared to the lipid protons and it was impossible to assign the chemical shifts for all the dye protons.

The lipid molecules of EggPC are a mixture of several structurally different lipids with varying lengths of the acyl chains with POPC (Palmitoyl, oleoyl Phosphatidyl choline, structure shown in figure 4.13) being the major component [7]. The one dimensional ¹H NMR spectrum of EggPC vesicles was identical to that reported in literature [231, 232] and hence the resonance assignments of all the individual protons belonging to the head group and the alkyl chain were straight forward. Upon the addition of the dye (5mM, dye:lipid ratio 1:5), significant change in the chemical shifts of the head group and alkyl protons were observed. Table 4.4 gives the chemical shifts obtained for various lipid protons with and without the dye. The lipid protons labelled a-i are indicated in figure

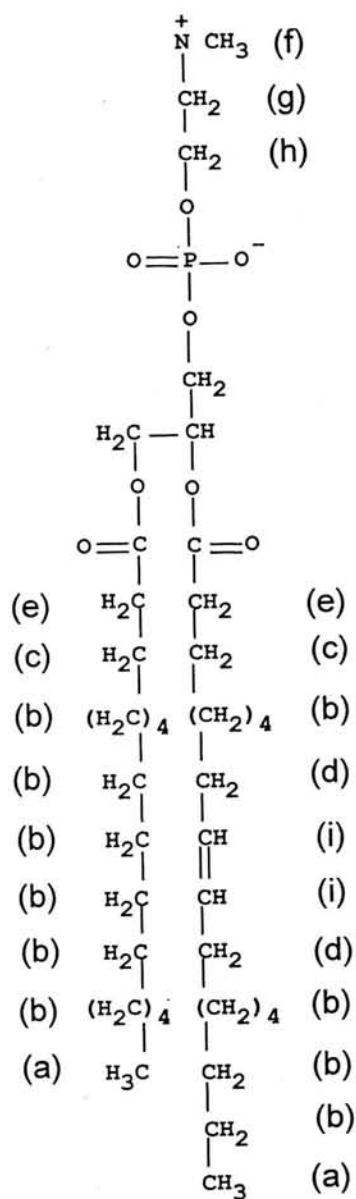


Figure 4.13: Structure of the lipid molecule POPC (C16:0/18:1, Palmitoyl, Oleoyl Phosphatidyl Choline). The chemical shifts of the labelled protons with and without the dye molecules are given in Table 4.4.

4.13. The protons labelled j were not identified. The change in the chemical shifts for some of the head group and alkyl protons induced by DODCI is opposite and different in magnitude to those observed with DiIC₁₈(5).

The aromatic proton resonances of the dye molecules in EggPC vesicles were observed in the 1D spectrum ($6 < \delta < 8$ ppm), but they were weak and broad. Hence, no crosspeaks could be observed between the aromatic protons of the dye and the protons of the lipid in the 2D-NOESY spectrum recorded with a mixing time of 500 ms. On the other hand, the alkyl protons of the dye molecules could not be identified as they overlapped with the lipid protons.

As seen in Table 4.4, large change in the chemical shifts are observed only for some protons of the lipid molecule when the dye molecule is intercalated in the membrane. This is useful to characterize the location of the dye molecule. In the case of DiIC₁₈(5), major changes in the chemical shifts occurred for the proton resonances belonging to the head group region (mainly CH₂-C-COO and CH₂N protons). The change in the chemical shifts of other aliphatic acyl chain proton is insignificant. This indicates that the DiIC₁₈(5) is located on the surface of the membrane in the vicinity of NCH₂ protons of the choline group and the CH₂-C-COO protons at the beginning of the acyl chain. In the case of DODCI also, major change in the chemical shift is observed for the CH₂-C-COO protons which is located near the surface indicating solubilization near the surface region of the membrane. However, in this case, protons of the alkyl chain, (CH₂)_n are also affected significantly and therefore one can infer that the molecule is present also in the core of the bilayer. In general, when compared to the changes in the chemical shifts of Egg PC protons in the presence of DiIC₁₈(5), the chemical shifts of the lipid protons are affected more strongly in the case of DODCI. This indicates that DODCI exists in multiple locations and multiple orientations in the bilayer. Although the chromophore structure is the same in the case of DODCI and DiIC₁₈(5), because of the long alkyl chains of 18 carbon atoms length, DiIC₁₈(5) gets solubilized near the surface of the membrane with its two alkyl chains oriented parallel to the lipid chains of the Egg PC bilayer.

It is interesting to note that the chemical shift of the CH₂-C-COO protons is affected

Table 4.4 NMR chemical shifts of Egg PC protons before and after the dye addition

Egg PC proton peak assignment (see figure 4.12)	Egg PC Chemical Shift $\delta(\text{ppm.})$	DODCI + Egg PC		DiIC ₁₈ (5) + Egg PC	
		Chemical Shift $\delta(\text{ppm.})$	Difference $\Delta\delta(\text{ppm.})$	Chemical Shift $\delta(\text{ppm.})$	Difference $\Delta\delta(\text{ppm.})$
(a) Terminal CH ₃ 's	0.86	0.86	0.00	0.86	0.00
(b) (CH ₂) _n	1.25	1.23	0.02	1.25	0.00
(c) CH ₂ -C-COO	1.55	1.50	0.05	1.62	-0.07
(d) CH ₂ -C=C	2.00	1.98	0.02	2.01	-0.01
(e) CH ₂ -COO	2.30	2.30	0.00	2.31	-0.01
(f) N(CH ₃) ₃	3.22	3.20	0.02	3.22	0.00
(g) CH ₂ N	3.66	3.64	0.02	3.62	0.04
(h) CH ₂ OP(polar chain)	4.26	4.25	0.01	4.27	-0.01
(i) CH=CH	5.27	5.25	0.02	5.28	-0.01

by the DODCI and DiIC₁₈(5) in opposite ways. Since it is the aromatic ring of the dye molecule which is responsible for the large change in the chemical shift it is possible to derive some conclusion about the orientation of the dye molecule with respect to these protons. In the case of DiIC₁₈(5) the chemical shift increases which indicates a ring current deshielding effect [233] on the lipid protons. Thus one may infer that the aromatic plane of the dye is perpendicular to the membrane surface such that the CH₂-C-COO protons are present on either side of the aromatic plane of the dye. In the case of DODCI, there is no evidence for the ring current effect on the CH₂-C-COO protons. On the other hand, the chemical shift is less for these protons indicating a diamagnetic shielding. Thus, one can infer that the orientation of the aromatic plane of DODCI is random with respect to these protons which is consistent with the increased orientational freedom for DODCI because of the absence of long alkyl chain as in the case of DiIC₁₈(5).

4.4.5 Oriented dye molecules in the core of the bilayer membrane

As discussed earlier, the dependence of the radiative rate of a membrane-bound fluorophore on the refractive index of the medium external to the membrane (here aqueous medium) depends on its orientation with respect to the interface, according to equation 4.4. Such effects can be observed only for dyes which have linear structure and the long axis of the molecule is oriented with respect to the membrane interface. Theory predicts that the fluorescence lifetime (inverse of the sum of radiative and nonradiative rates) decreases with the increase of refractive index of the aqueous solution when the radiative rate dominates over the nonradiative rate. This dependence can be used to extract the information about the probe orientation in the bilayer membrane. Of the fifteen organic dye molecules used in this study, only four dyes DPH, DODCI (DiOC₂(5)), DiSC₂(5) and DiSC₃(5) in Egg PC membrane showed a decrease in the fluorescence lifetime of the membrane-bound dye with the increase of sucrose concentration. It may be noted that this effect is observed only for the long lifetime component for which the nonradiative rate

is negligible. This is unambiguously the refractive index effect which is expected for the oriented dye molecules in the membrane. The decrease of fluorescence lifetime with the external refractive index is previously reported in literature [200] for DPH. Dicarbocyanine dye molecules are new addition to this class of oriented dyes.

Figure 4.14 shows the decrease in fluorescence lifetime with the refractive index of the aqueous medium in which the Egg PC vesicles were made. The experimental data have been fitted to $\tau \propto (n_0)^{-m}$ and the value of m for each dye is indicated in the respective plots. Among the three dicarbocyanines, DODCI shows maximum variation in the fluorescence lifetime with the external refractive index: $m = 2.6$ for DODCI, $m = 1.2$ for DiSC₂(5) and $m = 1.9$ for DiSC₃(5). A value of $m=5$ indicates that the dye is oriented normal to the membrane ($\theta=0$ in equation 4.4) and $m=1$ indicates an orientation parallel to the surface ($\theta=\pi/2$ in equation 4.4). The observed values of m for the four dyes suggest that they are oriented at different angles.

The immediate question that arises is how are these molecules oriented in the membrane. This is addressed in the next chapter (Chapter 5).

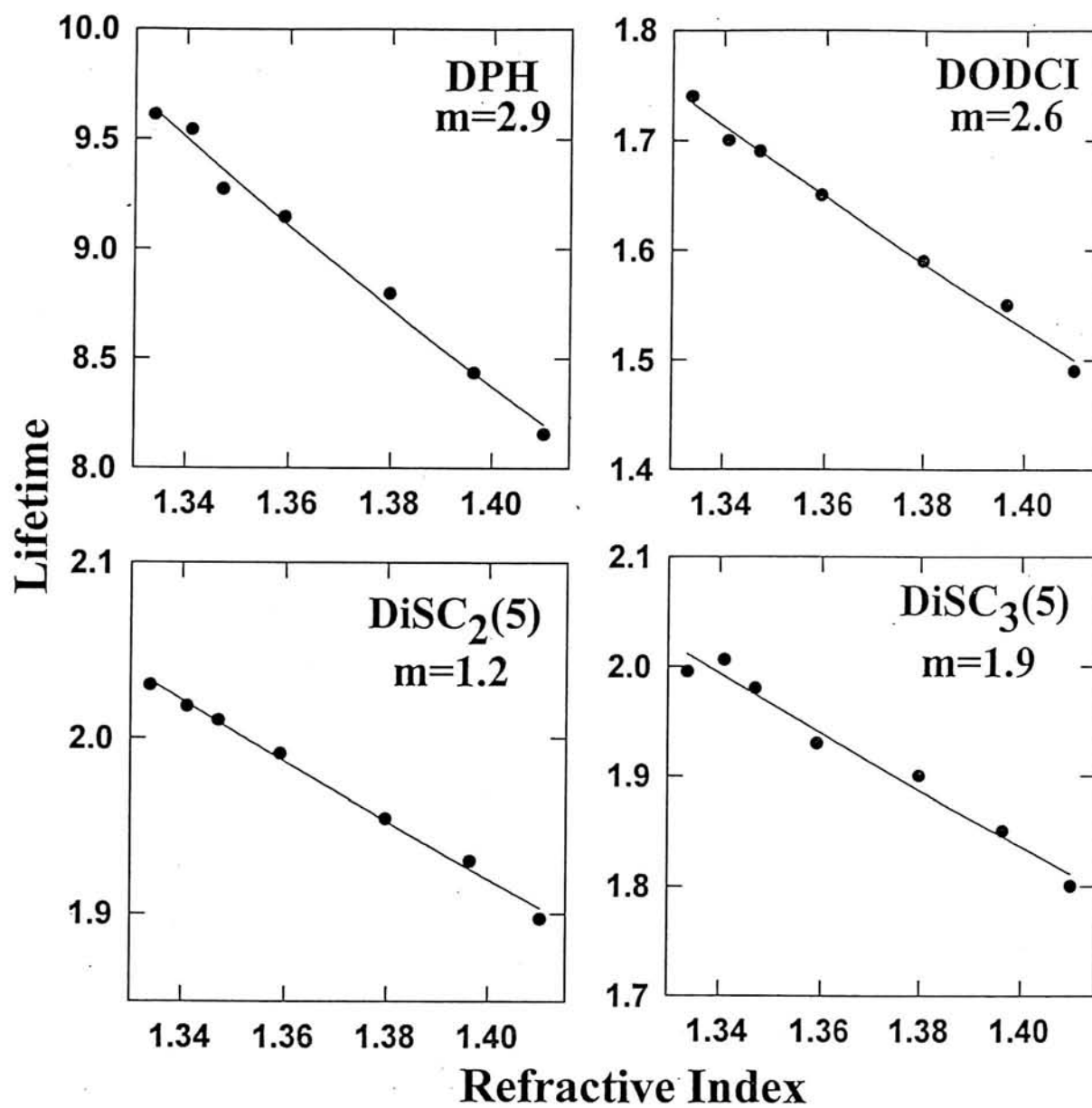


Figure 4.14: Variation of the long fluorescence lifetime of the four dyes DPH, DODCI, DiSC₂(5) and DiSC₃(5) in Egg PC vesicles with the external refractive index. The values of m obtained by fitting $\tau \propto (n_0)^{-m}$ are indicated in the plots.

Chapter 5

Orientational Distribution of Linear Dye Molecules in Bilayer Membranes

Many biological phenomena on/in membrane are orientation specific. The transport of ions and small molecules across the lipid bilayer membrane, action of drug molecules, function of receptors and other signal transmitting molecules, response of the voltage sensitive dyes to the voltage across a bilayer membrane are some of the well-known examples for the orientation dependent mechanisms. Organic fluorescent dye molecules are commonly used to study the structure, function and dynamics of biological membranes in relation with the membrane related functions [52, 223, 51, 53, 48]. The location and orientation of these fluorescent probes in the bilayer membrane must be known for unambiguous interpretation of membrane-based biological phenomena. Determination of the location of fluorescent probes in a bilayer membrane using the combined effects of viscosity and refractive index on the fluorescence lifetime of the membrane-bound dye was described in the last chapter (Chapter 4). This chapter answers the question of how the fluorescent dye molecules get oriented in a bilayer membrane.

Small and large molecules get randomly oriented in all possible directions in liquids. The anisotropic nature of the bilayer membrane may however restrict the orientational freedom of even small molecules in a lipid bilayer membrane. The membrane is a highly

ordered dynamic structure. The orientation of a dye molecule in a lipid bilayer membrane is facilitated by the van der Waals and electrostatic interactions between the dye molecule and the lipid acyl chains. Since the acyl chains of the membrane are oriented, a dye molecule will have a preferential orientation and the fluorescent probe cannot get oriented in all random directions in the lipid bilayer membrane. If the molecule is polar or ionic, then the polar end of the molecule will be oriented towards the aqueous phase. Hence the orientational distribution of a dye molecule in the membrane will be highly anisotropic.

Time resolved fluorescence anisotropy is commonly used to determine the orientational distribution of a fluorescent dye molecule in a bilayer membrane. Different orientational distributions were proposed in literature to explain the anisotropy decay kinetics of fluorescent probes in bilayer membranes and the use of time resolved anisotropy has not led to an unambiguous determination of the orientational distribution. Since the effect of external refractive index on the fluorescence lifetime of a dye molecule in a bilayer membrane is orientation dependent (section 4.2), one can also use this property to resolve the orientational distribution of linear dye molecules in a lipid bilayer membrane, in addition to the time resolved anisotropy measurements.

5.1 Order parameters

5.1.1 Theory

The orientational distribution is generally expressed in terms of order parameters [50, 54], some of which are experimentally measurable. The theory of order parameters is as follows. Let z-axis represents the symmetry axis of the probe orientational distribution in the lipid bilayer which is also called as the director axis. The direction of the director axis is controlled by the orientation of the lipid chains with respect to the membrane surface and this is generally parallel to the membrane normal. The orientational distribution of the fluorescent probe molecules in a bilayer membrane is determined by the mobility of the lipid chains and the free volume available for the probe molecules between the lipid

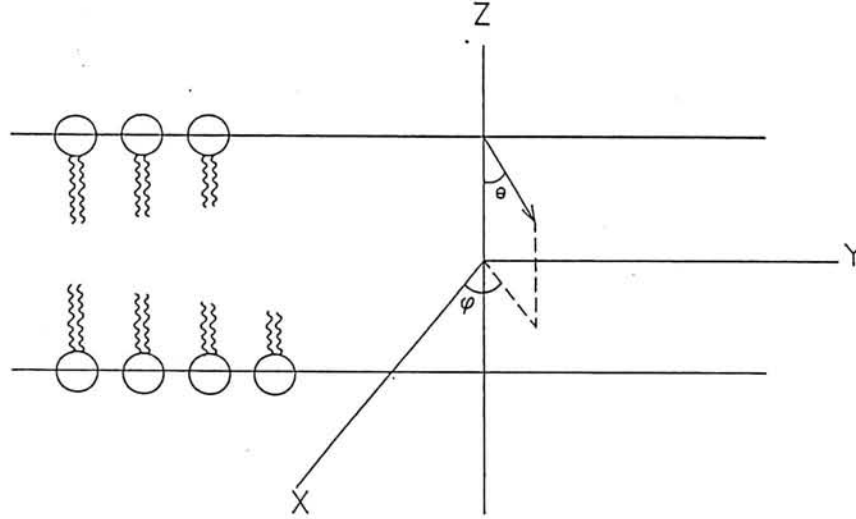


Figure 5.1: The two polar angles θ and ϕ required to specify the orientation of a linear probe molecule in a lipid bilayer

chains. The orientation of a fluorescent probe molecule can be represented by the two polar angles θ and ϕ in the coordinate system with the director axis as the z-axis and the xy-plane perpendicular to the z-axis (see figure 5.1). The orientational distribution $P(\Omega)$ then consists of two parts: $P(\theta)$ and $P(\phi)$. Since the symmetry of the bilayer membrane is uniaxial i.e., the probability of orientation of a molecule is independent of the angle ϕ , $P(\phi)$ becomes constant ($1/2\pi$). $P(\phi)$ will not be a constant in case of other ordered systems where the uniaxial symmetry fails. The orientational distribution $P(\theta)$ has to satisfy two conditions: (i) the symmetry condition of the lipid bilayer i.e., $P(\theta) = P(\pi - \theta)$ and (ii) normalization condition i.e., $\int P(\theta) \sin\theta d\theta = 1$. One can obtain complete information about $P(\theta)$ in experiments if $P(\theta)$ follows a simple distribution function such as $P(\theta) = \delta(\theta - \theta')$ where the dye molecules are oriented at a particular angle θ' . However, for arbitrary $P(\theta)$, $P(\theta)$ can be expressed as a linear combination of Legendre Polynomials, which are a complete set of orthogonal functions when integrated over $\sin\theta d\theta$. Using the two conditions which $P(\theta)$ has to satisfy, the orientational distribution becomes

$$P(\theta) = \sum_l \langle P_l \rangle P_l(\cos\theta) \quad (l \text{ even}) \quad (5.1)$$

The constants $\langle P_l \rangle$ which are known as the order parameters of the probe distribution, represent the set of orientational averages defined by

$$\langle P_l \rangle = \int P_l(\cos\theta) P(\theta) \sin\theta d\theta \quad (5.2)$$

When the system is perfectly aligned where the probe molecules are oriented along the director axis, the value of the order parameters becomes one. In the case of a completely disordered system where the probe molecules take all orientations, the order parameters become zero. Hence the variations in these represent the order of the system and hence these are called the order parameters. The knowledge of all these order parameters completely defines the orientational distribution of the probe molecules in the system. Except in the case of simple orientational distributions, all of these order parameters cannot be experimentally determined. However, the measurement of some of these makes us to rule out some of the possible orientational distributions for the probe molecules in the system and favour the others which should satisfy the experimentally measured order parameters. The second rank order parameter $\langle P_2 \rangle$, is the one which is generally obtained in fluorescence measurements.

$$\langle P_2(\cos\theta) \rangle = \frac{3 \langle \cos^2\theta \rangle - 1}{2} \quad (5.3)$$

For some distributions such as wobbling-in-a-cone model [95, 96], measurement of $\langle P_2 \rangle$ alone fully describes the orientational distribution. The fourth rank order parameter $\langle P_4 \rangle$ was also measured from fluorescence anisotropy measurements in some cases [54, 98, 234, 99, 235, 236]. Although the exact orientational distribution $P(\theta)$ cannot be experimentally obtained in most cases, the knowledge about the order parameters increases our knowledge on the system.

5.1.2 Measurement

The second rank order parameter $\langle P_2 \rangle$ (called as order parameter from now onwards) is measured in a model-independent way from the time resolved fluorescence anisotropy

[102, 103, 96, 54] as

$$\langle P_2 \rangle_a = \left(\frac{r_\infty}{r_0} \right)^{\frac{1}{2}} \quad (5.4)$$

where r_0 and r_∞ represent the fluorescence anisotropies at zero time and at 'infinite' time after excitation. The subscript a indicates that the order parameter is determined from the fluorescence anisotropy measurements. The value of the initial anisotropy r_0 depends on the probe molecule and the excitation and emission wavelengths whereas the anisotropy at infinite time, in addition to these parameters, depends on the orientational freedom of the molecule in the system. If the molecule is free to occupy all possible orientations in the system, then the initially created anisotropic population by the polarized excitation light decays to a random orientational distribution giving rise to $r_\infty = 0$ and hence the order parameter $\langle P_2 \rangle_a$ becomes zero in such a case. For a fluorescent probe molecule in a system such as bilayer membrane where the dye cannot orient in all random directions, the r_∞ will be non-zero and hence the order parameter $\langle P_2 \rangle_a$ becomes finite.

The order parameter can also be determined from fluorescence lifetime measurements. The fluorescence decay of a linear dye molecule intercalated in a lipid bilayer membrane is faster in the presence of sucrose in the aqueous solution (section 4.2). This is the consequence of the effect of refractive index on the radiative decay of an oriented dye molecule [228, 229, 200, 54]. The fluorescence lifetime of a dye molecule in a bilayer membrane depends on its orientation in the membrane and the refractive indices of the aqueous and lipid media (equation 4.4). This can be used to deduce the orientation of the dye molecule in the bilayer membrane. The order parameter $\langle P_2 \rangle$ can be determined from the variation of the radiative rate k_r with the external refractive index n_0 (refer to equation 4.4) [200] as

$$\langle P_2 \rangle_\tau = \frac{An_1^4 - \frac{1}{2}B}{An_1^4 + B} \quad (5.5)$$

where A and B are the slope and intercept of the linear plot

$$\frac{\left(\frac{1}{\tau} - k_{nr} \right)}{n_0} = An_0^4 + B \quad (5.6)$$

where n_0 and n_1 represent the refractive indices of the aqueous and lipid phases and k_{nr} is the nonradiative rate. The subscript τ indicates that the order parameter is determined

from the lifetime data. The calculation of $\langle P_2 \rangle_\tau$ requires the determination of n_1 , the refractive index of the bilayer membrane and k_{nr} , nonradiative rate of the membrane-bound dye.

5.2 Refractive index of the membrane

Refractive index of the bilayer membrane was measured according to the procedure described in [200]. The efficiency of light scattering by the lipid vesicles depends on the difference between the refractive indices of the membrane (n_1) and the external aqueous medium (n_0). The scattering will be minimum when the two refractive indices match. In the vicinity of $n_0 = n_1$, the scattering efficiency by the lipid vesicles can be described by the parabola

$$A = \alpha(n_0 - n_1)^2 + \beta \quad (5.7)$$

where A is the absorbance of the unlabelled vesicles, α and β are the constants. The above equation is obtained by the Taylor expansion of the function $A(n_0)$ in the vicinity of the minimum ($n_0 = n_1$) [200]. Absorbance estimates of scattering efficiency should be made on unlabelled vesicles at a wavelength outside the absorption band of the bilayer material and for this purpose, the wavelength 450nm was selected [200].

Figure 5.2 shows the variation of the absorbance of unlabelled Egg PC lipid vesicles with the external refractive index, measured at a lipid concentration of 1.43mg/ml and at the wavelength 450nm. Sucrose was used to vary the refractive index of the aqueous medium in which vesicles were prepared. This data was fitted to the parabolic equation 5.7 and the refractive index of the bilayer is obtained as $n_1=1.406$.

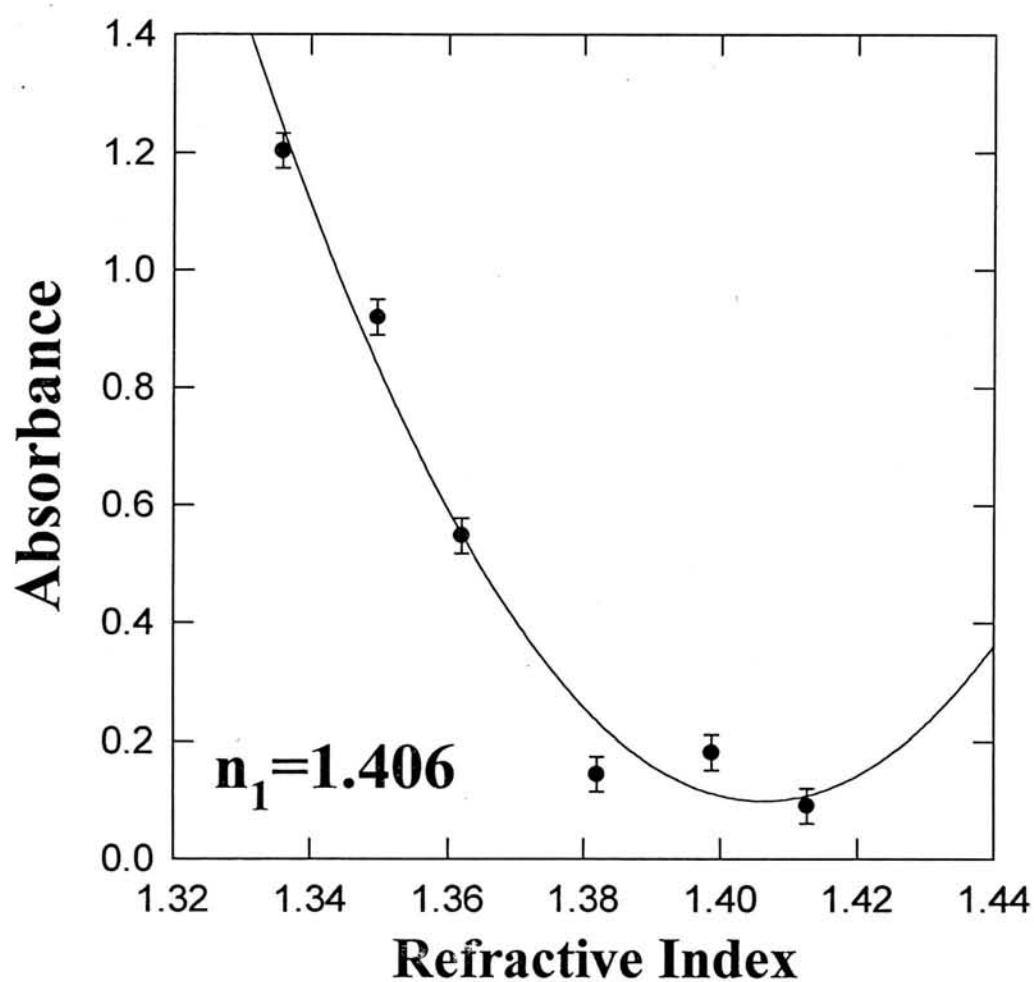


Figure 5.2: The plot of absorbance due to scattering of unlabelled Egg PC lipid vesicles at 450nm versus refractive index of the aqueous medium. The absorbance measurements were done at a lipid concentration of 1.43mg/ml and sucrose is used to vary the refractive index of the aqueous medium in which vesicles were prepared.

5.3 Orientation of the linear dye molecules: Dicarboxyanines and DPH

As described in the last chapter (section 4.2), the three dicarboxyanines DODCI (DiOC₂(5)), DiSC₂(5) and DiSC₃(5) and DPH are the only molecules which show the signature of an oriented dye molecule in the core of the bilayer, i.e., whose lifetime decreases with the increase of external refractive index (figure 4.14). Hence for these molecules, the order parameters can be determined from the lifetime measurements. For the measurement of $\langle P_2 \rangle_\tau$, one needs to know the value of the nonradiative rate k_{nr} for that species (the long lifetime component) inside the bilayer membrane (refer equation 5.6). The assumption made in using equation 5.6 to calculate $\langle P_2 \rangle_\tau$ is that k_{nr} is unchanged for the long lifetime of the membrane-bound dye located in the core of the bilayer with the addition of sucrose in the aqueous medium. For all the four dye molecules, the fluorescence decay is due to either two or three species. The measurement of nonradiative rate for a particular component requires the estimation of the number of excitation photons absorbed and the number of fluorescence photons emitted by that particular species. One can determine the amount of fluorescence photons by using the method of Decay Associated Spectra (DAS) but there is no way to determine the amount of excitation photons absorbed by a particular component in a multi-component system. This makes it impossible to determine the nonradiative rate for one species alone based on fluorescence quantum yield measurements in membranes. The nonradiative rate is assumed to be negligible for the long lifetime component of DPH and dicarboxyanines in the Egg PC membrane. This is a reasonable assumption because the long lifetime component value is comparable to or higher than its value in highly viscous glycerol, where the quantum yield approaches unity.

The order parameters $\langle P_2 \rangle_\tau$ for the four linear dyes were determined using the experimental results (τ versus n_0) and the value of the refractive index for the bilayer membrane $n_1=1.406$, assuming that $k_{nr}=0$. The calculated values of $\langle P_2 \rangle_\tau$ are 0.257 (DPH), 0.141 (DODCI), -0.137 (DiSC₃(5)) and -0.422 (DiSC₂(5)). It may be noted that

$\langle P_2 \rangle_\tau$ is negative for DiSC₂(5) and DiSC₃(5). The order parameters $\langle P_2 \rangle_a$ were also calculated from the time resolved anisotropy measurements from the limiting values $r(0)$ and $r(\infty)$ (equation 5.4). The calculated values are 0.267 (DPH), 0.513 (DODCI), 0.424 (DiSC₃(5)) and 0.320 (DiSC₂(5)). It is clear that the values of $\langle P_2 \rangle_\tau$ and $\langle P_2 \rangle_a$ are not equal.

The reason for the observed discrepancy between $\langle P_2 \rangle_\tau$ and $\langle P_2 \rangle_a$ is as follows: the order parameter $\langle P_2 \rangle_a$ from the anisotropy measurements is with respect to the director axis, i.e., the symmetry axis of the probe distribution in the bilayer whereas the measurement of the order parameter $\langle P_2 \rangle_\tau$ from the fluorescence lifetime measurements is with respect to the membrane normal. When these two reference axes are not equal, then the two order parameters $\langle P_2 \rangle_\tau$ and $\langle P_2 \rangle_a$ need not be equal. The measurement of $\langle P_2 \rangle_\tau$ in addition to $\langle P_2 \rangle_a$ offers an additional parameter in determining the orientational distribution of fluorescent probe molecules in a lipid bilayer membrane.

The question of the orientational distribution of linear dye molecules in a bilayer membrane has been addressed in several experimental studies using fluorescence anisotropy as the measured parameter [237, 95, 96, 50, 97, 98, 234, 99, 51, 236, 53, 100, 238, 54, 101, 239]. A fixed orientation of the dye in the membrane was ruled out by the low value of steady-state anisotropy and more importantly the anisotropy decay. Many models of orientational distribution were considered to explain the observed fluorescence anisotropy decays of the probe molecules in bilayer membranes. In many cases, it was found that the measurement of a single order parameter $\langle P_2 \rangle_a$ does not give complete information about the orientational distribution of the probe molecules in a bilayer. In some cases, the fourth rank order parameter $\langle P_4 \rangle_a$ was measured assuming a single population of the dye molecules inside the bilayer membrane and a higher order description of the fluorescence anisotropy decay for a rodlike fluorophore [98]. Using the two order parameters $\langle P_2 \rangle_a$ and $\langle P_4 \rangle_a$, attempts were made to obtain the orientational distribution of fluorescent dye molecules in bilayer membranes [98, 234, 99, 235, 236]. This approach cannot be used in our case as the fluorescence decay in most cases is from the dye located in two different sites in the membrane. Here we used the effect of refractive index on the fluorescence

lifetime of the membrane-bound dye to determine the order parameter $\langle P_2 \rangle_\tau$ which can be used, in addition to $\langle P_2 \rangle_a$, to deduce the information about the orientational distribution of the probe molecules in the lipid bilayer.

The observed discrepancy between the two order parameters is similar to the one observed in the case of DPH in DPPC [200]. In this case, the fluorescence decay is almost single exponential with 92% being the fractional amplitude of the long lifetime in the total fluorescence intensity decay. This fluorescence lifetime decreases with the increase of the external refractive index. The fluorescence lifetime data was fitted to the equation $\tau \propto n_0^{-m}$ and the m value was obtained as 2.6. The values of $\langle P_2 \rangle_\tau$ and $\langle P_2 \rangle_a$ measured in this case were 0.285 and 0.910 respectively [200].

The discrepancy between the two order parameters can be explained if the probe molecules are assumed to be oriented at an angle with respect to the membrane normal. The average orientation angle θ' of the probe molecules can be calculated from the ratio of the two order parameters as

$$\frac{3\cos^2\theta - 1}{2} = \frac{\langle P_2 \rangle_\tau}{\langle P_2 \rangle_a} \quad (5.8)$$

Toptygin and Brand [200] used this approach to calculate the orientation angle in the case of DPH in DPPC as 43° with respect to the membrane normal. It was suggested that the lipid chains may be oriented at such angles, thereby aligning DPH at the same angle. In the absence of any independent experimental evidence, it is quite unlikely that the lipid chains are oriented at such a large angle and hence the question of the orientation of DPH in the bilayer membrane was left open.

Following the same approach, the orientation angles for the dyes in the Egg PC membrane were calculated as 9° for DPH, 44° for DODCI and 70° for DiSC₂(5). The orientation angle cannot be calculated for DiSC₃(5) using equation 5.8. The orientation of the linear dyes in a bilayer membrane at extremely low concentrations of the dye used (1:500 dye to lipid ratio) will be entirely decided by the orientation of the lipid chains. The variation of orientation angles for different linear dyes in the same bilayer membrane cannot be explained in terms of the orientation of the lipid chain or any other reasonable model.

Hence a single population of the fluorescent probe molecules in a lipid bilayer membrane (unimodal orientational distribution) at a tilted angle from the membrane normal cannot explain the discrepancy between the two order parameters.

A bimodal orientational distribution of the fluorescent probe molecules in a bilayer membrane can satisfactorily explain the observed experimental results: (a) the negative values for $\langle P_2 \rangle_\tau$ for some dyes and (b) the difference in the values of the two order parameters obtained from lifetime and anisotropy measurements. In this model, the orientational distribution of the linear dye molecules in the core region (that is, the fraction with the long lifetime component) consists of two populations which are oriented about the parallel ($\theta=0$) and the perpendicular ($\theta=\pi/2$) axes with respect to the membrane normal. These two represent the orientations at which the probe molecule is stabilized to the maximum extent by the van der Waals interactions between the dye molecule and the lipid chains. $\theta = 0$ population represent the dye molecules oriented along the lipid chains and $\theta = \pi/2$ represent the dye molecules oriented perpendicular to the lipid chains, i.e., parallel to the membrane surface. The potential barrier for intermediate orientations is sufficiently high that the net population in the intermediate orientations is small. The order parameter determined by the lifetime method (refractive index effect) is with respect to the membrane normal and given by

$$\langle P_2 \rangle_\tau = f \langle P_2 \rangle_{\theta=0} + (1-f) \langle P_2 \rangle_{\theta=\pi/2} \quad (5.9)$$

where f is the fraction of molecules oriented about $\theta=0$, and $\langle P_2 \rangle_{\theta=0}$ and $\langle P_2 \rangle_{\theta=\pi/2}$ are the order parameters for the two populations. In the extreme case of fixed orientations at $\theta=0$ and $\theta=\pi/2$, $\langle P_2 \rangle_{\theta=0}=1$ and $\langle P_2 \rangle_{\theta=\pi/2}=-0.5$. Negative values for $\langle P_2 \rangle_\tau$ are therefore possible if $f < \frac{1}{3}$. The values of f calculated for this extreme case are 0.504 (DPH), 0.427 (DODCI), 0.242 (DiSC₃(5)) and 0.052 (DiSC₂(5)). In this model, $\langle P_2 \rangle_a$ represents the average orientational freedom in the two orthogonal populations and this value will be always positive and greater than or equal to $\langle P_2 \rangle_\tau$, irrespective of the value of f in the above model. However, realistic values for f can be calculated only when an accurate angular distribution is known.

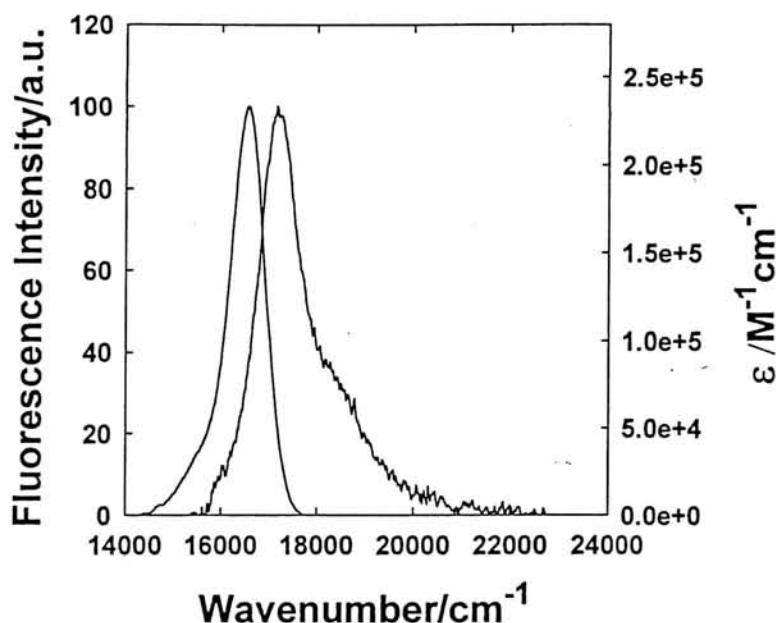


Figure 5.3: The normalized absorption and emission spectra of DODCI in 56% aqueous glycerol solution (refractive index 1.406)

Further discussion on the orientational distribution of linear dye molecules in bilayer membranes concentrates on determining the exact orientational distribution of one of the dicarbocyanines DODCI in Egg PC and DPH in DPPC (the values of the order parameters in the case of DPH in DPPC were taken from literature [200]). In the case of calculation of $\langle P_2 \rangle_\tau$ for DODCI in Egg PC, the assumed value of k_{nr} as zero can be improved. This is determined as follows. The radiative rate k_r for the membrane-bound dye is independent of its orientation when $n_0 = n_1$ (refer equation 4.4). Therefore, the value of k_r in membrane is taken to be equal to the value of k_r determined in an aqueous glycerol solution whose refractive index is n_1 . The value of k_r in aqueous glycerol was determined using the Strickler-Berg equation [145, 86] as described in Chapter 2 (section 2.3.3). Figure 5.3 shows the normalized absorption and fluorescence spectra of DODCI in 56% aqueous glycerol solution whose refractive index is that of the refractive index of the membrane (1.406). The 0-0 transition of $S_0 - S_1$ is the frequency at which the normalized absorption and fluorescence spectra intersect. The integration of the spectra according to the Strickler-Berg equation gave the value of k_r as $0.513(\text{ns})^{-1}$. The measured fluorescence lifetime for the membrane-bound dye for the same condition is 1.52 ns. The nonradiative rate for the dye is calculated as $0.145(\text{ns})^{-1} (\tau^{-1} - k_r)$. Using the values of the nonradiative

rate and the refractive index of the bilayer (n_1), the $\langle P_2 \rangle_\tau$ was calculated as 0.428 from the variation of the long lifetime (1.76ns) of the membrane bound dye as a function of the external refractive index (n_0).

The order parameter from anisotropy $\langle P_2 \rangle_a$ was obtained from the anisotropy values at zero time (r_0) and at infinite time (r_∞). The r_0 value is determined to be 0.375 from the time resolved anisotropy decay of DODCI in glycerol in which the rotational correlation time of the dye is very long. The anisotropy at infinite time (r_∞) was determined to be 0.099 from the time resolved anisotropy decay of DODCI in Egg PC membrane. It may be noted that fluorescence decay at times greater than 2ns is strongly weighted towards the long lifetime component (in this case the membrane-bound dye with lifetime of 1.76ns) and hence the experimentally determined r_∞ value is associated with the same species. The value of $\langle P_2 \rangle_a$ was calculated to be 0.513 for DODCI in Egg PC membrane.

For the case of DPH in DPPC [200], the fluorescence decay was almost single exponential. Hence Toptygin and Brand [200] was able to determine the k_{nr} of the dye in the membrane by fluorescence quantum yield measurements and used this value in the determination of the order parameter $\langle P_2 \rangle_\tau$. The calculated values of the two order parameters in this case are $\langle P_2 \rangle_\tau=0.285$ and $\langle P_2 \rangle_a=0.910$.

It is clear that the values of $\langle P_2 \rangle_\tau$ and $\langle P_2 \rangle_a$ are not equal in both the cases. $\langle P_2 \rangle_a$ and $\langle P_2 \rangle_\tau$ are expected to be equal only when the orientational distribution of the linear dye is unimodal and the director axis of the orientational distribution coincides with the membrane normal. Thus, it is necessary to examine different orientational distribution models which predict $\langle P_2 \rangle_\tau$ to be different from that of $\langle P_2 \rangle_a$.

(a) Unimodal distribution model. In this model it is assumed that the population of membrane-bound dye molecules associated with the long lifetime is orientationally distributed in the membrane as a single population about a local director axis. If the director axis is parallel to the membrane normal then $\langle P_2 \rangle_\tau$ and $\langle P_2 \rangle_a$ ought to be quantitatively identical. However, if the director axis is tilted by an angle θ' from the

membrane normal then,

$$\langle P_2(\cos\theta) \rangle_\tau = \langle P_2(\cos\theta') \rangle = \langle P_2(\cos\theta) \rangle_a \quad (5.10)$$

Application of this model by Tóptygin and Brand [200] to the experimental results of DPH in DPPC led to a result that $\theta' = 43^\circ$. It was speculated that the orientation of the acyl chains of the lipid is tilted from the normal and thus the linear dye molecules are also aligned in the same direction as the lipid molecules. It is quite unlikely that the lipid chains are tilted at such a large angle with the membrane normal. In the case of DODCI in Egg PC, the orientation angle θ' is 19° . As described before, application of this model to the experimental results of different cyanine dyes in Egg PC membrane gave dye-dependent orientation angles. It is unlikely that the orientation of the lipid chain would change with the dye molecule for lipid to dye ratio of 500:1. The model of unimodal distribution with a tilted director axis is therefore not valid.

(b) Bimodal distribution model. In this model it is assumed that the molecules are distributed as two populations which interconvert very slowly compared to the intra-population molecular dynamics. The simplest model is the case where the director axis of one population is oriented along the membrane normal and that of the other population is oriented parallel to the membrane. The usefulness of this model to explain the discrepancy between $\langle P_2 \rangle_a$ and $\langle P_2 \rangle_\tau$ has been examined.

The bimodal orientational distribution $P(\theta)$ is considered as a sum of two orientational populations, one centered about the membrane normal $P'(\theta)$ and the other parallel to the membrane surface $P''(\theta)$.

$$P(\theta) = P'(\theta) + P''(\theta) \quad (5.11)$$

where θ is the angle measured with respect to the membrane normal. $P(\theta)$ has to satisfy the normalization condition:

$$\int_0^\pi P(\theta) \sin\theta d\theta = 1 \quad (5.12)$$

$\langle P_2 \rangle_\tau$ is calculated with respect to the membrane normal as

$$\langle P_2(\cos\theta) \rangle_\tau = \int_0^\pi P_2(\cos\theta) P(\theta) \sin\theta d\theta \quad (5.13)$$

$\langle P_2 \rangle_a$ is calculated by taking into account the fact that the director axes for the two distributions are mutually perpendicular.

$$\langle P_2(\cos\theta) \rangle_a = \int_0^\pi [P'(\theta)P_2(\cos\theta) + P''(\theta)P_2(\cos(\pi/2 - \theta))] \sin\theta d\theta \quad (5.14)$$

For simplicity, the two distribution functions $P'(\theta)$ and $P''(\theta)$ are considered as Gaussians centered about the membrane normal and perpendicular to the membrane normal [99, 235] as

$$\begin{aligned} P'(\theta) &= a_1 \exp\left(-\frac{\theta^2}{w_1^2}\right), \\ P''(\theta) &= a_2 \exp\left(-\frac{\left(\frac{\pi}{2} - \theta\right)^2}{w_2^2}\right) \end{aligned} \quad (5.15)$$

where a_1 and a_2 are the amplitudes and w_1 and w_2 are the widths of the two Gaussians. The normalization condition (equation 5.12) restricts that only three of these four parameters are independent.

The parameters of the double Gaussian (DG) distribution function $P(\theta)$, namely the amplitudes a_1 , a_2 and widths w_1 , w_2 , were determined by an iterative method [155] for which $\langle P_2 \rangle_a$ and $\langle P_2 \rangle_\tau$ are in quantitative agreement. For this purpose, an initial set of parameters was assumed and it was ascertained that the final optimized values are independent of initial values of the parameters. The optimized values of the amplitudes and the widths, an average of ten trials, for the different experimental systems are given in Table 5.1. The fractions f_1 and f_2 of the two populations are also given in Table 5.1. Figure 5.4 shows the orientational distribution $P(\theta)$ and the population distribution $P(\theta)\sin\theta$ for these cases.

The results described above suggest that bimodal orientational distribution of dye molecules in membranes explains satisfactorily the discrepancy between the two experimental order parameters. However, gaussian distribution of orientations which is assumed in the above calculations may not be strictly valid [240]. A more reasonable distribution function is based on the Brownian rotational diffusion model (BRD) where the fluorescent probe molecule is moving in an effective potential created by the surrounding lipid

molecules in the system [50]. This effective potential will obey the same symmetry conditions as that of $P(\theta)$ and hence it can also be approximated as a linear combination of Legendre Polynomials, $P_l(\cos\theta)$.

$$U(\theta) = \sum c_l P_l(\cos\theta) \quad (5.16)$$

Here the coefficients c_l are proportional to the strength of the solute-solvent interaction between the probe molecule and the lipid molecules. Hence the orientational distribution can be calculated using the Boltzmann expression

$$P(\theta) = \frac{\exp\left(-\frac{U(\theta)}{kT}\right)}{\int d\theta \sin\theta \exp\left(-\frac{U(\theta)}{kT}\right)} \quad (5.17)$$

In the bimodal orientational distribution, the dye probes in the two populations are considered to experience two different orienting potentials [241]. In the simplest case of considering only upto P_2 term in the effective potential $U(\theta)$ (Maier-Saupe model [50]), one can write

$$\begin{aligned} P'(\theta) &= a_1 \exp(\lambda_1 P_2(\cos\theta)), \\ P''(\theta) &= a_2 \exp(-\lambda_2 P_2(\cos\theta)) \end{aligned} \quad (5.18)$$

where a_1 and a_2 are the amplitudes and $\lambda_1 (>0)$ and $\lambda_2 (>0)$ are the adjustable parameters consistent with the normalization condition (equation 5.12). As θ varies from 0 to $\pi/2$, $P_2(\cos\theta)$ varies from 1 to -0.5. Hence $P'(\theta)$ represents the orientational distribution of the population that is oriented parallel to the membrane normal and $P''(\theta)$ represents the orientational distribution of the population that is oriented perpendicular to the membrane normal in the bimodal orientational distribution. The parameters λ_1 and λ_2 decide the widths of the two distributions. As described above, these parameters were optimized using an iterative method [155] for which the two order parameters match. The optimized values which are independent of the initial values (ten trials) for the different experimental systems are given in Table 5.1. The orientational distribution function $P(\theta)$ and the population distribution function $P(\theta)\sin\theta$ are shown in figure 5.4.

Thus, the discrepancy between the two order parameters from lifetime and anisotropy measurements is satisfactorily explained by the bimodal distribution model. However,

Table 5.1: Bimodal orientational distributions for DODCI in Egg PC and DPH in DPPC. The table shows the two order parameters $\langle P_2 \rangle_\tau$ and $\langle P_2 \rangle_a$ determined from lifetime and anisotropy methods, the optimized parameters for the Double Gaussian (DG) and Brownian Rotational Diffusion (BRD) models and the two fractional amplitudes f_1 and f_2 in the two populations.

System	$\langle P_2 \rangle_\tau$	$\langle P_2 \rangle_a$	Model	w_1/λ_1^\dagger	w_2/λ_2^\dagger	a_1	a_2	f_1	f_2
DODCI+ Egg PC, pH 7.4 25°C	0.428	0.513	DG	40.3±	61.9±	0.0691±	0.0024±	0.8985±	0.1015±
				0.1	8.1	0.0002	0.0001	0.0083	0.0083
			BRD	2.26±	3.18±	0.0092±	0.0006±	0.9287±	0.0713±
				0.02	0.46	0.0001	0.0001	0.0025	0.0025
DPH+ DPPC, pH 7.4 20°C	0.285	0.910	DG	15.7±	20.7±	0.2559±	0.0255±	0.5374±	0.4626±
				0.7	1.3	0.0221	0.0013	0.0036	0.0036
			BRD	8.19±	11.04±	0.0001±	0.0002±	0.5581±	0.4419±
				0.26	1.50	0.0000	0.0001	0.0032	0.0032

[†] w_1, w_2 in the case of DG and λ_1, λ_2 in the case of BRD model.

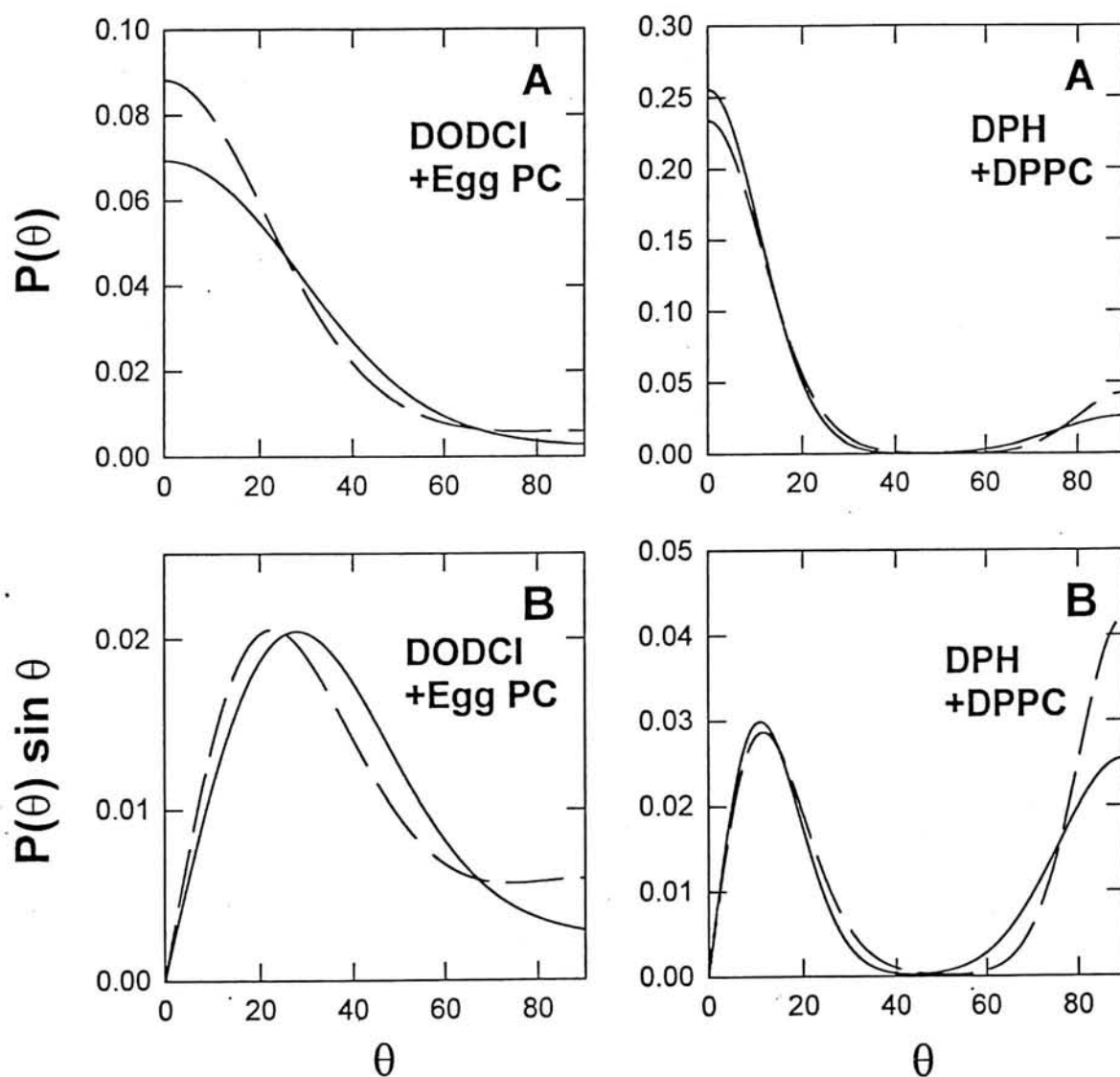


Figure 5.4: (A) Bimodal orientational distribution functions, $P(\theta)$, and (B) population distribution functions, $P(\theta) \sin \theta$ for DODCI in Egg PC and DPH in DPPC. The solid line shows the functions for double gaussian (DG) and the dashed line shows the functions for the BRD model.

the fractions of populations oriented parallel and perpendicular to the membrane and the shape of the population distribution depends upon the assumed functions for $P(\theta)$.

It may be noted that $P(\theta)$ gives the orientational probability distribution whereas $P(\theta)\sin\theta$ gives the actual number density of the dye molecules. Hence the number density appears significantly different from the orientational probability distribution. In the case of DODCI in Egg PC, the population distribution appears nearly unimodal with a peak at $\theta = 26^\circ$ because of large widths (Table 5.1) associated with the two populations. On the other hand, the population distribution for DPH in DPPC is unambiguously bimodal with peaks at $\theta = 12^\circ$ and $\theta = \pi/2$.

The orientational distribution of linear dye molecules in Egg PC membrane is clearly weighted in favour of two mutually orthogonal orientations: parallel and perpendicular to the membrane normal. The bimodal orientational distribution is favoured over the unimodal distribution in literature as a model for the orientational distribution of dye molecules in lipid bilayers, particularly in the case of linear dyes. The model of two orthogonal orientational distributions is found to satisfactorily explain the fluorescence anisotropy decay kinetics of linear DPH related probes in vesicles, planar bilayer membranes and lipid monolayers [234, 99, 235, 51, 236, 238, 101, 242]. Other physical techniques such as neutron scattering techniques [243] also supported the bimodal orientational distribution in lipid bilayers. The recent Monte Carlo dynamics simulations on the distribution of hydrophobic probe molecules in bilayer membranes also support the two population model [244]. These simulations have also shown that the relative proportion of the probe molecules in the two orthogonal orientational distributions depends on the location of the dye molecule in the bilayer membrane. In some cases [241], it was found that one population as well as two population models yield statistically equivalent solutions and it was concluded that the time resolved anisotropy experiments on macroscopically unoriented membranes do not provide sufficient information in order to fully characterize the orientational distribution of probe molecules in bilayers.

Here we have used fluorescence lifetime measurements to determine the orientational distribution of probe molecules in the bilayer in addition to the anisotropy studies. The use

of the order parameter determined from the lifetime variation with the external refractive index in addition to the order parameter from anisotropy measurements unequivocally favours the two population model over the one population model for the orientational distribution of linear probe molecules in a bilayer membrane. The effect of refractive index on the fluorescence decay of linear dyes in sucrose solutions described here has given a strong evidence for two distinct orientational distributions for linear probe molecules in bilayer membranes.

The results and analysis presented here uses fluorescence lifetime data in addition to the conventional fluorescence anisotropy data to deduce the orientational distribution of linear dye molecules in a bilayer membrane. It is shown that the experimental results are consistent with a bimodal orientational distribution and not a unimodal distribution.

5.4 Location and Orientation of a linear dye molecule DODCI in lipid bilayer membranes: Effects of chain length, unsaturation and temperature

Linear dye molecules such as DODCI exist in two different locations in the bilayer membrane: one on the surface/interface of the membrane and the other in the core of the bilayer membrane. The population which is on the surface/interface shows the fluorescence lifetime that is sensitive to external viscosity whereas the fluorescence lifetime corresponding to the other population in the core is insensitive to viscosity, but shows the effect of external refractive index. These dyes are oriented in the core of the bilayer membrane which is evident from the effect of refractive index on the fluorescence lifetime. The two order parameters obtained from fluorescence lifetime and anisotropy measurements do not match and these are consistent with the picture that the probe molecules are oriented in two mutually perpendicular orientational distributions whose interconversion rate is very slow compared to the intra-population dynamics. In summary, the linear dye molecules exist in two different locations in the bilayer and in two different orientations

in the core of the bilayer.

Here we report the experimental results on the location and orientation of DODCI carried out in bilayer membrane vesicles made up of different synthetic lipids. The lipids used were C12:0(DLPC, Dilauroyl Phosphatidyl Choline), C14:0 (DMPC, Dimyristoyl PC), C16:0 (DPPC, Dipalmitoyl PC), C18:0 (DSPC, Distearoyl PC), C20:0 (DAPC, Diarachidoyl PC), C14:1 (Dimyristoleoyl PC) and C16:1 (Dipalmitoleoyl PC). The nomenclature used here in representing a Phosphatidylcholine (PC) lipid is as follows. The lipid is represented as Cx:y where x represents the length of the alkyl chain and y represent the number of double bonds in the alkyl chain. The single double bond in the alkyl chain of some of the lipids (C14:1 and C16:1) is at the 9th position in the alkyl chain and is of cis type. The interplay between the two locations (surface versus core) and two different orientations in the core (parallel versus perpendicular orientations with respect to the membrane normal) is examined in terms of the alkyl chain length, unsaturation and the phase transition temperature of the lipid.

The experimental strategy is as follows. The fluorescence lifetime and anisotropy measurements were carried out on dye - lipid vesicle solutions prepared in seven different sucrose solutions. The amplitudes of the two lifetimes of the membrane-bound dye τ_{short} and τ_{long} which corresponds to that of the dye populations located on the surface and core of the bilayer are taken as the relative population in the two locations. The two order parameters $\langle P_2 \rangle_\tau$ and $\langle P_2 \rangle_a$ were determined from the variation of the long lifetime τ_{long} with the external refractive index and the anisotropy measurements. The bimodal orientational distribution was determined according to the BRD model which can satisfactorily explain these two order parameters. The fractional amplitudes of the two orthogonal distributions in the bimodal orientational distribution were taken as the relative population of the dye in the two orientations.

The estimation of $\langle P_2 \rangle_\tau$ is from the effect of refractive index on the radiative rate. As discussed earlier, calculation of this order parameter requires the estimation of k_{nr} for that particular lifetime which is impossible to determine in a multicomponent system. Hence it was estimated from the radiative rate of the dye determined in an aqueous

glycerol solution whose refractive index matches with that of the membrane. In order to minimize the errors associated with this method, we searched for the ways to increase the contribution of radiative rate to the fluorescence lifetime of the membrane-bound fluorophore.

One method of increasing the fluorescence lifetime is to decrease the pH. There were reports in literature that by lowering the pH of the aqueous medium, the fluorescence lifetimes of the fluorophores incorporated in membranes increases. With the increase of pH, the water mobility at the interface decreases resulting in the decrease in the lipid mobility [245, 246]. This results in the increase of the hydrophobicity which in turn increases the fluorescence lifetimes of the fluorophores in membranes [245].

Figure 5.5A shows the change in the fluorescence lifetime of DODCI incorporated in Egg PC lipid vesicles prepared by ether evaporation procedure with pH. With the decrease of pH from 7.4 to 3.5, the long fluorescence lifetime of DODCI increased from 1.68ns to 1.96ns. In the case of Egg PC vesicles prepared by sonication procedure, the long fluorescence lifetime of DODCI increases from 1.73ns to 1.97ns when the pH was decreased from 7.4 to 4.3. In saturated lipids such as C12:0, C14:0 etc., the increase was marginal. The same trend was observed in the case of unsaturated lipids (C14:1, C16:1 etc.) also. At present, we do not understand the reasons for the large change in the fluorescence lifetime of DODCI incorporated in Egg PC with the decrease of pH. All the fluorescence experiments described in this section were done at pH 4.3.

One another method of increasing k_r is lowering the temperature. With the decrease of the temperature, the fluorescence lifetime increases as the nonradiative process decreases [46]. Figure 5.5B shows the change in the fluorescence lifetime of DODCI incorporated in Egg PC vesicles prepared at pH 4.3 by ether evaporation method, with temperature. The fluorescence lifetime increases from 1.94ns to 2.10ns when the temperature is varied from 25°C to 5°C. In the case of Egg PC vesicles prepared at pH 7.4 by sonication method, the fluorescence lifetime increased from 1.73ns to 1.96ns when the temperature was decreased from 25°C to 5°C. Similar trends were observed in the case of DODCI incorporated in vesicles made up of other lipids used in this study. Hence most of the

experiments described in this section were done at 5°C.

5.4.1 Location of DODCI

In all the lipid bilayer vesicles made of different lipids used in this study, the membrane-bound DODCI showed two lifetimes, one close to 0.68ns and the other close to 1.76ns. With the increase of the sucrose concentration in the aqueous phase, 0.68ns component at first showed a slight decrease or no variation and then increased with the increase of sucrose concentration. This indicates that this lifetime corresponds to the dye located on the surface/interface region of the membrane as discussed before (section 4.2). The long lifetime steadily decreases which is the refractive index effect indicating that this lifetime corresponds to that of the dye located in the core of the bilayer membrane. The relative amplitudes of these two lifetimes were taken as the relative population of the dye molecules in these two locations.

Effect of chain length:

Figure 5.6 shows the variation of the amplitudes of the long and short lifetimes of the membrane bound dye with the alkyl chain length. Figure 5.6A shows the case for the saturated lipids C12:0, C14:0 and C16:0 and figure 5.6B shows the case of unsaturated lipids C14:1 and C16:1. As discussed before, the amplitudes of the short and long lifetimes of the membrane-bound DODCI represent the populations of the dye in two different locations: surface and core of the bilayer respectively. It is clear that from the figure that in both the cases of saturated and unsaturated lipids, the dye population located in the core decreases compared to that located on the surface of the bilayer with the increase of the alkyl chain length. That means, the dye penetrating into the core of the membrane decreases with the increase of the chain length. This effect is so severe that in the case of lipids with longer alkyl chains such as C18:0 (DSPC) and C20:0 (DAPC), the dye penetrating into the core is very less and, either there is no long lifetime component or the amplitude of the long lifetime is near-zero in these lipid membranes.

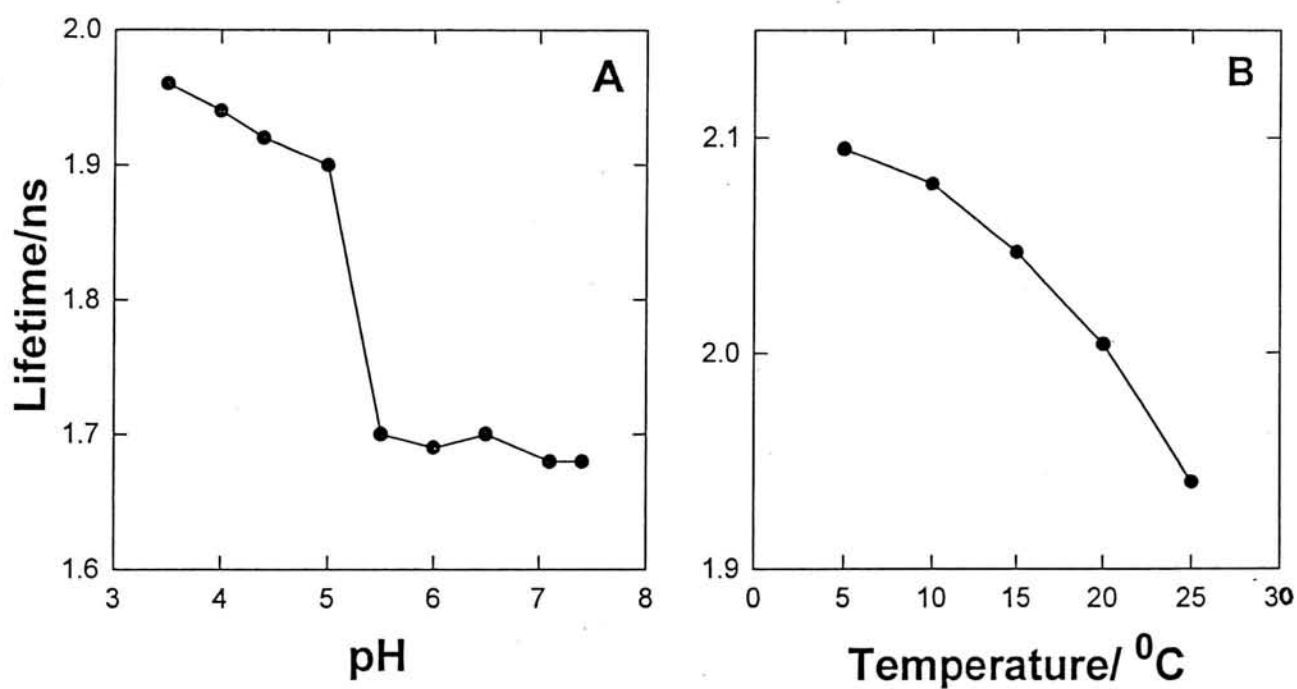


Figure 5.5: Variation of the fluorescence lifetime of DODCI incorporated in lipid vesicles prepared by ether evaporation procedure with (A) pH (at 25°C) and (B) temperature (at pH 4.3) of the medium.

The variation of the penetration of the dye into the bilayer with the alkyl chain length suggests that the free volume available for the dye decreases or the packing density of the lipids increases in the core of the bilayer membrane with the increase of the alkyl chain length. It is known that the interaction between the lipid chains of the two leaves of a bilayer is minimal in membranes made up of lipids of shorter alkyl chain lengths compared to that of longer alkyl chain lengths [1, 11]. That is, the lipid packing density in the core of the bilayer made up of lipids with longer alkyl chain lengths will be much higher than that of the membranes made up of shorter alkyl chain lengths and hence the amount of dye penetrating into the core of the bilayer decreases with the increase of the chain length.

Effect of unsaturation:

The effect of lipid unsaturation on the amplitudes of the short and long lifetimes of membrane-bound DODCI are shown in figure 5.7. Figure 5.7A and B shows the variation with the presence of one double bond for the case where the lipid chain length is kept constant at 14 (C14:0 and C14:1) and 16 carbon atoms (C16:0 and C16:1) respectively. It is clear from the figure that the dye located in the core of the bilayer increases compared to the dye located on the surface of the bilayer with the introduction of a double bond in the alkyl chain. That is, the penetration of the dye increases with the increase of unsaturation in the lipid chain.

The variation of the dye populations in the core and surface regions of the bilayer with the change in the unsaturation of the lipid chain suggests that more free volume is available for the dye in the core of the bilayer made up of unsaturated lipids compared to those made up of saturated lipids. In other words, the packing density of unsaturated lipids is less compared to that of saturated lipids in the core of the bilayer. In the case of unsaturated lipids such as C14:1 and C16:1, there is an additional *cis* double bond present at the 9th position along the alkyl chain. This introduces a kink in the structure of an unsaturated lipid molecule [4, 1]. Such units cannot be closely packed compared to the saturated lipids and hence the rigidity (or the packing density) of the membrane core decreases with the increase of the unsaturation. This is also evident from the increased hydration levels

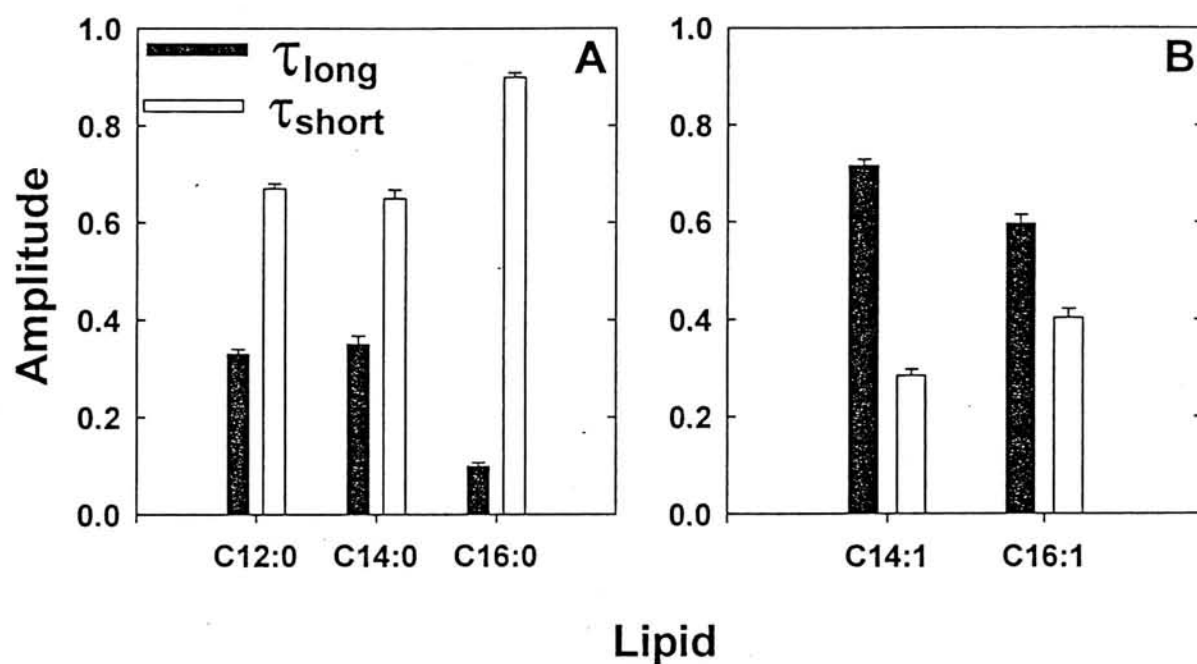


Figure 5.6: Variation of the amplitudes of the long and short lifetimes of the membrane bound DODCI with the alkyl chain length. These two amplitudes represent the relative fraction of the dye located at two different sites: core and surface regions of the bilayer respectively. The sum of the two amplitudes is normalized to unity. Figure A and B indicate the variation for saturated and unsaturated lipids respectively.

of the bilayer with the increase of lipid unsaturation [99, 247, 248, 249, 250, 251]. Therefore the number of dye molecules penetrating into the core of the bilayer increases with the increase of unsaturation.

Effect of temperature:

The variation of the amplitudes of short and long lifetimes with temperature are shown in figure 5.8. Figure 5.8A and B show the variation of the amplitudes for C12:0, C14:0 and C16:0 at two temperatures 5°C and 25°C. In general, the dye molecules penetrating into the core of the bilayer decreases with the increase of temperature. The observed trend can be explained by the fact that the lipid bilayer undergoes a phase transition with temperature. The phase transition temperatures of C12:0, C14:0 and C16:0 are -2°C, 24°C and 41°C respectively [18, 1, 19]. Below the phase transition temperature, the lipid bilayer exists in the gel phase whereas it exists in the liquid crystalline phase above the phase transition temperature [1]. Hence at 5°C, C12:0 exists in the liquid crystalline phase whereas C14:0 and C16:0 exist in the gel phase. At the other temperature 25°C, C12:0 exists in the liquid crystalline phase, C14:0 is in the gel-liquid crystalline phase whereas C16:0 exists in the gel phase. As can be seen from the figures, the dye located in the core (giving rise to the long lifetime) is more compared to the dye located on the surface (giving rise to the short lifetime) in liquid crystalline bilayers compared to the gel phase bilayers. The observed behaviour agrees well with the other experimental observations that the small molecules penetrates more into the bilayer as the fluidity of the lipid chains increases with the phase transition [1]. In the case of these saturated lipids, two factors are involved in determining the population of the dye at the two sites in the membrane: chain length and the phase transition. The increase of chain length decreases the core population whereas the phase transition from gel to liquid crystalline bilayer increases the core population.

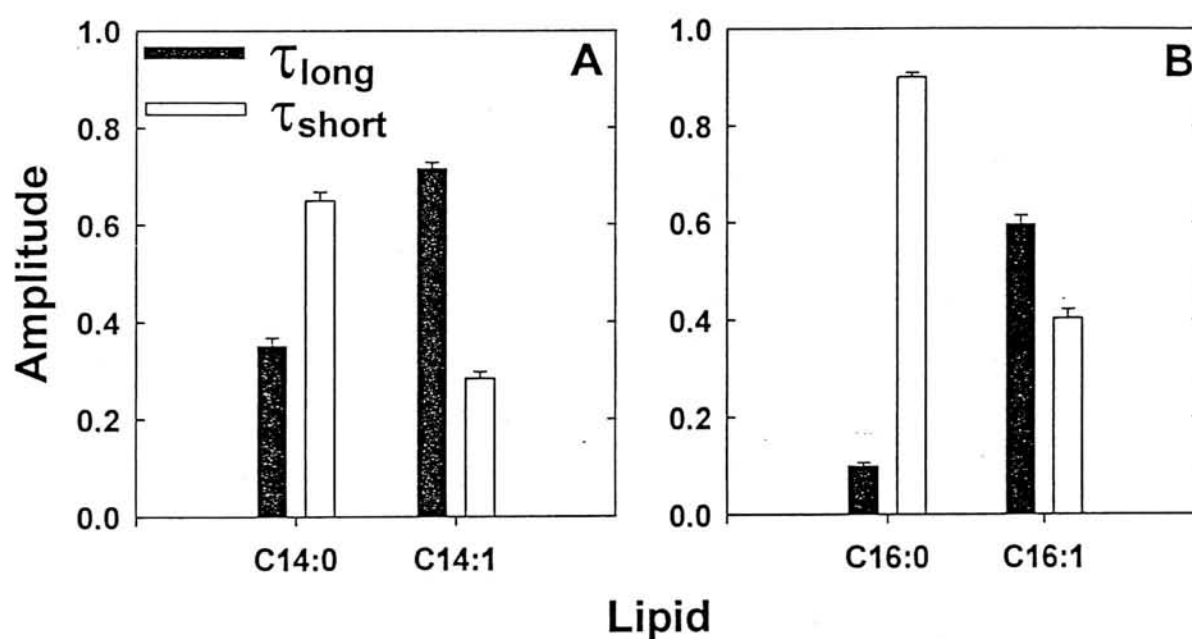


Figure 5.7: Variation of the amplitudes of the long and short lifetimes of the membrane bound DODCI with unsaturation. These two amplitudes represent the relative fraction of the dye located at two different sites: core and surface regions of the bilayer respectively. The sum of the two amplitudes is normalized to unity. Figure A and B indicate the variation for the case of C14:0 and C14:1; and C16:0 and C16:1 respectively.

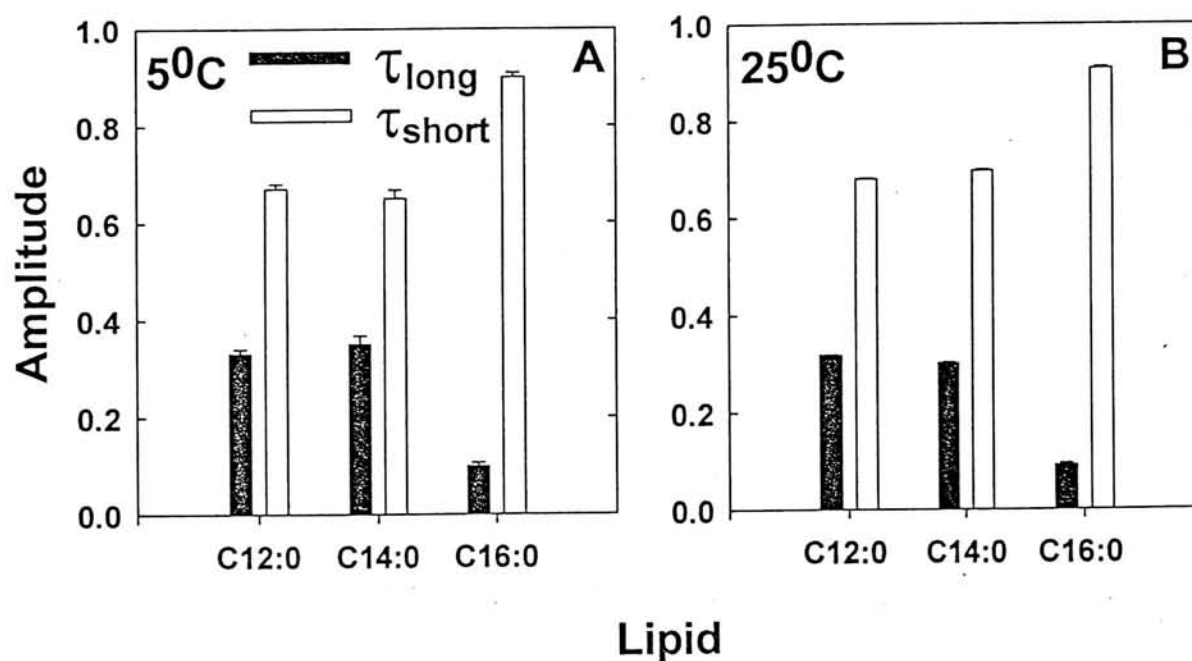


Figure 5.8: Variation of the amplitudes of the long and short lifetimes of the membrane bound DODCI with temperature. These two amplitudes represent the relative fraction of the dye located at two different sites: core and surface regions of the bilayer respectively. The sum of the two amplitudes is normalized to unity. Figure A and B indicate the variation for the case of C12:0, C14:0 and C16:0 at two temperatures 5°C and 25°C respectively. The phase transition temperatures of C12:0, C14:0 and C16:0 are -2°C, 24°C and 41°C respectively.

5.4.2 Orientation of DODCI

As mentioned before, the dye population in the core of the bilayer membrane made up of lipids of higher alkyl chain length, C18:0 and C20:0, is very less and hence the variation in the long lifetime and the orientational distribution cannot be accurately determined for these two cases. For the other cases, the order parameter $\langle P_2 \rangle_\tau$ was determined from the refractive index effect on the long lifetime and $\langle P_2 \rangle_a$ was determined from the time resolved measurements. These two order parameters do not match. Table 5.2 shows the long lifetimes and the two order parameters obtained in different lipid vesicles. The two order parameters were used to obtain the bimodal orientational distribution of DODCI in different lipid bilayer membranes, according to the BRD model (equations 5.11 and 5.18). The fractional amplitudes f_1 and f_2 in the two distributions were taken as the populations of the dye in the two orientations.

DODCI being positively charged, the orientational distribution was weighted towards the parallel orientation of the dye molecules along the membrane normal. For example, DODCI in DPPC at 25°C shows the fractional amplitudes of the two distributions f_{para} (or f_1) and f_{perp} (or f_2) oriented parallel and perpendicular to the membrane normal as 85% and 15% respectively. In the case of DPH in DPPC at 20°C (Table 5.1), the respective populations in the two orientational distributions were 54% and 46%. DPH, being a neutral molecule, can go deeper into the core of the bilayer membrane compared to DODCI. Since the fluidity of the lipid chains increases towards the core of the bilayer membrane [1, 13, 14], the population of the dye molecules oriented perpendicular to the lipid chains is higher in the case of DPH (46%) compared to that of DODCI (15%). This experimental finding confirms the conclusion drawn from the recent Monte Carlo dynamics [244] on the orientational distribution of fluorescent molecules in bilayer membranes that the relative proportion of the probe molecules in the two orientational distributions depends on the location of the probe molecule and at the centre of the bilayer, the dye population oriented parallel to the membrane surface increases.

In general, the width of the population oriented perpendicular to the membrane normal

Table 5.2: Order parameters of DODCI in bilayer membranes made up of different lipids. $\langle P_2 \rangle_\tau$ and $\langle P_2 \rangle_a$ represents the two order parameters determined from fluorescence lifetime and anisotropy measurements. τ_{long} represents the long lifetime of the membrane-bound dye and m value is obtained by fitting this lifetime data to the equation $\tau_{long} \propto (n_0)^{-m}$ where n_0 is the refractive index of the external aqueous medium in which vesicles were made. The values of anisotropy at infinite time (r_∞) determined from time resolved anisotropy decay were also shown in the table. Anisotropy at zero time (r_0) is estimated to be 0.375 from the time resolved anisotropy decay of DODCI in glycerol.

Lipid	Temp. °C	τ_{long} ns	m	$\langle P_2 \rangle_\tau$	r_∞	$\langle P_2 \rangle_a$
C12:0	5	1.87	2.9	0.510	0.23	0.778
C14:0	5	2.10	3.3	0.485	0.22	0.761
C16:0	5	1.88	3.1	0.645	0.24	0.795
C14:1	5	1.95	2.6	0.341	0.23	0.788
C16:1	5	1.96	3.1	0.605	0.26	0.833
C12:0	25	1.76	2.8	0.568	0.18	0.688
C16:0	25	1.79	2.7	0.435	0.15	0.628

is higher than that oriented parallel to the membrane normal in the bimodal orientational distribution. This observation indicates that the dye molecules oriented parallel to the lipid chains can take fewer orientations compared to the dye molecules oriented perpendicular to the lipid chains. With temperature, the widths of the two populations in the bimodal orientational distributions increases.

The fluorescence experiments carried out on C14:0 at 25°C have shown that the observed trend in the fluorescence lifetime with the sucrose concentration at this temperature is not in line with the expected trend ($m > 5$ was obtained when lifetime τ is fitted to the equation $\tau \propto (n_0)^{-m}$). This is because the phase transition temperature of C14:0 exactly falls at 24°C and the local environment of the membrane-bound dye may not be the same in all sucrose solutions. It is well known that at the phase transition temperature, the lipid bilayer is very fluid resulting in the very high penetration of the aqueous phase solutes [1].

Effect of chain length:

The variation of the fractional amplitudes in the two orthogonal orientational distributions with the chain length are shown in figure 5.9. Figure 5.9A shows the case for saturated lipids (C12:0, C14:0 and C16:0) and figure 5.9B shows the variation in the case of unsaturated lipids (C14:1 and C16:1). f_{para} and f_{perp} (or f_1 and f_2) represent the fractional amplitudes in the two orientational distributions whose director axes are parallel and perpendicular to the membrane normal respectively. As can be seen from the figure, the fraction of the probe molecules oriented parallel to the lipid chains increases with the increase of the chain length.

The observed trend in the orientation of the probe molecules with the increase of chain length can be explained with the same explanation given previously for the variation in the location of the probe molecules. With the increase of the chain length, the packing density of the lipid chains increases in the core of the bilayer. Hence the probe molecules which are oriented parallel to the membrane surface decreases in the core and more probe molecules get oriented parallel to the lipid chains. Therefore, the relative population of the probe molecules oriented parallel to the membrane normal (f_{para}) increases with the

increase of the chain length.

Effect of unsaturation:

Figure 5.10 shows the variation in the fractional amplitudes of the two orientational distributions with the unsaturation in the lipid chain. Figure 5.10A and B shows the variation with the presence of one double bond for the case where the lipid chain length is kept constant at 14 (C14:0 and C14:1) and 16 carbon atoms (C16:0 and C16:1) respectively. The probe molecules that are oriented parallel to the membrane normal decreases with the introduction of a double bond in the lipid chain.

The observed trend in the relative populations of the two orientational distributions can be explained as follows. The additional *cis* double bond in the case of C14:1 and C16:1 present at the 9th position along the alkyl chain introduces a kink in the structure of each individual lipid molecule. If we can think of a saturated lipid (such as C14:0 and C16:0) as a rod, then the case of C14:1 and C16:1 becomes that of a rod which is bent at the 9th position as indicated in the cartoon in figure 5.10. The organization of such individual units into a bilayer makes more free volume available for the dyes which are oriented parallel to the membrane surface compared to those oriented parallel to the lipid chains. Hence, the fractional amplitude of the dye molecules oriented perpendicular to the membrane normal increases compared to those oriented parallel to the membrane normal.

Effect of temperature:

The effect of temperature on the orientational distribution of membrane-bound DODCI was examined in the case of saturated lipids. Figure 5.11A represent the variation at 5°C for the two lipids C12:0 and C14:0 whereas figure 5.11B shows the variation at 25°C for the two lipids C12:0 and C16:0. The observed trend can be explained with the phase transition of the lipid with temperature. As mentioned before, the gel to liquid crystalline phase transition occurs at -2°C, 24°C and 41°C for C12:0, C14:0 and C16:0 respectively [18, 1, 19]. At 5°C, the lipid C12:0 exists in liquid crystalline phase whereas C14:0 exists in the gel phase. At 25°C, the lipid C12:0 exists in liquid crystalline phase whereas C16:0

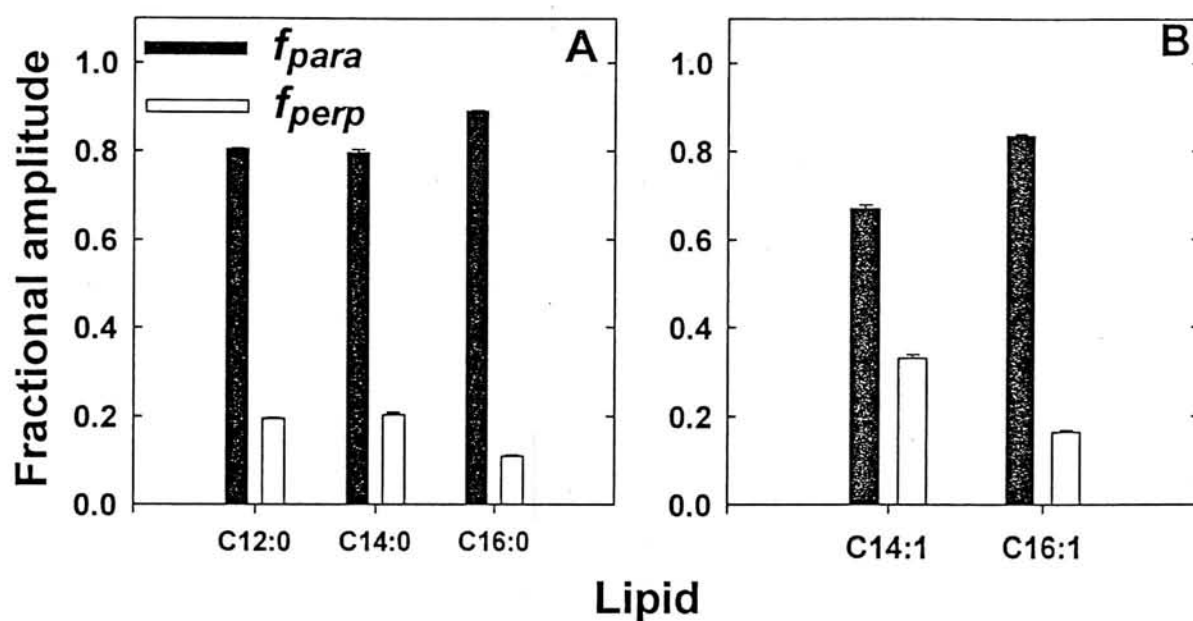


Figure 5.9: Variation of the fractional amplitudes in the two orthogonal orientational distributions of the bimodal orientational distribution with the chain length. f_{para} and f_{perp} represent the population of the probe molecules oriented in the two distributions with the respective director axes parallel and perpendicular to the bilayer membrane normal. The sum of these were normalized to unity. Figures A and B indicate the variation in the case of saturated lipids C12:0, C14:0 and C16:0; and in the case of unsaturated lipids C14:1 and C16:1 respectively.

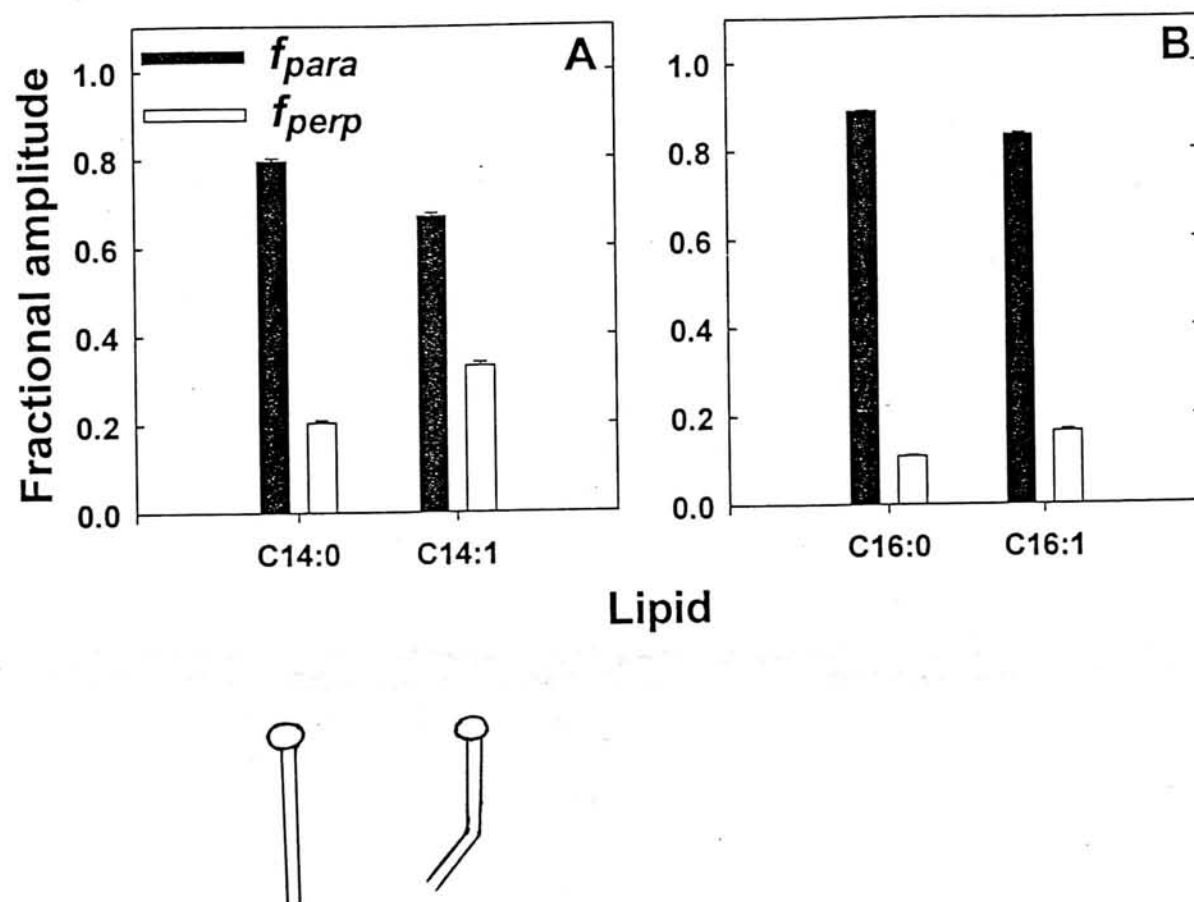


Figure 5.10: Variation of the fractional amplitudes in the two orthogonal orientational distributions of the bimodal orientational distribution with lipid unsaturation. f_{para} and f_{perp} represent the population of the probe molecules oriented in the two distributions with the respective director axes parallel and perpendicular to the bilayer membrane normal. The sum of these were normalized to unity. Figures A and B indicate the variation in the case of C14:0 and C14:1; and C16:0 and C16:1 respectively. The cartoon below figure A indicate the kink associated with the unsaturated lipids compared to the saturated lipids.

exists in gel phase. It is clear from the figure 5.11 that the relative population of the dye molecules oriented parallel to the membrane normal is higher in liquid crystalline bilayers compared to the bilayers that exist in gel phase. The difference is very clear in the case of experiments carried out on C12:0 and C16:0 lipids at 25°C in spite of the earlier observation that the population of the dye molecules oriented parallel to the membrane normal increases with the increase of alkyl chain length from the experiments carried out at 5°C (figure 5.9). The relative population in the two orientational distributions is controlled by two factors: alkyl chain length and the phase transition temperature. Increase of the alkyl chain length as well as the gel to liquid crystalline phase transition increases the dye population that is oriented parallel to the membrane normal. The alkyl chain length effect is dominant at lower temperatures (5°C, figures 5.9A and 5.11A) whereas the phase transition temperature effect is dominant at higher temperatures (25°C, figure 5.11B).

The observed trend can be explained with the changes associated with the lipid bilayer upon phase transition. In liquid crystalline phase, the alkyl chains of the lipid molecules are aligned parallel to one another compared to those in the gel phase [1]. When the lipid bilayer undergoes a gel to liquid crystalline phase transition, the thickness of the bilayer membrane decreases and the area per lipid molecule increases. For example, in the case of DPPC bilayers, the thickness of the bilayer decreases from 47 Å to 41 Å whereas the area per lipid molecule increases from 46 Å² to 56 Å² upon phase transition [1]. Therefore, available free volume is more for the dye molecules to get oriented parallel to the lipid chains in the liquid crystalline phase. Hence the relative population of the dye molecules oriented parallel to the membrane normal is higher in liquid crystalline bilayers compared to the gel phase bilayers.

Figure 5.12 shows the variation of the relative population of the membrane-bound dye in the two orientations in a lipid bilayer membrane as a function of temperature. Figure 5.12A and B represent the variation of the fractional amplitudes at two temperatures 5°C and 25°C in the case of the lipids C12:0 and C16:0 respectively. The phase transition temperatures of C12:0 and C16:0 are -2°C and 41°C respectively and hence at these two temperatures (5°C and 25°C) C12:0 is in the liquid crystalline phase whereas C16:0 is

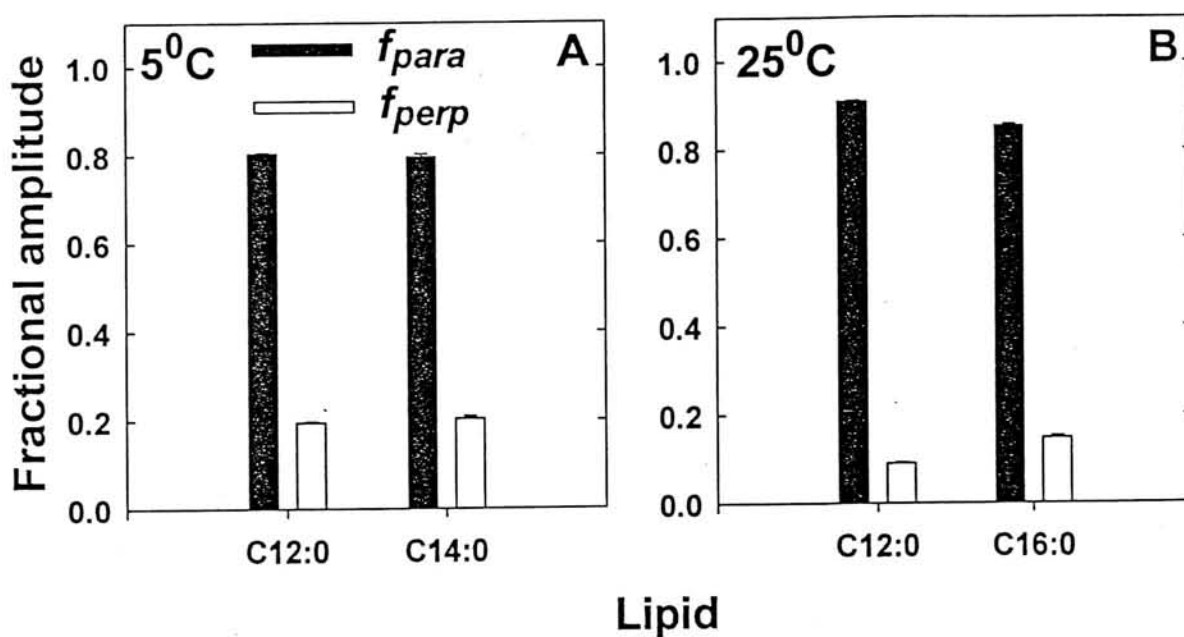


Figure 5.11: Variation of the fractional amplitudes in the two orthogonal orientational distributions of the bimodal orientational distribution with temperature. f_{para} and f_{perp} represent the population of the probe molecules oriented in the two distributions with the respective director axes parallel and perpendicular to the bilayer membrane normal. The sum of these were normalized to unity. Figures A and B indicate the variation at two temperatures 5° and 25° respectively. The phase transition temperatures of C12:0, C14:0 and C16:0 are -2°C, 25°C and 41°C respectively.

in the gel phase. Therefore, figure 5.12 represent the trends in the fractional amplitudes of the probe molecules with temperature when the lipid exists in gel phase (C16:0) or in liquid crystalline phase (C12:0). It is clear from the figure that when the lipid bilayer is in the gel phase (C16:0), the population of the dye molecules oriented perpendicular to the membrane normal increases with temperature whereas for the lipid membrane which is in the liquid crystalline phase (C12:0), the probe molecules oriented parallel to the lipid chains increases with temperature. That is, the observed trends in the relative populations of the two orientational distributions are opposite for the case of gel and liquid crystalline bilayers.

The observed opposite trends in the variation of the fractional amplitudes of the probe molecules in the two orientations with temperature for gel and liquid crystalline bilayer membranes can be explained as follows. With the increase of the temperature in the case of gel phase bilayers, the dynamics of the lipid chains increases in the direction parallel to the plane of the membrane (segmental motion) and hence available free volume will be more for the dye molecules to get oriented parallel to the lipid membrane compared to those oriented parallel to the lipid chains. Therefore, the relative population of the probe molecules oriented parallel to the membrane normal decreases with temperature in the case of lipid bilayers in the gel phase (C16:0). In the other case where the lipid bilayer is in the liquid crystalline phase, the lipid chains are aligned parallel to one another and the dynamics in the direction parallel to the lipid chains or perpendicular to the membrane increases. The increase of temperature increases the number of gauche-trans-gauche kinks (also known as 2g1 kinks) in the all trans chain of the lipid chains leading to more free volume between the lipid chains [1, 11, 15, 252]. Hence, more molecules will get oriented parallel to the lipid chains and the relative population of the probe molecules oriented parallel to the membrane normal increases with temperature in the case of lipid bilayers in the liquid crystalline phase (C12:0).

In summary, we have used the fluorescent probe molecule DODCI in different lipid bilayer membranes to understand how the location and orientation of molecules in bilayer membranes are controlled by the lipid parameters such as alkyl chain length, unsaturation

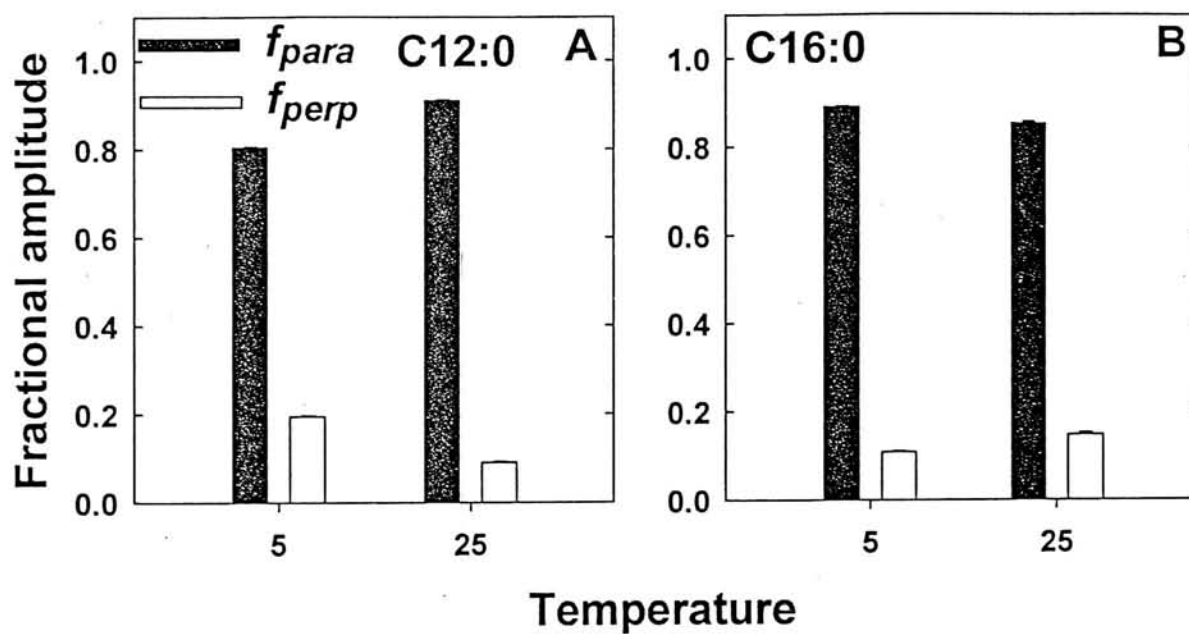


Figure 5.12: Variation of the fractional amplitudes in the two orthogonal orientational distributions of the bimodal orientational distribution with temperature. f_{para} and f_{perp} represent the population of the probe molecules oriented in the two distributions with the respective director axes parallel and perpendicular to the bilayer membrane normal. The sum of these were normalized to unity. Figures A and B indicate the variation in the case of C12:0 and C16:0 respectively. The phase transition temperatures of C12:0 and C16:0 are -2°C and 41°C respectively.

and the phase transition temperature. The order parameter $\langle P_2 \rangle_r$ and the relative populations in the two orientations in the bimodal orientational distribution, f_{para} and f_{perp} are new parameters used in characterizing the orientational distribution of linear dye molecules in lipid bilayer membranes in addition to the conventional order parameter $\langle P_2 \rangle_a$. Fluorescent probes are preferentially located in the core of the bilayer compared to the surface in the membranes made up of lipids with shorter alkyl chain lengths or with unsaturated alkyl chains or in the liquid crystalline phase and vice versa. In the core of the bilayer, the probe molecules get preferentially oriented parallel to the membrane normal compared to the population that is oriented parallel to the membrane surface in membranes made up of lipids with longer alkyl chains, or with no unsaturation or in the liquid crystalline phase and vice versa.

After addressing the location and orientation of fluorescent probe molecules in lipid bilayer membranes, the question of the dynamics of these molecules in bilayer membranes and how they are different from the dynamics in homogeneous solvents is addressed in the next Chapter.

Chapter 6

Translational and Rotational Diffusion of Surface Probes: Monte Carlo Simulations and Fluorescence Anisotropy Experiments

Time resolved fluorescence anisotropy measurements provide important information about the dynamics of the fluorophore in the excited state [46, 94, 92]. When the initial ground state population oriented at random directions in liquids (or a non-random orientational distribution in anisotropic media such as lipid bilayer membranes) is excited with a polarized light, an anisotropic population is created in the excited state at zero time. The fluorescence anisotropy decay measures the relaxation of this anisotropic population to the equilibrium orientational distribution. The anisotropy decay parameters of a fluorophore are sensitive to its shape, size and local environment.

The fluorescence anisotropy decay of a 'spherical' fluorophore in a homogeneous medium such as non-interacting solvent is single exponential. The fluorescence anisotropy decay becomes double exponential when the fluorophore is an oblate or a prolate ellipsoid and the dipole axis is not along one of the two axes (minor or major) of the ellipsoid [94].

Although it is theoretically shown that the anisotropy decay of a fluorophore of any shape can never exceed five exponentials [93, 94, 92], it was observed that in most cases, two exponentials can satisfactorily explain the experimentally measured fluorescence anisotropy decay of most of the fluorophores. The rotational correlation time of a fluorophore is directly proportional to its molecular volume and viscosity and inversely proportional to the temperature of the medium.

When the fluorophore is in a biological microheterogeneous system such as membranes, micelles or proteins, the fluorescence depolarization is caused by both the dynamics of the fluorophore and the dynamics of the system in which the fluorophore is incorporated. The surrounding anisotropic medium restricts the equilibrium orientational distribution of the fluorophore to a nonrandom one (as discussed in Chapter 5) and hence the fluorescence anisotropy of the fluorophore does not decay to zero at infinite time. This is true in most cases of the fluorophores incorporated in lipid bilayer membranes where the lipid chains restrict the orientational distribution of the fluorophores. But when the fluorophore is incorporated in a micelle or attached to a protein, the fluorescence anisotropy decays to zero with a very slow rotational correlation time that is characteristic of the size of the micelle or protein. In the case of lipid bilayer vesicles, the rotational dynamics of the vesicle does not contribute to the fluorescence anisotropy decay of the fluorophore as the rotational correlation times of vesicles (μs to ms) are much longer than the lifetimes of the fluorophores in the excited state (ns). Microviscosity of the fluorophore environment in a biological system is generally estimated by comparing the rotational correlation time with that in a solvent of known viscosity [46]. This method assumes that the dynamics of the fluorophore in a microheterogeneous system follows Brownian dynamics with Stokes-Einstein relation for the diffusion coefficient.

The rotational dynamics of the fluorophores in homogeneous media can be described by an unhindered free rotation of the fluorophore in all directions. In the case of biological systems, the anisotropic nature of the surrounding medium does not allow the fluorophore to undergo a free rotation in all directions. Different models were considered in literature to explain the restricted rotational freedom of the fluorophores in these

microheterogeneous media.

6.1 Models for the rotational dynamics of fluorophores in biological systems

Many models were proposed to describe the rotational dynamics of the fluorophores in biological systems. The most commonly employed model is the "wobbling-in-a-cone" model where the fluorophore wobbles in a cone whose semiangle is related to the order of the probe environment [95, 96]. In this model, the equilibrium orientational distribution $P(\theta)$ is assumed to be uniform in a cone of semiangle θ_0 . That is,

$$\begin{aligned} P(\theta) &= [2\pi(1 - \cos\theta_0)]^{-1} \text{ for } 0 \leq \theta \leq \theta_0 \\ &= 0 \text{ for } \theta > \theta_0 \end{aligned} \quad (6.1)$$

The model-independent order parameter $\langle P_2 \rangle$ is related to the cone semiangle θ_0 as

$$S = \langle P_2(\cos\theta) \rangle = \left(\frac{r(\infty)}{r(0)} \right)^{\frac{1}{2}} = \frac{1}{2} \cos\theta_0 (1 + \cos\theta_0) \quad (6.2)$$

In this model, the equation for the time resolved anisotropy becomes

$$\frac{r(t)}{r(0)} = S^2 + (1 - S^2) \exp(-t/\tau_w) \quad (6.3)$$

where τ_w is the wobbling time constant which is inversely related to the wobbling diffusion coefficient, D_w . From the values of S and τ_w , D_w can be calculated using the relation [96]

$$\begin{aligned} D_w \tau_w (1 - S^2) &= -x_0^2 (1 + x_0)^2 [\log[(1 + x_0)/2] + (1 - x_0)/2] / [2(1 - x_0)] \\ &\quad + (1 - x_0)(6 + 8x_0 - x_0^2 - 12x_0^3 - 7x_0^4)/24 \end{aligned} \quad (6.4)$$

where $x_0 = \cos\theta_0$, θ_0 being the cone semiangle.

The above model is found to explain the fluorescence anisotropy decay of fluorophores in most of the biological systems such as membranes [253, 51, 52, 53], micelles [104, 254, 105] and proteins [164, 92, 255, 201]. In this model, the probe molecules are assumed

to be experiencing uniform orienting potential within the cone which may not be correct. Different orienting potentials such as gaussian orienting potential [50] was used to obtain the anisotropy decay equation similar to equation 6.3 and used in explaining the fluorescence anisotropy kinetics of probe molecules in biological systems. A higher order analysis of the hindered rotational diffusion of fluorescent probes in anisotropic media was proposed with which the fourth rank order parameter can also be determined in addition to the second rank order parameter. This has been applied in many cases to explain the fluorescence anisotropy decay kinetics of fluorescent probes in lipid membranes [98, 234, 99, 235, 236, 54].

6.2 Fluorescence anisotropy decay of Fluorescent Probes in bilayer membranes

The anisotropy decays of all the fifteen dyes studied (section 4.2) in Egg PC membrane are multiexponential (figure 6.1) and Table 6.1 gives the quantitative parameters for the multiexponential fit (equation 6.5) which includes a constant, r_∞ .

$$r(t) = r_\infty + (r_0 - r_\infty) \sum_{i=1}^2 \alpha_i \exp(-t/\phi_i) \quad (6.5)$$

where ϕ_i and α_i represent the rotational correlation times and the respective amplitudes such that $\sum_i \alpha_i = 1$. As discussed earlier, the fluorescence anisotropy decay of a dye molecule in the membrane is determined by the rotational/wobbling dynamics of the molecule during its excited state lifetime. Hence, it depends upon the local environment around the probe molecule, that is, the site of solubilization. The anisotropy decay ought to be consistent with the site of solubilization of the dye (which is determined in section 4.2), at least for those cases where a single site is predominant.

The interpretation of experimentally determined fluorescence anisotropy decay of fluorophores in membranes have been studied and discussed [256, 257, 234]. The anisotropy decay is generally multi-exponential, often with a residual anisotropy, r_∞ . Theoretical models for the rotational/wobbling dynamics of the fluorophore in membrane have been

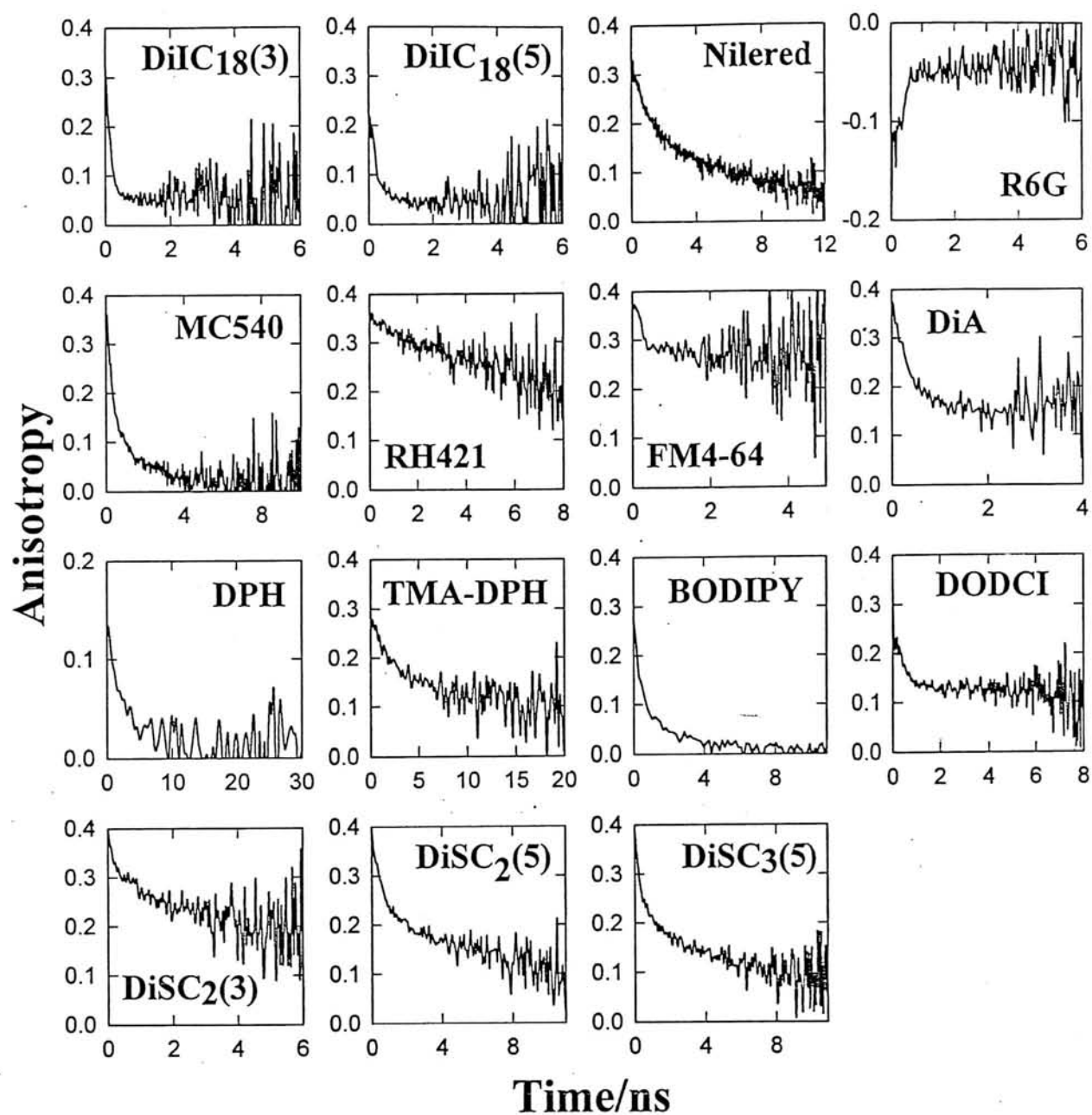


Figure 6.1: Fluorescence anisotropy decay of the fifteen dye molecules in EggPC membrane. The excitation and emission wavelengths are given in Table 6.1.

Table 6.1: Fluorescence anisotropy decay parameters (equation 6.5) for the fifteen organic dyes in Egg PC membrane

Dye	λ_{ex}	λ_{em}	r_0	ϕ_1	ϕ_2	α_1	α_2	r_∞
DiIC18(3)	570	650	0.33	0.16	-	1	-	0.05
DiIC18(5)	600	750	0.24	0.24	-	1	-	0.05
Nilered	570	615	0.31	1.11	7.53	0.47	0.53	0.01
Rhodamine 6G	300	630	-0.16	0.35	-	1	-	-0.04
Merocyanine 540	570	680	0.38	0.34	2.43	0.68	0.32	0.01
RH421	570	700	0.35	12.69	-	1	-	0.05
FM4-64	570	690	0.39	0.29	-	1	-	0.27
DiA	570	630	0.39	0.32	-	1	-	0.16
DPH	300	500	0.14	1.27	4.19	0.46	0.54	0.01
TMA DPH	300	470	0.28	1.67	10	0.45	0.55	0.08
DiOC2(5) (DODCI)	580	690	0.37	0.3	5.67	0.86	0.14	0.1
DiSC2(3)	570	690	0.39	0.15	2.47	0.29	0.71	0.18
DiSC2(5)	630	760	0.39	0.53	9.57	0.46	0.54	0.04
DiSC3(5)	630	760	0.39	0.33	4.78	0.5	0.5	0.07
BODIPY 611/627	610	730	0.27	0.4	2.63	0.67	0.33	0.004

discussed [95, 96] to explain the anisotropy decay for an ideal case, namely, a single species in a single site of solubilization and oriented normal to the surface. An ideal system is difficult to obtain in practice. Existence of multiple species or multiple sites of solubilization implies that the anisotropy decay is mathematically complex and experimental data cannot be meaningfully interpreted. The fluorescence studies of several dyes described in this paper suggests that a single site of solubilization is the predominant one in several cases ($a > 0.8$ in Table 4.2) : Nilered, RH421, DiSC₃(5) and BODIPY. The following discussion on the anisotropy decay is confined to these cases only.

The fluorescence anisotropy decays of Nilered and BODIPY show that the residual anisotropy, r_∞ is very small. The calculated values of order parameters $\left(\left(\frac{r_\infty}{r_0}\right)^{\frac{1}{2}}\right)$ for Nilered (0.150) and BODIPY (0.121) are also small suggesting that the equilibrium orientational distribution is almost random and the rotational dynamics of these dyes is therefore similar to that in a free solvent of high viscosity. This is consistent with the structure of the dye which is not charged and the major fraction of fluorescence is associated with a single site of solubilization in the core of the membrane. The single exponential fits of the anisotropy decays of Nilered and BODIPY gave the rotational correlation times to be 2.71ns and 0.90ns. Comparing these values with those measured for Nilered and BODIPY in 1-butanol (viscosity of 2.59 cP at 25°C), 0.52ns and 0.22ns, respectively, one obtains the viscosity near the site of solubilization to be 13.5cP and 10.6cP. These values are well within the range obtained using other probes [258] for the core region of the EggPC membrane.

In the case of RH421, the fluorescence is again predominantly due to one species solubilized in the interfacial region. The order parameter is 0.378 and the anisotropy decay time is 12.69ns which indicates a very slow rotational dynamics. Such a slow dynamics is conceivable for RH421 if the orientation of the chromophore is in the interfacial region and is parallel to the surface. The behaviour is similar to DiSC₂(5) which is discussed below.

The fluorescence of some linear dye molecules consisted of a long lifetime component which showed refractive index effect. Based on the refractive index effect the dye was

inferred to be oriented with respect to the membrane normal as two mutually orthogonal populations in the core region: orientation along the membrane normal and along the membrane plane. The rotational dynamics of the former population is more reasonably be the wobbling-in-a-cone model [95, 96, 98] which predicts one decay component (τ_w) followed by a static component ($S^2r(0)$). The rotational dynamics of the latter population is essentially rotation in the plane of the membrane. Such a rotational motion of a linear molecule will be highly hindered by the lipid chains. There is no experimental example for the rotational dynamics for such cases of rotation in membrane plane. One expects the rotational motion of a lengthy linear molecule in two dimensions to be single exponential with a very slow decay constant (τ_s). The anisotropy decay due to both the populations is therefore given by equation 6.6.

$$r(t) = r_0 \left[f \left[S^2 + (1 - S^2) \exp(-t/\tau_w) \right] + (1 - f) \exp(-t/\tau_s) \right] \quad (6.6)$$

where f and $(1 - f)$ represent the populations in the two orientational distributions. The above equation assumes that the dye molecule exists as one population in the core which is closely satisfied by DiSC₃(5) since the long lifetime is the dominant fraction (corresponding amplitude being 84%). The refractive index effect on lifetime and the analysis indicated that $f \approx 0.242$ (Chapter 5) and the anisotropy decay ought to be dominated by the slow component which is the case (figure 6.1). Quantitative fit of the experimental data has given $\tau_w = 0.33\text{ns}$ and $\tau_s = 4.78\text{ns}$ which are reasonable values for the model.

For other linear dyes the long lifetime component (the fraction of the dye in the core) is not the dominant fraction and hence the validity of equation 6.6 is less certain. It is noted however that the anisotropy decay of DiSC₂(5) consists of a long correlation time of 9.57ns (figure 6.1 and Table 6.1) that corresponds to the rotational dynamics of the fluorophore oriented parallel to the membrane surface.

6.3 Dynamics of surface probes: Diffusion on the surface of a macroparticle

When a fluorophore is attached to a macroparticle, the diffusion of the fluorophore on the surface of the macroparticle can also lead to fluorescence depolarization. There are two types of diffusion for the fluorophore on the surface: translational and rotational diffusion. In liquids, the fluorescence anisotropy decay is not affected by the translational diffusion dynamics of the fluorophore. On the other hand, in the case of a fluorophore bound noncovalently to the surface of nanometer-size particles such as vesicle membranes, micelles and proteins, the fluorescence depolarization dynamics is determined by both the rotational and translational dynamics of the dye. In addition, the anisotropy decay depends upon the orientation of the transition dipole and the shape of the particle. In spite of the numerous studies of fluorescence dynamics of fluorophores bound to micelle [259, 260, 104, 254, 105], membrane [96, 95] and proteins [164], analytical equation is not available for the anisotropy decay due to translational diffusion for surface-bound fluorophores. This led to the use of incorrect equations [104, 254] for the interpretation of the data for fluorescence depolarization due to lateral diffusion of dye molecules on spherical micelles. Similar equations are applicable for the spin relaxation due to surface transport in the Nuclear Magnetic Resonance studies in micelles and membranes [261, 262]. These translational diffusion equations are necessary for understanding biological transport phenomena at molecular level where the translational diffusion of solutes bound to different surfaces directly influence the rate of metabolism or the rate at which the chemical signals are conveyed [263].

In section 6.4, we obtain the fluorescence anisotropy decay parameters due to the translational and rotational diffusion of surface probes on the surface of a sphere using Monte Carlo simulations. The problem of surface diffusion has also been of wide importance in many areas of Physical Sciences such as polymer entanglement, depolarized light scattering, magnetic behaviour of spin-less bosons etc. [264, 265, 266, 267, 268]. The framework of solving the translational and rotational dynamics of a fluorophore on

the surface of a spherical particle can be extended to fluorophores of different characteristics and surfaces of different shapes. Experimentally measured anisotropy decay of fluorophores in micelles, small and large vesicle membranes are interpreted in accord with the theoretical results.

6.4 Monte Carlo Simulations

The main theme of the Monte Carlo simulations [155] used in this study is to mimic the surface diffusion of the molecular dipoles on a spherical surface. In these simulations, the probe molecules were treated as point dipoles oriented at a particular angle with respect to the normal to the surface of the sphere. The simulation is done with multiple dipoles diffusing on a spherical surface. The random numbers were generated using a random number generator '*ran2*' supplied in "Numerical Recipes in C" [156]. The random numbers generated by '*ran2*' depends on the seed used in the algorithm. If the same seed is used, the set of random numbers generated will be the same. Hence to obtain different sets of random numbers in the simulations carried out repeatedly to make sure that the obtained results are independent of the set of random numbers used to simulate the diffusion process, computer clock time was used as the variable seed for *ran2*. The simulation procedure can be mainly divided into three parts: selecting the initial distribution of the molecular dipoles, diffusion of the dipoles on the spherical surface and calculation of the anisotropy function.

6.4.1 Translational diffusion

Monte Carlo simulations were carried out for obtaining the anisotropy decay equations due to translational diffusion of the dipoles on a spherical surface. The simulation was carried out for the case where the dipoles are oriented parallel to the normal to the spherical surface and for the other cases where the dipoles are oriented at an angle α with the normal to the spherical surface. The simulation procedure mainly consists of three parts as mentioned before and these are described below. This procedure is summarized

in terms of a flow chart as shown in figure 6.2.

(i) Selecting the initial distribution of the point dipoles

Let R be the radius of the sphere on which the dipoles are undergoing translational diffusion and D_{tr} be the corresponding translational diffusion coefficient of the point dipole. Let θ and ϕ be the standard polar angles of the dipole vector (figure 6.3A). The initial distribution of the dipoles in the excited state was selected in the following steps. The ground state distribution of the molecular dipoles making an angle α with the respective radial vectors distributed randomly over the entire spherical surface was selected. Then the excited state distribution of the dipoles was obtained after 'excitation by a light pulse' polarized in z-axis, with the probability of excitation being $\cos^2\theta$. This distribution of excited state dipoles thus obtained will be identical to that in a real experiment.

The probability of a radial vector \bar{R} making an angle θ with the z-axis is proportional to $\sin\theta$. This probability has to be satisfied during the selection of random radial vectors. The random number generator *ran2* generates real numbers distributed uniformly from 0 to 1. From these uniform deviates, the random numbers satisfying the required probability distribution, say $P(\theta)$ (here $\sin\theta$), has to be generated. For this purpose, the "Transformation Method" [155, 156] was adopted. The method can be described as follows. Let $P(x)$ represents the probability of the random numbers uniformly distributed between 0 and 1.

$$\begin{aligned} P(x) &= 1 \text{ for } 0 \leq r \leq 1 \\ &= 0 \text{ otherwise} \end{aligned} \tag{6.7}$$

The conservation of probability requires

$$|P(x)dx| = |P(\theta)d\theta| \tag{6.8}$$

and hence

$$\int_{x=-\infty}^x P(x)dx = \int_{\theta=-\infty}^{\theta} P(\theta)d\theta \tag{6.9}$$

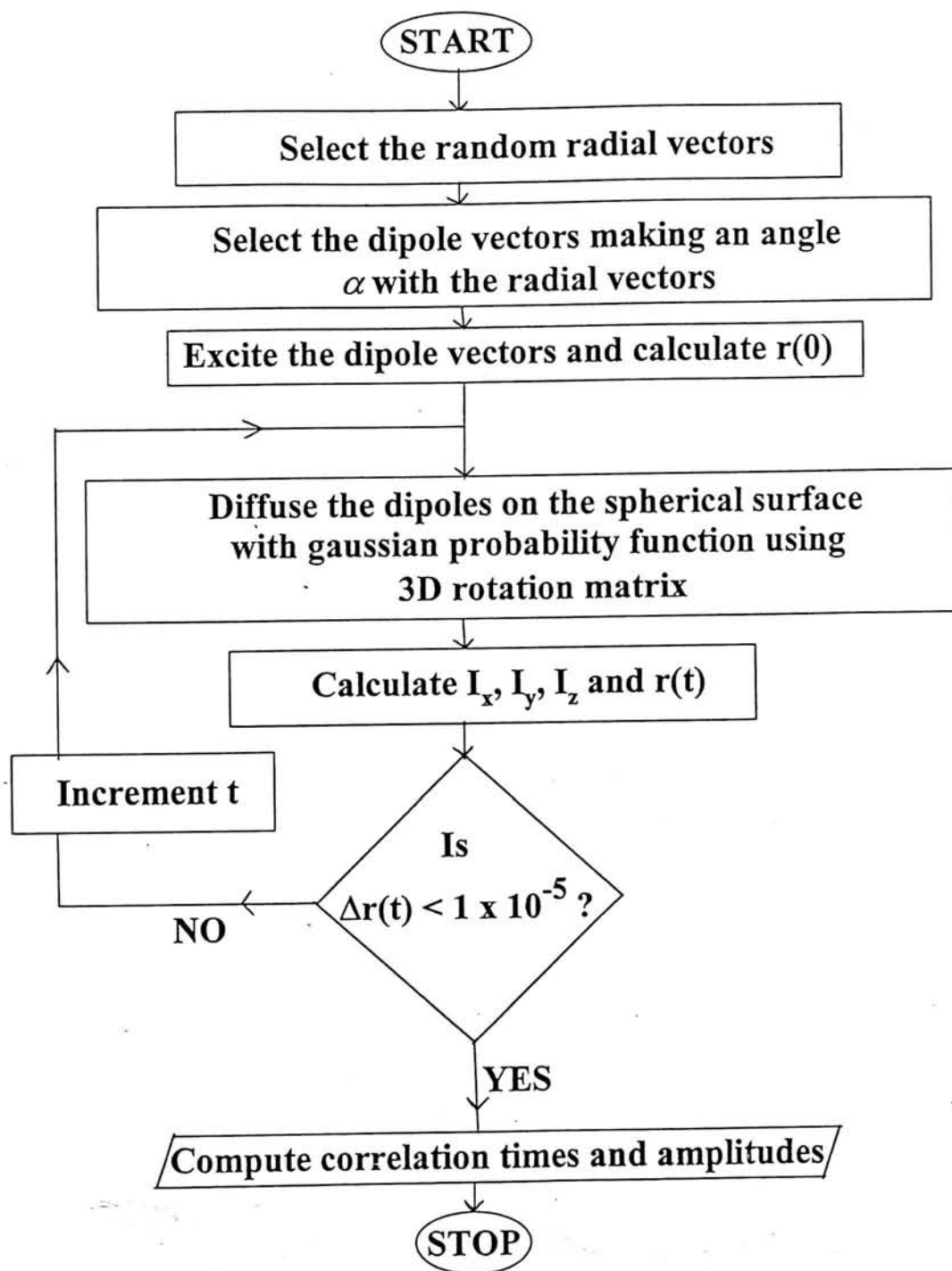


Figure 6.2: Flow chart for the Monte Carlo simulations of the translational diffusion of molecular dipoles on the surface of a sphere. This involves three steps as described in the text: (i) selection of the initial distribution of the point dipoles in the excited state, (ii) diffusion of dipoles on the spherical surface, and (iii) calculation of the anisotropy function.

The above equation becomes

$$x = \int_{\theta=0}^{\theta} P(\theta) d\theta \quad (6.10)$$

Therefore first choose a random number x between 0 to 1, then find the value of θ where the area under the probability curve from 0 to θ is x times that of the total area under the probability curve. The cartesian coordinates of the radial vector was calculated from the θ value and a randomly selected ϕ value between 0 and 2π .

The dipole oriented at an angle α with respect to the radial vector \bar{R} was obtained as follows. Initially a normal unit vector \hat{N} perpendicular to the radial vector \bar{R} was obtained such that $\bar{R} \cdot \hat{N} = 0$. If (x_1, x_2, x_3) represent the components of \bar{R} on the three cartesian axes, then the components of the normal unit vector \hat{N} , (n_1, n_2, n_3) has to satisfy the two equations

$$x_1 n_1 + x_2 n_2 + x_3 n_3 = 0 \quad (6.11)$$

and

$$n_1^2 + n_2^2 + n_3^2 = 1 \quad (6.12)$$

With the thus obtained normal unit vector $\bar{N} = (n_1, n_2, n_3)$ as the axis of rotation, the radial vector \bar{R} is rotated through the angle α to obtain a new vector \bar{V} that is oriented at the angle α with the radial vector (figure 6.3B). The rotation was done using the three dimensional rotation matrix $D_{\hat{N}}(\alpha)$ whose form is given in part (ii) of this section. The unit vector \hat{V} along this new vector is the dipole vector oriented at the angle α with the radial vector.

In selecting the normal unit vector $\hat{N} = (n_1, n_2, n_3)$ using the equations 6.11 and 6.12, random numbers were used such that the selected normal unit vectors are randomly distributed in the plane perpendicular to \bar{R} . This was done as follows. Initially a specific normal vector was chosen depending on the values of the three components of the radial vector $\bar{R} = (r_1, r_2, r_3)$. If all the components of the radial vector are non-zero, then the normal vector chosen was $(-r_2, r_1, 0)$. If some of the components are equal to zero, then the corresponding components of the normal vector are taken as one and for other components which are non-zero, the corresponding components were equated to zero. Using this

specific normal vector and a randomly chosen angular variable ϕ_1 between 0 to 2π , the rotation matrix $D_{\hat{R}}(\phi_1)$ was used to rotate the specific normal vector through the angle ϕ_1 about the unit vector along the radial vector \bar{R} , to obtain the random normal vector in the plane perpendicular to the radial vector. The selection of random normal vectors to the radial vector makes sure that the obtained dipole vectors are randomly oriented at the angle α with the respective radial vectors.

The probability of a dipole getting excited is proportional to $\cos^2\theta$ where θ is the angle made by the dipole with the z-axis. In selecting the excited dipoles with this probability, the same Transformation method described previously was adopted. A random number is chosen and if this random number matches with the fraction of the area under the probability curve with the total area, then that dipole was retained. Otherwise, the procedure was repeated from the initial step of selecting the ground state distribution.

(ii) Diffusion of the dipoles on the spherical surface

Let \hat{V} , \bar{R} and \hat{V}' , \bar{R}' represents the point dipole vectors and respective radial vectors before and after the diffusion in one iteration. The amount of diffusion is the same in the case of radial vector and dipole vector in one iteration. So the diffusion of the dipoles on the spherical surface was performed by rotation of the radial and dipole vectors by the three dimensional rotation matrix about the randomly chosen normal vector to the radial vector. If $\hat{n} \equiv (n_1, n_2, n_3)$ represents the unit normal vector which is the axis of rotation and β is the angle of rotation, then the three dimensional rotation matrix $D_{\hat{n}}(\beta)$ is given as [269]

$$D_{\hat{n}}(\beta) = \begin{pmatrix} \cos\beta + (1 - \cos\beta)n_1^2 & (1 - \cos\beta)n_1n_2 - \sin\beta n_3 & (1 - \cos\beta)n_1n_3 + \sin\beta n_2 \\ (1 - \cos\beta)n_1n_2 + \sin\beta n_3 & \cos\beta + (1 - \cos\beta)n_2^2 & (1 - \cos\beta)n_2n_3 - \sin\beta n_1 \\ (1 - \cos\beta)n_3n_1 - \sin\beta n_2 & (1 - \cos\beta)n_3n_2 + \sin\beta n_1 & \cos\beta + (1 - \cos\beta)n_3^2 \end{pmatrix} \quad (6.13)$$

The angle of rotation β was obtained as follows. The probability of finding a particle at r at time t given that the initial position is r_0 at $t = 0$ for diffusion on a two dimensional

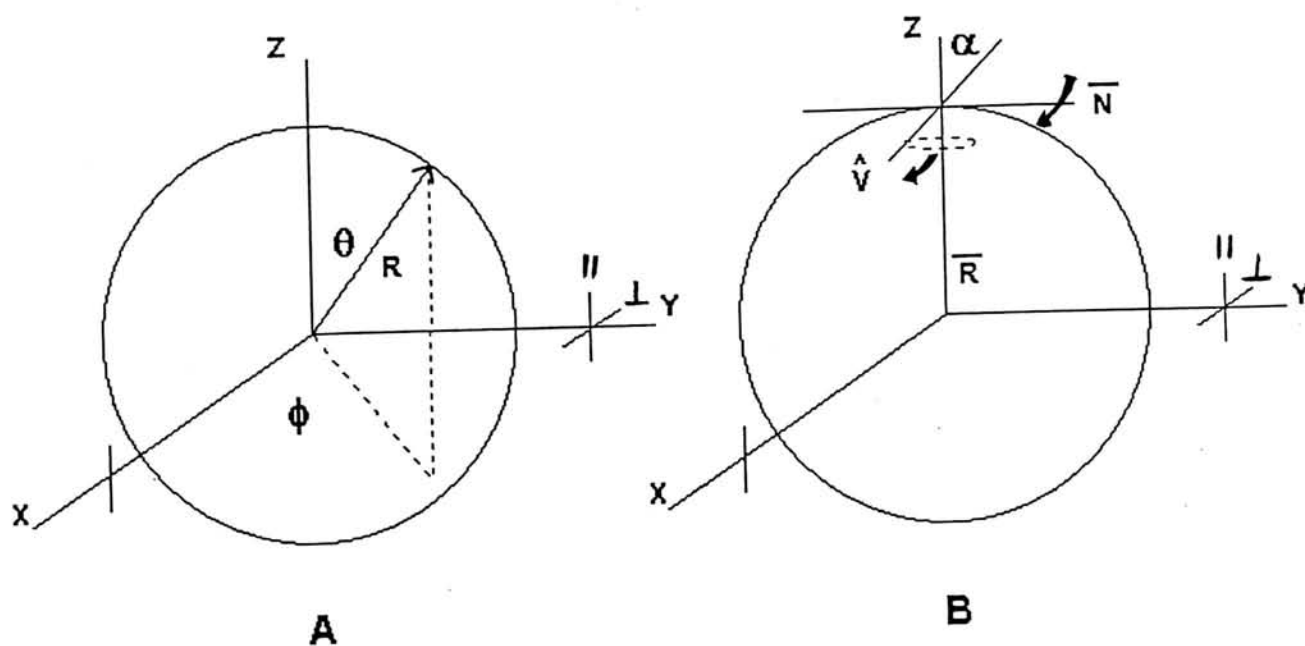


Figure 6.3: (A) The figure shows the two polar angles θ and ϕ of a radial vector on the surface of a sphere with radius R in the xyz laboratory frame. The excitation light is polarized along the z -direction. The fluorescence anisotropy is calculated using the intensities along the parallel and perpendicular directions with respect to the polarization of the exciting laser beam. (B) This figure illustrates the selection of a random dipole vector \hat{V} which makes an angle α with the radial vector \bar{R} with the selection of a random normal vector \bar{N} . See text for details.

planar surface [270] is given by

$$W(r, t; r_0, 0) = \frac{1}{4\pi Dt} \exp\left(-\frac{|r - r_0|^2}{4Dt}\right) \quad (6.14)$$

where D is the diffusion coefficient. In our case, replacing the displacement $|r - r_0|$ by $R\beta$ (which is valid for small displacements) and multiplying by $\sin\beta$, the probability of the angle of rotation β satisfies the equation 6.15:

$$W(\beta) = \frac{1}{4\pi D_{tr}t} \exp\left(-\frac{R^2\beta^2}{4D_{tr}t}\right) \sin\beta \quad (6.15)$$

The β values satisfying equation 6.15 were calculated using the random numbers by the Transformation method described earlier. After getting a value for β and the randomly chosen unit normal vector components (as described in part (i) of this section), the three dimensional rotation matrix was computed. The new vectors \hat{V}' and \bar{R}' were then obtained by multiplying \hat{V} and \bar{R} with the matrix $D_{\hat{n}}(\beta)$.

(iii) Calculation of the anisotropy function

After 'excitation', the excited dipoles were allowed to diffuse randomly on the spherical surface with the given diffusion constant for a unit time (one iteration). The 'fluorescence intensity' along the x, y and z-axes were calculated as squares of the respective components of the dipole vector \hat{V} . The components along x and y-axes ought to be equal which serves to check the algorithm. The anisotropy was calculated as

$$r(t) = \frac{I_{\parallel} - I_{\perp}}{I_{\parallel} + 2I_{\perp}} = \frac{I_z - I_x}{I_x + I_y + I_z} = \frac{I_z - I_y}{I_x + I_y + I_z} \quad (6.16)$$

The random diffusion of the dipoles was continued until there is no change in the calculated anisotropy between successive iterations.

The C program developed for the Monte Carlo simulations is given in the Appendix A. The validity of each and every step in this simulation procedure was checked with the help of Computer graphics. If the initial selection of excited dipoles follows $\cos^2\theta$ distribution, then the initial anisotropy r_0 value should be independent of the orientation angle α and should be equal to 0.4 [46], which was observed. The selection of random normal vectors

and the use of the rotation matrix $D_{\hat{n}}(\beta)$ for the surface diffusion of dipoles were also tested. The simulation was done for varying values of α with about 85000 dipoles diffusing on a spherical surface, using a DEC Alpha OSF/1 Computer system. The simulation was also carried out for varying values of radius of the sphere R and translational diffusion coefficient D_{tr} . The results are discussed in section 6.5.1.

6.4.2 Rotational diffusion

Monte Carlo simulations were also carried out to obtain the fluorescence anisotropy decay equations due to the rotational diffusion of dipoles on a spherical surface. The procedure is similar to the one described before for simulating the translational diffusion. It involves three steps: initial selection of the excited dipoles, rotational diffusion of the dipoles on the spherical surface with no translational diffusion and calculation of the anisotropy function.

The ground state population of the dipoles were selected to be parallel to the membrane surface, i.e., making the angle $\alpha = 90^\circ$ with the respective radial vector. These were excited with the probability of excitation. The rotational diffusion of the excited dipoles was performed by rotating the dipoles through the specified angle (1° in one iteration) about the radial vector using the rotation matrix. The anisotropy function was calculated after each iteration. The decay is simulated for the two cases (i) where all the dipoles are situated in a plane (no spherical averaging) and (ii) where all the dipoles are distributed over the entire spherical surface and the simulated anisotropy decay is the average of all the dipoles (spherical averaging). Figure 6.4 illustrates the experimental examples for these two cases. As shown in the figure, the samples include (i) the rotational diffusion of surface probes in a planar bilayer membrane and the fluorescence anisotropy is measured for the fluorophores from a small area (diameter of $\approx 1.2 \pm 0.2 \mu\text{m}$ [150]) of the planar membrane under a fluorescence microscope (no spherical averaging) and (ii) when the fluorescence anisotropy is observed from the dye incorporated in sonicated vesicles in a cuvette where the collected fluorescence anisotropy is from the probes distributed over

the entire spherical vesicle.

6.5 Translational Diffusion: Simulations and Experiment

6.5.1 Results of the Monte Carlo Simulations

The translational diffusion of excited dipoles oriented along the normal to the spherical surface is shown in figures 6.5 and 6.6 at different stages of the Monte Carlo simulation. Figure 6.5 shows the surface diffusion for the case when all the initially excited dipoles are oriented parallel to the z -axis, to illustrate the random diffusion process modelled in these Monte Carlo simulations. Figure 6.6 shows the case when the dipoles are excited with the excitation probability $\cos^2\theta$. The corresponding intensities along the three axes and the calculated anisotropy is shown in figure 6.7. The anisotropy decay is identical if the excited dipoles are distributed with the excitation probability $\cos^2\theta$ such that $r(0)=0.4$ or with the initial excited state population along the z -axis with $r(0)=1.0$. The decay is single exponential. The residuals are shown in the bottom panel of figure 6.7. From the values of the translational diffusion coefficient D_{tr} and the radius of the sphere R , the correlation time is found to be equal to $R^2/6D_{tr}$.

The fluorescence anisotropy decays generated from the Monte Carlo simulations of the translational diffusion when the dipoles are oriented at an angle α (from 0° to 90° at an interval of 15°) with the respective radial vectors are shown in figure 6.8. These curves clearly show that the anisotropy decay depends on the orientation angle α . These individual decays can not be fitted to single exponential functions at all non-zero values of α . When we analyzed the anisotropy decay at $\alpha=90^\circ$ for a two exponential function, we found that the decay fits well. The two correlation times are in the ratio of $\approx 1:3$ and these are $R^2/6D_{tr}$ and $R^2/2D_{tr}$. The anisotropy decays simulated at the other orientation angles were also found to fit to a two exponential function with the same correlation times

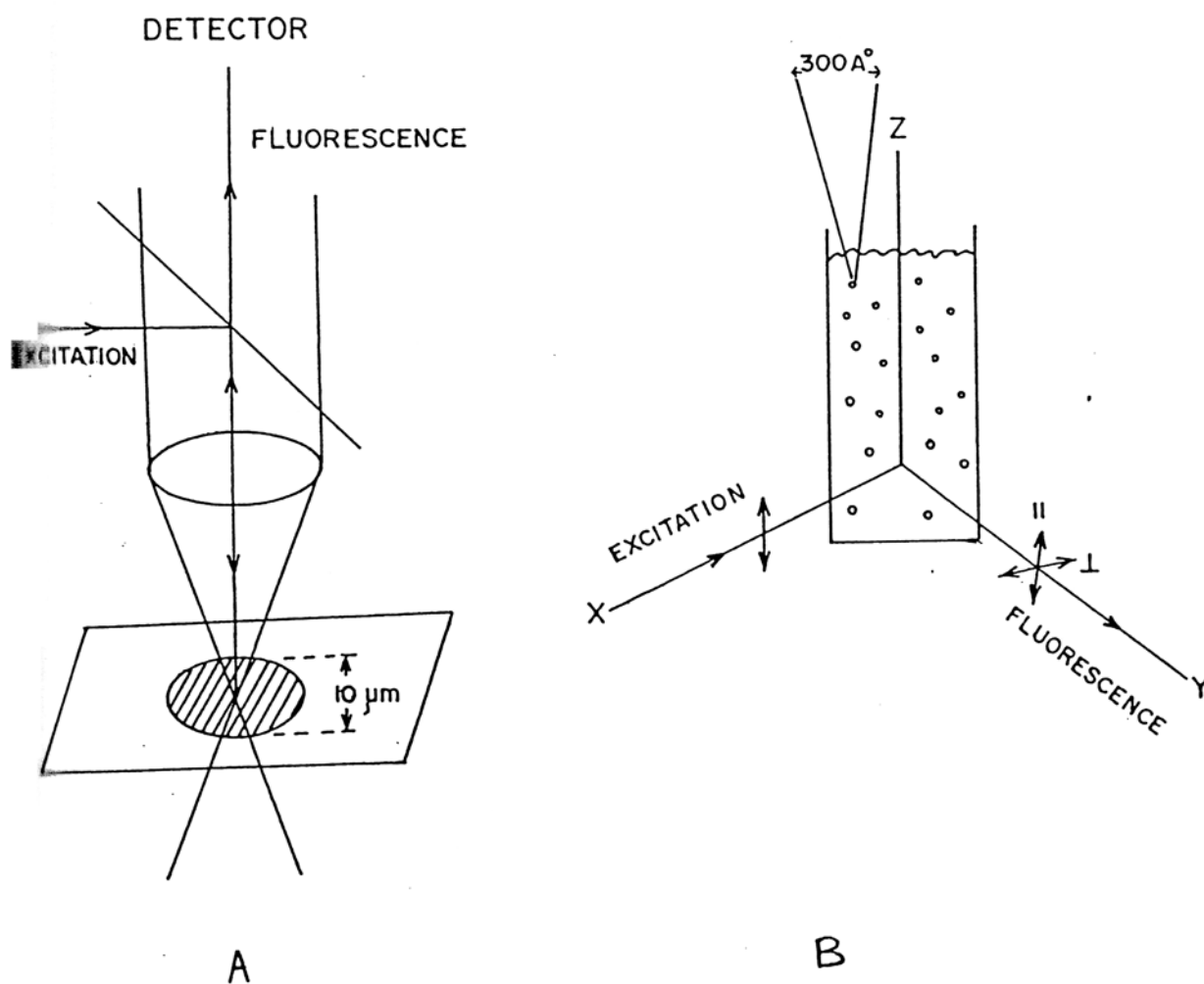


Figure 6.4: Rotational diffusion of surface probes. The calculation of the fluorescence anisotropy in the case of a planar bilayer membrane (Fig. A) does not involve spherical averaging due to the fluorophore distribution as in the case of sonicated vesicles in a cuvette (Fig. B)

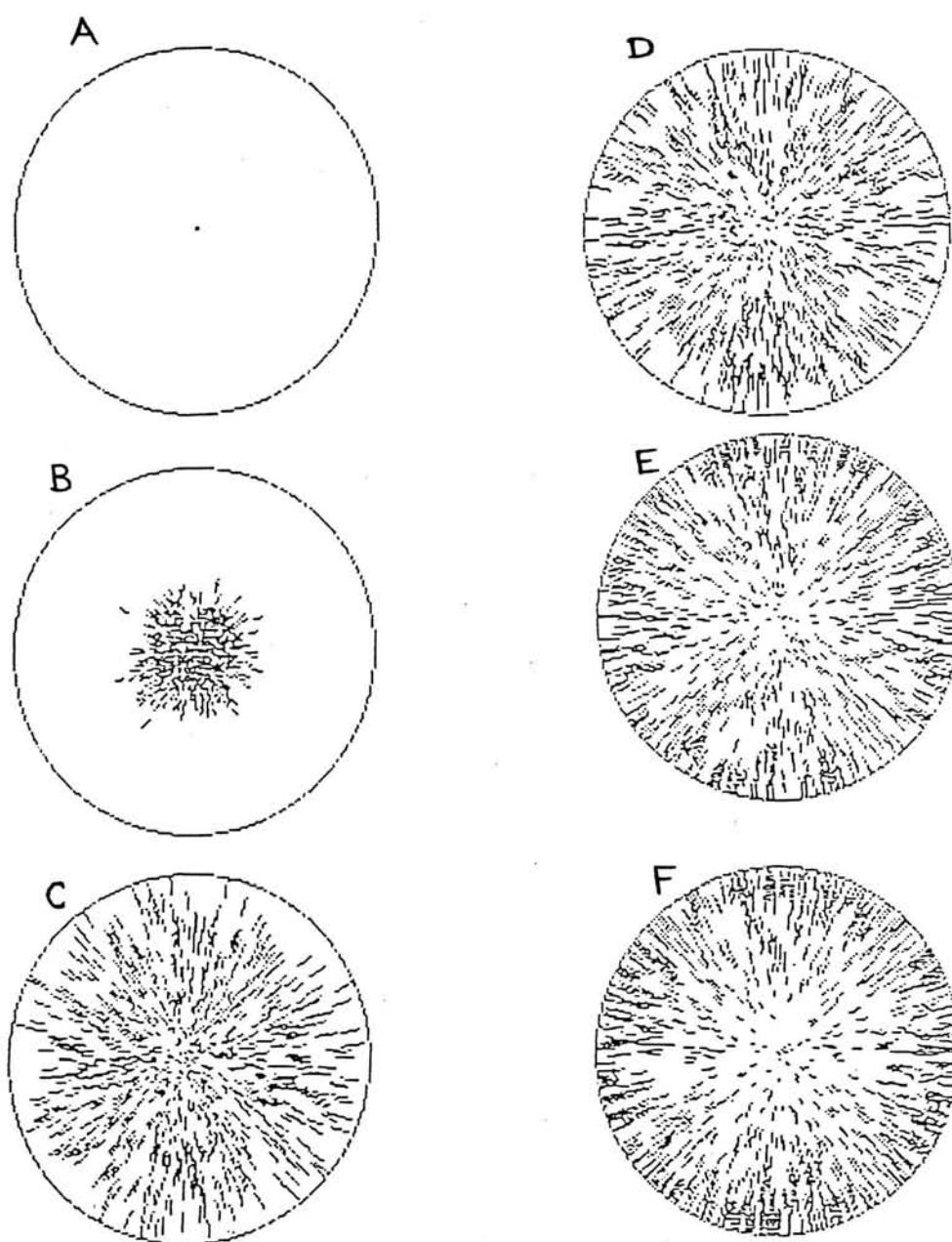


Figure 6.5: Translational diffusion of the dipoles oriented along the radial vectors on the surface of the sphere as viewed from the top of the sphere. A to F show the distribution of the dipoles on the surface of the sphere at different stages of the translational diffusion. Here the excited dipoles are initially oriented parallel to the z -axis which is the axis of polarization of the excitation light.

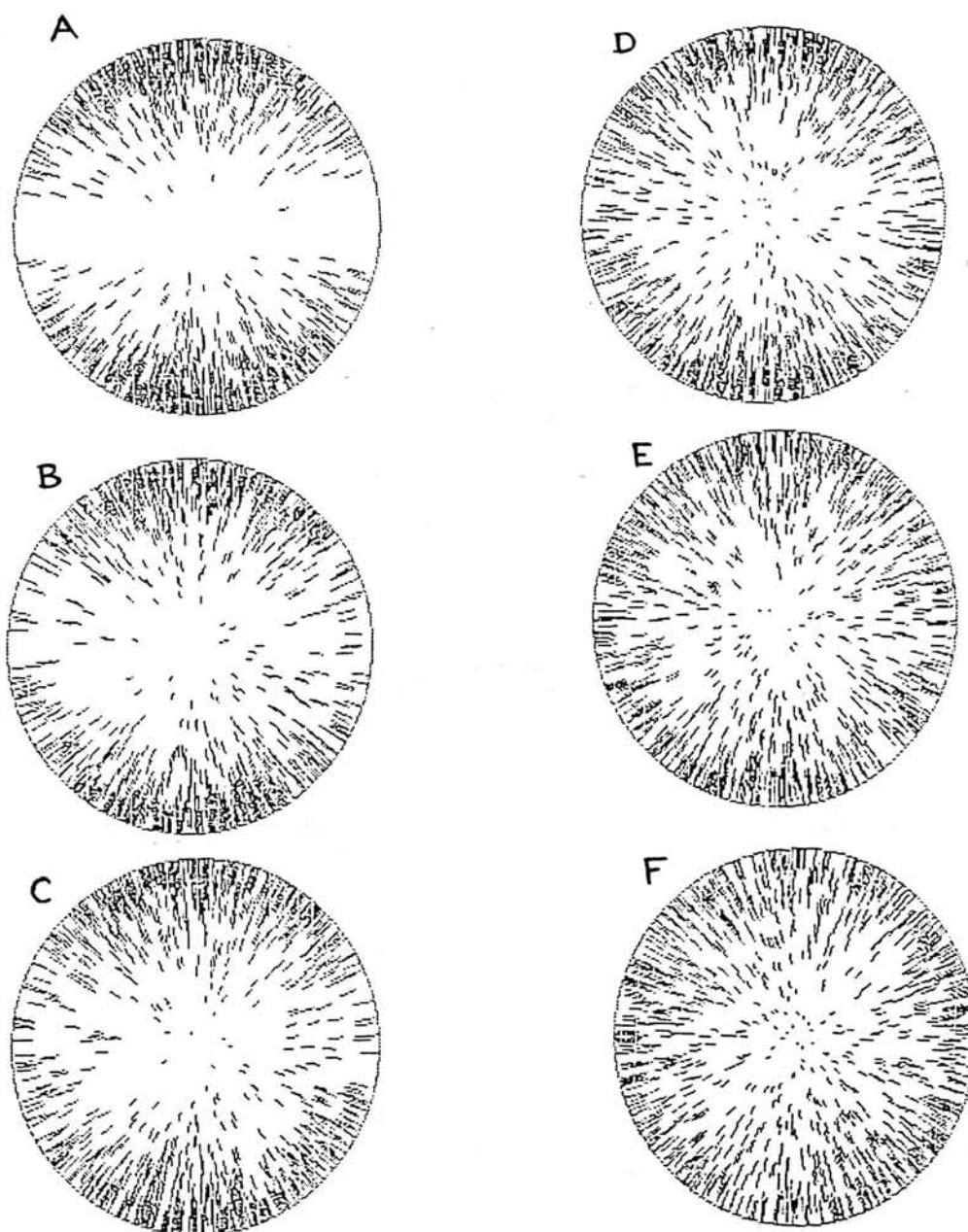


Figure 6.6: Translational diffusion of the dipoles oriented along the radial vectors on the surface of the sphere as viewed from the side of the sphere. A to F show the distribution of the dipoles on the surface of the sphere at different stages of the translational diffusion. Here the excited dipoles are initially selected with the probability $\cos^2\theta$ where θ is the angle made with the z-axis which is the axis of polarization of the excitation light. The corresponding fluorescence anisotropy decay curve is shown in figure 6.7.

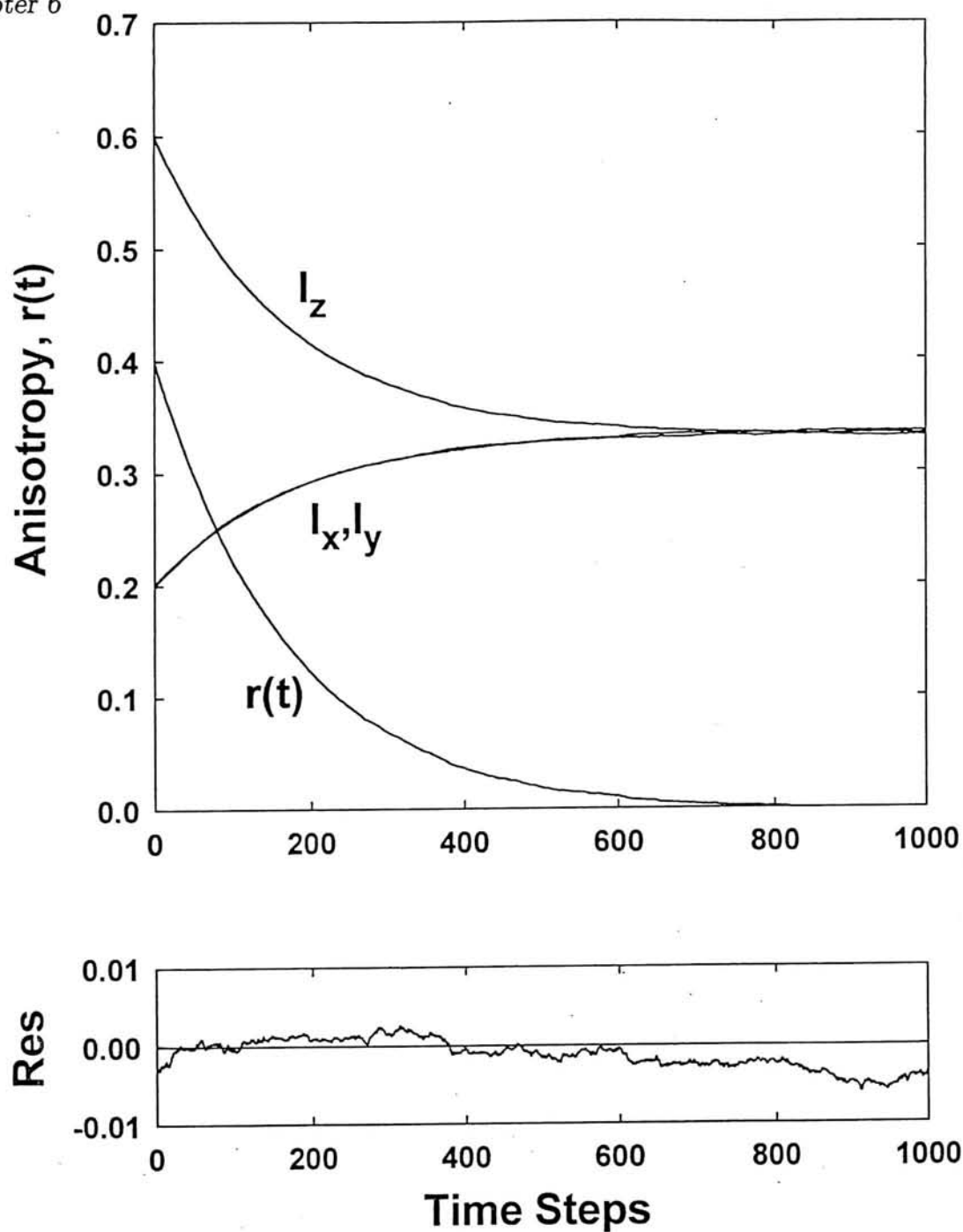


Figure 6.7: Fluorescence anisotropy decay due to the translational diffusion of dipoles oriented along the radial vectors on the surface of a sphere. I_x , I_y and I_z represent the intensities along the three directions. Residuals for a single exponential fit of the anisotropy decay are shown in the bottom panel.

according to the equation

$$\frac{r(t)}{r(0)} = a(\alpha) \exp\left(-\frac{6D_{tr}t}{R^2}\right) + (1 - a(\alpha)) \exp\left(-\frac{2D_{tr}t}{R^2}\right) \quad (6.17)$$

The preexponential factors $a(\alpha)$ and $1 - a(\alpha)$ of these two correlation times in the anisotropy decay due to translational diffusion depend only on the orientation angle α . The variation is shown in the figure 6.9. The error bars on $a(\alpha)$ indicated in the figure are from multiple simulations carried out with different sets of random numbers for a particular orientation angle α .

The preexponential factors of the two correlation times were not following any known relationship with the orientation angle α and hence it was difficult to find the analytical relationship between $a(\alpha)$ and α from the observed trend. The translational diffusion process was modelled with the appropriate equations and an analytical solution was obtained as described in the next section [271]. All the seven simulated decays at different orientation angles α could be fitted to this equation 6.18 which contains three exponential terms.

$$r(t) = \frac{2}{5}(\cos^2\alpha - \frac{1}{2}\sin^2\alpha)^2 \exp\left(-6D_{tr}t/R^2\right) + \frac{6}{5}\sin^2\alpha\cos^2\alpha \exp\left(-5D_{tr}t/R^2\right) + \frac{3}{10}\sin^4\alpha \exp\left(-2D_{tr}t/R^2\right) \quad (6.18)$$

Figure 6.10 shows the fitting of the simulated data to the above equation. Note that the preexponential factors of the three exponentials depend only on the orientation angle α . For $\alpha=0$, i.e., when the transition dipole is parallel to the radial vector, the anisotropy decay is single exponential with the correlation time $R^2/6D_{tr}$. This is the exact result obtained by solving the diffusion equation for the rotational dynamics of a molecule in liquids [94] with an isotropic rotational diffusion constant $D_{rot} (=D_{tr} / R^2)$. The appearance of the other two exponentials with the anisotropy decay times of $(5D_{tr}/R^2)^{-1}$ and $(2D_{tr}/R^2)^{-1}$ when the transition dipole is oriented ($\alpha \neq 0$), is an unanticipated new result. In the extreme case, for $\alpha=90^\circ$, the anisotropy decay is two exponential with the correlation times $(6D_{tr}/R^2)^{-1}$ and $(2D_{tr}/R^2)^{-1}$ with the respective amplitudes in the ratio 1:3. Although the above equation for the translational diffusion contains three

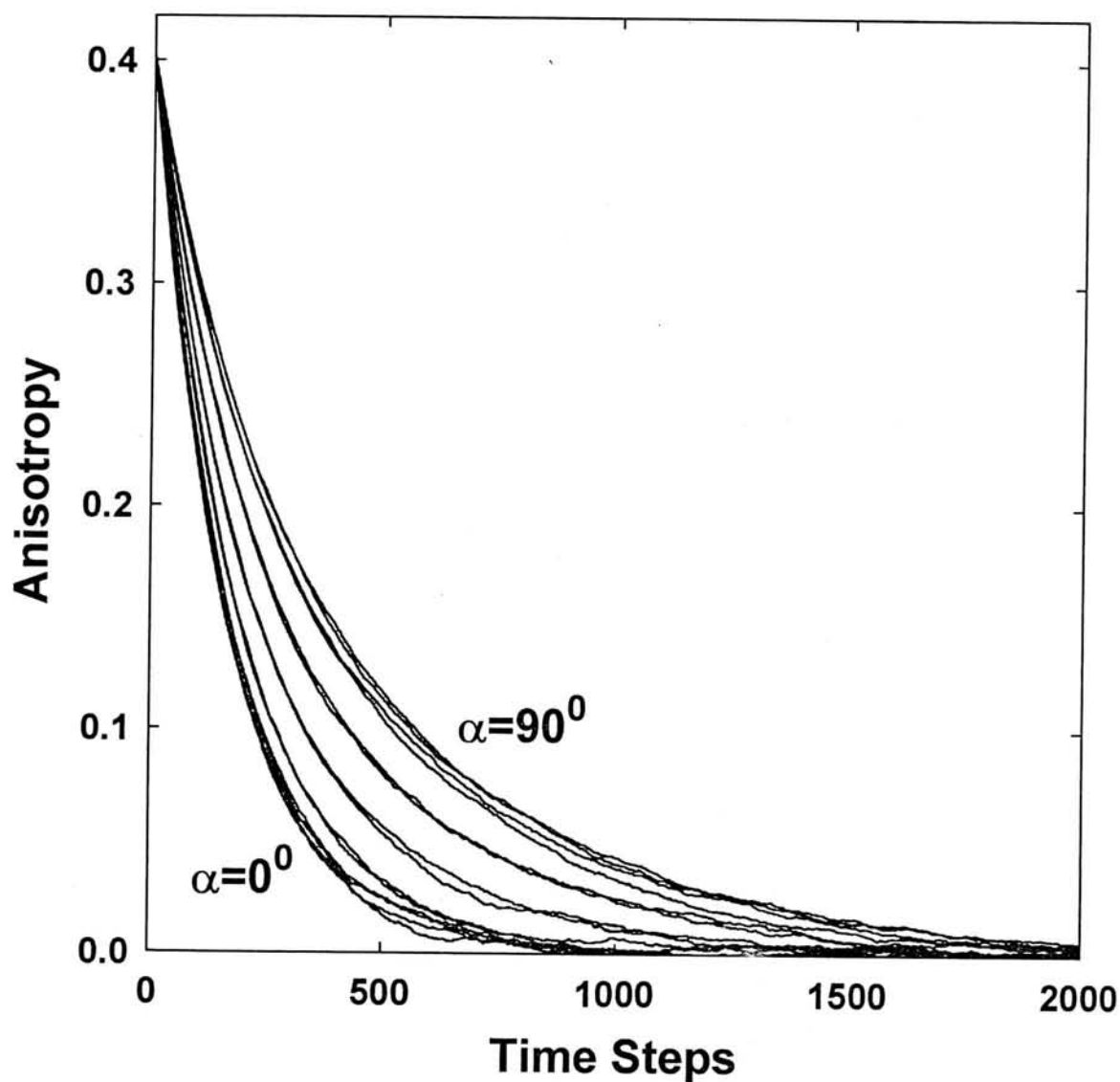


Figure 6.8: Fluorescence anisotropy decays obtained from the Monte Carlo simulations of the translational diffusion of dipoles on the surface of a sphere at different orientation angles α made by the dipoles with the respective radial vectors. The figure shows two decays for each value of α , simulated using different sets of random numbers.

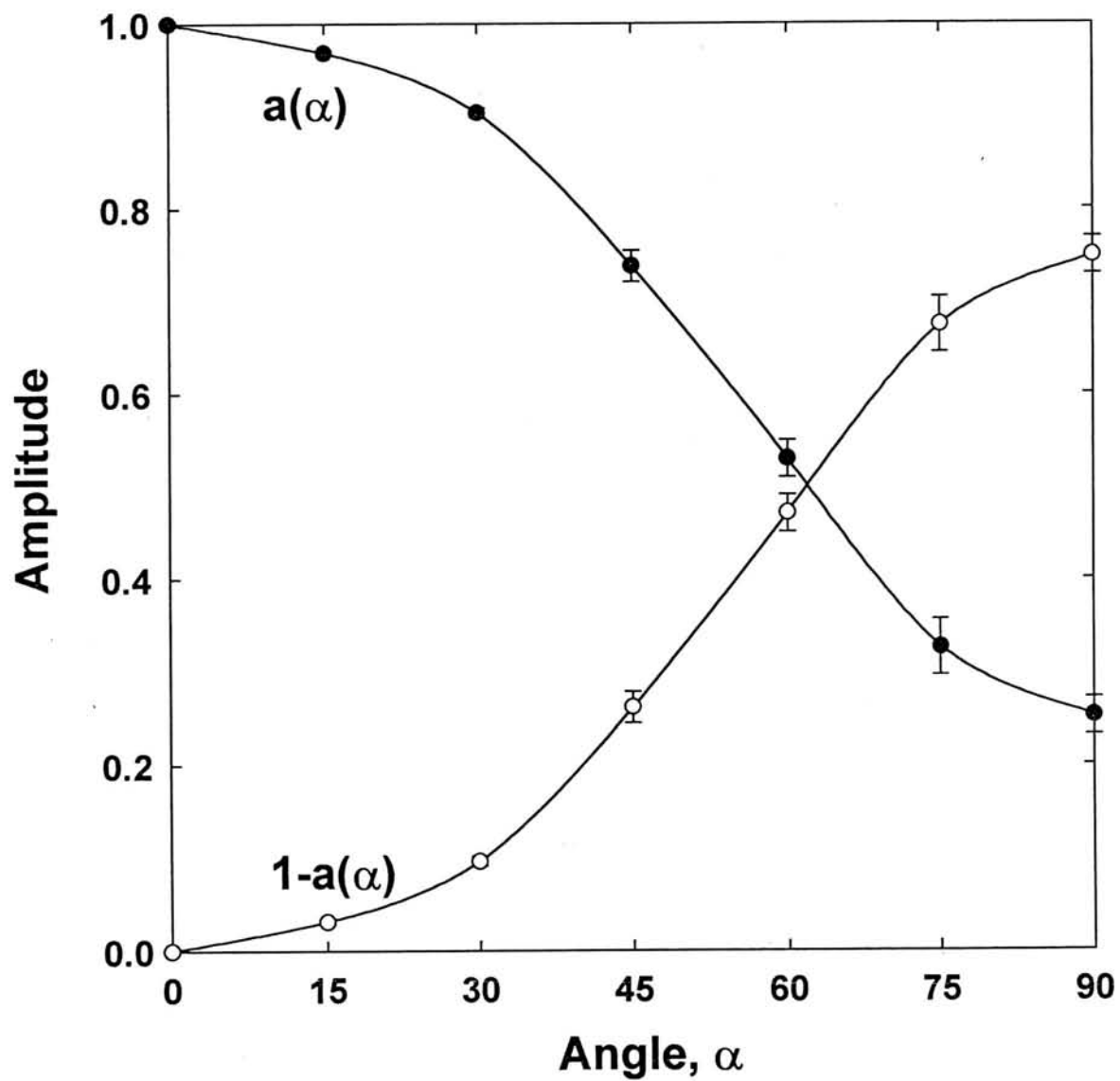


Figure 6.9: Variation of the preexponential factors of the two correlation times $R^2/6D_{tr}$ and $R^2/2D_{tr}$ with the orientation angle α (Refer to equation 6.17)

exponentials, there are only two fitting parameters α and D_{tr}/R^2 that has to be optimized in the analysis of the experimental data.

6.5.2 Theoretical justification of the simulation results

When the dipoles are oriented parallel to the radial vectors, the diffusion equation becomes the usual spherical harmonics equation [272] with the radial coordinate being a constant at the radius of the sphere, R .

$$\frac{\partial}{\partial t} P(\theta, \phi, t) = D_{tr} \nabla^2 P(\theta, \phi, t) \quad (6.19)$$

where $P(\theta, \phi, t)$ is the probability of finding the dipole at the angular coordinates θ and ϕ at time t , ∇^2 is the Laplacian in the spherical polar coordinates. Here θ and ϕ represent the polar and azimuthal angles of the dipole, respectively. This equation can be easily separated into the two angular parts (θ and ϕ parts) using the method of separation of variables [191]. The θ part becomes

$$\frac{1}{R^2 \sin \theta} \frac{\partial}{\partial \theta} \left(\sin \theta \frac{\partial}{\partial \theta} \right) P(\theta, t) = -\frac{\lambda}{D_{tr}} P(\theta, t) \quad (6.20)$$

The general solution which satisfy the above equation is

$$P(\theta, t) = \sum_l A_l P_l(\cos \theta) \exp \left(-\frac{l(l+1)D_{tr}}{R^2} t \right) \quad (6.21)$$

where $P_l(\cos \theta)$ are the l th order Legendre Polynomial and A_l is the corresponding scaling factor.

In this case where the dipoles are oriented parallel to radial vectors, the fluorescence anisotropy equation is defined by

$$r(t) = \langle P_2(\cos \Omega) \rangle_t = \langle P_2(\cos \theta) \rangle_t \quad (6.22)$$

where Ω is the angle made by the dipole with the z -axis. Using the above solution (equation 6.21) for the θ part, the anisotropy equation becomes a single exponential as

$$r(t) = c \exp \left(-\frac{6D_{tr}t}{R^2} \right) \quad (6.23)$$

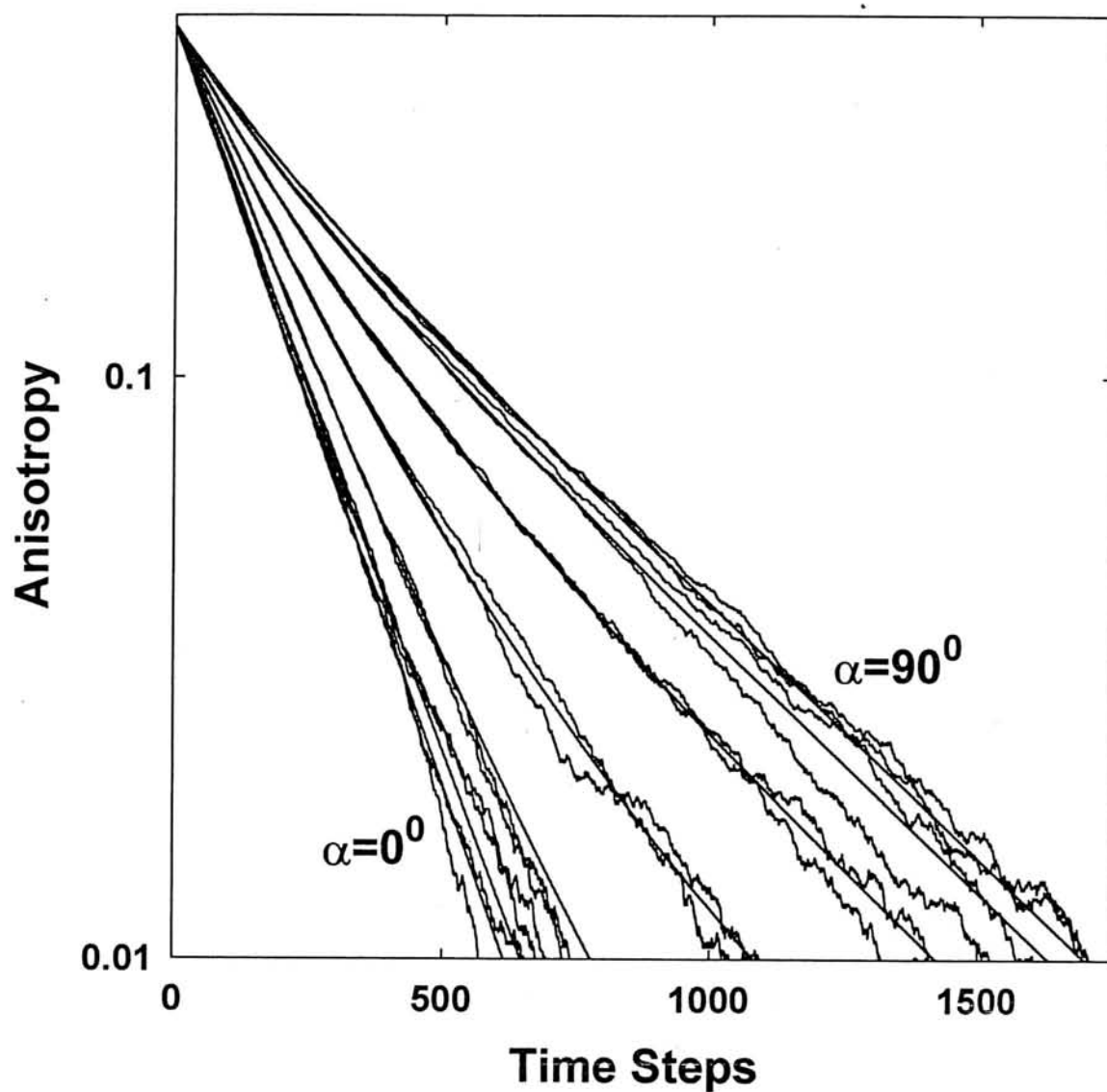


Figure 6.10: Fitting of the anisotropy decay data simulated by the Monte Carlo methods for the translational diffusion of oriented dipoles making an angle α with the normal to the spherical surface, to the analytical equation 6.18. The simulated decays are the same as in figure 6.8, except that they are plotted in log scale here.

where c is a constant. That means, the fluorescence anisotropy decays exponentially with the correlation time of $R^2/6D_{tr}$ when the dipoles are oriented parallel to the radial vectors. This is in agreement with the Monte Carlo simulations.

The theory and the Monte Carlo simulations predict that the translational correlation time is $R^2/6D_{tr}$, not $R^2/4D_{tr}$ as assumed in interpreting the experimental fluorescence anisotropy decay data of fluorescent dyes in micelles [104].

The theoretical derivation of the fluorescence anisotropy equation becomes complex in the case where the dipoles are oriented at a particular angle α with the radial vectors. A diffusion equation similar to equation 6.19 has to be set up for the translational diffusion in such a case and has to be solved to obtain the solution similar to equation 6.21. The main difference that arises when $\alpha \neq 0$ is the Berry's phase factor [273]. When the dipole is oriented at an angle with the respective radial vector, the direction at which the dipole points at a given time during the translational diffusion depends on the path it followed to arrive at that particular position. That means the phases of the different dipole vectors starting at the same initial position and arriving at the same final position but following different paths will be different. This Berry's phase factor has to be taken care of in setting up and solving the diffusion equation. This requires a different formalism which should include one extra degree of freedom which takes account of the phase factor for the diffusion process on the surface of a sphere. This was done as follows [271].

For solving the problem of translational diffusion of oriented dipoles, we consider an additional frame associated with the dipole in addition to the space-fixed axes x, y and z . Let an orthonormal set of three vectors \vec{a} , \vec{b} and \vec{c} be the frame attached with the dipole that is undergoing translational diffusion. The vector \vec{c} is selected such that it is parallel to the radial vector and the dipole is tilted at an angle α with respect to \vec{c} in the plane of vectors \vec{b} and \vec{c} . Hence the unit dipole vector that is undergoing translational diffusion becomes $\vec{c} \cos \alpha + \vec{b} \sin \alpha$. The model for translational diffusion which was simulated here by the Monte Carlo methods gives this abc frame infinitesimal random rotations around the body fixed \vec{a} and \vec{b} axes. In this process, the \vec{c} axis moves and with it the location of the dipole on the surface of the sphere. When the \vec{c} returns to its original value in

the process of this diffusion process, the dipole has returned to the same point on the sphere, but because of the geometric phase effect (Berry's phase) discussed before, the \vec{a} and \vec{b} axes would not in general return to their original values, and hence the dipole will be different. By working on this formalism of two frames (space fixed and body fixed), we have ensured that the extra degree of freedom required to take account of the Berry's phase factor is explicitly included.

With the excitation light polarized along the z-axis, the probability of excitation of the dipole located at $\vec{a}, \vec{b}, \vec{c}$ is equal to the square of the component of the dipole vector on the z-axis, i.e., $(c_z \cos \alpha + b_z \sin \alpha)^2$. After time t , let the dipole diffuses to $\vec{a}', \vec{b}', \vec{c}'$ with the probability $P(\vec{a}', \vec{b}', \vec{c}' : \vec{a}, \vec{b}, \vec{c} : t)$. Projecting it back to the space fixed z axis and squaring, the intensity I_z becomes

$$I_z = (c_z \cos \alpha + b_z \sin \alpha)^2 (c'_z \cos \alpha + b'_z \sin \alpha)^2 \quad (6.24)$$

The expression for anisotropy can be written as

$$r(t) = \frac{3 I_z(t)}{2 I(t)} - \frac{1}{2} \quad (6.25)$$

where $I = I_x + I_y + I_z$ is the total fluorescence intensity.

For calculating $r(t)$, one needs to compute the ensemble average of I_z that can be obtained by multiplying the expressions for I_z and the probability P and integrating over $\vec{a}, \vec{b}, \vec{c}$ and $\vec{a}', \vec{b}', \vec{c}'$. The conditional probability P is the solution of the diffusion equation which at $t = 0$ is a delta function centered around the initial frame. This is the Green's function of the diffusion equation. It can be expressed in a similar manner to the Green's function of the Schrodinger equation, in terms of eigenfunctions. Schematically,

$$P(a', b', c' : a, b, c : t) = \sum_p \Psi_p(a', b', c') \Psi_p(a, b, c) \exp(-E_p t) \quad (6.26)$$

Here Ψ_p, E_p are the eigenfunctions and eigenvalues, (labelled by the index p) of the corresponding diffusion operator on the group.

For the case of interest, i.e., highly hindered rotation about the radial direction to the spherical surface, the diffusion operator will be proportional to $J_a^2 + J_b^2$. The absence

of J_c^2 shows that we have built in the constraint of no rotation about the normal to the sphere. This operator is similar to that of the symmetric top. Hence the eigenvalues and eigenfunctions will be similar to those which occur in the quantum-mechanical treatment of the symmetric top [274]. The appropriate quantum numbers are (i) J which enters the eigenvalue of the square of the angular momentum as $J(J+1)$ (ii) M , which is the eigenvalue of the z component of the angular momentum, i.e., along the space fixed z axis and (iii) K which is the eigenvalue of the \vec{c} component of angular momentum, i.e., along the body fixed z axis. These three operators commute and their eigenvalues are sufficient to label states for the top, whose wave functions depend on three variables. The conventional choice for these three variables is the set of Euler angles giving the orientation of the body fixed frame with respect to the space fixed frame [275]. But for the problem considered here, it is convenient to use the components of \vec{a}, \vec{b} and \vec{c} which in turn can be expressed in terms of Euler angles. The intensity I_z is already expressed in terms of these components (equation 6.24). The eigenvalues of the diffusion operator $J_a^2 + J_b^2$ are obtained by adding and subtracting J_c^2 (since $J^2 = J_a^2 + J_b^2 + J_c^2$) and hence these are $J(J+1) - K^2$. Taking account of the angular diffusion coefficient D_{tr}/R^2 , the eigenvalues of the diffusion equation becomes $(J(J+1) - K^2)D_{tr}/R^2$.

Each of the factors in I_z can be expressed as a sum of eigenfunctions. This ensures that when it is multiplied by P and do the integration needed to compute the average of I_z over the ensemble, only those eigenfunctions will contribute and the rest will disappear by the orthogonality relations. The three relevant eigenfunctions are

$$\sqrt{\frac{45}{4}}(c_z^2 - 1/3),$$

$$\sqrt{15}b_z c_z,$$

and

$$\sqrt{\frac{15}{4}}(b_z^2 - a_z^2) \quad (6.27)$$

All the three functions have $J = 2$, and $M = 0$, but have different $|K|$ values as 0, 1, 2, and hence the eigenvalues are 6, 5, and 2.

One of the factors in the intensity expression (equation 6.24) can be written as

$$(c_z \cos \alpha + b_z \sin \alpha)^2 = \sqrt{\frac{4}{45}}(\cos^2 \alpha - \frac{1}{2} \sin^2 \alpha) \sqrt{\frac{45}{4}}(c_z^2 - 1/3) + \sqrt{\frac{4}{15}}(\sin \alpha \cos \alpha) \sqrt{15} b_z c_z + \sqrt{\frac{1}{15}} \sin^2 \alpha \sqrt{\frac{15}{4}}(b_z^2 - a_z^2) + \frac{1}{3} \cdot 1 \quad (6.28)$$

The constant term corresponds to $J = 0$, with the normalized eigenfunction to 1, which is non-decaying under diffusion (zero eigenvalue). The second factor in I_z can be similarly written in terms of primed quantities. Multiplying I_z by P and integrating over the initial and final parameters of the frame, the expression for I_z was obtained. It can also be calculated that $I = \frac{1}{3}$ and is independent of α and time. Hence the anisotropy r can be computed as

$$r(t) = \frac{2}{5}(\cos^2 \alpha - \frac{1}{2} \sin^2 \alpha)^2 \exp\left(\frac{-6D_{tr}t}{R^2}\right) + \frac{6}{5} \sin^2 \alpha \cos^2 \alpha \exp\left(\frac{-5D_{tr}t}{R^2}\right) + \frac{3}{10} \sin^4 \alpha \exp\left(\frac{-2D_{tr}t}{R^2}\right) \quad (6.29)$$

The constant $J = 0$ term cancels against the $-\frac{1}{2}$ in the expression for $r(t)$ (equation 6.25).

This is the expression tested in the previous section against the results obtained from the Monte Carlo simulations of the translational diffusion of oriented dipoles on the surface of a sphere. At zero time, $r(t)$ takes the value 0.4 independent of α (equation 6.29), as expected. The slower decays occur only if α is nonzero. Although the translational diffusion is happening with the same diffusion coefficient, the depolarization of the fluorescence anisotropy is slower for the case of dipoles oriented away from the normal to the spherical surface because of the presence of non-zero $|K|$ modes of diffusion. For the case of the dipole normal to the sphere, only $K = 0$ contributes, and the equation for the time resolved fluorescence anisotropy is $\exp(-6D_{tr}t/R^2)$ which can also be obtained more simply from the eigenvalue $l(l+1)$ of the Laplacian on the sphere, for $l = 2$ (equations 6.19 and 6.21).

6.5.3 Experiment: Nile red in SDS micelles

Nilered solubilizes in SDS micelle and a very low concentration ratio of the dye (2.27 μM) to micelle (0.99 mM) is maintained so that the probability of finding more than one dye per micelle is <0.2% [105]. SDS micelles were prepared as described before (section 3.2) by stirring the surfactant in warm deionized water for about one hour. SDS micelle is known to be spherical formed by the aggregation of 60 surfactant molecules [28, 25]. The fluorescence decay of Nile red in SDS collected at the emission maximum is single exponential with the lifetime 2.53 ns. The fluorescence anisotropy decay is shown in figure 6.12. The fluorescence depolarization for the dye in micelle is caused by three depolarizing motions: (i) wobbling dynamics of the dye in the micelle [95, 96] (part I in equation 6.30), (ii) the translational motion of the dye on the spherical surface of the micelle (part II in equation 6.30) and (iii) the rotational diffusion of the spherical micelle (part III in equation 6.30) as shown in the figure 6.11. Hence the anisotropy consists of contribution from these three parts.

$$\begin{aligned}
 \frac{r(t)}{r(0)} &= \text{PartI} \times \text{PartII} \times \text{PartIII} \\
 &= [S^2 + (1 - S^2) \exp(-t/\tau_w)] \times \\
 &\quad \left[\left(\cos^2 \alpha - \frac{1}{2} \sin^2 \alpha \right)^2 \exp\left(\frac{-6D_{tr}t}{R^2}\right) + 3 \sin^2 \alpha \cos^2 \alpha \exp\left(\frac{-5D_{tr}t}{R^2}\right) + \right. \\
 &\quad \left. \frac{3}{4} \sin^4 \alpha \exp\left(\frac{-2D_{tr}t}{R^2}\right) \right] \times \exp\left(-\frac{t}{\tau_m}\right) \quad (6.30)
 \end{aligned}$$

Here S is the order parameter, τ_w is the wobbling diffusion time which is related to the wobbling diffusion constant D_w by the relation 6.4 (according to the wobbling-in-cone model [96]), D_{tr} is the translational diffusion constant, R is the hydrodynamic radius of the micelle ($r_H=21 \text{ \AA}$), α is the average orientation angle of the dipoles with the normal to the surface of the micelle and τ_m is the rotational time constant for the spherical micelle. Part II in the above equation is the same as obtained from Monte Carlo simulations (equation 6.18) except that it is made equal to one at $t=0$. τ_m is estimated from the molecular volume (hydrodynamic radius, $r_H = 21 \text{ \AA}$) and Stokes-Einstein equation ($\tau_m = \eta V/kT$) to be 8.3ns at 25°C.

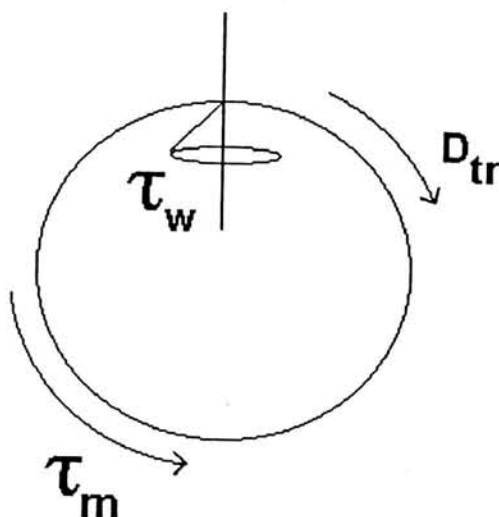


Figure 6.11: The three depolarizing motions for the fluorescent probes in micelles: (i) wobbling dynamics of the dye in the micelle, (ii) the translational motion of the dye on the spherical surface of the micelle and (iii) the rotational diffusion of the spherical micelle. τ_w , D_{tr} and τ_m are the physical parameters that can be associated with these three processes respectively. D_{tr} is the translational diffusion coefficient and τ_w and τ_m are the wobbling time constant of the dye in the micelle and the rotational correlation time of the micelle.

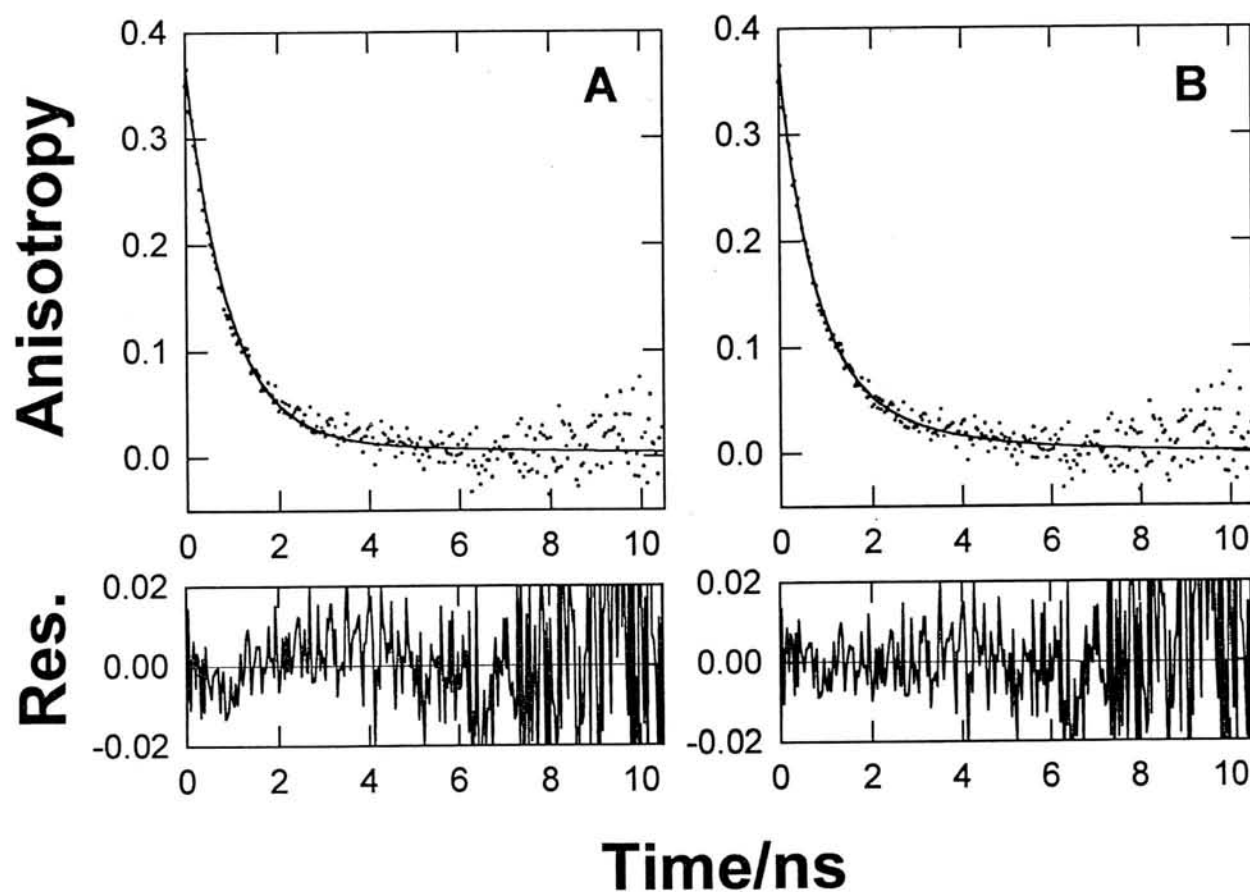


Figure 6.12: Fluorescence anisotropy decay of Nilered in SDS micelles. The concentrations used were $[\text{nilered}] = 2.27\mu\text{M}$ and $[\text{SDS}] = 68.34\text{mM}$ (or $[\text{micelle}] = 0.98\text{mM}$). The fluorescence anisotropy decay is collected at the emission wavelength 650nm with the excitation at 570nm at 25°C. A and B show the fittings without ($D_{tr}=0$) and with ($D_{tr} \neq 0$) the translational diffusion, respectively.

The experimental anisotropy decay shown in figure 6.12 was initially fitted by neglecting the translational diffusion; that is, $D_{tr} = 0$ in equation 6.30. The best fit for this equation was obtained for $S^2 = 0.04$ and $D_w = 1.65 \times 10^8 \text{ s}^{-1}$. Figure 6.12A shows the fit, and the residuals are shown in the bottom panel of figure 6.12A. Neglecting the translational diffusion leads to misfit of experimental data. In addition, the value of the order parameter ($S = 0.2$) is also low for the dye intercalated in the micelle.

In a separate experiment, the order parameter of Nile red in SDS was determined independently. Surfactants are known to form large worm like micelles (or rod-like micelles) at high concentrations or with the addition of electrolytes such as NaCl [25]. Because of the worm like structure, the mechanisms of D_{tr} and τ_m (in equation 6.30) are absent in depolarizing the initial anisotropy. Hence, the order parameter S can be measured in this case from the ratio of the fluorescence anisotropy at zero time (r_0) and at infinite time (r_∞). Worm-like micelles containing the dye are prepared by mixing the dye (1.73mM) with the concentrated solution of the surfactant (1.73M, dye to surfactant ratio of 1:1000) and then drying the solution on a glass plate until it becomes a film of thick paste. The anisotropy decay is collected from this film by placing the glass plate at an angle of 45° to the exciting laser beam. From the values of r_0 and r_∞ , the order parameter S is calculated as 0.47. Hence the order parameter S in the case of Nile red in SDS spherical micelles ought to be close to this value.

The experimental anisotropy decay data of Nile red in SDS spherical micelles was fitted to the equation 6.30 including the translational diffusion part. It was found that the optimized values for S , D_w , D_{tr} and α are dependent on the starting values in the minimization procedure. This indicates that these parameters are highly correlated. Hence the values of S and the initial anisotropy r_0 , whose values were obtained independently, are fixed at 0.47 and 0.37, respectively, in the fitting procedure. To see the correlation among the rest of the parameters, the angle α was fixed at different values and the other two parameters that fits the experimental data were obtained. The residuals for all these fits were equally good. The wobbling diffusion time τ_w remains constant at $1.07 \pm 0.05 \text{ ns}$ whereas the translational diffusion time defined as $\tau_t = R^2/D_{tr}$ shows a strong correla-

tion with α . This correlation between τ_t and α is shown in the figure 6.13. Because of this strong correlation between these two parameters, it was not possible to determine the accurate values of the orientation angle α and the translational diffusion parameters (τ_t or D_{tr}) from the experimental anisotropy decay data. This correlation is purely an experimental artifact. The other two depolarizing motions, wobbling-in-a-cone diffusion and the rotation of the entire micelle explain the observed fluorescence anisotropy decay to a large extent (as indicated by the residuals in the figure 6.12A) indicating that the contribution of translational diffusion to the fluorescence depolarization is less. However, these fits do confirm that the translational diffusion is necessary to obtain a good fit of the experimental data. The translational diffusion coefficient falls in the range of $3.14 \pm 1.23 \times 10^{-10} \text{ m}^2/\text{s}$. The wobbling diffusion coefficient is calculated as $1.76 \pm 0.08 \times 10^8 \text{ s}^{-1}$ using the values of S and τ_w using the relation 6.4. From the value of S , the cone semiangle θ_0 [95, 96] is calculated as 53.7° .

A possible orientation angle for Nile red in SDS can be assigned based on the polarity sensitive emission maximum of Nile red. As discussed in the previous chapters, the emission maximum of Nile red highly depends on the polarity of the surrounding environment and it varies from 524 nm in hexane to 665 nm in water [90]. The emission maximum of Nile red in SDS occurs at 640 nm indicating that the Nile red is located in a polar environment. Considering the radius of the SDS micelles as 19 Å [105] and the length of the Nile red molecule as 17 Å [88], the average orientation angle of Nile red can not be close to the normal to the spherical surface in which case the emission maximum should be close to that in nonpolar solvents. Nile red must be close to the surface and oriented nearly parallel to the surface of the micelle. A simple geometrical modelling indicates that the average orientation angle should be close to $25 \pm 7^\circ$ with respect to the surface. For this case, the translational diffusion coefficient D_{tr} is $4.2 \times 10^{-10} \text{ m}^2/\text{s}$ that best fits the experimental anisotropy data.

The values for the wobbling diffusion coefficient D_w , the translational diffusion coefficient D_{tr} and the order parameter S for Nile red in SDS micelle are reasonable. The reported values for these parameters for a few other dyes in other micelles are in the same

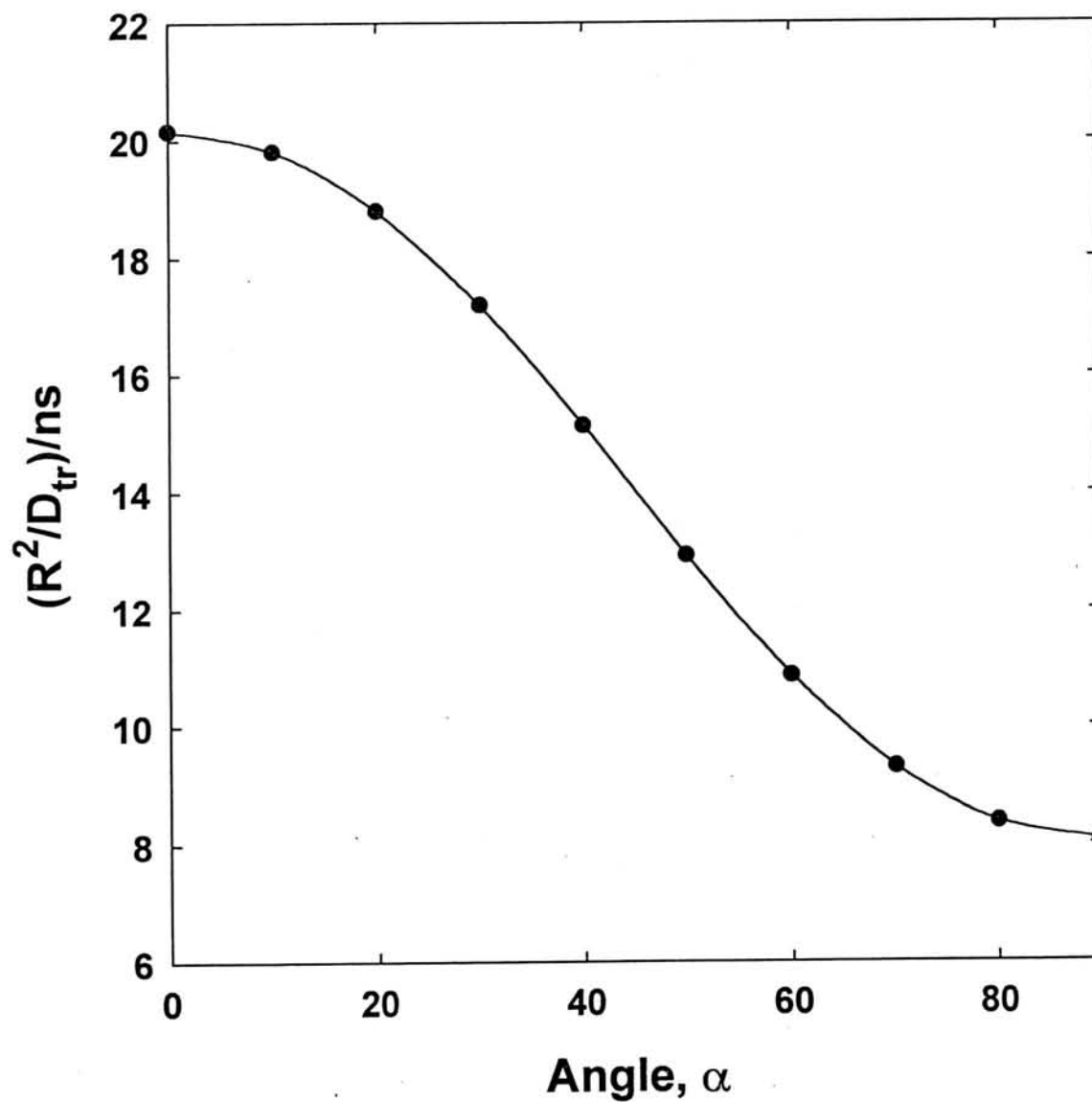


Figure 6.13: Variation of the translational diffusion time $\tau_t = R^2/D_{tr}$ with the orientation angle α obtained from the anisotropy decay data fitting in the case of Nile red in SDS micelles

range [254, 104, 259, 260, 105], even though the anisotropy data were analyzed by simpler equations than equation 6.30.

6.6 Rotational Diffusion: Simulations and Experiment

6.6.1 Results of the Monte Carlo Simulations

The fluorescence anisotropy decays obtained from the Monte Carlo simulations of the rotational diffusion of dipoles on the surface of a plane and on the surface of a sphere are as shown in figure 6.14. These two cases were illustrated in figure 6.4. As explained in section 6.4.2, anisotropy decay in the latter case is computed by spherical averaging because of distribution of dipoles with respect to the z-axis. From the figure, one can clearly see that the anisotropy decays to zero ($r_\infty=0$) in the case of diffusion on a plane whereas it decays to a non-zero value ($r_\infty \neq 0$) in the case where the dipoles are undergoing rotational diffusion on the surface of a sphere.

Both the fluorescence anisotropy decays are single exponential. The fluorescence anisotropy decays to one-fourth of its initial value in the case of rotational diffusion on the surface of a sphere. These results can be summarized as follows. The anisotropy decay due to rotational diffusion of the molecular dipoles on the surface is

$$\frac{r(t)}{r(0)} = c \exp(-4D_{rot}t) + (1 - c) \quad (6.31)$$

where $c = 1$ for the case where the anisotropy decay was simulated with the dipoles situated in a plane (no spherical averaging) and $c = \frac{3}{4}$ for the case where the dipoles are distributed over the entire sphere and the anisotropy function is calculated with spherical averaging (i.e., averaging over all the dipoles).

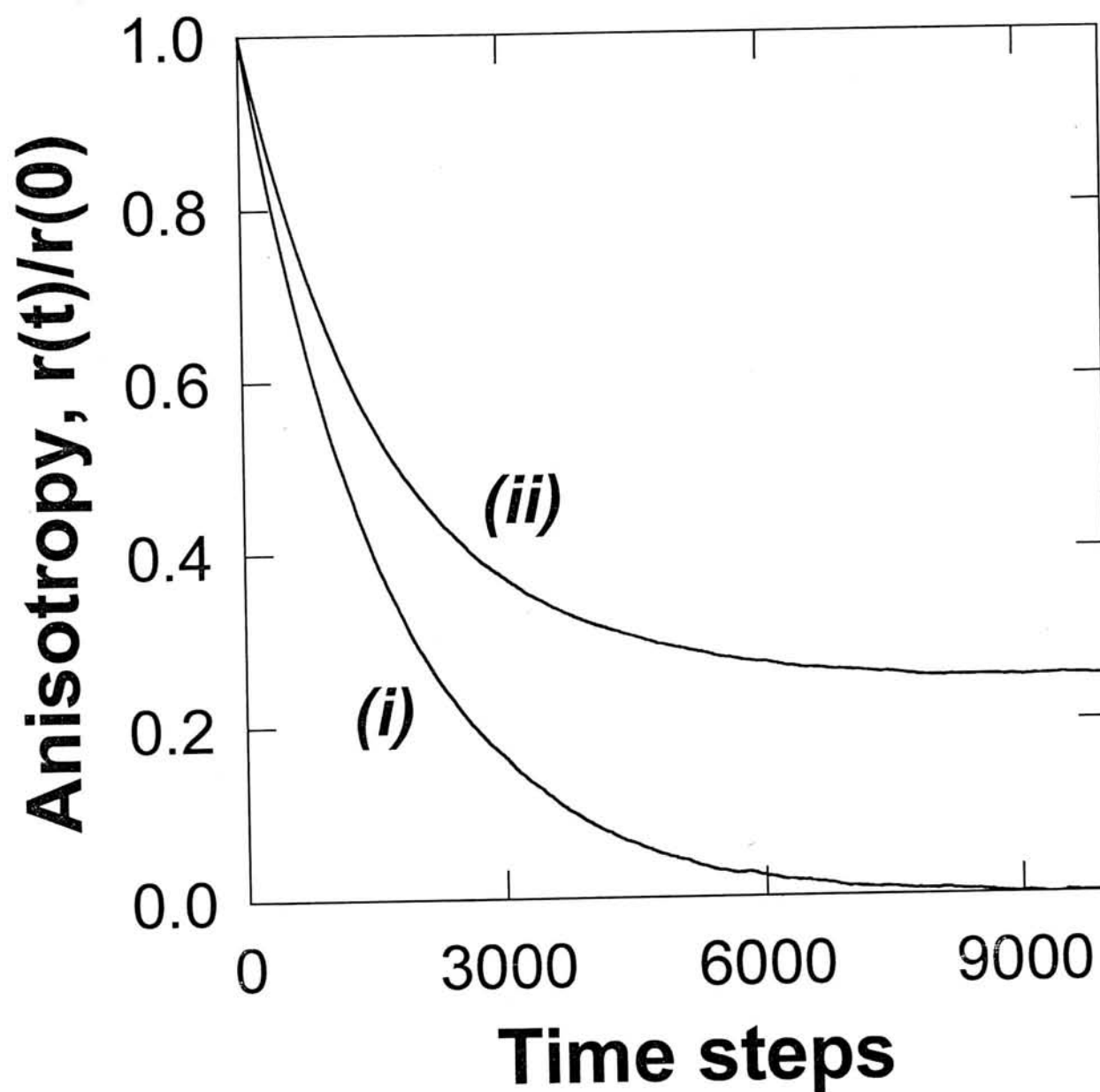


Figure 6.14: Fluorescence anisotropy decays obtained from the Monte Carlo simulations of the rotational diffusion of dipoles (i) on the surface of a plane and (ii) on the surface of a sphere.

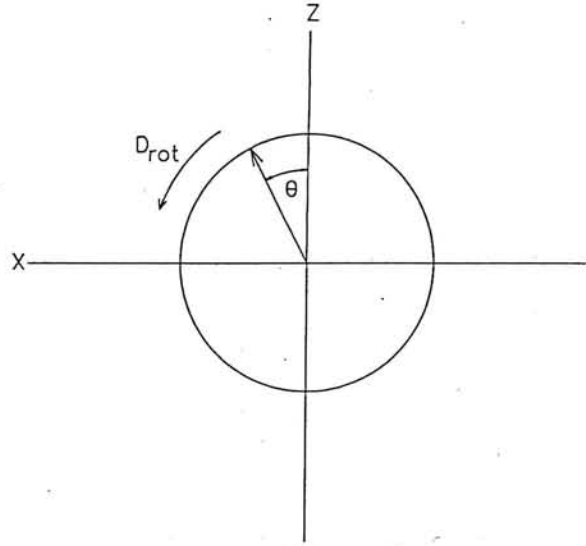


Figure 6.15: The figure shows the angular coordinate θ made by the rotating dipole with the z-axis which is the polarization axis of the exciting beam.

6.6.2 Theoretical justification of the simulation results

Let θ represent the angle made by the rotating dipole with the axis of polarization of the exciting light (z-axis) as shown in figure 6.15. This angular coordinate is enough to define the position of a rotating dipole at any time t during the rotation. The diffusion equation in this case [272] becomes

$$\frac{\partial}{\partial t} P(\theta, t) = D_{rot} \nabla^2 P(\theta, t) \quad (6.32)$$

where $P(\theta, t)$ is the probability of finding the dipole at the angle θ at time t , ∇^2 is the laplacian in θ . Hence equation 6.32 becomes

$$\frac{\partial^2}{\partial \theta^2} P(\theta, t) = -\frac{\lambda}{D_{rot}} P(\theta, t) \quad (6.33)$$

The general solution which satisfy the above differential equation is

$$P(\theta, t) = \sum_l A_l \exp(\pm i l \theta) \exp(-l^2 D_{rot} t) \quad (6.34)$$

where A_l are the scaling factors. In this case where the dipoles are located on a plane, the fluorescence anisotropy becomes

$$r(t) = \langle \cos 2\theta \rangle_t \quad (6.35)$$

Using the solution (equation 6.34), the equation for the fluorescence anisotropy is obtained as

$$r(t) = k \exp(-4D_{rot}t) \quad (6.36)$$

where k is a constant. That is, the anisotropy decay due to the rotational diffusion of the dipoles on a plane is single exponential with the correlation time $(4D_{rot})^{-1}$. This is the exact result which was also obtained by the Monte Carlo simulations.

The reason for the different values of c (equation 6.31) in the two cases where the dipoles are distributed over a planar membrane and on a sphere, can be understood as follows. In the case of a planar membrane, the initially excited anisotropic population of dipoles undergoes random rotational diffusion in the plane resulting in equal intensities along the two axes on the plane. This makes the anisotropy at infinite time, r_∞ , which is $(1-c)$ in the above equation as zero. But in the case of a sphere, the initially excited population of dipoles centered about the z -axis upon random rotational diffusion and no translational diffusion, results in the intensities along the three axes in the ratio $I_z:I_x:I_y$ as 2:1:1 at infinite time. This makes the r_∞ equal to $\frac{1}{4}$ and hence c becomes $\frac{3}{4}$.

6.6.3 Rotational Dynamics of DiIC₁₈(5) in Egg PC

DiIC₁₈(5) is a linear chromophore attached with two octadecyl chains. This dye is insoluble in water and it is easily solubilised in bilayer vesicle membranes of EggPC. By virtue of the structure, the chromophore lies on the surface of the membrane [276]. The fluorescence decay is biexponential with lifetimes (amplitudes) 1.29ns (0.36) and 0.39ns (0.64). The lifetime values are unchanged upon four-fold dilution. Both the lifetimes are therefore associated with the monomer of the dye and the anisotropy function $r(t)$ associated with the two lifetimes is the same. The translational diffusion coefficient of the lipid in the membrane is typically of the order of $10^{-12} \text{ m}^2 \text{ s}^{-1}$, which is also the value for most molecules of comparable molecular weight [277]. The diffusion length in two dimensions ($\langle r^2 \rangle^{1/2} = 2(D_{tr}\tau_f)^{1/2}$) of the dye during the lifetime of the excited state is 0.7 Å which is far less than the diameter of the sonicated vesicle ($\approx 300 \text{ Å}$) or giant liposome ($\approx 10 \text{ μm}$). The contribution due to the translational diffusion on the curved surface of the membrane for the fluorescence depolarization may therefore be neglected. The fluorescence depolarization is essentially determined by the wobbling/rotational dynamics of

the dye on the plane of the membrane.

The fluorescence anisotropy decay of DiIC₁₈(5) solubilized on a single giant liposome was obtained by fluorescence microscopy. For the preparation of giant liposomes, the dye DiIC₁₈(5) was mixed with the Egg PC lipid (in the ratio 1:118) in chloroform:methanol mixture and was dried to form a thin layer. The thin layer was hydrated to get the giant liposomes of typical size 10 μ m [144]. The anisotropy decay of DiIC₁₈(5) in a single giant liposome is shown in figure 6.16. Theory and Monte Carlo simulation predicts that the anisotropy decay for this case should be single exponential:

$$\frac{r(t)}{r(0)} = \exp(-4D_{rot}t) \quad (6.37)$$

where D_{rot} is the rotational diffusion constant on the surface of the membrane. Experimentally measured fluorescence anisotropy decay is consistent with this. The experimental data is fitted to equation 6.37 and the value of D_{rot} is obtained as $D_{rot} = 1.56 \times 10^8 \text{ s}^{-1}$.

The fluorescence anisotropy decay of DiIC₁₈(5) solubilized in sonicated vesicles was obtained for the sample in a cuvette. Typical size of these vesicles are about 300 Å [142]. In this case, the fluorescence anisotropy is the average measured over several vesicles (figure 6.4). Figure 6.17 shows the anisotropy decay. Unlike the single liposome experiment, the anisotropy does not decay to zero. This is the expected result. As described earlier, the anisotropy decay obtained by Monte Carlo simulation for this case should be single exponential with a constant term.

$$\frac{r(t)}{r(0)} = \frac{3}{4} \exp(-4D_{rot}t) + \frac{1}{4} \quad (6.38)$$

The rotational dynamics of the molecule on the surface is expected to be identical for the giant liposome and sonicated vesicles and hence D_{rot} to be nearly same. The best fit of the anisotropy decay to equation 6.38 shows that the data is poorly fitted. The misfit is due to a fast depolarization component. The experimental data were then fitted to equation 6.39, as shown in figure 6.17, containing a fast relaxation term in addition to the rotational diffusion term ($\tau_r = 1/4D_{rot}$) term:

$$\frac{r(t)}{r(0)} = p + q \exp(-4D_{rot}t) + r \exp\left(-\frac{t}{\tau_{fast}}\right) \quad (6.39)$$

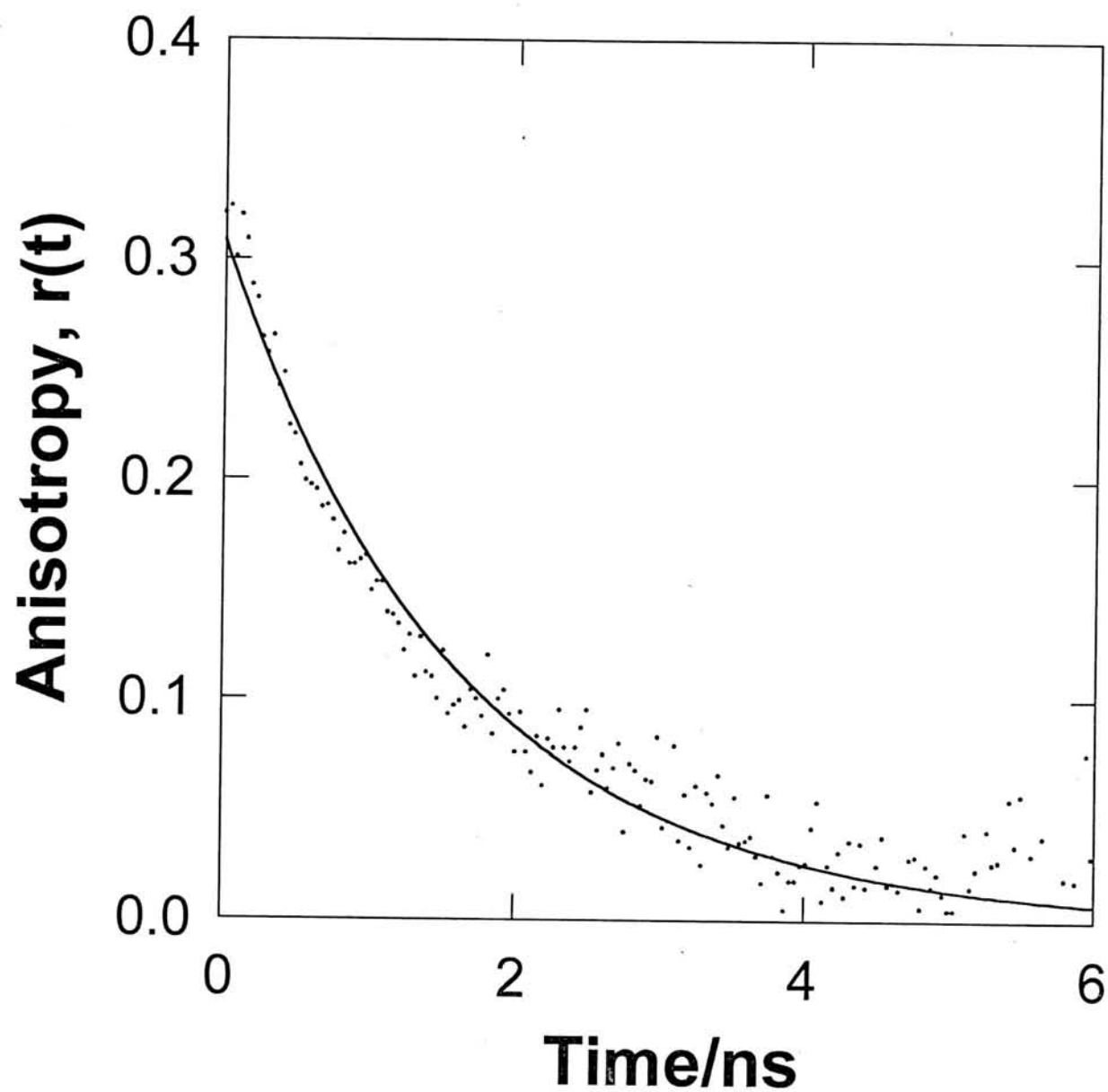


Figure 6.16: Fluorescence anisotropy decay of DiIC₁₈(5) in a single giant liposome. The concentration ratio was [DiIC₁₈(5)]:[lipid] = 1:118. The decay was collected at the excitation wavelength 600nm and the emission over 645nm at 25°C.

The best fit parameters are $p = 0.17$, $q = 0.08$, $r = 0.75$, $D_{rot} = 1.56 \times 10^8 \text{ s}^{-1}$, $\tau_{fast} = 0.18\text{ns}$. Considering the molecular length ($\approx 16 \text{ \AA}$) as the radius of the circle on which the dipole is rotating, the D_{tr} was calculated as $4.01 \times 10^{-10} \text{ m}^2/\text{s}$.

The fast relaxation time of $\tau_{fast} = 0.18\text{ns}$ is not due to scattered light from the vesicles. The scattering intensity ($\lambda_{ex} = 600 \text{ nm}$) was negligible at the emission wavelength $\lambda_{em} = 670 \text{ nm}$ because of the 645 nm cut-off filter used. Considering the structure of the dye and its anchoring on the surface of the membrane, the molecule has the freedom to wobble in a cylinder of volume $\pi R^2 l$ (l is the length of the dye molecule which is the length of the cylinder and R is the radius of the cylinder (mean displacement of the dye)) about the surface of the membrane, apart from the rotational diffusion (D_{rot}) on the surface. The wobbling-in-cylinder dynamics is the surface equivalent to the wobbling-in-cone model [95, 96] for a linear dye molecule which is intercalated inside the membrane. The fast relaxation is therefore attributed to the wobbling-in-cylinder dynamics of DiIC₁₈(5). Figure 6.18 illustrates the proposed model of wobbling-in-a-cylinder dynamics for the surface dynamics of DiIC₁₈(5).

The fluorescence anisotropy experiments were also carried out on DiIC₁₈(5) in Egg PC sonicated liposomes prepared in buffers of different pH to characterize this fast relaxation component. The values of τ_{fast} (equation 6.39) obtained from the best fits to the experimental data were 0.31ns, 0.18ns and 0.36ns at the pH values 4.0, 7.0 and 9.0 respectively. Variation of the pH is known to affect the packing of lipid molecules and consequently the dynamics [245, 246]. This effect will be larger in the head group region which contains polar groups compared to the hydrophobic tail region. The strong dependence of the fast rotational correlation time with the pH supports the argument that the process causing this fast depolarization is the one associated with the surface of the membrane. This fast anisotropy component was also observed in the case of other lipids such as DMPC (C14:0, 1,2-Dimyristoyl Phosphatidyl Choline) and DPPC (C16:0, 1,2-Dipalmitoyl Phosphatidyl Choline) and is of the same order ($0.18 \pm 0.05\text{ns}$). In the case of Egg PC vesicles prepared in sucrose solutions, this fast correlation time increases from 0.18ns to 0.27ns with the increase of sucrose concentration from 0%w/w to 44.4%w/w, supporting the argument that

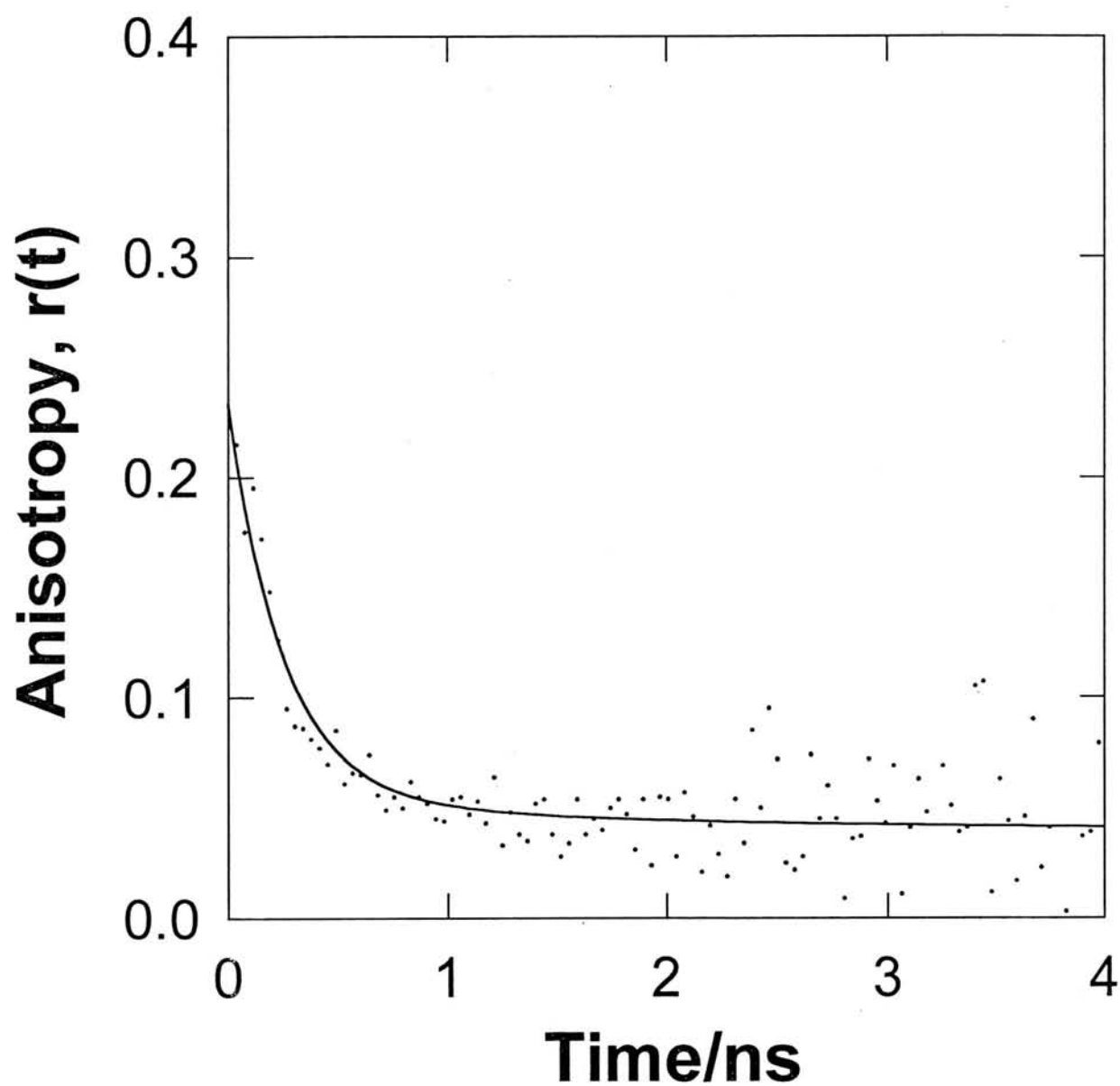


Figure 6.17: Fluorescence anisotropy decay of DiIC₁₈(5) in sonicated vesicles. The concentrations used were [DiIC₁₈(5)] = 0.80 μ M and [lipid] = 0.14 mM. The decay was collected at the emission wavelength 670nm with the excitation wavelength of 600nm at 25°C.

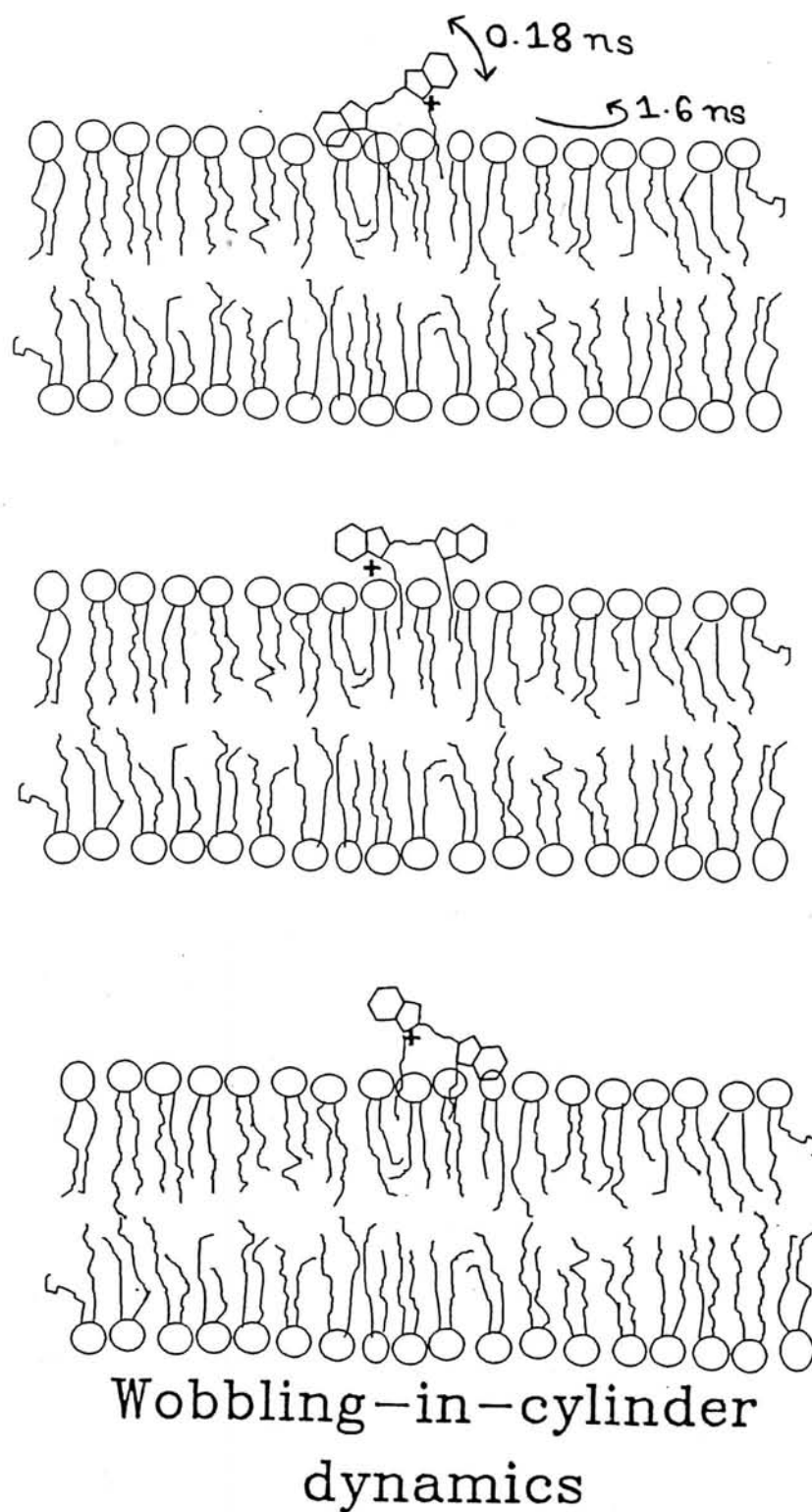


Figure 6.18: Proposed Wobbling-in-a-cylinder model for the surface dynamics of DiIC₁₈(5)

the process associated with this fast relaxation is the one that can be associated with the surface of the membrane. The slow correlation time due to the rotational diffusion on the surface also increases from 1.60ns to 2.78ns with the increase of sucrose concentration in the aqueous medium.

Therefore, in the case of the surface probe DiIC₁₈(5) in Egg PC vesicles, two depolarizing motions contribute to the fluorescence anisotropy decay: rotational diffusion on the membrane surface (1.60ns) and wobbling-in-a-cylinder dynamics about the membrane surface (0.18ns).

It may be noted that the fast relaxation was not observed in the depolarization dynamics of DiIC₁₈(5) in single giant liposomes. This is understood as follows. In single giant liposomes, the fluorescence depolarization is measured in two dimensions (on the surface of the membrane). In this case, rotational motion on the surface depolarizes the fluorescence whereas the wobbling-in-cylinder dynamics does not depolarize the fluorescence.

Chapter 7

Summary

7.1 Summary

The dynamics of fluorescent probes in biological systems has been addressed in this thesis using mainly the methodologies based on fluorescence spectroscopy. Main attention was focussed on one particular biological system, namely, lipid bilayer membranes, and to some extent, on surfactant micelles and proteins. In the course of this work, new methods were developed and the underlying assumptions in the usage of existing methods were examined. Effects of viscosity and refractive index on the fluorescence lifetimes of probes in biological systems were studied. These were used in the determination of the location and orientation of fluorescent probes in bilayer membranes. This thesis makes use of the refractive index effect on the fluorescence lifetimes of fluorophores, which has been generally ignored in the past. Monte Carlo simulations were used to address one important aspect of the dynamics of fluorescent probes in biological systems, namely, the surface diffusion. The relevant equations were applied in explaining the fluorescence depolarization kinetics. The main summary of this thesis is as follows.

A new method of Spectrally Constrained Global Analysis (SCGA) of multiple fluorescence decays was developed for the accurate estimate of fluorescence lifetimes and spectra of fluorescent dye molecules in lipid bilayer membranes. This method takes advantage

of the known spectrum and lifetime of one of the components. Using this method, the fluorescence lifetimes and spectra of the membrane-bound fluorescent probe DODCI were estimated with the prior knowledge of the lifetime and spectra of the dye present in the aqueous phase.

It was identified that the fluorescence decay of Nile red in lipid vesicles, surfactant micelles and viscous organic solvents is biexponential with a negative fraction for the short lifetime indicating subnanosecond excited state kinetics. Species Associated Spectra of the two species were determined using the fluorescence decay kinetics derived for an irreversible and a reversible kinetics in the excited state. The observed excited state kinetics was attributed to that of the viscous media. This observation points out that the multiple lifetimes of a fluorophore in a biological system may not be always from the fluorophore located at different sites or in multiple environments.

Association of fluorescence lifetimes with tryptophans in a multi-tryptophan protein was done by making use of the crosspeak patterns in the 2D NMR measurements. The two lifetimes in the HSPI protein were found to be associated with the two sterically constrained tryptophans.

Effects of aqueous viscosity and refractive index on the tryptophan fluorescence were examined in the case of two proteins Barstar and HSPI. Increase of viscosity increases the fluorescence lifetime whereas the increase of refractive index decreases the lifetime. Solvent exposed tryptophans show a predominant viscosity effect whereas the tryptophan that is buried inside a protein matrix does not show viscosity effect.

The sites of solubilization (or location) of thirteen organic dyes in a bilayer membrane (Egg PC) were identified to be surface, interface or core region based on the combined effects of viscosity and refractive index on the fluorescence lifetimes. The fluorescence lifetime of the fluorophores whose location is near the surface of the membrane, increases with the increase of the aqueous viscosity whereas the fluorophores that stay in the core of the bilayer exhibit fluorescence lifetimes that decrease with the increase of the external refractive index. The fluorophores located in the interface region show a mixed behaviour.

Dicarbocyanines such as DODCI, and DPH are the only fluorescent probes that exhibit

the effect of refractive index on the fluorescence lifetimes, i.e., the fluorescence lifetime decreases with the increase of the refractive index. These are identified to be oriented in the core of the bilayer.

The second rank order parameters determined from fluorescence lifetime and anisotropy differed significantly in the case of DODCI in bilayer membranes, similar to the case of DPH. This discrepancy was explained by a bimodal orientational distribution with one population centered about the membrane normal and the other parallel to the membrane surface, where the molecules in the two populations interconvert very slowly compared to the intra-population molecular dynamics. A unimodal distribution was not adequate to explain the discrepancy.

DODCI exists in two different locations in the membrane, on the surface and in the core, and in two different orientations inside the core of the bilayer. The effect of lipid chain parameters such as chain length, unsaturation and temperature on the location and orientation of DODCI were examined. The ratio of the surface to core population of DODCI in bilayer membranes increases with the increase of the chain length or with the decrease of the unsaturation of the lipid hydrocarbon chains. In the core of the bilayer, the dye molecules oriented perpendicular to the membrane surface increases with the increase of chain length or with the decrease of unsaturation of lipid chains. Phase transition from gel to liquid crystalline bilayer increases the core population relative to the surface population whereas in the core, it increases the relative population of the probes oriented parallel to the membrane normal compared to those oriented parallel to the membrane surface.

Monte Carlo methods were used in simulating the surface diffusion of dipoles on the surface of a sphere. A computer program was developed for this purpose. This program was used in estimating the fluorescence depolarization of fluorescent probes due to translational and rotational diffusion.

The fluorescence anisotropy decay due to translational diffusion of oriented dipoles on the surface of a sphere is found to be multi exponential. The obtained fluorescence decays were fitted to the theoretical equation derived for this case. The decay is three

exponential with the correlation times $R^2/6D_{tr}$, $R^2/5D_{tr}$ and $R^2/2D_{tr}$ where R is the radius of the sphere and D_{tr} is the translational diffusion coefficient. The amplitudes of these correlation times depend on the angle made by the dipoles with the surface normal. These equations were used in explaining the fluorescence anisotropy decay of Nile red in SDS micelles.

The fluorescence anisotropy decay due to the rotational diffusion of surface dipoles on the surface of a sphere decays exponentially to a residual anisotropy that is one fourth of the initial value. The rotational correlation time is $1/4D_{rot}$ where D_{rot} is the rotational diffusion coefficient. This is the same rotational correlation time that is obtained in the case of rotational diffusion of dipoles on a planar surface where the anisotropy decays to zero. These equations were applied in explaining the fluorescence anisotropy decays of DiIC₁₈(5) in sonicated and giant liposomes.

A fast depolarization was observed in the case of DiIC₁₈(5) in lipid vesicles that is attributed to the wobbling-in-cylinder dynamics of the dye around the surface of the membrane.

7.2 Future Directions

The location and orientation of fluorescent probes in bilayer membranes determined here can be further extended to see how these parameters vary with the incorporation of membrane-soluble agents such as cholesterol, and in the case of mixed bilayers, i.e., the bilayers made up of more than one lipid. Although a simplistic model of bimodal orientational distribution of linear probes in the core of the bilayer explains the measured properties, it will be good to take account of the slight tilt associated with the lipid chains in the bilayer that occurs under some conditions [1]. Moreover, the functional forms used for the two populations in the bimodal orientational distribution are approximated as either Gaussian type or based on Maier-Saupe potentials. A search for an experimental method is required that can directly give the exact orientational distribution of probes which does not require any approximations. The same methodologies applied here can be

applied in the case of other systems, such as planar supported membranes, lipid monolayers, surfactant-lipid bicelles, to identify the location, orientation and dynamics of small molecules.

The usefulness of any experiment depends on the accuracy of the parameters that tell about the system under study. Data analysis methods such as global analysis methods need to be developed for this purpose in the investigation of complex systems, especially biological ones. Methods similar to SCGA that use the known properties of the complex system to extract the unknown properties can be generalized for other experimental systems also.

Effect of refractive index on the fluorescence properties of fluorophores in biological and microheterogeneous systems has not been paid much attention before. These effects can be very severe for the probes oriented in a particular orientation at the interfaces where the refractive index difference between the two phases is high. These effects have to be studied in detail in different systems where the difference in the refractive index is controlled. Because of the finite length of the molecular dipoles, the probe may experience a variation of refractive index through its length when it is located in the interface where a gradual variation of refractive index is expected. Theoretical formalisms and experimental protocols are challenging problems to understand these effects, which are undoubtedly relevant in the context of usage of fluorescent probes in biological applications.

Dynamics of fluorescent probes in biological systems or microheterogeneous systems is more complex. The same principles which apply to the dynamics in homogeneous solvents are not true in these systems. Validity of Stokes-Einstein relation in microheterogeneous systems has to be verified. Monte Carlo methods provide a tool to simulate the dynamics of small molecules in restricted environments. The next step in the Monte Carlo simulation described in this thesis is to combine both surface diffusion and the dynamics of the probe inside the macroparticle (like wobbling-in-a-cone dynamics) where the angle made by the molecular dipole with the normal to the surface changes continuously. The effect of this motion on the fluorescence depolarization, and the validity of the assumptions involved in separating the translational and rotational motions as a product of independent mo-

tions can be examined. The same Monte Carlo simulations developed in this study can also be used in visualizing dynamics in more complex restricted environments such as in geometrical models for a living cell.

The assignment of multiple lifetimes to individual tryptophans in a multi-tryptophan protein is still an unsolved problem. This problem lies at the heart of the protein fluorescence, without resolving it, it impairs the use of tryptophan fluorescence for the study of the structural dynamics of proteins. New methods have to be developed for this purpose.

Appendix A

C program developed for Monte Carlo simulations of the translational diffusion of surface probes on the surface of a sphere

This appendix gives the source code (DIF.C) for the program developed to simulate the translational diffusion of the dipoles on the surface of a sphere by Monte Carlo techniques. The program used to simulate the rotational diffusion of dipoles on the spherical surface is similar to the program described here. The details of the procedures followed are described in section 6.4.

```

/*
DIF.C
Monte Carlo simulation of the translational diffusion of oriented
dipoles on the surface of a sphere
Written in Microsoft Quick C V 2.5
Requires the subroutines nrutil.c, qsimp.c and trapzd.c and
the random number generator ran2.c from "Numerical Recipes in C", Second
Edition [156]
Inputs: Diffusion Coefficient, sphere radius, number of iterations,
angle between the dipole and the normal to the sphere
Output will be printed in the file DIFOUT
M. M. G. Krishna
1996-99
*/

#include <stdio.h>
#include <string.h>
#include <stdlib.h>
#include <math.h>
#include <malloc.h>
#include <errno.h>
#include <time.h>
#include <graph.h>

#define PI 3.14159265
#define RDP 1.      /* dipole vector length */
#define NDP 85000 /* Number of dipoles */
#define DT 1.      /* in picoseconds */ /* Sampling time interval */
#define EPSILON 0.001 /* convergence factor */
#define square(x) (x*x)

float ran2(long *idum);
float func(float x);
float func1(float x);
float qsimp(float (*func)(float), float a, float b);

void plotini(float x);
void plotdata(float x, float y);
void plotdata1(float rad, float x, float y, float z);
void plotdata2(float x, float y, float x1, float y1);
void finish();

static float dt, rm;

main()
{
    int i, j, ni, m, l, a;
    int maxiter;
    float d, delt, rp, norm, test, k, itot, temp, dev, test1, test2;
    float t, corr, corrx, corry, corrz;
    float posc[NDP][3], poscv[NDP][3];
    /* Here posc represents normal vector (to the sphere surface)
       coordinates and poscv represents dipole vector coordinates */
    float angle;
    /* angle between the dipole and the normal to the sphere surface */
    float x[3], x1[3], n[3], n1[3], rotate[3][3], theta, phi;
    long seed1, seed2;
    float thet[1001], ifun[1001];
    FILE *fopen(),
        *file_pointer;

    seed1 = (unsigned)time( NULL );
    seed1 *= (-1);
    printf("Enter values for diff.coefft (cm2/sec), \nsphere radius (Angs), "

```

```

        " \n& max.no. of iterations:\n");
scanf("%f %f %d",&d,&rm,&maxiter);
printf("Enter the angle between the dipole and the normal to the sphere"
        " surface: (should be between 0 and 90 degrees)\n");
scanf("%f",&angle);
file_pointer = fopen("difout","a");
fprintf(file_pointer,"\n*****\n");
fprintf(file_pointer,"Diff. coeff. = %f (cm2/sec)\nsphere radius = %f "
        "(Angstroms.)\n",d,rm);
fprintf(file_pointer,"Here the angle between the dipole and the normal "
        "to the sphere surface is %f (degrees).\n",angle);
fprintf(file_pointer,"The sampling interval is %f (ps.)\n",DT);
fprintf(file_pointer,"Here corr[ni] represents correlation function "
        "at time t[ni].\n");
fprintf(file_pointer,"\n1st col.: ni , 2nd col.: t , 3rd col.: corr, "
        "4th col.: corrx, 5th col.: corry, 6th col.: corrz \n");
angle *= (PI/180.); /* in radians */
d = d*1.e4; /* now d in Ang^2/ps */
delt = DT;
rp = 2.*(double) sqrt((double) (d*delt));
/* rp, possible radius spanned in DT in Angs */
printf("\nrp=%fA, Max. iterations =%d Okay?",rp,maxiter);
getchar();

/* generating the deviates satisfying the probability distribution
for diffusion*/
dt = d*delt;
itot = qsimp((float *) (float)) (func),0.,5.*rp/rm);
thet[0] = 0.;
ifun[0] = 0.;
for(i=1;i<1001;i++)
{
    thet[i] = i*0.005*rp/rm;
    ifun[i] = qsimp((float *) (float)) (func),0.,thet[i])/itot;
}

t=0.;
corr=0.;
corrx=0.;
corry=0.;
corrz=0.;
plotini(rm);

/* initial distribution of the dipoles */
for(i=0;i<NDP;i++)
{
repeat1:
    theta = acos(1-2*ran2(&seed1));
    phi = ran2(&seed1)*2.*PI;
    x[0] = rm*sin(theta)*cos(phi);
    x[1] = rm*sin(theta)*sin(phi);
    x[2] = rm*cos(theta);
    /* sin dependence*/

    /* finding a vector perpendicular to the radial vector */
    m=0;
    for(j=0;j<=2;j++)
        if(x[j]==0.) m++;
    if(m==0)
    {
        n1[0]=-x[1];
        n1[1]=x[0];
        n1[2]=0.;
    }
}

```

```

if (m==1 || m==2)
{
    for (j=0;j<=2;j++)
    {
        if (x[j]==0) n1[j]=1;
        else n1[j]=0;
    }
}
norm=sqrt(n1[0]*n1[0]+n1[1]*n1[1]+n1[2]*n1[2]);
n1[0]=n1[0]/norm;
n1[1]=n1[1]/norm;
n1[2]=n1[2]/norm;

phi=ran2(&seed1)*2.*PI;

/* finding the rotation matrix */
for(j=0;j<=2;j++)
    rotate[j][j]=cos(phi)+(1-cos(phi))*x[j]*x[j]/(rm*rm);
rotate[0][1]=(1-cos(phi))*x[0]*x[1]/(rm*rm)-sin(phi)*x[2]/rm;
rotate[0][2]=(1-cos(phi))*x[0]*x[2]/(rm*rm)+sin(phi)*x[1]/rm;
rotate[1][0]=(1-cos(phi))*x[1]*x[0]/(rm*rm)+sin(phi)*x[2]/rm;
rotate[1][2]=(1-cos(phi))*x[1]*x[2]/(rm*rm)-sin(phi)*x[0]/rm;
rotate[2][0]=(1-cos(phi))*x[2]*x[0]/(rm*rm)-sin(phi)*x[1]/rm;
rotate[2][1]=(1-cos(phi))*x[2]*x[1]/(rm*rm)+sin(phi)*x[0]/rm;

/*rotating the specific normal vector to an angle phi to get a
random normal vector */

n[0]=rotate[0][0]*n1[0]+rotate[0][1]*n1[1]+rotate[0][2]*n1[2];
n[1]=rotate[1][0]*n1[0]+rotate[1][1]*n1[1]+rotate[1][2]*n1[2];
n[2]=rotate[2][0]*n1[0]+rotate[2][1]*n1[1]+rotate[2][2]*n1[2];
norm = sqrt(n[0]*n[0]+n[1]*n[1]+n[2]*n[2]);
if(fabs(norm-1.) > .001)
{
    printf("Norm %f is not 1! I am Quitting.\n",norm);
    getch();
    exit();
}

test = n[0]*x[0]+n[1]*x[1]+n[2]*x[2];
if (fabs(test) > .001)
{
    printf("test %f is not 0! I am Quitting.\n",test);
    getch();
    exit();
}

/* finding the rotation matrix */
for(j=0;j<=2;j++)
    rotate[j][j] = cos(angle) + (1-cos(angle))*n[j]*n[j];
rotate[0][1] = (1-cos(angle))*n[0]*n[1] - sin(angle)*n[2];
rotate[0][2] = (1-cos(angle))*n[0]*n[2] + sin(angle)*n[1];
rotate[1][0] = (1-cos(angle))*n[1]*n[0] + sin(angle)*n[2];
rotate[1][2] = (1-cos(angle))*n[1]*n[2] - sin(angle)*n[0];
rotate[2][0] = (1-cos(angle))*n[2]*n[0] - sin(angle)*n[1];
rotate[2][1] = (1-cos(angle))*n[2]*n[1] + sin(angle)*n[0];

/* rotating the radial vector to get the dipole vector oriented at
an angle "angle"*/
x1[0] = (rotate[0][0]*x[0] + rotate[0][1]*x[1] +
        rotate[0][2]*x[2])/rm;
x1[1] = (rotate[1][0]*x[0] + rotate[1][1]*x[1] +
        rotate[1][2]*x[2])/rm;

```



```

x1[2] = (rotate[2][0]*x[0] + rotate[2][1]*x[1] +
        rotate[2][2]*x[2])/rm;

/* checking cos square dependence */
test = acos(x1[2]);
test1 = test - 0.05*PI/180.;
test2 = test + 0.05*PI/180.;
if (test1 < 0.) test1 = 0.;
if (test2 > PI) test2 = PI;
temp = ran2(&seed1);
if (temp < func1(test1) || temp > func1(test2)) goto repeat1;
posc[i][0] = x[0];
posc[i][1] = x[1];
posc[i][2] = x[2];

poscv[i][0] = x1[0];
poscv[i][1] = x1[1];
poscv[i][2] = x1[2];

plotdata2(posc[i][0],posc[i][2],poscv[i][0],poscv[i][2]);
corr += square(poscv[i][2]) -
      (square(poscv[i][1])+square(poscv[i][0]))/2;
corrx += square(poscv[i][0]);
corry += square(poscv[i][1]);
corrz += square(poscv[i][2]);
}
corr /= (RDP*RDP*NDP);
corrx /= (RDP*RDP*NDP);
corry /= (RDP*RDP*NDP);
corrz /= (RDP*RDP*NDP);
printf("\nni=%d t[ni]=%f corr[ni]=%f",0,t,corr);
fprintf(file_pointer,"\n%5d %10.4f %7.4f %7.4f %7.4f",0,
        t,corr,corrx,corry,corrz);

finish();

seed2 = (unsigned)time( NULL );
seed2 *= (-1);
for(ni=1;(corrz>EPSILON) && (ni<=maxiter);ni++)
/* starting iterations from 1 to maxiter */
{
    t = (float)ni*DT;
    corr = 0;
    corrx = 0;
    corry = 0;
    corrz = 0;
    plotini(rm);
    for(i=0;i<NDP;i++)/* starting iteration for NDP dipoles */
    {
        x[0] = posc[i][0];
        x[1] = posc[i][1];
        x[2] = posc[i][2];

        x1[0] = poscv[i][0];
        x1[1] = poscv[i][1];
        x1[2] = poscv[i][2];

/* finding a vector perpendicular to the radial vector */
        m=0;
        for(j=0;j<=2;j++)
            if(x[j]==0.) m++;
        if(m==0)
        {
            n1[0]=-x[1];

```

```

        n1[1]=x[0];
        n1[2]=0.;
    }
    if (m==1 || m==2)
    {
        for (j=0;j<=2;j++)
        {
            if (x[j]==0) n1[j]=1;
            else n1[j]=0;
        }
    }
    norm=sqrt(n1[0]*n1[0]+n1[1]*n1[1]+n1[2]*n1[2]);
    n1[0]=n1[0]/norm;
    n1[1]=n1[1]/norm;
    n1[2]=n1[2]/norm;

    phi=ran2(&seed1)*2.*PI;

/* finding the rotation matrix */
    for(j=0;j<=2;j++)
        rotate[j][j]=cos(phi)+(1-cos(phi))*x[j]*x[j]/(rm*rm);
    rotate[0][1]=(1-cos(phi))*x[0]*x[1]/(rm*rm)-sin(phi)*x[2]/rm;
    rotate[0][2]=(1-cos(phi))*x[0]*x[2]/(rm*rm)+sin(phi)*x[1]/rm;
    rotate[1][0]=(1-cos(phi))*x[1]*x[0]/(rm*rm)+sin(phi)*x[2]/rm;
    rotate[1][2]=(1-cos(phi))*x[1]*x[2]/(rm*rm)-sin(phi)*x[0]/rm;
    rotate[2][0]=(1-cos(phi))*x[2]*x[0]/(rm*rm)-sin(phi)*x[1]/rm;
    rotate[2][1]=(1-cos(phi))*x[2]*x[1]/(rm*rm)+sin(phi)*x[0]/rm;

/*rotating the specific normal vector to an angle phi to get a
random normal vector */

    n[0]=rotate[0][0]*n1[0]+rotate[0][1]*n1[1]+rotate[0][2]*n1[2];
    n[1]=rotate[1][0]*n1[0]+rotate[1][1]*n1[1]+rotate[1][2]*n1[2];
    n[2]=rotate[2][0]*n1[0]+rotate[2][1]*n1[1]+rotate[2][2]*n1[2];

    norm = sqrt(n[0]*n[0]+n[1]*n[1]+n[2]*n[2]);
    if(fabs(norm-1.) > .001)
    {
        printf("Norm %f is not 1! I am Quitting.\n",norm);
        getch();
        exit();
    }

    test = n[0]*x[0]+n[1]*x[1]+n[2]*x[2];
    if (fabs(test) > .001)
    {
        printf("test %f is not 0! I am Quitting.\n",test);
        getch();
        exit();
    }

/* selecting a random deviate for diffusion
from the calculated values */
    temp = ran2(&seed2);
    dev = 0.;
    for(l=1;l<1001;l++)
    {
        if(temp >= ifun[l-1] && temp < ifun[l])
        {
            if(fabs(temp-ifun[l-1])<fabs(temp-ifun[l]))
                dev = thet[l-1];
            else dev = thet[l];
        }
        if (dev != 0.) break;
    }

```

```

    }
    theta = dev;

    /* finding the rotation matrix */
    for(j=0;j<=2;j++)
        rotate[j][j] = cos(theta) + (1-cos(theta))*n[j]*n[j];
    rotate[0][1] = (1-cos(theta))*n[0]*n[1] - sin(theta)*n[2];
    rotate[0][2] = (1-cos(theta))*n[0]*n[2] + sin(theta)*n[1];
    rotate[1][0] = (1-cos(theta))*n[1]*n[0] + sin(theta)*n[2];
    rotate[1][2] = (1-cos(theta))*n[1]*n[2] - sin(theta)*n[0];
    rotate[2][0] = (1-cos(theta))*n[2]*n[0] - sin(theta)*n[1];
    rotate[2][1] = (1-cos(theta))*n[2]*n[1] + sin(theta)*n[0];

    /* rotating the radial and dipole vectors */
    posc[i][0] = rotate[0][0]*x[0] + rotate[0][1]*x[1] +
        rotate[0][2]*x[2];
    posc[i][1] = rotate[1][0]*x[0] + rotate[1][1]*x[1] +
        rotate[1][2]*x[2];
    posc[i][2] = rotate[2][0]*x[0] + rotate[2][1]*x[1] +
        rotate[2][2]*x[2];

    poscv[i][0] = rotate[0][0]*x1[0] + rotate[0][1]*x1[1] +
        rotate[0][2]*x1[2];
    poscv[i][1] = rotate[1][0]*x1[0] + rotate[1][1]*x1[1] +
        rotate[1][2]*x1[2];
    poscv[i][2] = rotate[2][0]*x1[0] + rotate[2][1]*x1[1] +
        rotate[2][2]*x1[2];

    plotdata2(posc[i][0],posc[i][2],poscv[i][0],poscv[i][2]);
    corr += square(poscv[i][2]) -
        (square(poscv[i][1]) + square(poscv[i][0]))/2;
    corrx += square(poscv[i][0]);
    corry += square(poscv[i][1]);
    corrz += square(poscv[i][2]);
}
corr /= (RDP*RDP*NDP);
corrx /= (RDP*RDP*NDP);
corry /= (RDP*RDP*NDP);
corrz /= (RDP*RDP*NDP);
printf("\nni=%d t[ni]=%f corr[ni]=%f",ni,t,corr);
fprintf(file_pointer,"\n%5d %10.4f %7.4f %7.4f %7.4f %7.4f",ni,
        t,corr,corrx,corry,corrz);
if (ni==maxiter) getch();
finish();
}
fprintf(file_pointer,"\n*****\n");
fclose(file_pointer);
printf("\n\nThe results are appended in the file DIFOUT.\n");
}

float func(float x)
{
    return (rm*rm*sin(x)*exp(-rm*rm*x*x/(4*dt))/(2*dt));
}

float func1(float x)
{
    return((x+0.5*sin(2*x))/PI);
    /* integral of cos square from 0 to x, normalised */
}

void plotini(float x)
{

```

```

float xmin, xmax, ymin, ymax;
xmin = -x;
xmax = x;
ymin = -x;
ymax = x;
_setvideomode(_VRES16COLOR);
_setviewport(120, 40, 520, 440);
_setwindow(1, xmin, ymin, xmax, ymax);
_setcolor(0);
_rectangle_w(_GBORDER, xmin, ymin, xmax, ymax);
_setcolor(4);
_ellipse_w(_GBORDER, xmin, ymin, xmax, ymax);
_setcolor(7);
}

void plotdata(float x, float y)
{
    _setcolor(7);
    _setpixel_w((double)x, (double)y);
    _setcolor(2);
    _setpixel_w(0., 0.);
    _setcolor(7);
}

void plotdata1(float rad, float x, float y, float z)
{
    float norm;
    norm = sqrt(x*x+y*y+z*z);
    x *= rad/norm;
    y *= rad/norm;
    z *= rad/norm;
    norm = sqrt(x*x+y*y+z*z);
    _setcolor(8);
    _setpixel_w((double)x, (double)z);
    _moveto_w((double)x, (double)z);
    _lineto_w(0., 0.);
    _setcolor(7);
}

void plotdata2(float x, float y, float x1, float y1)
{
    _setcolor(7);
    _setpixel_w((double)x, (double)y);
    _moveto_w((double)x, (double)y);
    _lineto_w((double)(x-x1), (double)(y-y1));
}

void finish()
{
    _setvideomode(_DEFAULTMODE);
}

```

Bibliography

- [1] Jain, M. K.; Wagner, R. C. *Introduction to Biological Membranes* John Wiley and Sons, 1980.
- [2] Jain, M. K. *The Bimolecular Lipid Membrane: A System* Van Nostrand Reinhold Company, New York, 1972.
- [3] Singer, S. J.; Nicolson, G. L. *Science* **1972**, *175*, 723.
- [4] Alberts, B.; Bray, D.; Lewis, J.; Raff, M.; Roberts, K.; Watson, J. D. *Molecular Biology of the Cell* third edn Garland Publishing Inc., New York, 1994.
- [5] Cantor, C. R.; Schimmel, P. R. *Biophysical Chemistry* W. H. Freeman and Company, New York, 1980.
- [6] Stryer, L. *Biochemistry* fourth edn W. H. Freeman and Company, New York, 1995.
- [7] Ladbrooke, B. D.; Chapman, D. *Chem. Phys. Lipids* **1969**, *3*, 304.
- [8] Szoka Jr., F.; Papahadjopoulos, D. *Ann. Rev. Biophys. Bioeng.* **1980**, *9*, 467.
- [9] Woodle, M. C.; Papahadjopoulos, D. *Meth. Enzymol.* **1989**, *171*, 193.
- [10] Nayar, R.; Hope, M. J.; Cullis, P. R. *Biochim. Biophys. Acta* **1989**, *986*, 200.
- [11] Tanford, C. *The Hydrophobic Effect: Formation of Micelles and Biological Membranes* second edn John Wiley and Sons, 1980.

- [12] Benz, R.; Frohlih, O.; Lauger, P.; Montal, M. *Biochim. Biophys. Acta* **1975**, *394*, 323.
- [13] Griffith, O. H.; Dehlinger, P. J.; Van, S. P. *J. Membrane Biol.* **1974**, *15*, 159.
- [14] Jain, M. K.; Wu, N. M. *J. Membrane Biol.* **1977**, *34*, 157.
- [15] Trauble, H. J. *Membrane Biol.* **1971**, *4*, 193.
- [16] Jain, M. K.; White, H. B. *Adv. Lipid Res.* **1977**, *15*, 1.
- [17] Lee, A. G. *Biochim. Biophys. Acta* **1977**, *422*, 237.
- [18] Lewis, B. A.; Engelman, D. M. *J. Mol. Biol.* **1983**, *166*, 211.
- [19] In *Liposomes: From Physical Structure to Therapeutic Applications*, (ed. Knight, C. G.). Elsevier 1981.
- [20] Compassi, S.; Werder, M.; Boffelli, D.; Weber, F. E.; Hauser, H.; Schulthess, G. *Biochemistry* **1995**, *34*, 16473.
- [21] Staggers, J. E.; Hernell, O.; Stafford, R. J.; Carey, M. C. *Biochemistry* **1990**, *29*, 2028.
- [22] Shiau, Y. F. *Am. J. Physiol.* **1981**, *240*, G1.
- [23] Lindstrom, M. B.; Sternby, B.; Borgstrom, B. *Biochim. Biophys. Acta* **1988**, *959*, 178.
- [24] Lehninger, A. L.; Nelson, D. L.; Cox, M. M. *Principles of Biochemistry* CBS Publishers and Distributors, India, 1993.
- [25] Kalyanasundaram, K. *Photochemistry in Microheterogeneous systems* Academic Press, New York, 1991.
- [26] Mittal, K. L. *Solution Chemistry of Surfactants* Plenum Press, New York, 1979.

- [27] Client, J. H. *Surfactant Aggregation* Chapman Hall, New York, 1991.
- [28] Langevin, D. *Annu. Rev. Phys. Chem.* **1992**, *43*, 341.
- [29] Israelachvili, J. N.; Mitchell, D. J.; Ninham, B. W. *J. Chem. Soc. Faraday Trans. II* **1976**, *72*, 1525.
- [30] Menger, F. M. *Acc. Chem. Res.* **1979**, *12*, 111.
- [31] Menger, F. M.; Jerkunica, J. M. *J. Am. Chem. Soc.* **1978**, *100*, 688.
- [32] Hayashi, S.; Ikeda, S. *J. Phys. Chem.* **1980**, *84*, 744.
- [33] Berr, S. S.; Jones, R. R. M. *Langmuir* **1988**, *4*, 1247.
- [34] Zubay, G. L. *Biochemistry* fourth edn Wm. C. Brown Publishers, Dubuque, IA, 1998.
- [35] Creighton, T. E. *Proteins: Structure and Molecular Properties* second edn W. H. Freeman Co., New York, 1993.
- [36] Lubieniski, M. J.; Bycroft, M.; Freund, S. M. V.; Fersht, A. R. *Biochemistry* **1994**, *33*, 8866.
- [37] Lakey, J. H.; Baty, D.; Pattus, F. *J. Mol. Biol.* **1991**, *218*, 639.
- [38] Lala, A. K.; Raja, S. M. *J. Biol. Chem.* **1995**, *270*, 11348.
- [39] Ghosh, A. K.; Rukmini, R.; Chattopadhyay, A. *Biochemistry* **1997**, *36*, 14291.
- [40] Keith, A. D.; Sharnoff, M.; Cohn, G. E. *Biochim. Biophys. Acta* **1973**, *300*, 379.
- [41] Gaffney, B. J.; Chen, S. C. Spin-label studies of membranes In *Methods in Membrane Biology*, Vol. 8, (ed. Korn, E. D.). Plenum Press, New York 1977.
- [42] Waggoner, A. S. *Annu. Rev. Biophys. Bioeng.* **1979**, *8*, 47.
- [43] Loew, L. M.; Simpson, L. L. *Biophys. J.* **1981**, *34*, 353.

- [44] Das, T. K.; Periasamy, N.; Krishnamoorthy, G. *Biophys. J.* **1993**, *64*, 1122.
- [45] Visser, N. V.; Van Hoek, A.; Visser, A. J. W. G.; Frank, J.; Apell, H. J.; Clarke, R. J. *Biochemistry* **1995**, *34*, 11777.
- [46] Lakowicz, J. R. *Principles of Fluorescence Spectroscopy* Plenum Press, New York, 1983.
- [47] In *Topics in Fluorescence Spectroscopy, Vol. 1-3*, (ed. Lakowicz, J. R.). Plenum Press, New York 1991-92.
- [48] Haugland, R. P. *Handbook of Fluorescent Probes and Research Chemicals* sixth edn Molecular Probes Inc., 1996.
- [49] Andersen, H. C. *Annu. Rev. Biochem.* **1978**, *47*, 359.
- [50] Zannoni, C.; Aricioni, A.; Cavatorta, P. *Chem. Phys. Lipids* **1983**, *32*, 179.
- [51] Lentz, B. R. *Chem. Phys. Lipids* **1989**, *50*, 171.
- [52] Stubbs, C. D.; Williams, B. W. Fluorescence in membranes In *Topics in Fluorescence Spectroscopy, Vol. 3*, (ed. Lakowicz, J. R.) Vol. 3. Plenum Press, New York 1992 ch. 5.
- [53] Lentz, B. R. *Chem. Phys. Lipids* **1993**, *64*, 99.
- [54] Tóptygin, D.; Brand, L. *J. Fluorescence* **1995**, *5*, 39.
- [55] Lee, A. G.; Birdsall, N. J. M.; Metcalfe, J. C. Nuclear magnetic relaxation and the biological membrane In *Methods in Membrane Biology, Vol. 2*, (ed. Korn, E. D.). Plenum Press, New York 1974 1.
- [56] Bocian, D. F.; Chan, S. I. *Annu. Rev. Phys. Chem.* **1978**, *29*, 307.
- [57] Davis, J. H. *Biochim. Biophys. Acta* **1983**, *737*, 117.
- [58] Brown, M. F.; Williams, G. D. *J. Biochem. Biophys. Methods* **1985**, *11*, 71.

- [59] Fenske, D. B. *Chem. Phys. Lipids* **1993**, *64*, 143.
- [60] Auger, M. *Biophys. Chem.* **1997**, *68*, 233.
- [61] Shipley, G. G. Recent x-ray diffraction studies of biological membranes and membrane components In *Biological Membranes*, (eds Chapman, D.; Wallach, D. F. H.). Academic Press, London 1973 1.
- [62] Makowski, L.; Li, J. X-ray diffraction and electron microscopic studies of the molecular structure of biological membranes In *Biomembrane Structure and Function*, (ed. Chapman, D.). Verlag Chemie GmbH, Weinheim 1984 43.
- [63] Caffrey, M.; Wang, J. *Annu. Rev. Biophys. Biomol. Struct.* **1995**, *24*, 351.
- [64] Freed, J. H. *Annu. Rev. Biophys. Biomol. Struct.* **1994**, *23*, 1.
- [65] Bach, D. Calorimetric studies of model and natural biomembranes In *Biomembrane Structure and Function*, (ed. Chapman, D.). Verlag Chemie GmbH, Weinheim 1984 1.
- [66] Schoenborn, B. P. *Biochim. Biophys. Acta* **1976**, *457*, 41.
- [67] Amey, R. L.; Chapman, D. Infrared spectroscopic studies of model and natural membranes In *Biomembrane Structure and Function*, (ed. Chapman, D.). Verlag Chemie GmbH, Weinheim 1984 199.
- [68] Verma, S. P.; Wallach, D. F. H. Raman spectroscopy of lipids and biomembranes In *Biomembrane Structure and Function*, (ed. Chapman, D.). Verlag Chemie GmbH, Weinheim 1984 167.
- [69] Hansma, H. G.; Hoh, J. H. *Annu. Rev. Biophys. Biomol. Struct.* **1994**, *23*, 115.
- [70] Shao, Z.; Yang, J.; Somlyo, A. P. *Annu. Rev. Cell Dev. Biol.* **1995**, *11*, 241.
- [71] Saxton, M. J.; Jacobson, K. *Annu. Rev. Biophys. Biomol. Struct.* **1997**, *26*, 373.

- [72] Martin, J. L.; Vos, M. H. *Annu. Rev. Biophys. Biomol. Struct.* **1992**, *21*, 199.
- [73] Martin, J. L.; Vos, M. H. *Methods Enzymol.* **1994**, *232*, 416.
- [74] Fleming, G. R.; Van Grondelle, R. *Curr. Opin. Struct. Biol.* **1997**, *7*, 738.
- [75] Nie, S.; Zare, R. N. *Annu. Rev. Biophys. Biomol. Struct.* **1997**, *26*, 567.
- [76] Rigler, R. *J. Biotechnol.* **1995**, *41*, 177.
- [77] Schwille, P.; Bieschke, J.; Oehlenschlaeger, F. *Biophys. Chem.* **1997**, *66*, 211.
- [78] Meixner, A. J.; Knepe, H. *Cell Mol. Biol.* **1998**, *44*, 673.
- [79] Squier, T. C.; Bigelow, D. J.; de Ancos, J. G.; Inesi, G. *J. Biol. Chem.* **1987**, *262*, 4748.
- [80] Bishop, J. E.; Squier, T. C.; Bigelow, D. J.; Inesi, G. *Biochemistry* **1988**, *27*, 5233.
- [81] Gryczynski, I.; Wicz, W.; Inesi, G.; Squier, T.; Lakowicz, J. R. *Biochemistry* **1989**, *28*, 3490.
- [82] Brinkley, M. *Bioconjugate Chem.* **1992**, *3*, 2.
- [83] Means, G. E.; Feeney, R. E. *Chemical Modification of Proteins* Holden-Day Inc., San Francisco, 1971.
- [84] Rai, S. S.; Kasturi, S. R. *Biophys. Chem.* **1994**, *48*, 359.
- [85] Neville, D. C.; Rozanas, C. R.; Tulk, B. M.; Townsend, R. R.; Verkman, A. S. *Biochemistry* **1998**, *37*, 2401.
- [86] Birks, J. B. *Photophysics of Aromatic Molecules* Wiley - Interscience, 1970.
- [87] Rohatgi-Mukherjee, K. K. *Fundamentals of Photochemistry* Wiley Eastern Limited, New Delhi, 1986.

- [88] Dutt, G. B.; Doraiswamy, S.; Periasamy, N.; Venkataraman, B. *J. Chem. Phys.* **1990**, *93*, 8498.
- [89] Dutt, G. B.; Doraiswamy, S.; Periasamy, N. *J. Chem. Phys.* **1991**, *94*, 5360.
- [90] Sackett, D. L.; Wolff, J. *Anal. Biochemistry* **1987**, *167*, 228.
- [91] Datta, A.; Mandal, D.; Pal, S. K.; Bhattacharyya, K. *J. Phys. Chem. B* **1997**, *101*, 10221.
- [92] Steiner, R. F. Fluorescence anisotropy: Theory and applications In *Topics in Fluorescence Spectroscopy, Vol. 2*, (ed. Lakowicz, J. R.). Plenum Press, New York 1991 1.
- [93] Belford, G. G.; Belford, R. L.; Weber, G. *Proc. Nat. Acad. Sci. USA* **1972**, *69*, 1392.
- [94] Fleming, G. R. *Chemical Applications of Ultrafast Spectroscopy* Oxford University Press, New York, 1986.
- [95] Kinosita, K. J.; Kawato, S.; Ikegami, A. *Biophys. J.* **1977**, *20*, 289.
- [96] Lipari, G.; Szabo, A. *Biophys. J.* **1980**, *30*, 489.
- [97] Szabo, A. *J. Chem. Phys.* **1984**, *81*, 150.
- [98] Van der Meer, W.; Pottel, H.; Herrman, W.; Ameloot, M.; Hendrickx, H.; Schroder, H. *Biophys. J.* **1984**, *46*, 515.
- [99] Straume, M.; Litman, B. *Biochemistry* **1987**, *26*, 5113.
- [100] Van der Sijis, D. A.; Van Faasen, E. E.; Levine, Y. K. *Chem. Phys. Lett.* **1993**, *216*, 559.
- [101] Van der Heide, U. A.; Van Ginkel, G.; Levine, Y. K. *Chem. Phys. Lett.* **1996**, *253*, 118.

- [102] Heyn, M. P. *FEBS Lett.* **1979**, *108*, 359.
- [103] Jahnig, F. *Proc. Natl. Acad. Sci. USA* **1979**, *76*, 6361.
- [104] Quitevis, E. L.; Marcus, A. H.; Fayer, M. D. *J. Phys. Chem.* **1993**, *97*, 5762.
- [105] Maiti, N. C.; Krishna, M. M. G.; Britto, P. J.; Periasamy, N. *J. Phys. Chem. B* **1997**, *101*, 11051.
- [106] Maroncelli, M.; Fleming, G. R. *J. Chem. Phys.* **1987**, *86*, 6221.
- [107] Rocker, C.; Heilemann, A.; Fromherz, P. *J. Phys. Chem.* **1996**, *100*, 12172.
- [108] Siano, D. B.; Metzler, D. E. *J. Chem. Phys.* **1969**, *51*, 1856.
- [109] Demchenko, A. P. Fluorescence and dynamics in proteins In *Topics in Fluorescence Spectroscopy, Vol. 3*, (ed. Lakowicz, J. R.). Plenum Press, New York 1992 65.
- [110] Brand, L.; Gohlike, J. R. *J. Biol. Chem.* **1971**, *246*, 2317.
- [111] Gafni, A.; DeToma, R. P.; Manrow, R. E.; Brand, L. *Biophys. J.* **1977**, *17*, 155.
- [112] Okamura, T.; Sumitani, M.; Yoshihara, K. *Chem. Phys. Lett.* **1983**, *94*, 339.
- [113] Donzel, B.; Gauduchon, P.; Wahl, P. *J. Am. Chem. Soc.* **1974**, *96*, 801.
- [114] Knutson, J. R.; Baker, S. H.; Cappuccino, A. G.; Walbridge, D. G.; Brand, L. *Photochem. Photobiol.* **1983**, *37*, s21.
- [115] Mantulin, W. W.; Beechem, J. M. *J. Cell Biol.* **1988**, *107*, 842a.
- [116] Knutson, J. R.; Davenport, L.; Brand, L. *Biochemistry* **1986**, *25*, 1805.
- [117] Davenport, L.; Knutson, J. R.; Brand, L. *Biochemistry* **1986**, *25*, 1811.
- [118] Eftink, M. R. Fluorescence quenching: Theory and applications In *Topics in Fluorescence Spectroscopy*, (ed. Lakowicz, J. R.). Plenum Press, New York 1991 53–126.

- [119] Periasamy, N.; Doraiswamy, S.; Maiya, G. B.; Venkataraman, B. *J. Chem. Phys.* **1988**, *88*, 1638.
- [120] Periasamy, N.; Doraiswamy, S.; Venkataraman, B.; Fleming, G. R. *J. Chem. Phys.* **1988**, *89*, 4799.
- [121] Periasamy, N.; Joshi, G. C.; Das, R. *Chem. Phys. Lett.* **1989**, *160*, 457.
- [122] Das, R.; Periasamy, N. *Chem. Phys.* **1989**, *136*, 361.
- [123] Joshi, G. C.; Bhatnagar, R.; Doraiswamy, S.; Periasamy, N. *J. Phys. Chem.* **1990**, *94*, 2908.
- [124] Eftink, M. R.; Ghiron, C. A. *Biochemistry* **1976**, *15*, 672.
- [125] Eftink, M. R.; Ghiron, C. A. *Anal. Biochem.* **1981**, *114*, 199.
- [126] Calhoun, D. B.; Vanderkooi, J. M.; Woodrow, G. V.; Englander, S. W. *Biochemistry* **1983**, *22*, 1526.
- [127] Chattopadhyay, A.; London, E. *Biochemistry* **1987**, *26*, 39.
- [128] Moore, H. P. H.; Raftery, M. A. *Proc. Natl. Acad. Sci. U. S. A.* **1980**, *77*, 4509.
- [129] Vanderkooi, J. M.; Calhoun, C. D.; Englander, S. W. *Science* **1987**, *236*, 568.
- [130] Farinas, J.; Van Hoek, A. N.; Shi, L. B.; Erikson, C.; Verkman, A. S. *Biochemistry* **1993**, *32*, 11857.
- [131] Krishna, M. M. G.; Rastogi, V. K.; Periasamy, N.; Chary, K. V. R. *J. Phys. Chem. B* **1998**, *102*, 5520.
- [132] Stryer, L. *Annu. Rev. Biochem.* **1978**, *47*, 819.
- [133] Remedios, C. G.; Moens, P. D. J. *J. Struct. Biol.* **1995**, *115*, 175.
- [134] Cheung, H. C. Resonance energy transfer In *Topics in Fluorescence Spectroscopy*, Vol. 2, (ed. Lakowicz, J. R.). Plenum Press, New York 1991 128.

- [135] Wu, P.; Brand, L. *Anal. Biochem.* **1994**, *218*, 1.
- [136] Dale, R. E.; Eisinger, J.; Blumberg, W. E. *Biophys. J.* **1979**, *26*, 161.
- [137] Rice, K. G.; Wu, P.; Brand, L.; Lee, Y. C. *Biochemistry* **1991**, *30*, 6646.
- [138] Merino, C. G.; Centeno, F.; Martin, E. G.; Merino, J. M. *Biochem. Soc. Trans.* **1994**, *22*, 784.
- [139] Clegg, R. M. *Curr. Opin. Biotech.* **1995**, *6*, 103.
- [140] Eis, P. S.; Millar, D. P. *Biochemistry* **1993**, *32*, 13852.
- [141] Deamer, D.; Bangham, A. D. *Biochim. Biophys. Acta* **1976**, *443*, 629.
- [142] Krishnamoorthy, G. *Biochemistry* **1986**, *25*, 6666.
- [143] Klein, R. A. *Biochim. Biophys. Acta* **1970**, *210*, 486.
- [144] Riquelme, G.; Lopez, E.; Garcia-Segura, L. M.; Ferragut, J. A.; Gonzalez-Ros, J. M. *Biochemistry* **1990**, *29*, 11215.
- [145] Strickler, S. J.; Berg, R. A. *J. Chem. Phys.* **1962**, *37*, 814.
- [146] Doraiswamy, S.; Krishnamoorthy, G.; Periasamy, N.; Venkataraman, B. *Proc. Indian Nat. Sci. Acad.* **1988**, *54A*, 782.
- [147] Bankar, K. V.; Bhagat, V. R.; Das, R.; Doraiswamy, S.; Ghangrekar, A. S.; Kamat, D. S.; Periasamy, N.; Srivatsovoy, V. J. P.; Venkataraman, B. *Indian J. Pure Appl. Chem.* **1989**, *27*, 416.
- [148] O'Connor, D. V.; Philips, D. *Time Correlated Single Photon Counting* Academic Press, London, 1984.
- [149] Birch, D. J. S.; Imhof, R. E. In *Topics in Fluorescence Spectroscopy, Vol. 1*, (ed. Lakowicz, J. R.). Plenum Press, New York 1991 1.

- [150] Krishnamoorthy, G.; Srivastava, A. *Curr. Science* **1997**, 72, 835.
- [151] Srivastava, A.; Krishnamoorthy, G. *Anal. Biochem.* **1997**, 249, 140.
- [152] Srivastava, A.; Krishnamoorthy, G. *Arch. Biochem. Biophys.* **1997**, 340, 159.
- [153] Kumar, A.; Wagner, G.; Ernst, R. R.; Wuthrich, K. *Biochem. Biophys. Res. Commun.* **1980**, 96, 1156.
- [154] Marquardt, D. W. *Journal of the Society for Industrial and Applied Mathematics* **1963**, 11, 431.
- [155] Bevington, P. R.; Robinson, D. K. *Data Reduction and Error Analysis for the Physical Sciences* second edn McGraw-Hill Inc., New York, 1994.
- [156] Press, W. H.; Teukolsky, S. A.; Vetterling, W. T.; Flannery, B. P. *Numerical Recipes in C: The Art of Scientific Computing* second edn Cambridge University Press, 1992.
- [157] Grinvald, A.; Steinberg, I. Z. *Anal. Biochem.* **1974**, 59, 583.
- [158] Yguerabide, J.; Yguerabide, E. In *Optical Techniques in Biological Research*, (ed. Rouseou, D. L.). Academic Press Inc., Orlando, FLA 1984 206.
- [159] Periasamy, N. *Biophys. J.* **1988**, 54, 961.
- [160] Bajzer, Z.; Zelic, A.; Prendergast, F. G. *Biophys. J.* **1995**, 69, 1148.
- [161] Knutson, J. R.; Beechem, J. M.; Brand, L. *Chem. Phys. Lett.* **1983**, 102, 501.
- [162] Beechem, J. M.; Knutson, J. R.; Ross, J. B. A.; Turner, B. W.; Brand, L. *Biochemistry* **1983**, 22, 6054.
- [163] Gratton, E.; Limkeman, M.; Lakowicz, J. R.; Maliwal, B.; Cherek, H.; Laczko, G. *Biophys. J.* **1984**, 46, 479.
- [164] Beechem, J. M.; Brand, L. *Ann. Rev. Biochem.* **1985**, 54, 43.

- [165] Beechem, J. M.; Ameloot, M.; Brand, L. *Anal. Instrum.* **1985**, *14*, 379.
- [166] Beechem, J. M.; Knutson, J. R.; Brand, L. *Biochem. Soc. Trans.* **1986**, *14*, 832.
- [167] Beechem, J. M.; Gratton, E.; Ameloot, M.; Knutson, J. R.; Brand, L. The global analysis of fluorescence intensity and anisotropy decay data: Second-generation theory and programs In *Topics in Fluorescence Spectroscopy, Vol. 2*, (ed. Lakowicz, J. R.). Plenum Press, New York 1991 241.
- [168] Knutson, J. R.; Walbridge, D. G.; Brand, L. *Biochemistry* **1982**, *21*, 4671.
- [169] Lofroth, J. *J. Phys. Chem.* **1986**, *90*, 1160.
- [170] Walbridge, D. G.; Knutson, J. R.; Brand, L. *Anal. Biochem.* **1987**, *161*, 467.
- [171] Han, M. K.; Walbridge, D. G.; Knutson, J. R.; Brand, L.; Roseman, S. *Anal. Biochem.* **1987**, *161*, 479.
- [172] Beechem, J. M.; Haas, E. *Biophys. J.* **1989**, *55*, 1225.
- [173] Barkley, M. D.; Kowalczyk, A.; L., B. *J. Chem. Phys.* **1981**, *75*, 3581.
- [174] Brochon, J. *Methods in Enzymology* **1994**, *240*, 262.
- [175] Livesey, A. K.; Brochon, J. C. *Biophys. J.* **1987**, *52*, 693.
- [176] Skilling, J.; Bryan, R. K. *Mon. Not. R. Astron. Soc.* **1984**, *211*, 111.
- [177] Skilling, J. In *Maximum Entropy in Action*, (eds Buck, B.; Macaulay, V. A.). Oxford Univ. Press (Clarendon), Oxford 1991 19.
- [178] Swaminathan, R.; Periasamy, N. *Proc. Indian Acad. Sci.: Chem. Sci.* **1996**, *108*, 39.
- [179] Jaynes, E. T. In *Papers on Probability Statistics and Statistical Physics*, (ed. Rosenkrantz, R. D.). Reidel, Dordrecht 1983.

- [180] Romoino, P.; Margallo, E.; Nicolo, G. *J. Lipid Res.* **1996**, *37*, 1207.
- [181] Kinnunen, P. K.; Rytono, M.; Koiv, A.; Lehtonan, J.; Mustonan, P.; Aro, A. *Chem. Phys. Lipids* **1993**, *66*, 75.
- [182] Sarkar, N.; Datta, A.; Das, S.; Bhattacharyya, K. *J. Phys. Chem.* **1996**, *100*, 15483.
- [183] Ruvinov, S. B.; Yang, X. J.; Parris, K. D.; Banik, U.; Ahmed, S. A.; Miles, E. W.; Sackett, D. L. *J. Biol. Chem.* **1995**, *270*, 6357.
- [184] Sackett, D. L.; Knutson, J. R.; Wolff, J. *J. Biol. Chem.* **1990**, *265*, 14899.
- [185] Greenspan, P.; Mayer, E. P.; Fowler, S. D. *J. Cell Biol.* **1985**, *100*, 965.
- [186] Sarkar, N.; Das, K.; Nath, D. N.; Bhattacharyya, K. *Langmuir* **1994**, *10*, 326.
- [187] Choi, M.; Jin, D.; Kim, H.; Kang, T. J.; Jeoung, S. C.; Kim, D. *J. Phys. Chem. B* **1997**, *101*, 8092.
- [188] Dutta, A. K.; Kamada, K.; Ohta, K. *Chem. Phys. Lett.* **1996**, *258*, 369.
- [189] Ira; Krishnamoorthy, G. *Biochim. Biophys. Acta* **1998**, *1414*, 255.
- [190] Dutta, A. K.; Kamada, K.; Ohta, K. *J. Photochem. Photobiol. A: Chem* **1996**, *93*, 57.
- [191] Kreyszig, E. *Advanced Engineering Mathematics* seventh edn John Wiley, New York, 1993.
- [192] Drexhage, K. H. *Prog. in Optics* **1974**, *12*, 163.
- [193] Haroche, S.; Kleppner, D. *Physics Today* **1989**, *42(1)*, 24.
- [194] Walther, H. *Physics Reports* **1992**, *219*, 263.
- [195] Haroche, S.; Raimond, J. M. *Scientific American* **1993**, *268(4)*, 54.
- [196] Rempe, G. *Contemporary Physics* **1993**, *34*, 119.

- [197] Hulet, R. G.; Hilfer, E. S.; Kleppner, D. *Phys. Rev. Lett.* **1985**, *55*, 2137.
- [198] Jhe, W.; Anderson, A.; Hinds, E. A.; Meschede, D.; Moi, L.; Haroche, S. *Phys. Rev. Lett.* **1987**, *58*, 666.
- [199] Goy, P.; Raimond, J. M.; Gross, M.; Haroche, S. *Phys. Rev. Lett.* **1983**, *50*, 1903.
- [200] Toptygin, D.; Brand, L. *Biophys. Chem.* **1993**, *48*, 205.
- [201] Swaminathan, R.; Nath, U.; Udgaonkar, J. B.; Periasamy, N.; Krishnamoorthy, G. *Biochemistry* **1996**, *35*, 9150.
- [202] Rastogi, V. K.; Chary, K. V. R.; Govil, G. *Curr. Science* **1997**, *72*, 69.
- [203] Ross, J. B. A.; Schmidt, C. J.; Brand, L. *Biochemistry* **1981**, *20*, 4369.
- [204] Borkman, R. F.; Douhal, A.; K., Y. *Biochemistry* **1993**, *32*, 4787.
- [205] Tanaka, F.; Mataga, N. In *Dynamics and Mechanisms of Photoinduced Transfer and Related Phenomena*, (eds Mataga, N.; Okada, T.; Masuhara, H.). Elsevier Science, New York 1992 501.
- [206] Bismuto, E.; Gratton, E.; Sirangelo, I.; Irace, G. *Eur. J. Biochem.* **1993**, *218*, 213.
- [207] Kim, S. J.; Chowdhury, F. N.; Younathan, W. S. E. S.; Rosso, P. S.; Barkley, M. D. *Biophys. J.* **1993**, *65*, 215.
- [208] Swaminathan, R.; Krishnamoorthy, G.; Periasamy, N. *Biophys. J.* **1994**, *67*, 2013.
- [209] Waldman, A. D. B.; Clarke, A. R.; Wigley, D. B.; Hart, K. W.; Chia, W. N.; Barstow, D.; Atkinson, T.; Munro, I.; Holbrook, J. J. *Biochim. Biophys. Acta* **1987**, *913*, 66.
- [210] Shen, W. H. *Biochemistry* **1993**, *32*, 13925.
- [211] Willaert, K.; Loewenthal, R.; Sancho, J.; Froeyen, M.; Fersht, A.; Engelborghs, Y. *Biochemistry* **1992**, *31*, 711.

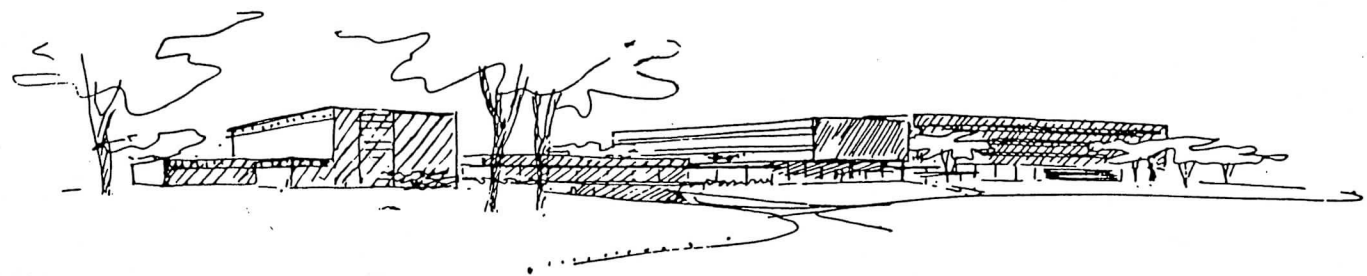
- [212] Chen, L. X. Q.; Longworth, J. W.; Fleming, G. R. *Biophys. J.* **1987**, *51*, 865.
- [213] Chen, R. F.; Knutson, J. R.; Ziffer, H.; Porter, D. *Biochemistry* **1991**, *30*, 5184.
- [214] Harris, D. L.; Hudson, B. S. *Biochemistry* **1990**, *29*, 5276.
- [215] Chabbert, M.; Hillen, W.; Hansen, D.; Takahashi, M.; Bousquet, J. A. *Biochemistry* **1992**, *31*, 1951.
- [216] Szabo, A. G.; Rayner, D. M. *J. Am. Chem. Soc.* **1980**, *102*, 554.
- [217] Ross, J. B. A.; Wyssbrod, H. R.; Porter, R. A.; Schwartz, G. P.; Michaels, C. A.; Laws, W. R. *Biochemistry* **1992**, *31*, 1585.
- [218] Colucci, W. J.; Tilstra, L.; Sattler, M. C.; Fronczek, F. R.; Barkley, M. D. *J. Am. Chem. Soc.* **1990**, *112*, 9182.
- [219] McMahon, L. P.; Colucci, W. J.; McLaughlin, M. L.; Barkley, M. D. *J. Am. Chem. Soc.* **1992**, *114*, 8442.
- [220] Rastogi, V. K. *NMR Studies of Proteins and Nucleic Acids*. PhD thesis Chemical Physics Group, Tata Institute of Fundamental Research, Mumbai 400 005, INDIA 1996.
- [221] McGimpsey, W. G.; Gorner, H. *Photochem. Photobiol.* **1996**, *64*, 501.
- [222] Bent, D. V.; Hayon, E. *J. Am. Chem. Soc.* **1975**, *97*, 2612.
- [223] In *Biophysical and Biochemical Aspects of Fluorescence Spectroscopy*, (ed. Dewey, T. G.). Plenum Press, New York 1991.
- [224] Smith, J. C. *Biochim. Biophys. Acta* **1990**, *1016*, 1.
- [225] Clarke, R. J.; Zouni, A.; Holzworth, J. F. *Biophys. J.* **1995**, *68*, 1406.
- [226] Visser, N. V.; Van Hoek, A.; Visser, A. J. W. G.; Clarke, R. J.; Holzworth, J. F. *Chem. Phys. Lett.* **1994**, *231*, 551.

- [227] Lukosz, W. *Phys. Rev. B* **1980**, *22*, 3030.
- [228] Toptygin, D.; Svobodova, J.; Konopasek, I.; Brand, L. *J. Chem. Phys.* **1992**, *96*, 7919.
- [229] Toptygin, D.; Svobodova, J.; Konopasek, I.; Brand, L. In *Time Resolved Laser Spectroscopy in Biochemistry III, SPIE 1640*. 1992 739.
- [230] Macklin, J. J.; Trautman, J. K.; Harris, T. D.; Bruis, L. E. *Science* **1996**, *272*, 255.
- [231] Finer, E. G.; Flook, A. G.; Hauser, H. *FEBS Letters* **1971**, *18*, 331.
- [232] Finer, E. G.; Flook, A. G.; Hauser, H. *Biochim. Biophys. Acta* **1972**, *260*, 49.
- [233] Silverstein, R. M.; Bassler, G. C.; Morrill, T. C. *Spectrometric Identification of Organic Compounds* fifth edn John Wiley Sons, Inc., 1991.
- [234] Ameloot, M.; Hendrickx, H.; Herreman, W.; Pottel, H.; Cauvelaert, F. V.; Van der Meer, W. *Biophys. J.* **1984**, *46*, 525.
- [235] Straume, M.; Litman, B. *Biochemistry* **1987**, *26*, 5121.
- [236] Wang, S.; Beechem, J. M.; Gratton, E.; Glaser, M. *Biochemistry* **1991**, *30*, 5565.
- [237] Badley, R. A.; Martin, W. G.; Schneider, H. *Biochemistry* **1973**, *12*, 268.
- [238] Muller, J. M.; Van Faassen, E. E.; Van Ginkel, G. *Chem. Phys.* **1994**, *185*, 393.
- [239] Holmes, A. S.; Birch, D. J. S.; Sanderson, A.; Aloisi, G. G. *Chem. Phys. Lett.* **1997**, *266*, 309.
- [240] Levine, Y. K. Personal Communication.
- [241] Van Zandvoort, M. A. M. J.; Gerritsen, H. C.; Van Ginkel, G.; Levine, Y. K.; Tarroni, R.; Zannoni, C. *J. Phys. Chem. B* **1997**, *101*, 4149.
- [242] Zhai, X.; Kleijn, J. M. *Biophys. J.* **1997**, *72*, 2651.

- [243] Pebay-Peyroula, E.; Dulfourc, E. J.; Szabo, A. G. *Biophys. Chem.* **1994**, *53*, 45.
- [244] Van Zandvoort, M. A. M. J.; Gerritsen, H. C.; Levine, Y. K. *J. Phys. Chem. B* **1997**, *101*, 4142.
- [245] Cerbon, J. *Biochim. Biophys. Acta* **1970**, *211*, 389.
- [246] Massari, S.; Folena, E.; Ambrosin, V.; Schiavo, G.; Colonna, R. *Biochim. Biophys. Acta* **1991**, *1067*, 131.
- [247] Demel, R. A.; Bruckdorfer, K. R.; Van Deenen, L. L. M. *Biochim. Biophys. Acta* **1972**, *255*, 321.
- [248] Ghosh, D.; Williams, M. A.; Tinoco, J. *Biochim. Biophys. Acta* **1973**, *291*, 351.
- [249] Jendrasiak, G. L.; Hasty, J. H. *Biochim. Biophys. Acta* **1974**, *348*, 45.
- [250] Jendrasiak, G. L.; Hasty, J. H. *Biochim. Biophys. Acta* **1974**, *337*, 79.
- [251] Levine, Y. K.; Birdsall, N. J. M.; Lee, A. G.; Metcalfe, J. C. *Biochemistry* **1972**, *11*, 1416.
- [252] Thompson, T. E.; Huang, C. In *Physiology of Membrane Disorders*, (eds Andriolo, T. E.; Hoffman, J. F.; Fanestil, D. D.; Schultz, S. G.). Plenum, New York 1986.
- [253] Kawato, S.; Kinoshita, K. J.; Ikegami, A. *Biochemistry* **1977**, *16*, 2319.
- [254] Maiti, N. C.; Mazumdar, S.; Periasamy, N. *J. Phys. Chem.* **1995**, *99*, 10708.
- [255] Swaminathan, R.; Periasamy, N.; Udgaonkar, J. B.; Krishnamoorthy, G. *J. Phys. Chem.* **1994**, *98*, 9270.
- [256] Ludescher, R. D.; Peting, L.; Hudson, S.; Hudson, B. *Biophys. Chem.* **1987**, *28*, 59.
- [257] Van der Heide, U. A.; Zandvoort, M. A. M. J.; Van Faasen, E.; Van Ginkel, G.; Levine, Y. K. *J. Fluorescence* **1993**, *3*, 271.

- [258] Cogen, U.; Shinitzky, M.; Weber, W.; Nishida, T. *Biochemistry* **1973**, *12*, 521.
- [259] Klein, U. K. A.; Haar, H. P. *Chem. Phys. Lett.* **1978**, *58*, 531.
- [260] Visser, A. J. W. G.; Vos, K.; Hoek, A. V.; Santema, J. S. *J. Phys. Chem.* **1988**, *92*, 759.
- [261] Walderhaug, H.; Soderman, O.; Stilbs, P. *J. Phys. Chem.* **1984**, *88*, 1655.
- [262] Nery, H.; Soderman, O.; D., C.; Walserhaug, H.; Lindman, B. *J. Phys. Chem.* **1986**, *90*, 5802.
- [263] Berthon, H. A.; Kuchel, P. W. *Adv. Mol. Cell Biol.* **1995**, *11*, 147.
- [264] Brece-ton, M. G.; Butler, C. *J. Phys. (London) A* **1987**, *20*, 3955.
- [265] Khandekar, D. C.; Wiegel, F. W. *J. Phys. (London) A* **1988**, *21*, L563.
- [266] Khandekar, D. C.; Wiegel, F. W. *J. Stat. Phys.* **1988**, *53*, 1073.
- [267] In *Geometric Phases in Physics*, (eds Shapere, A.; Wilczek, F.). World Scientific, Singapore 1989.
- [268] Sinha, S.; Samuel, J. *Phys. Rev. B* **1994**, *50*, 13871.
- [269] Jansen, L.; Boon, M. *Theory of Finite Groups. Application in Physics: Symmetry Groups of Quantum Mechanical Systems* North - Holland Publishing Company, Amsterdam, 1967.
- [270] Chandrasekhar, S. *Rev. Modern Phys.* **1943**, *15*, 1.
- [271] Nityananda, R. Personal Communication.
- [272] Abragam, A. *The Principles of Nuclear Magnetism* Oxford University Press, London, 1961.
- [273] Zwanziger, J. W.; Koenig, M.; Pines, A. *Annu. Rev. Phys. Chem.* **1990**, *41*, 601.

- [274] Landau, L. D.; Lifshitz, E. M. *Quantum Mechanics: Non-relativistic Theory* third edn Pergamon Press, Oxford, U. K., 1977.
- [275] Townes, C. H.; Schawlow, A. L. *Microwave Spectroscopy* McGraw-Hill Book Company, New York, 1955.
- [276] Axelrod, D. *Biophys. J.* **1979**, 26, 557.
- [277] Kleinfeld, A. M.; Dragsten, P.; Klausner, R. D.; Pjura, W. J.; Matayoshi, E. D. *Biochim. Biophys. Acta* **1981**, 649, 471.



TIFR Sketch: Helmuth Bartsch